AD_____

Award Number: W81XWH-10-1-0226

TITLE: Function of ZFAND3 in the DNA Damage Response

PRINCIPAL INVESTIGATOR: Bianca M. Sirbu

CONTRACTING ORGANIZATION: Vanderbilt University
Nashville, TN 37232

REPORT DATE: June 2013

TYPE OF REPORT: Annual Summary

PREPARED FOR: U.S. Army Medical Research and Materiel Command
Fort Detrick, Maryland 21702-5012

REPORT DOCUMENTATION PAGE

Form Approved
OMB No. 0704-0188

1. REPORT DATE *(DD-MM-YYYY)*	2. REPORT TYPE	3. DATES COVERED *(From - To)*
June 2013	Annual Summary	1 June 2010 – 31 May 2013

4. TITLE AND SUBTITLE
Function of ZFAND3 in the DNA damage response

5a. CONTRACT NUMBER

5b. GRANT NUMBER
W81XWH-10-1-0226

5c. PROGRAM ELEMENT NUMBER

6. AUTHOR(S)
Bianca M. Sirbu

E-mail: bianca.m.sirbu@vanderbilt.edu; bia.sirbu@gmail.com

5d. PROJECT NUMBER

5e. TASK NUMBER

5f. WORK UNIT NUMBER

7. PERFORMING ORGANIZATION NAME(S) AND ADDRESS(ES)
Vanderbilt University
Nashville, TN 37232

8. PERFORMING ORGANIZATION REPORT NUMBER

9. SPONSORING / MONITORING AGENCY NAME(S) AND ADDRESS(ES)
U.S. Army Medical Research and Material Command
Fort Detrick, Maryland 21702-5012

10. SPONSOR/MONITOR'S ACRONYM(S)

11. SPONSOR/MONITOR'S REPORT NUMBER(S)

12. DISTRIBUTION / AVAILABILITY STATEMENT
Approved for Public Release; Distribution Unlimited

13. SUPPLEMENTARY NOTES

14. ABSTRACT
Tumors exhibit genomic instability that arises from environmental and endogenous sources of DNA damage. To prevent the propagation of unstable genomes, the DNA damage response (DDR) pathway is activated during each cell cycle to ensure accurate DNA replication, repair of damaged DNA and apoptosis of heavily damaged cells. Thus, the DDR pathway functions as a barrier to cancer. DDR activation has been observed in precancerous lesions and has led to the idea that unresolved problems accumulated during DNA replication promote tumorigenesis. Such damaged sites halt the progression of DNA polymerases and cause 'replication stress' that activates the DDR. Repair and restart of damaged replication forks requires the concerted effort of several DNA repair proteins, including the tumor suppressor BRCA1 (breast cancer 1) and other DDR proteins that have yet to be characterized.
I hypothesized that multiple DDR pathways prevent the accumulation of replication stress observed in precancerous and cancerous lesions of the breast. I identified one putative novel replication stress response protein (Zfand3) and characterized its regulation and function during the DDR. I also developed a new biochemical purification method termed iPOND (isolation of proteins on nascent DNA) to examine Zfand3 and other replication stress proteins that function at moving and stalled replication forks in human cells. These findings suggest that multiple DDR pathways coordinated at replication forks prevent genome instability and have implications for understanding breast cancer etiology.

15. SUBJECT TERMS
cancer, DNA damage response, genome maintenance, epigenome maintenance, DNA replication, replication stress

16. SECURITY CLASSIFICATION OF:			17. LIMITATION OF ABSTRACT	18. NUMBER OF PAGES	19a. NAME OF RESPONSIBLE PERSON
a. REPORT	b. ABSTRACT	c. THIS PAGE			USAMRMC
U	U	U	UU	109	19b. TELEPHONE NUMBER *(include area code)*

Table of Contents

Introduction

The faithful maintenance of genomic integrity is crucial to prevent tumorigenesis (Hoeijmakers 2001; Ciccia and Elledge 2010). DNA damage occurs in each and every cell cycle from both exogenous and endogenous sources and threatens genome stability. Thousands of DNA lesions in the form of UV light, carcinogen exposure, reactive oxidative by-products of normal metabolism, lack of sufficient nucleotides and other types of stress are encountered during each round of cell division. To prevent the propagation of damaged DNA, cells have evolved a signaling pathway called the DNA damage response (DDR) that halts cell cycle progression to allow time for DNA repair, and initiates apoptosis of heavily damaged cells (Schar 2001; Cimprich and Cortez 2008).

When damage is encountered during DNA replication, replication forks stall at the damage site activating the DNA damage response pathway (Cimprich and Cortez 2008). Such 'replication stress' is a hallmark of pre-cancerous lesions and has been hypothesized to arise in genomic areas that are difficult to replicate and that eventually degenerate into toxic double-strand breaks (Gorgoulis et al. 2005). While the sources of replication stress remain poorly characterized, different repair factors are recruited to damaged replication forks to restore accurate copies of DNA (Sirbu and Cortez 2013). For example, the breast cancer tumor suppressor BRCA1 (breast cancer 1) functions in homologous recombination repair of DNA double-strand breaks (Kee and D'Andrea 2010), which may occur at persistently stalled replication forks. BRCA1 also prevents the aberrant processing of damaged replication forks (Schlacher et al. 2012). Mutations in BRCA1 cause one form of hereditary breast cancer and underline the importance of DDR genes for cell survival and prevention of breast cancer.

Identifying novel DDR genes is significant for understanding breast cancer etiology and can inform the design of new cancer therapeutics. Functional genomic screens in our laboratory aimed at finding genes implicated in the DNA damage response have identified ZFAND3 (zinc finger AN1-type domain containing protein 3) as a potential new DDR gene (Lovejoy et al. 2009). Preliminary data indicates that ZFAND3 prevents premature entry into mitosis in the presence of DNA damage and is a putative interacting partner of TopBP1 (topoisomerase II binding protein 1), a proposed breast cancer susceptibility gene (Forma et al. 2012). This project tested the hypothesis that ZFAND3 functions in the DNA damage response pathway to promote genome integrity.

Body

Accordingly with the statement of work, this proposal aimed to: characterize ZFAND3 function in the DDR, identify ZFAND3 interacting proteins, and examine ZFAND3 regulation after DNA damage.

Task 1: Characterize the function of ZFAND3 in the DNA damage response (completed)

DNA damage response proteins can control proper progression through the cell cycle, for example to halt cells from entering mitosis in the presence of DNA damage (G2/M checkpoint). My preliminary data showed that ZFAND3 contributes to the G2/M checkpoint cell after ionizing radiation, suggesting that ZFAND3 is a DDR checkpoint protein. To examine whether ZFAND3, also known as TEX27, promotes normal cell cycle progression in the absence of exogenous DNA damage, the cell cycle profile of cells silenced with two siRNAs targeting FAND3 (TEX27_1 and TEX27_2) was examined. Only a slight difference in the percent of cells in G1 phase was observed in the absence of ZFAND3 (Fig. 1), suggesting that ZFAND3 is not essential for cell cycle progression in the absence of damage. It is formally possible that ZFAND3 knock-down is insufficient in these experiments, which was addressed in Task 2.

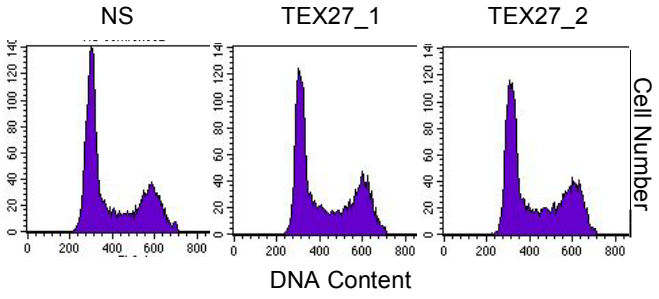

Figure 1. Cell cycle analysis of ZFAND3 depleted cells. ZFAND3 was silenced using two distinctive siRNAs targeting ZFAND3, also known as TEX27 (siRNAs TEX27_1 and TEX27_2), cells were stained with propidium iodide, and DNA content was examined by flow-cytometry.

DNA damage response proteins contribute to maintaining cellular viability following exposure to DNA damaging agents. The replication stress reagent hydroxyurea (HU) stalls replication forks, and

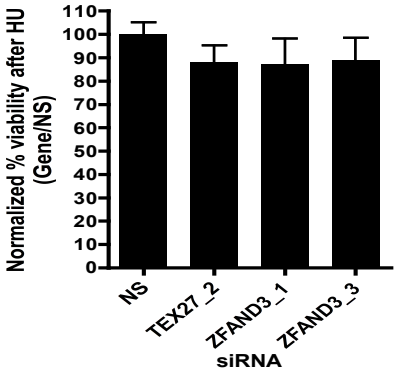

Figure 2. ZFAND3 silencing does not hypersensitize cells to HU. Sensitivity to HU was determined after depletion of ZFAND3 (using siRNAs labeled TEX27_2, ZFAND3_1, and ZFAND3_3) by measuring the cell viability in a colorimetric proliferation assay. Normalized % cellular viability after HU was calculated as the ratio of treated/untreated for each ZFAND3/non-targeting (NS) siRNA. Error bars represent SEM from three independent repeats. Statistical significance was calculated using a t-test as described (Lovejoy 2009).

activates the DDR that ensures the repair and restart of damaged replication forks (Cimprich and Cortez 2008). As proposed in the statement of work, the cellular viability of ZFAND3 depleted cells was examined after HU treatment. No significant change in cell viability was observed relative to controls in the absence of ZFAND3 under the HU concentration and time point tested (Fig. 2). This data suggests that ZFAND3 is not essential for survival during the replication stress observed in these conditions.

The role of ZFAND3 following a variety of damaging agents was examined as proposed in the body of work. The major coordinators of the DDR are a family of related kinases that include the ATR (ATM and Rad3-related) kinase that responds to a wide range of DNA lesions, especially those observed during DNA replication (Lovejoy and Cortez 2009). Such damage can be observed during each cell cycle and ATR's role under various damage types makes it essential for the viability of replicating cells (de Klein et al. 2000; Cortez et al. 2001). ATR phosphorylation of the Chk1 checkpoint kinase amplifies signaling following replication stress and reduced Chk1 phosphorylation on serine 317 corresponds to disrupted DDR signaling.

Depletion of ATR impaired Chk1 phosphorylation after treatment with ionizing radiation (IR), HU and UV radiation relative to a non-targeting siRNA (NS) (Fig. 3A). However, ZFAND3 silencing with two independent siRNAS displayed slightly reduced signaling through Chk1 only after IR (Fig. 3A). In time

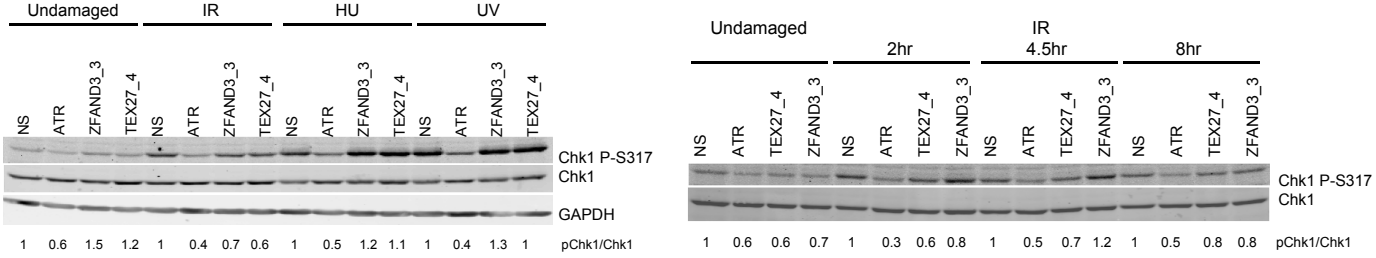

Figure 3. ZFAND3 regulation of DDR signaling. **(A)** Cells were treated with 5Gy of IR, 2mM of HU, or 50J/M^2 of UV radiation and collected after 1.5hr, 6hr, or 1hr, respectively. Immunoblotting with indicated antibodies against phosphorylated Chk1 or total Chk1 was detected and quantified with an Odyssey scanner. **(B)** Cells treated with 5Gy of IR were collected at the indicated time-points. Immunoblotting was performed as above.

course experiments, ZFAND3 depletion affected Chk1 phosphorylation early after IR treatment (2 hours), but not after prolonged exposure to IR (4.5 and 8 hours) (Fig. 3B). Together, this data supports the idea that ZFAND3 contributes minimally to early checkpoint signaling through ATR after ionizing radiation.

Task 2: Identify ZFAND3 interacting proteins (completed)

Preliminary data supporting the role of ZFAND3 in the DNA damage response identified a potential interaction between ZFAND3 and the breast cancer protein TopBP1. To confirm this yeast-two-hybrid interaction, affinity purifications using recombinant TopBP1 and HA-tagged GST-tagged ZFAND3 were performed to examine the in vitro binding. Cell lysates expressing ZFAND3-HA were incubated with GST-tagged TopBP1 fragments that included the previously observed ZFAND3-interacting domain (TopBP1 fragments 7&8, see (Mordes et al. 2008). The ATR interacting protein ATRIP was confirmed to bind TopBP1 in these assays, however no detectable ZFAND3-TopBP1 interaction was observed (Fig. 4).

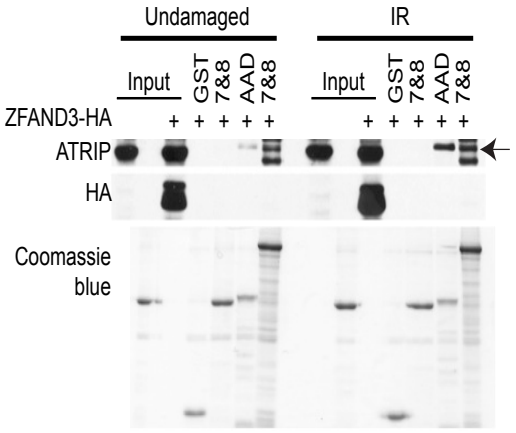

Figure 4. ZFAND3 interaction with TopBP1 is undetectable in TopBP1-GST pulldown assays. Nuclear extracts left untreated or damaged with 5Gy IR were prepared from 293T cells transfected with vectors encoding ZFAND3-HA or empty vector. Extracts were incubated with GST-tagged recombinant TopBP1 fragments (BRCT repeats 7&8 and ATR activation domain (AAD)) immobilized on glutathione beads (Mordes 2008). Proteins bound to TopBP1 were eluted, resolved by SDS-PAGE, and immunoblotted with the indicated antibodies. Input is 5% of total cell extract from the pulldown assays. Arrow indicates band corresponding to ATRIP.

To further examine the potential ZFAND3-TopBP1 interaction, co-immunoprecipitation experiments under varying stringencies of cell lysis buffers were performed, but no binding was observed (data not shown). Taken together, the potential interaction between ZFAND3 and TopBP1 observed in preliminary yeast-two-hybrid studies could not be confirmed using the proposed biochemical methods.

Furthermore, an antibody was raised in rabbits to attempt to detect endogenous ZFAND3. Although antibodies recognized overexpressed and tagged ZFAND3-HA in U2OS and Phoenix ampho cells (Fig. 5, see U2OS ZFAND3-HA, NS lane), ZFAND3 depletion with siRNAs did not significantly change the two protein bands visible in ZFAND3-HA expressing cells. Therefore, this antibody may recognize

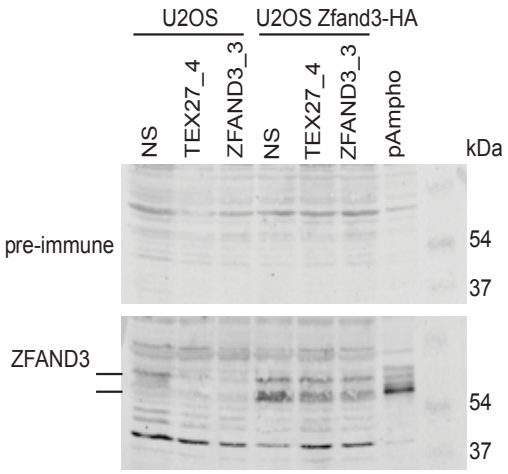

Figure 5. Antibody raised targeting FAND3. Cell lines expressing HA-tagged Zfand3 or no overexpressed protein were tested using pre-immune and ZFAND3 antibody after depletion of endogenous ZFAND3 using siRNA. pAmpho cells over-express HA-tagged ZFAND3 (above 54kDa). Two lines indicate potential bands for ZFAND3 protein.

some endogenous ZFAND3 protein (see bands in untagged cell line), but further testing would confirm the validity of this antibody. A good antibody targeting ZFAND3 (commercially not available or our custom designed antibody) was essential to studies assessing the knockdown efficiency of ZFAND3 in functional studies and further biochemical interaction experiments.

Task 3: Determine ZFAND3 regulation after DNA damage (completed)

Preliminary data supporting a role for ZFAND3 in the DDR showed that ZFAND3 protein levels increase in response to ionizing radiation. To determine whether ZFAND3 protein stability is DNA-damage dependent, the half-life of HA-tagged ZFAND3 was examined before and after IR treatment (Fig. 6). In these experiments, ZFAND3 protein half-life was not reproducibly altered by ionizing radiation. Furthermore, published datasets on DNA-damage responsive mRNA transcripts did not identify ZFAND3. Therefore, we do not believe ZFAND3 expression is regulated by DNA damage.

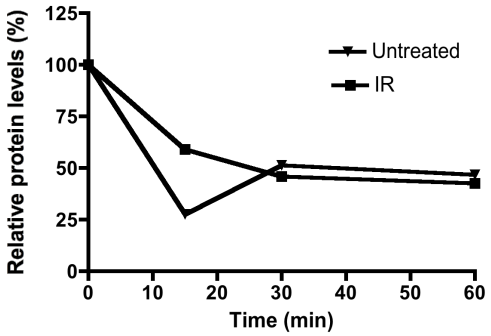

Figure 6. Analysis of ZFAND3 protein half-life. Relative protein levels of ZFAND3-HA were determined over time after cycloheximide treatment in the presence and absence of IR. Protein levels were quantified using an Odyssey system.

Additional research direction:

The results examining ZFAND3's role in genome maintenance prompted the search for a more encompassing understanding of breast cancer etiology resulting from replication stress. The *in vivo* analysis of the events that protect genomic and epigenomic integrity during DNA replication has been a challenging task. The proteins that ensure the accurate inheritance of the genome act directly at replication forks and have eluded identification in mammalian cells because the location of elongating forks is difficult to predict. To understand genome and epigenome pathways disrupted in cancers, I developed a biochemical purification technique called iPOND (isolation of Proteins On Nascent DNA) (Sirbu et al. 2011; Sirbu et al. 2012). iPOND permits the isolation, analysis and discovery of proteins that localize to replication forks during active DNA replication and following conditions of DNA damage. The iPOND technique provides a useful tool to investigate the coordinated mechanisms that maintain

the genome and epigenome through DNA replication and has been adapted and reviewed by several independent researchers studying genome and epigenome instability observed in cancer (Alabert and Groth 2012; Lubelsky et al. 2012; Lopez-Contreras et al. 2013). Lastly, I coupled iPOND to semi-quantitative spectometry to identify proteins associated with replication forks that are moving (active), stalled, and collapsed replication forks (Sirbu et al. 2013). ZFAND3 was not identified in the three iPOND-MS datasets as a replication fork protein.

Key Research Accomplishments

- Tested the function of ZFAND3 during the response to DNA damage and found a minor role for ZFAND3 in early signaling through the ATR pathway after ionizing radiation, but not after replication stress (HU or UV radiation).
- ZFAND3 does not appear to play a significant role in cell cycle progression or in protecting cell viability after replication stress.
- ZFAND3 protein-protein biochemical studies were unable to confirm an interaction with TopBP1.
- An antibody raised to recognize endogenous ZFAND3 requires further testing.
- ZFAND3 protein half-life is not regulated by DNA damage.

Training

My training in molecular cancer biology has been extensive over the last four years of funding and has included weekly and monthly attendance and participation at various seminar series including: bi-monthly Vanderbilt-Ingram Cancer Center seminars, weekly seminars in the Center in Molecular Toxicology, monthly seminar in the Department of Biochemistry, and yearly Genome Maintenance and Breast Cancer SPORE seminars. I presented my research findings at 3 national and international conferences and at 3 research symposia at Vanderbilt University. At the 2011 DOD Era of Hope Conference, I interacted with breast cancer survivors and advocates, which heightened my dedication and understanding of the clinical consequences of breast cancer.

Lastly, my scientific progress included weekly meetings with my research advisor, Dr. David Cortez, and regular meetings with my thesis committee. My training culminated in the defense of my thesis dissertation in June 2013.

Reportable outcomes

I. Coursework and seminars:
   1. All proposed coursework indicated in Statement of Work has been completed
   2. Attended Vanderbilt Ingram Cancer Center bi-monthly seminars (2009-2013)
   3. Attended yearly seminars (2009-2013) at Vanderbilt relevant to cancer within the Genome Maintenance and Molecular Toxicology Seminar series

II. Dissertation defense on June 10, 2013 (Vanderbilt University, Nashville TN)
   Title: Analyzing genome integrity during DNA replication using iPOND (isolation of Proteins On Nascent DNA)

III. Honors, Awards, and Fellowships:
   1. Vanderbilt Ingram Cancer Center Graduate Student of the Year Award 2012
   2. Vanderbilt Prize Scholar 2011 (best female graduate student in biomedical sciences)
   3. Received funding from Swim Across America $50,000 to support cancer research 2012
   4. 1st Place Poster Award, Vanderbilt Cancer Center retreat 2011
   5. Leon Cunningham Award for Excellence in Biochemistry 2010

IV. Presentations of research findings:
   1. Oral presentations of iPOND methodology
      i. **Sirbu BM.** Annual Cunningham Award Biochemistry Lecture at Vanderbilt University
      Title: Maintaining genome integrity during DNA replication
      ii. **Sirbu BM.** Gordon Research Conference, Cell Growth and Proliferation, June 29, 2011, Biddeford, ME.
      Title: Analysis of protein dynamics at active, stalled and collapsed replication forks.

   2. Poster presentation of iPOND methodology
      i. **Sirbu BM**, Couch FB, Feigerle JT, Bhaskara S, Hiebert SW, Cortez D
      Analysis of protein dynamics at active, stalled and collapsed replication forks
      Gordon Research Seminar, Cell Growth and Proliferation, June 26, 2011, Biddeford, ME.
      ii. **Sirbu BM**, Couch FB, Feigerle JT, Bhaskara S, Hiebert SW, Cortez D.
      Analysis of protein dynamics at active, stalled and collapsed replication forks
      Retreat: Vanderbilt Ingram Cancer Center Retreat, Nashville, TN, May 2011
      iii. **Sirbu BM**, Couch FB, Feigerle JT, Bhaskara S, Hiebert SW, Cortez D.
      Analysis of protein dynamics at active, stalled and collapsed replication forks
      Department of Defense Breast Cancer Program Era of Hope Conference August 2011
      iv. **Sirbu BM**, Couch FB, Feigerle JT, Bhaskara S, Hiebert SW, Cortez D.
      Analysis of protein dynamics at active, stalled and collapsed replication forks;
      Vanderbilt Institute of Chemical and Physical Biology August 2011

V. Publications (by year):

1. **Sirbu BM**, Couch FB, Feigerle JT, Bhaskara S, Hiebert SW, Cortez D. 2011. Analysis of protein dynamics at active, stalled, and collapsed replication forks. *Genes Dev* **25**: 1320-1327.
2. **Sirbu BM**, Couch FB, Cortez D. 2012. Monitoring the spatiotemporal dynamics of proteins at replication forks and in assembled chromatin using isolation of proteins on nascent DNA. *Nature protocols* **7**: 594-605.
3. Betous R, Mason AC, Rambo RP, Bansbach CE, Badu-Nkansah A, **Sirbu BM**, Eichman BF, Cortez D. 2012. SMARCAL1 catalyzes fork regression and Holliday junction migration to maintain genome stability during DNA replication. *Genes Dev* **26**: 151-162.
4. Nagarajan P, Ge Z, **Sirbu B**, Doughty C, Agudelo Garcia PA, Schlederer M, Annunziato AT, Cortez D, Kenner L, Parthun MR. 2013. Histone acetyl transferase 1 is essential for Mammalian development, genome stability, and the processing of newly synthesized histones h3 and h4. *PLoS Genet* **9**: e1003518.
5. **Sirbu BM**, Cortez D. 2013. DNA damage response: three levels of DNA repair regulation. *Cold Spring Harbor perspectives in biology* **5**: a012724.
6. Wells CE, Bhaskara S, Stengel KR, Zhao Y, **Sirbu B**, Chagot B, Cortez D, Khabele D, Chazin WJ, Cooper A et al. 2013. Inhibition of histone deacetylase 3 causes replication stress in cutaneous T cell lymphoma. *PloS one* **8**: e68915.
7. **Sirbu BM**, McDonald WH, Dungrawala H, Badu-Nkansah A, Kavanaugh GM, Chen Y, Tabb DL, Cortez D. 2013. Identification of Proteins at Active, Stalled, and Collapsed Replication Forks Using Isolation of Proteins on Nascent DNA (iPOND) Coupled with Mass Spectrometry. *J Biol Chem* **288**: 31458-31467.

Conclusions

My research on ZFAND3 has characterized a new potential DNA damage response protein that my preliminary data showed functions in the G2/M checkpoint, interacts with TopBP1, and whose protein levels increase following DNA damage. Based on my studies, ZFAND3 likely has only a minor role in protecting genome integrity in breast cancer cell lines. While this conclusion is disappointing, I have made significant progress on the larger goal of understanding how maintaining genome and epigenome integrity prevents cancer. To this end, I developed and implemented the iPOND technology to identify and characterize proteins at elongating and damaged replication forks. Together, this work resulted in 3 first author publications, 3 co-author publications, 1 co-author review on DNA repair, several awards, a research fellowship supporting cancer research, and successful defense of my doctoral thesis.

References

Alabert C, Groth A. 2012. Chromatin replication and epigenome maintenance. *Nature reviews Molecular cell biology* **13**: 153-167.

Ciccia A, Elledge SJ. 2010. The DNA damage response: making it safe to play with knives. *Mol Cell* **40**: 179-204.

Cimprich KA, Cortez D. 2008. ATR: an essential regulator of genome integrity. *Nature reviews Molecular cell biology* **9**: 616-627.

Cortez D, Guntuku S, Qin J, Elledge SJ. 2001. ATR and ATRIP: partners in checkpoint signaling. *Science* **294**: 1713-1716.

de Klein A, Muijtjens M, van Os R, Verhoeven Y, Smit B, Carr AM, Lehmann AR, Hoeijmakers JH. 2000. Targeted disruption of the cell-cycle checkpoint gene ATR leads to early embryonic lethality in mice. *Current biology : CB* **10**: 479-482.

Forma E, Krzeslak A, Bernaciak M, Romanowicz-Makowska H, Brys M. 2012. Expression of TopBP1 in hereditary breast cancer. *Molecular biology reports* **39**: 7795-7804.

Gorgoulis VG, Vassiliou LV, Karakaidos P, Zacharatos P, Kotsinas A, Liloglou T, Venere M, Ditullio RA, Jr., Kastrinakis NG, Levy B et al. 2005. Activation of the DNA damage checkpoint and genomic instability in human precancerous lesions. *Nature* **434**: 907-913.

Hoeijmakers JH. 2001. Genome maintenance mechanisms for preventing cancer. *Nature* **411**: 366-374.

Kee Y, D'Andrea AD. 2010. Expanded roles of the Fanconi anemia pathway in preserving genomic stability. *Genes Dev* **24**: 1680-1694.

Lopez-Contreras AJ, Ruppen I, Nieto-Soler M, Murga M, Rodriguez-Acebes S, Remeseiro S, Rodrigo-Perez S, Rojas AM, Mendez J, Munoz J et al. 2013. A proteomic characterization of factors enriched at nascent DNA molecules. *Cell reports* **3**: 1105-1116.

Lovejoy CA, Cortez D. 2009. Common mechanisms of PIKK regulation. *DNA Repair (Amst)* **8**: 1004-1008.

Lovejoy CA, Xu X, Bansbach CE, Glick GG, Zhao R, Ye F, Sirbu BM, Titus LC, Shyr Y, Cortez D. 2009. Functional genomic screens identify CINP as a genome maintenance protein. *Proc Natl Acad Sci U S A* **106**: 19304-19309.

Lubelsky Y, MacAlpine HK, MacAlpine DM. 2012. Genome-wide localization of replication factors. *Methods* **57**: 187-195.

Mordes DA, Glick GG, Zhao R, Cortez D. 2008. TopBP1 activates ATR through ATRIP and a PIKK regulatory domain. *Genes Dev* **22**: 1478-1489.

Schar P. 2001. Spontaneous DNA damage, genome instability, and cancer--when DNA replication escapes control. *Cell* **104**: 329-332.

Schlacher K, Wu H, Jasin M. 2012. A distinct replication fork protection pathway connects Fanconi anemia tumor suppressors to RAD51-BRCA1/2. *Cancer cell* **22**: 106-116.

Sirbu BM, Cortez D. 2013. DNA damage response: three levels of DNA repair regulation. *Cold Spring Harbor perspectives in biology* **5**: a012724.

Sirbu BM, Couch FB, Cortez D. 2012. Monitoring the spatiotemporal dynamics of proteins at replication forks and in assembled chromatin using isolation of proteins on nascent DNA. *Nature protocols* **7**: 594-605.

Sirbu BM, Couch FB, Feigerle JT, Bhaskara S, Hiebert SW, Cortez D. 2011. Analysis of protein dynamics at active, stalled, and collapsed replication forks. *Genes Dev* **25**: 1320-1327.

Sirbu BM, McDonald WH, Dungrawala H, Badu-Nkansah A, Kavanaugh GM, Chen Y, Tabb DL, Cortez D. 2013. Identification of Proteins at Active, Stalled, and Collapsed Replication Forks Using Isolation of Proteins on Nascent DNA (iPOND) Coupled with Mass Spectrometry. *J Biol Chem* **288**: 31458-31467.

Analysis of protein dynamics at active, stalled, and collapsed replication forks

Bianca M. Sirbu, Frank B. Couch, Jordan T. Feigerle, et al.

Genes Dev. 2011 25: 1320-1327
Access the most recent version at doi:10.1101/gad.2053211

Analysis of protein dynamics at active, stalled, and collapsed replication forks

Bianca M. Sirbu, Frank B. Couch, Jordan T. Feigerle, Srividya Bhaskara, Scott W. Hiebert, and David Cortez[1]

Department of Biochemistry, Vanderbilt University School of Medicine, Nashville, Tennessee 37232, USA

Successful DNA replication and packaging of newly synthesized DNA into chromatin are essential to maintain genome integrity. Defects in the DNA template challenge genetic and epigenetic inheritance. Unfortunately, tracking DNA damage responses (DDRs), histone deposition, and chromatin maturation at replication forks is difficult in mammalian cells. Here we describe a technology called iPOND (isolation of proteins on nascent DNA) to analyze proteins at active and damaged replication forks at high resolution. Using this methodology, we define the timing of histone deposition and chromatin maturation. Class 1 histone deacetylases are enriched at replisomes and remove predeposition marks on histone H4. Chromatin maturation continues even when decoupled from replisome movement. Furthermore, fork stalling causes changes in the recruitment and phosphorylation of proteins at the damaged fork. Checkpoint kinases catalyze H2AX phosphorylation, which spreads from the stalled fork to include a large chromatin domain even prior to fork collapse and double-strand break formation. Finally, we demonstrate a switch in the DDR at persistently stalled forks that includes MRE11-dependent RAD51 assembly. These data reveal a dynamic recruitment of proteins and post-translational modifications at damaged forks and surrounding chromatin. Furthermore, our studies establish iPOND as a useful methodology to study DNA replication and chromatin maturation.

[*Keywords*: DNA replication; chromatin; DNA damage response; H2AX; histone acetylation; EdU; click chemistry]

Supplemental material is available for this article.

Received March 22, 2011; revised version accepted May 16, 2011.

In human cells, more than 6 billion base pairs of DNA need to be replicated and packaged into chromatin every cell division cycle. Failures lead to mutation, epigenetic changes, and other chromosomal aberrations that ultimately cause diseases such as cancer. DNA replication is coordinated with chromatin assembly (Probst et al. 2009). The replisome, containing the proteins necessary to complete replication, is a dynamic machine that must work with speed and precision. DNA lesions, insufficient nucleotides, and other types of replication stress cause fork stalling. In these circumstances, the DNA damage response (DDR) mobilizes repair activities to stabilize the fork, resolve the problem, and complete DNA synthesis (Harper and Elledge 2007; Cimprich and Cortez 2008).

The DDR to replication stress is poorly understood in comparison with the response to double-strand breaks (DSBs). For example, there are extensive modifications to the chromatin surrounding a DSB, including destabilization of nucleosomes, chromatin remodeling, and histone post-translational modifications (Morrison and Shen 2009; van Attikum and Gasser 2009; Rossetto et al. 2010; Venkitaraman 2010). These changes increase access to the repair machinery and recruit proteins involved in repair and DDR signaling. The extent to which chromatin changes at a stalled fork mimic those at a DSB is unknown.

Replication provides a unique landscape and set of challenges compared with a DSB. The immediate vicinity of the replisome lacks nucleosomes. Also, half of the histones on the nascent DNA are newly synthesized and require changes in post-translational modifications to restore the proper chromatin structure. Finally, several mechanisms exist to recover stalled replication forks, which necessitate the recruitment of multiple enzymatic activities and, perhaps, different chromatin changes.

The difference in our knowledge of the responses at stalled forks compared with DSBs is due primarily to the increased technical challenges of studying replication stress. For example, several investigators have used site-specific DSBs combined with chromatin immunoprecipitation (ChIP) to examine proteins at breaks with high resolution (Rudin and Haber 1988; Rodrigue et al. 2006; Soutoglou et al. 2007; Berkovich et al. 2008). Thus far, site-specific analysis of active and stalled replisomes in mammalian cells has not been achieved. We addressed this technical limitation by developing the iPOND (isolation of proteins on nascent DNA) methodology. iPOND

[1]**Corresponding author.**
E-mail david.cortez@vanderbilt.edu.
Article is online at http://www.genesdev.org/cgi/doi/10.1101/gad.2053211.

permits the isolation and analysis of proteins at active, stalled, and collapsed replication forks. It can also probe the changes that accompany chromatin deposition and maturation following DNA synthesis. We demonstrate the power of iPOND by defining the dynamics of proteins and post-translational modifications in the replisome and on the newly deposited chromatin.

Results

Development of iPOND

Tracking the location of any single replisome in a mammalian cell is not possible, limiting the utility of ChIP-based technologies. To overcome this technical limitation, we used the thymidine analog 5-ethynyl-2′-deoxyuridine (EdU) (Salic and Mitchison 2008), which contains an alkyne functional group. Covalent linkage to a biotin-azide using click chemistry (Moses and Moorhouse 2007) facilitates single-step purification of the EdU-labeled nascent DNA and associated proteins at replication forks (Fig. 1A).

To validate this methodology we first asked whether we could detect replisome proteins. We labeled cells with EdU for 10 min then performed iPOND. We detected proliferating cell nuclear antigen (PCNA), chromatin assembly factor 1 (CAF-1), replication protein A (RPA), and two subunits of polymerase ϵ (Fig. 1B). These results indicate that iPOND can purify replisome proteins, including those indirectly bound to DNA such as CAF-1 (Shibahara and Stillman 1999). Furthermore, they indicate that iPOND is a highly sensitive methodology. We are able to detect proteins such as POLE2 and POLE3, which are expected to be at a density of only one or two molecules per fork (Fig. 1B). Thus, unlike immunofluorescence, iPOND does not require high concentrations of proteins within a small nuclear region to track protein localization. Of note, proteins not present at replication forks, such as GAPDH, are not detectable in iPOND captures (data not shown).

In time-course experiments, we detected PCNA and CAF-1 after a 2.5-min pulse of EdU, histones H2B and H3 after 5 min, and the linker histone H1 at 20 min after EdU addition (Fig. 1C). Thus, with short labeling times, we selectively purify proteins at the replication fork, and longer labeling times permit analysis of chromatin assembly. The order of histone deposition supports previous fractionation data indicating that H1 is added 10–20 min after DNA replication to create higher-order chromatin structures (Worcel et al. 1978).

The resolution of this technique depends on the length of the EdU pulse, the rate of DNA synthesis, and the size of the DNA fragments generated after cell lysis. In practice, the first two parameters are the most important, since we consistently obtain DNA fragments of ~150 base pairs (bp) (Supplemental Fig. 1). In mammalian cells, the rate of DNA synthesis varies between 0.75 and 2.5 kb/min (Herrick and Bensimon 2008). Thus, a 2.5-min EdU pulse labels ~2–6 kb, although this is likely a significant overestimation, since EdU must enter the cell and be phosphorylated before incorporation into DNA. Thus, iPOND resolution is on the order of a few thousand base pairs.

Importantly, iPOND can be combined with pulse-chase methods to track how proteins assemble and disassemble from a nascent DNA segment with high spatial and temporal resolution. Increasing chase times monitor DNA-associated proteins at greater and greater distances from the moving fork. In these experiments, histone levels remain constant, indicating that the procedure effectively captures a maturing chromatin segment of constant length (Fig. 1D). However, PCNA and CAF-1 levels purified with the EdU-labeled segment decline with a half-life of considerably <10 min of chase time (Fig. 1D). These data indicate that iPOND isolates chromatin-associated proteins specifically located at the replication fork, and are consistent with rapid unloading of PCNA and CAF-1 once Okazaki fragment DNA synthesis is complete.

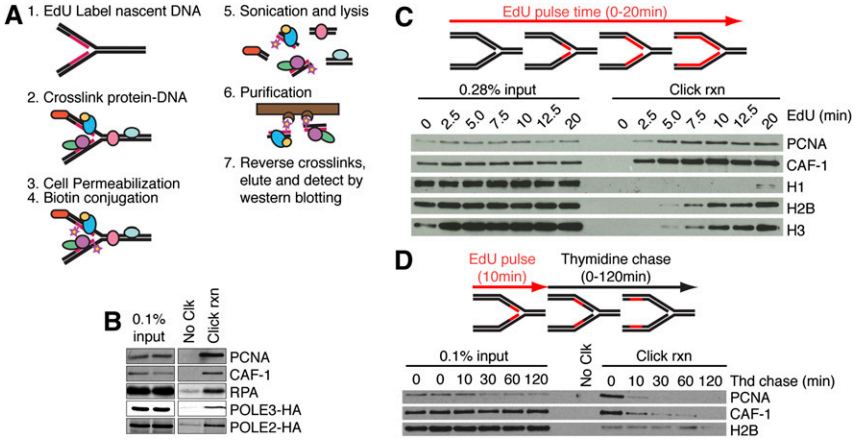

Figure 1. Development of the iPOND technology. (*A*) iPOND begins by adding EdU to cultured cells. The cells are then treated with formaldehyde to cross-link protein–DNA complexes, washed, and permeabilized with detergent. Copper catalyzes the cycloaddition of biotin-azide to the EdU-labeled DNA. The cells are then lysed in denaturing conditions with sonication. The biotin-labeled DNA–protein complexes are purified using streptavidin-coated beads, cross-links are reversed, and the eluted proteins are analyzed by immunoblotting or other methods like mass spectrometry. (*B*) Cells were incubated with EdU for 10 min prior to performing iPOND. Cells expressing POLE2-HA or POLE3-HA were used to detect these proteins with the HA antibody. (*C*) Cells were incubated in EdU-containing medium for increasing times prior to performing the iPOND protocol. (*D*) Cells were incubated with EdU for 10 min. The EdU-containing medium was removed and cells were washed once before incubating for increasing times in medium containing 10 μM thymidine prior to performing iPOND. In all experiments, the No Clk control is the input sample in the first lane processed with no biotin-azide.

Analysis of chromatin maturation using iPOND

Maturation of the new chromatin requires addition and removal of histone post-translational modifications. Newly synthesized histone H4 is acetylated on two lysines (5 and 12), and these evolutionarily conserved marks are removed after deposition (Sobel et al. 1995; Taddei et al. 1999). Our time course experiments indicate that acetylated H4K5 (H4K5ac) is removed rapidly and H4K12ac deacetylation is slightly delayed (Fig. 2A,B). The delay in K12 deacetylation could be due to the activity of chromatin-associated histone acetyltransferases (HATs) that promote the acetylation of this site in some chromatin domains. Indeed, in the presence of the nonselective HAT inhibitor anacardic acid, the rate of H4K12 deacetylation becomes identical to H4K5, with a half-life of <20 min (Fig. 2C,D).

In principle, chromatin maturation—as measured by H4K5,K12 deacetylation—could be coupled to fork progression. To test this possibility, we used high concentrations of hydroxyurea (HU) to stall active replisomes and stop DNA synthesis. HU addition stalls the fork effectively in these cells, since the amount of histone capture does not increase appreciably during the HU treatment (Fig. 2E). Deacetylation of newly deposited H4 proceeds at the same rate regardless of whether DNA synthesis is inhibited. Thus, chromatin maturation can be uncoupled from replisome movement.

The histone deacetylase (HDAC) in human cells that catalyzes the deacetylation of H4K5 and K12 is unknown. HDAC1 and HDAC2 associate with CAF-1 (Ahmad et al. 1999), and HDAC3 is required—perhaps in late S phase or G2—to remove H4K5ac (Bhaskara et al. 2010). Indeed, in pulse-chase experiments, we found an enrichment of HDAC1, HDAC2, and HDAC3 near the fork (Fig. 2A), and the selective class I HDAC inhibitor FK228 (Furumai et al. 2002) prevented deacetylation of H4 (Fig. 2F), suggesting that all three of these HDACs are involved.

DDR response at stalled replication forks

HU treatment causes DDR activation to stabilize the stalled fork and induce a cell cycle checkpoint. Previous studies suggest that HU-stalled forks remain stable and competent to resume DNA synthesis for several hours; however, eventually, the stalled fork collapses and DSBs are formed (Petermann et al. 2010). To further examine this process, we monitored recruitment and modification of proteins at stalled forks. The amounts of PCNA and CAF-1 that are captured at the stalled fork decrease initially after adding HU to the medium, and then reach a steady state level of between 20% and 30% of that found at an elongating fork (Fig. 3A). This PCNA pattern is likely due to unloading of PCNA from the completed Okazaki fragments. We detected RPA associated with the fork both before and after HU addition (Fig. 3A). The amount of RPA detected remained constant even though RPA accumulates at stalled forks (Cimprich and Cortez 2008). This discrepancy is explained because RPA binds only to the single-stranded, template strand of DNA, which lacks incorporated EdU. Therefore, iPOND detects only the RPA immediately adjacent to the newly synthesized dsDNA (Supplemental Fig. 2).

In these experiments, we noticed that at 120 and 240 min after addition of HU, the electrophoretic mobility of RPA decreased, consistent with phosphorylation (Fig. 3A). RPA S33 phosphorylation could be detected within 10 min of HU addition, and S4/S8 phosphorylation appeared at 2 h

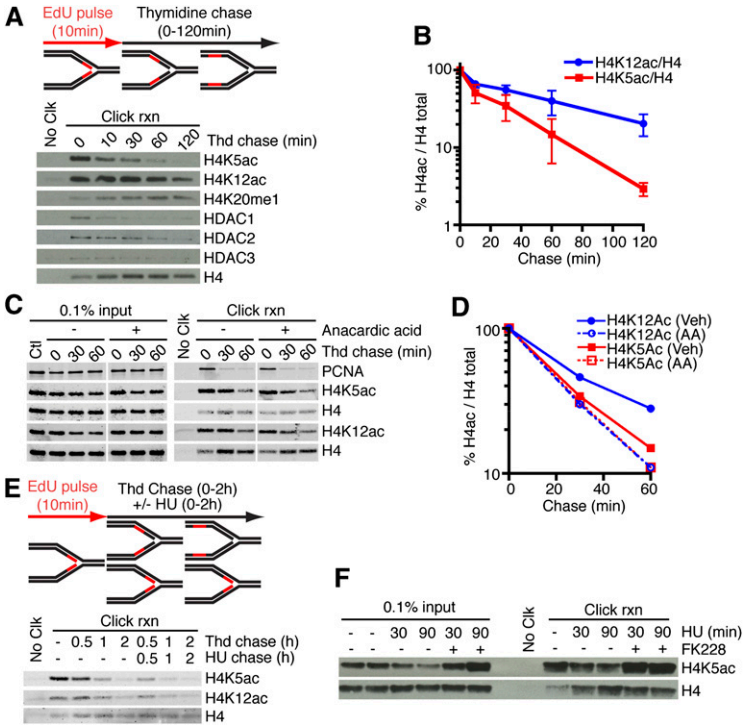

Figure 2. HDACs are enriched at replication forks and deacetylate newly deposited histone H4 regardless of fork movement. (*A–E*). Cells were labeled with EdU for 10 min followed, by a chase into thymidine-containing medium for the indicated times prior to performing iPOND. (*B*) Quantitation of H4 acetylation levels compared with total H4 in the click reaction samples from three independent experiments. Error bars in all figures are standard deviations. (*C*,*D*) Anacardic acid (30 μM) was added to the indicated samples. (*E*) HU (3 mM) was added to the indicated samples. (*F*) Cells labeled with EdU were chased into 3 mM HU medium with or without 100 nM FK228 prior to performing iPOND.

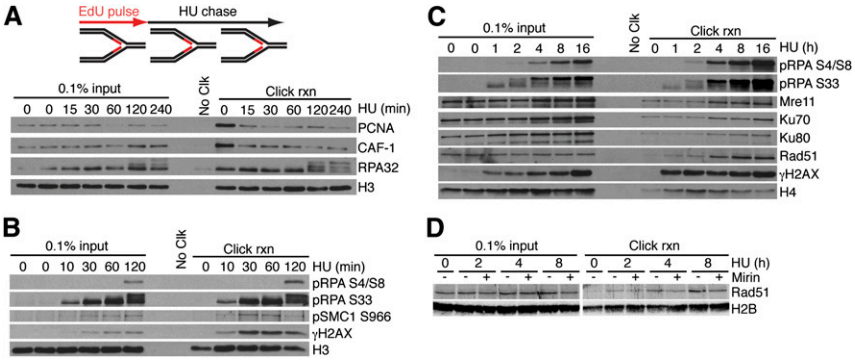

Figure 3. iPOND monitors post-translational modifications and recruitment of DDR proteins to stalled and collapsed replication forks. (*A–D*) Cells were labeled with EdU for 15 min (*A*) or 10 min (*B–D*), followed by a chase into HU for the indicated times prior to performing iPOND. (*D*) HU-treated cells were additionally coincubated with or without the Mre11 inhibitor mirin (100 μM) as indicated.

(Fig. 3B). DNA-PK catalyzes S4/S8 phosphorylation and ATR catalyzes S33 phosphorylation (Anantha et al. 2007), suggesting that ATR phosphorylates RPA immediately after fork stalling, and DNA-PK phosphorylates RPA only at persistently stalled forks.

H2AX phosphorylation (γH2AX) is often considered a marker for DSBs (Dickey et al. 2009). However, we observed γH2AX at stalled replication forks at even the earliest time points (10 min) after HU addition (Fig. 3B), well before evidence of DSB formation (Petermann et al. 2010). These data prompted us to examine the timing of recruitment of DSB repair proteins. MRE11, KU70, and KU80 exhibited a recruitment profile in which low amounts were observable before the addition of HU, and remained unchanged for 2 h after HU addition (Fig. 3C). However, by 4 h in HU, we detected a significant increase in all of these proteins near the stalled fork (Fig. 3C). RAD51 was first detectable after HU addition, but its levels also increased significantly by 4 h, suggesting that DSBs may form between 2 and 4 h after the fork is stalled. KU70 and KU80 may bind to some of the single-ended breaks, and RAD51 may bind to others.

At DSBs, MRE11-dependent end resection is required to load RAD51 (Mimitou and Symington 2009). At collapsed forks, RAD51 may function to promote recombination-based methods to re-establish the replication fork (Errico and Costanzo 2010). To test whether the loading of RAD51 at stalled forks also requires MRE11, we treated cells with the MRE11 nuclease inhibitor mirin (Dupre et al. 2008). Although the early recruitment of RAD51 occurred independently of MRE11, the late accumulation required MRE11 activity (Fig. 3D), suggesting that end resection promotes this loading. The timing of MRE11 recruitment also correlated with a large increase in RPA S4/S8 phosphorylation (Fig. 3C), which was previously linked to end resection at camptothecin-damaged forks (Sartori et al. 2007).

γH2AX spreading from stalled forks before and after fork collapse

We noticed that the rapid phosphorylation of H2AX near the fork saturates within 30 min; however, global levels continue to increase (Fig. 3B, cf. the click rxn lanes and the input lanes). Therefore, we hypothesized that the global increase stems from γH2AX spreading from the stalled fork, as is observed near DSBs (Berkovich et al. 2007; Savic et al. 2009). To test this hypothesis, we first labeled cells with EdU, then chased with thymidine for various lengths of time to extend the distance between the EdU-labeled fragment and the fork, and finally added HU to stall the fork. We again observed maximum γH2AX at the fork 30 min after HU addition; however, the chromatin region distant from the fork contained low but detectable levels of γH2AX that increased when examined at 60 min after HU addition (Fig. 4A, cf. lanes 4–6 and 7–9). A more detailed analysis revealed that the density of γH2AX gradually declined as a function of distance from the stalled fork (Fig. 4B,C). Compared with the saturated density at the fork, the γH2AX density decreased approximately twofold for every 15 min of thymidine chase time when cells were treated with HU for 1 h. By 2 h, we observed increased γH2AX density in all chromatin segments analyzed, suggesting that γH2AX spreading contributes significantly to the global change in γH2AX levels.

To examine the chromatin at a single location distant from the fork, we repeated this experiment holding the thymidine chase time constant at 30 min, and treated with HU for varying times. We observed a steady increase in γH2AX at this distance from the fork (Fig. 4D). Importantly, these results indicate considerable spreading of the γH2AX signal even shortly after fork stalling. Assuming a conservative rate of fork elongation of 1 kb/min, these data imply that, within 1 h of fork stalling, γH2AX spreads to include a large domain containing tens of thousands of base pairs of DNA.

To identify the kinases that phosphorylate H2AX adjacent to the stalled fork and that promote spreading, we used small molecule kinase inhibitors. The selective DNA-PK and ATM inhibitors NU7441 (Leahy et al. 2004) and KU55933 (Hickson et al. 2004) had minimal effects on the spreading or total levels of γH2AX induced by a short (30- to 60-min) HU treatment (Fig. 5A; Supplemental Fig. 3A). However, these inhibitors did significantly reduce γH2AX levels at all chromosomal positions relative to the fork in cells treated with HU for 4 h (Fig. 5B,C; Supplemental Fig. 3B). These results indicate that DNA-PK/ATM contributes to maintenance and spreading of γH2AX at persistently stalled forks. In contrast,

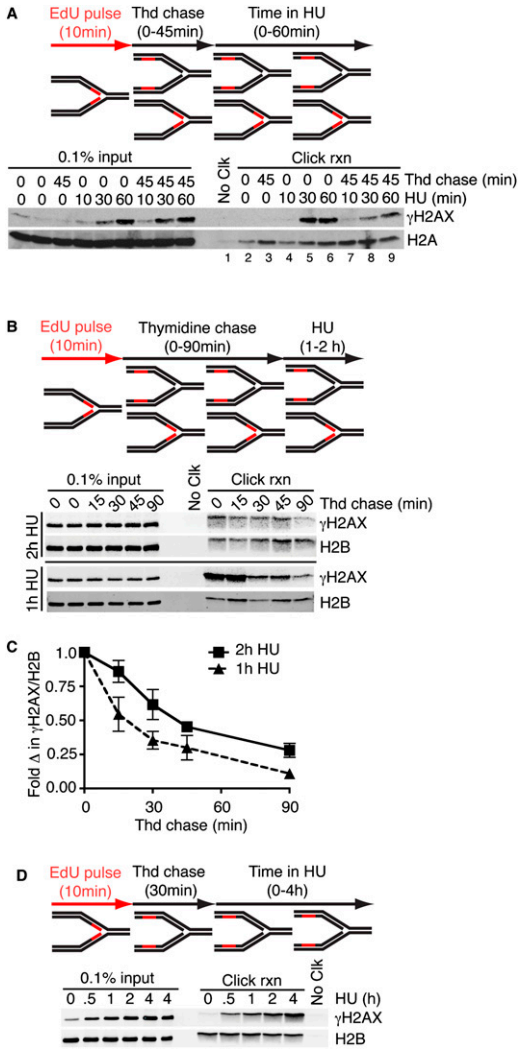

Figure 4. γH2AX spreads from a stalled replication fork. (*A–D*) Cells labeled with EdU for 10 min were chased into thymidine-containing medium prior to addition of HU, then processed using iPOND. The length of the thymidine and HU treatments is indicated. Quantitation of the click reaction samples in *C* at the 2-h HU-treated samples is from three independent experiments, and at the 1-h HU-treated samples is from two independent experiments.

treatment with caffeine, which preferentially inhibits ATR (Sarkaria et al. 1999), significantly reduced γH2AX formation and spreading shortly after the fork is stalled (Fig. 5D). These results are consistent with a model in which ATR phosphorylates H2AX at a stalled fork and promotes initial spreading. At later time points, when DSBs likely form at the fork, ATM and DNA-PKcs maintain and further propagate the H2AX phosphorylation (Supplemental Fig. 4).

Discussion

Previous studies of the replisome and DDR responses at stalled forks relied largely on immunofluorescent imaging to track protein localization. While useful, immunofluorescence has the significant disadvantages of low resolution and low sensitivity. For example, proteins that exist at only single-copy levels at replication forks cannot be tracked with immunofluorescent imaging. In contrast, iPOND technology has dramatically improved sensitivity,

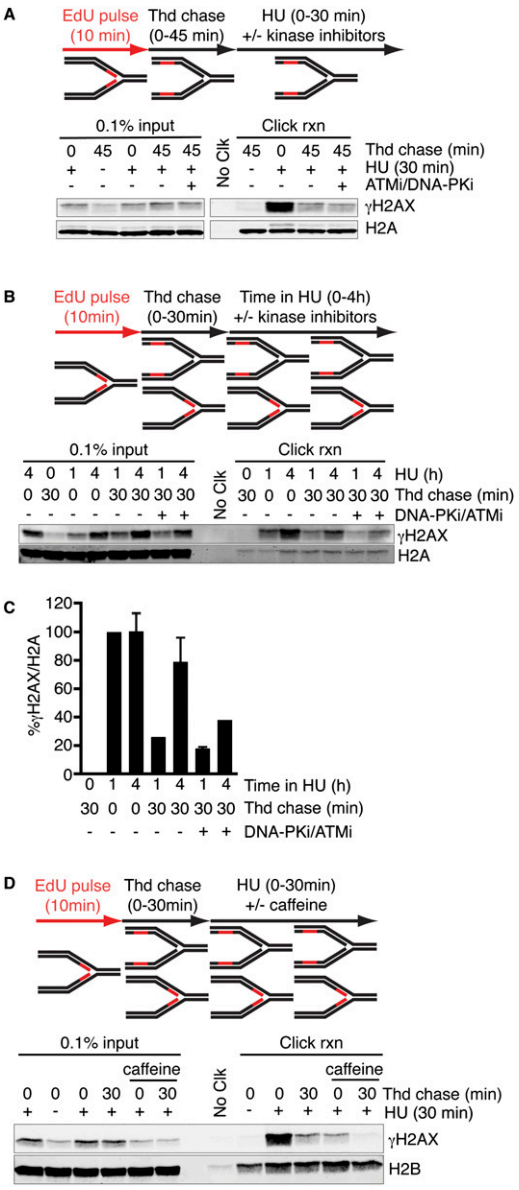

Figure 5. Checkpoint kinases propagate H2AX phosphorylation from stalled replication forks. (*A–C*) Cells labeled with EdU for 10 min were chased into thymidine, followed by treatment with HU. The length of thymidine and HU treatments are indicated. DNA-PK (KU7441, 1 μM) and ATM (KU5593, 10 μM) inhibitors were added at the same time as HU in the indicated samples. (*C*) Quantitation of the click reaction samples is the average from two independent experiments and is normalized to the 1-h HU treatment. (*D*) Cells labeled with EdU for 10 min were chased into thymidine for either 0 or 30 min, followed by a 30-min treatment with HU. Caffeine (10 mM) was added at the same time as HU in the indicated samples.

allowing us to detect even proteins such as polymerases. Furthermore, combining iPOND with pulse-chase methods provides high spatial and temporal resolution of protein dynamics. Finally, iPOND also facilitates analysis of post-translational modifications, which is often impossible with immunofluorescent imaging due to poor antibody quality or specificity.

Recently, the Helleday group (Petermann and Helleday 2010) isolated CldU-labeled DNA using an antibody to show that Rad51 is bound to recently synthesized DNA. However, they used a 40-min labeling time, so it is unclear whether this method is sufficiently sensitive or specific to produce high spatial and temporal resolution like iPOND. Also, unlike CldU-IP, iPOND does not require ssDNA to permit antibody access to an antibody epitope, and the biotin–streptavidin purification procedure is compatible with highly stringent conditions (1% SDS and 1 M NaCl), thereby improving specificity.

iPOND is an ensemble methodology. Thus, it provides an average picture of events in different cells at stalled forks throughout the genome. iPOND can be combined with cell synchronization to examine replication and chromatin maturation in early and late replicating genomic regions. In principle, iPOND should be applicable to any process involving DNA synthesis, such as analysis of DNA excision repair.

A disadvantage of iPOND over ChIP methods is the lack of a PCR amplification step. Thus, much larger amounts of input material are necessary to achieve sufficient protein for detection. Fortunately, the covalent coupling of EdU and biotin during the click reaction permits a single-step, highly efficient purification in stringent buffer, salt, and detergent conditions. A significant advantage of iPOND compared with ChIP is its compatibility with unbiased screening approaches. We anticipate coupling iPOND to mass spectrometry to identify all proteins at active and damaged replisomes. Furthermore, mass spectrometry analysis of iPOND-captured histones will facilitate studies of chromatin assembly and maturation.

Chromatin assembly is thought to occur by a stepwise deposition of the core histones, followed by linker histones and changes in post-translational modifications (Probst et al. 2009). Our data confirm this assembly process in vivo in cultured mammalian cells. Furthermore, we found that at least some chromatin maturation processes, such as the removal of acetylation on H4K5 and H4K12, proceed even when decoupled from replisome movement. HDAC1, HDAC2, and HDAC3 are enriched on newly synthesized DNA, and an inhibitor that targets all three of these enzymes prevents H4K5ac and H4K12ac deacetylation. Intriguingly, deacetylation of H4K5ac and H4K12ac occurred at the same rate, but acetyltransferases rapidly reacetylated H4K12, suggesting a specific need for this modification in some chromatin domains.

In the yeast *Saccharomyces cerevisiae*, H3K56 acetylation is also associated with newly deposited histones during DNA replication, and promotes survival in response to replication stress (Masumoto et al. 2005). We were unable to detect this acetylation mark on newly deposited histones or after HU treatment (data not shown). This observation is consistent with other human cell studies that found low levels of this post-translational modification in total chromatin that further decreased in response to DNA damage (Tjeertes et al. 2009).

Prominent changes in response to replication stress include protein phosphorylation. Importantly, our data indicate that H2AX phosphorylation spreads to a large chromatin domain early in the response to fork stalling. This early phosphorylation is catalyzed by ATR and is unlikely to be due to the processing of the fork into a DSB intermediate. Our data are consistent with previous analyses implicating both ATR-dependent (Ward and Chen 2001) and ATR-independent (Brown and Baltimore 2003; Gilad et al. 2010) H2AX phosphorylating activities in response to fork arrest. Most models of ATR function suggest that it is active only when bound to the ssDNA at the stalled fork through an ATRIP–RPA interaction (Cimprich and Cortez 2008), but our data indicate that ATR helps spread the γH2AX signal. One possibility is that the early spreading of γH2AX is due to looping of the newly synthesized chromatin that brings it into proximity of ATR. Alternatively, ATR may have a method of spreading its signal beyond the immediate ssDNA vicinity, similar to the ability of active ATM to spread along the dsDNA away from the DSB end (You et al. 2007). MDC1 may be involved in such a process (Ichijima et al. 2011; Wang et al. 2011).

Persistent stalling of the fork for longer than 1–2 h causes a switch in the DDR. RPA is hyperphosphorylated on DNA-PK-dependent phosphorylation sites, ATM/DNA-PK catalyzes further γH2AX spreading, and DSB repair proteins like MRE11, KU70/80, and RAD51 accumulate. RAD51 assembly at these persistently stalled forks depends on MRE11 activity, suggesting a requirement for end resection. The end resection may be on the template DNA strand, since we continued to capture EdU-labeled DNA and associated proteins. Resecting the leading strand template would yield a 3′ overhang of newly synthesized DNA, which could be used in recombination-based methods of fork repair and restart (Petermann and Helleday 2010).

Overall, these data provide the first high-resolution, time-dependent analyses of protein dynamics at active, stalled, and collapsed replication forks in mammalian cells. Furthermore, they validate iPOND as a powerful method to study DDRs, chromatin deposition, and chromatin maturation during DNA replication.

Materials and methods

Cell culture

HEK293T cells were cultured in DMEM supplemented with 7.5% FBS. Stable cell lines expressing POLE2-HA and POLE3-HA were generated by retroviral infection and selection in puromycin-containing medium.

Plasmid constructs

POLE2-HA and POLE3-HA retroviral vectors were generated by gateway cloning. pENTR POLE2 and pENTR POLE3 were

recombined with pLPCX-GW-HA3X (pDC1127) to generate a C-terminal HA-tagged POLE2 and POLE3 retroviral vectors. pDC1127 was created by subcloning a 3XHA epitope into pLPCX between the Not1 and Cla1 restriction sites, then subcloning the gateway cassette containing attR1, *ccdB* gene, and attR2 as an EcoRV fragment between EcoR1 and Not1 sites.

iPOND

EdU-labeled sample preparation HEK 293T cells (~1.5×10^8 cells per sample) were incubated with 10–12 μM EdU (Vanderbilt Synthesis Core). For pulse-chase experiments with thymidine (Sigma), EdU-labeled cells were washed once with temperature- and pH-equilibrated medium containing 10 μM thymidine to remove the EdU, then chased into 10 μM thymidine. Other chemicals were added to the cell cultures at the following concentrations: HU (3 mM; Sigma), HAT inhibitor anacardic acid (30 μM; Enzo), HDAC inhibitor FK228 (100 nM; kindly provided by Dineo Khabele), Mre11 inhibitor Mirin (100 μM; Sigma), ATM inhibitor (KU55933, 10 μM; AstraZeneca), DNA-PK inhibitor (KU57788, 1 μM; AstraZeneca), and caffeine (10 mM; ICN Biomedicals). DMSO was used as a vehicle control where appropriate.

After labeling, cells were cross-linked in 1% formaldehyde/PBS for 20 min at room temperature, quenched using 0.125 M glycine, and washed three times in PBS. Collected cell pellets were frozen at −80°C, then resuspended in 0.25% Triton-X/PBS to permeabilize. Pellets were washed once with 0.5% BSA/PBS and once with PBS prior to the click reaction.

Click reaction Cells were incubated in click reaction buffer for 1–2 h at a concentration of 2×10^7 cells per milliliter of click reaction buffer. The click reaction buffer contains Invitrogen's Click-iT cell reaction buffer and cell buffer additive (C10269), 2 mM copper (II) sulfate ($CuSO_4$), and 1 μM photocleavable biotin-azide (Kim et al. 2009) (kindly provided by Ned Porter). DMSO was added instead of biotin-azide to the negative control samples (no clk in all figures). Cell pellets were washed once with 0.5% BSA/PBS and once with PBS.

Cell lysis Cells were then resuspended in lysis buffer containing 1% SDS, 50 mM Tris (pH 8.0), 1 μg/mL leupeptin, and 1 μg/mL aprotinin. Samples were sonicated (Micro-tip, Misonix 4000 or Fisher Scientific Sonic Dismembrator model 500) using the following settings: 13–16 W, 20-sec constant pulse, and 40- to 59-sec pause for a total of 4–5 min. Samples were centrifuged at 13,200 rpm for 10 min, filtered through a 90-μm nylon mesh, and diluted 1:1 (v/v) with PBS containing 1 μg/mL leupeptin and 1 μg/mL aprotinin prior to purification.

Purification Streptavidin–agarose beads (Novagen) were washed 1:1 (v/v) twice in lysis buffer and once in PBS. Washed beads were incubated with the samples for 14–20 h at 4°C in the dark. The beads were washed once with lysis buffer, once with 1 M NaCl, and then twice with lysis buffer. Captured proteins were eluted and cross-links were reversed in SDS sample buffer by incubating for 25 min at 95°C. Proteins were resolved on SDS-PAGE and detected by immunoblotting. In most cases, quantitative immunoblotting was performed using the Odyssey infrared imaging system.

Antibodies

Antibodies used were as follows: PCNA (Santa Cruz Biotechnology); CAF-1 p60, RPA32, pRPA32 S4/S8, pRPA32 S33, and pSMC1 S966 (Bethyl Laboratories); FK2 (Calbiochem); RAD51, H2B, H2A, H3, H4, H4K5Ac, KU70, KU80, HDAC1, HDAC2, and HDAC3 (Abcam); γH2AX, H1 (Millipore); MRE11 (Genetex); H4K12Ac and H4K20me1 (Active Motif); and anti-HA (Covance).

Determination of DNA fragment size

To determine DNA fragment size, 5 μL of pre- and post-sonication samples were incubated at 65°C to reverse the DNA–protein cross-links, then incubated with RNaseA and proteinase K. DNA samples were resolved on a 1.5% agarose gel, stained with ethidium bromide, and visualized under UV light. DNA fragment sizes ranged between 100–300 bp. It should be noted that we determined that the $CuSO_4$ in the click reaction catalyzes cleavage of the phosphodiester bond and assists in generating the small fragment size.

Acknowledgments

We thank Drs. Ned Porter, Keri Tallman, Dineo Khabele, Janel McLean, Kathy Gould, Mahesh Chandrasekharan, Simona Codreanu, Daniel Liebler, and Larry Marnett for supplying reagents and advice. This work was supported by NIH grant R01CA136933 to D.C. Additional support was provided by the Vanderbilt-Ingram Cancer Center (CA06485) and the Ingram Charitable Fund. B.M.S. is supported by a Department of Defense Breast Cancer Research Program predoctoral fellowship (W81XWH-10-1-0226). F.B.C is supported by the Molecular Toxicology training grant (T32 CA09582).

References

Ahmad A, Takami Y, Nakayama T. 1999. WD repeats of the p48 subunit of chicken chromatin assembly factor-1 required for in vitro interaction with chicken histone deacetylase-2. *J Biol Chem* **274:** 16646–16653.

Anantha RW, Vassin VM, Borowiec JA. 2007. Sequential and synergistic modification of human RPA stimulates chromosomal DNA repair. *J Biol Chem* **282:** 35910–35923.

Berkovich E, Monnat RJ Jr, Kastan MB. 2007. Roles of ATM and NBS1 in chromatin structure modulation and DNA double-strand break repair. *Nat Cell Biol* **9:** 683–690.

Berkovich E, Monnat RJ Jr, Kastan MB. 2008. Assessment of protein dynamics and DNA repair following generation of DNA double-strand breaks at defined genomic sites. *Nat Protoc* **3:** 915–922.

Bhaskara S, Knutson SK, Jiang G, Chandrasekharan MB, Wilson AJ, Zheng S, Yenamandra A, Locke K, Yuan JL, Bonine-Summers AR, et al. 2010. Hdac3 is essential for the maintenance of chromatin structure and genome stability. *Cancer Cell* **18:** 436–447.

Brown EJ, Baltimore D. 2003. Essential and dispensable roles of ATR in cell cycle arrest and genome maintenance. *Genes Dev* **17:** 615–628.

Cimprich KA, Cortez D. 2008. ATR: an essential regulator of genome integrity. *Nat Rev Mol Cell Biol* **9:** 616–627.

Dickey JS, Redon CE, Nakamura AJ, Baird BJ, Sedelnikova OA, Bonner WM. 2009. H2AX: functional roles and potential applications. *Chromosoma* **118:** 683–692.

Dupre A, Boyer-Chatenet L, Sattler RM, Modi AP, Lee JH, Nicolette ML, Kopelovich L, Jasin M, Baer R, Paull TT, et al. 2008. A forward chemical genetic screen reveals an inhibitor of the Mre11-Rad50-Nbs1 complex. *Nat Chem Biol* **4:** 119–125.

Errico A, Costanzo V. 2010. Differences in the DNA replication of unicellular eukaryotes and metazoans: known unknowns. *EMBO Rep* **11:** 270–278.

Furumai R, Matsuyama A, Kobashi N, Lee KH, Nishiyama M, Nakajima H, Tanaka A, Komatsu Y, Nishino N, Yoshida M, et al. 2002. FK228 (depsipeptide) as a natural prodrug that inhibits class I histone deacetylases. *Cancer Res* **62:** 4916–4921.

Gilad O, Nabet BY, Ragland RL, Schoppy DW, Smith KD, Durham AC, Brown EJ. 2010. Combining ATR suppression with oncogenic Ras synergistically increases genomic instability, causing synthetic lethality or tumorigenesis in a dosage-dependent manner. *Cancer Res* **70:** 9693–9702.

Harper JW, Elledge SJ. 2007. The DNA damage response: ten years after. *Mol Cell* **28:** 739–745.

Herrick J, Bensimon A. 2008. Global regulation of genome duplication in eukaryotes: an overview from the epifluorescence microscope. *Chromosoma* **117:** 243–260.

Hickson I, Zhao Y, Richardson CJ, Green SJ, Martin NM, Orr AI, Reaper PM, Jackson SP, Curtin NJ, Smith GC. 2004. Identification and characterization of a novel and specific inhibitor of the ataxia-telangiectasia mutated kinase ATM. *Cancer Res* **64:** 9152–9159.

Ichijima Y, Ichijima M, Lou Z, Nussenzweig A, Camerini-Otero RD, Chen J, Andreassen PR, Namekawa SH. 2011. MDC1 directs chromosome-wide silencing of the sex chromosomes in male germ cells. *Genes Dev* **25:** 959–971.

Kim HY, Tallman KA, Liebler DC, Porter NA. 2009. An azido-biotin reagent for use in the isolation of protein adducts of lipid-derived electrophiles by streptavidin catch and photorelease. *Mol Cell Proteomics* **8:** 2080–2089.

Leahy JJ, Golding BT, Griffin RJ, Hardcastle IR, Richardson C, Rigoreau L, Smith GC. 2004. Identification of a highly potent and selective DNA-dependent protein kinase (DNA-PK) inhibitor (NU7441) by screening of chromenone libraries. *Bioorg Med Chem Lett* **14:** 6083–6087.

Masumoto H, Hawke D, Kobayashi R, Verreault A. 2005. A role for cell-cycle-regulated histone H3 lysine 56 acetylation in the DNA damage response. *Nature* **436:** 294–298.

Mimitou EP, Symington LS. 2009. DNA end resection: many nucleases make light work. *DNA Repair (Amst)* **8:** 983–995.

Morrison AJ, Shen X. 2009. Chromatin remodelling beyond transcription: the INO80 and SWR1 complexes. *Nat Rev Mol Cell Biol* **10:** 373–384.

Moses JE, Moorhouse AD. 2007. The growing applications of click chemistry. *Chem Soc Rev* **36:** 1249–1262.

Petermann E, Helleday T. 2010. Pathways of mammalian replication fork restart. *Nat Rev Mol Cell Biol* **11:** 683–687.

Petermann E, Orta ML, Issaeva N, Schultz N, Helleday T. 2010. Hydroxyurea-stalled replication forks become progressively inactivated and require two different RAD51-mediated pathways for restart and repair. *Mol Cell* **37:** 492–502.

Probst AV, Dunleavy E, Almouzni G. 2009. Epigenetic inheritance during the cell cycle. *Nat Rev Mol Cell Biol* **10:** 192–206.

Rodrigue A, Lafrance M, Gauthier MC, McDonald D, Hendzel M, West SC, Jasin M, Masson JY. 2006. Interplay between human DNA repair proteins at a unique double-strand break in vivo. *EMBO J* **25:** 222–231.

Rossetto D, Truman AW, Kron SJ, Cote J. 2010. Epigenetic modifications in double-strand break DNA damage signaling and repair. *Clin Cancer Res* **16:** 4543–4552.

Rudin N, Haber JE. 1988. Efficient repair of HO-induced chromosomal breaks in *Saccharomyces cerevisiae* by recombination between flanking homologous sequences. *Mol Cell Biol* **8:** 3918–3928.

Salic A, Mitchison TJ. 2008. A chemical method for fast and sensitive detection of DNA synthesis in vivo. *Proc Natl Acad Sci* **105:** 2415–2420.

Sarkaria JN, Busby EC, Tibbetts RS, Roos P, Taya Y, Karnitz LM, Abraham RT. 1999. Inhibition of ATM and ATR kinase activities by the radiosensitizing agent, caffeine. *Cancer Res* **59:** 4375–4382.

Sartori AA, Lukas C, Coates J, Mistrik M, Fu S, Bartek J, Baer R, Lukas J, Jackson SP. 2007. Human CtIP promotes DNA end resection. *Nature* **450:** 509–514.

Savic V, Yin B, Maas NL, Bredemeyer AL, Carpenter AC, Helmink BA, Yang-Iott KS, Sleckman BP, Bassing CH. 2009. Formation of dynamic γ-H2AX domains along broken DNA strands is distinctly regulated by ATM and MDC1 and dependent upon H2AX densities in chromatin. *Mol Cell* **34:** 298–310.

Shibahara K, Stillman B. 1999. Replication-dependent marking of DNA by PCNA facilitates CAF-1-coupled inheritance of chromatin. *Cell* **96:** 575–585.

Sobel RE, Cook RG, Perry CA, Annunziato AT, Allis CD. 1995. Conservation of deposition-related acetylation sites in newly synthesized histones H3 and H4. *Proc Natl Acad Sci* **92:** 1237–1241.

Soutoglou E, Dorn JF, Sengupta K, Jasin M, Nussenzweig A, Ried T, Danuser G, Misteli T. 2007. Positional stability of single double-strand breaks in mammalian cells. *Nat Cell Biol* **9:** 675–682.

Taddei A, Roche D, Sibarita JB, Turner BM, Almouzni G. 1999. Duplication and maintenance of heterochromatin domains. *J Cell Biol* **147:** 1153–1166.

Tjeertes JV, Miller KM, Jackson SP. 2009. Screen for DNA-damage-responsive histone modifications identifies H3K9Ac and H3K56Ac in human cells. *EMBO J* **28:** 1878–1889.

van Attikum H, Gasser SM. 2009. Crosstalk between histone modifications during the DNA damage response. *Trends Cell Biol* **19:** 207–217.

Venkitaraman AR. 2010. Modifying chromatin architecture during the response to DNA breakage. *Crit Rev Biochem Mol Biol* **45:** 2–13.

Wang J, Gong Z, Chen J. 2011. MDC1 collaborates with TopBP1 in DNA replication checkpoint control. *J Cell Biol* **193:** 267–273.

Ward IM, Chen J. 2001. Histone H2AX is phosphorylated in an ATR-dependent manner in response to replicational stress. *J Biol Chem* **276:** 47759–47762.

Worcel A, Han S, Wong ML. 1978. Assembly of newly replicated chromatin. *Cell* **15:** 969–977.

You Z, Bailis JM, Johnson SA, Dilworth SM, Hunter T. 2007. Rapid activation of ATM on DNA flanking double-strand breaks. *Nat Cell Biol* **9:** 1311–1318.

Monitoring the spatiotemporal dynamics of proteins at replication forks and in assembled chromatin using isolation of proteins on nascent DNA

Bianca M Sirbu, Frank B Couch & David Cortez

Department of Biochemistry, Vanderbilt University School of Medicine, Nashville, Tennessee, USA. Correspondence should be addressed to D.C. (david.cortez@vanderbilt.edu).

Published online 1 March 2012; doi:10.1038/nprot.2012.010

Understanding the processes of DNA replication, chromatin assembly and maturation, and the replication stress response requires the ability to monitor protein dynamics at active and damaged replication forks. Detecting protein accumulation at replication forks or damaged sites has primarily relied on immunofluorescence imaging, which is limited in resolution and antibody sensitivity. Here we describe a procedure to isolate proteins on nascent DNA (iPOND) that permits a high-resolution spatiotemporal analysis of proteins at replication forks or on chromatin following DNA replication in cultured cells. iPOND relies on labeling of nascent DNA with the nucleoside analog 5-ethynyl-2′-deoxyuridine (EdU). Biotin conjugation to EdU-labeled DNA using click chemistry facilitates a single-step streptavidin purification of proteins bound to the nascent DNA. iPOND permits an interrogation of any cellular process linked to DNA synthesis using a 3- to 4-d protocol.

INTRODUCTION

During S-phase, DNA replication and chromatin assembly are coordinated at the replication fork to duplicate the genome and epigenome rapidly and accurately. DNA template damage and other forms of replication stress challenge genetic stability and activate a DNA damage response[1]. This signaling pathway protects and repairs damaged replication forks to promote successful completion of chromosome replication and prevent diseases such as cancer[2].

Immunofluorescence imaging is a useful method to detect proteins in active replisomes or proteins recruited to damaged forks. However, immunofluorescence imaging suffers from low resolution, poor sensitivity and a requirement for highly specific antibodies[3]. Other methods such as chromatin immunoprecipitation (ChIP) have limited applicability to mammalian cell replication because of difficulties in obtaining synchronous cultures and the lack of highly efficient, sequence-specified origins of replication[4]. Purification of replisome protein complexes through protein-protein interactions is useful to identify potential components, but it provides limited spatial information about protein localization.

To overcome these technical challenges, we developed iPOND[5]. In addition to its use for monitoring replisome dynamics, iPOND provides a method for examining protein recruitment and modification at damaged replication forks and for analyzing chromatin deposition and maturation.

Overview of iPOND

The iPOND methodology enables the purification of proteins bound directly or indirectly to the nascent DNA at replication forks. The method relies on labeling short fragments of nascent DNA with EdU, a nucleoside analog of thymidine[6]. EdU contains an alkyne functional group that permits copper-catalyzed cycloaddition (click chemistry)[7] to a biotin azide to yield a stable covalent linkage (**Fig. 1**). This facilitates a single-step purification of DNA-protein complexes based on the high-affinity biotin-streptavidin interaction.

The iPOND procedure (**Fig. 2**) begins by incubating cells with EdU for a short period of time (typically 2–15 min). The cells are then fixed with formaldehyde, which serves to both stop DNA replication and cross-link protein-DNA complexes. A click reaction in the presence of copper to conjugate biotin to EdU is completed in detergent-permeabilized cells. Some DNA fragmentation occurs during this step because of copper-catalyzed hydrolysis of the DNA. Cells are then lysed in denaturing conditions and sonication completes the DNA fragmentation producing solubilized DNA-protein complexes. Streptavidin-coated beads purify the nascent, EdU-labeled DNA-protein complexes. Finally, the proteins are eluted from the complexes. Standard immunoblotting or mass spectrometry (MS) methodologies can be used to detect the purified proteins and post-translational modifications.

The spatial and temporal resolution achieved with iPOND depends on EdU incubation time, the rate of DNA synthesis and chromatin fragment size. Experimentally, EdU incubation time and replication rate are the major determinants of iPOND resolution, as the protocol consistently yields chromatin fragments of 100–300 bp. The shortest EdU incubation time we have used to purify replisome components is 2.5 min (ref. 5). As forks move between 750 and 2,000 bp min^{-1} (ref. 8), as much as 5,000 bp could contain EdU during a 2.5-min incubation, yielding a resolution of 5 kb. This is likely to be a substantial underestimation of the resolution because EdU must enter the cell and be phosphorylated before incorporation. Our analysis indicates that a 2.5-min incubation with EdU is sufficient to capture replisome proteins and that longer incubations with EdU are required to isolate newly deposited chromatin[5].

Applications

Thus far, we have used iPOND in three major applications. First, iPOND is useful for identifying proteins associated with active replisomes. This application requires combining iPOND within a pulse-chase experimental framework (**Figs. 3** and **4**). Cells are labeled with EdU for a short time (the pulse), and then EdU is replaced with thymidine for increasing periods of time (the chase). Samples are collected at the end of the pulse and chase periods. A true replisome protein should be detected only in the pulse sample

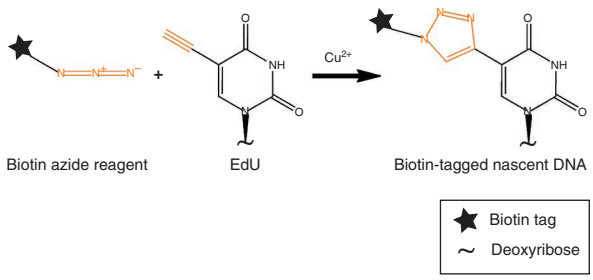

Figure 1 | Click chemistry addition of biotin tags to nascent DNA. EdU incorporated into nascent DNA is covalently tagged with biotin in the copper-catalyzed click reaction. Orange color represents the functional groups involved in the click chemistry reaction.

and not the chase sample. In contrast, other chromatin-bound proteins such as histones may be detected in both samples.

The pulse-chase experimental design is also the method of choice for the second major iPOND application—monitoring changes in chromatin located at various distances from the replication fork. Chromatin reassembly after passage of the replication fork occurs as a function of time and hence distance from the elongating fork[9]. The use of iPOND to purify histones on a segment of EdU-labeled DNA after various times of thymidine chase permits an analysis of how chromatin architecture is restored behind the elongating fork. For example, we used iPOND to document the timing of the deacetylation of newly synthesized histone H4 after deposition[5].

Finally, iPOND can be used to detect protein recruitment or post-translational modifications of proteins at damaged forks. The procedure in this case is to pulse for a short time with EdU, then to add a replication stress agent such as hydroxyurea (HU) or camptothecin (**Fig. 3b**). HU is particularly useful as high concentrations largely stop fork movement, facilitating an analysis of transiently or persistently stalled forks. Combining the DNA damaging protocol with the pulse-chase procedure also enables an examination of DNA damage–dependent events at different distances from the damaged fork. For example, we used this procedure to demonstrate spreading of H2AX phosphorylation from an HU-stalled fork[5]. Thus, the high spatial resolution of iPOND is derived from the capacity to measure the position of protein changes in relation to the replication fork. Theoretically, this system can also be used to monitor long-term changes in chromatin structure after DNA damage or replication stress by simply extending the time frame of the chase.

These three major applications are quite powerful, especially when combined with genetic or small molecule–mediated inactivation of specific pathways that regulate DNA replication, chromatin deposition and maturation, and DNA repair. iPOND is compatible with all proliferating cell types. We have used it successfully in HEK293T, HCT116, NIH3T3 and mouse embryonic fibroblasts (B.M.S. and D.C., unpublished observations). Thus, cell lines engineered to have mutations in specific pathways can be used directly with iPOND without any major modifications to the protocol. iPOND can also be extended for use beyond mammalian cell culture. Any cell type that can incorporate EdU during DNA synthesis (or be engineered to use EdU) can be used. In fact, we have used iPOND to purify DNA-protein complexes from the yeast *Saccharomyces cerevisiae*, although substantial optimization will be required to improve purification efficiency (F.B.C. and D.C., unpublished observations).

In addition to these three documented applications, iPOND can be used to study other processes that involve DNA or even RNA synthesis. An example would be DNA repair synthesis outside of S-phase. Synchronized or terminally differentiated cell cultures could be exposed to DNA damaging agents in the presence of EdU. The late steps in repair of that damage or the re-establishment of chromatin following repair synthesis can be monitored with iPOND. Synchronized cell cultures could also be used to examine the differences in DNA replication, chromatin deposition or DNA repair that occur in early versus late S-phase cells. This approach was recently used by Kliszczak *et al.*[10] to describe a methodology similar to iPOND. Another application could be to monitor DNA synthesis outside of the nucleus such as in mitochondrial DNA if iPOND is combined with a purification step that isolates this organelle. iPOND could theoretically be adapted to analyze even proteins on nascent RNA, as click chemistry has been used to label newly synthesized RNA with the uridine analog 5-ethynyluridine[11].

Finally, combining iPOND with quantitative MS should be a powerful methodology for identifying new replisome and DNA damage response proteins, as well as for monitoring the substantial numbers of post-translational modifications at damaged forks.

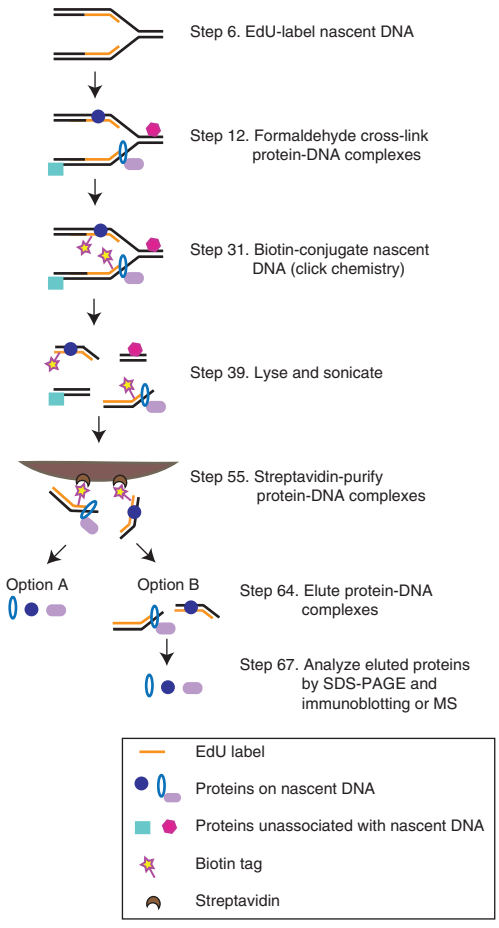

Figure 2 | Schematic overview of the iPOND procedure. The iPOND procedure consists of pulsing cells with EdU to label nascent DNA *in vivo*, formaldehyde cross-linking protein-DNA complexes, covalently tagging EdU-labeled DNA with biotin by using click chemistry, lysing and sonicating cells, purifying the solubilized protein-DNA complexes and eluting bound proteins for analysis by SDS-PAGE, and immunoblotting or MS.

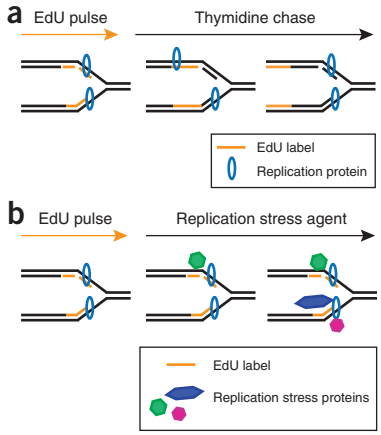

Figure 3 | Schematic of the experimental procedures used to identify replisome or DNA damage proteins and modifications at the replication fork. (**a**) To identify replisome proteins, a pulse-chase variation of the iPOND protocol uses a thymidine chase to move the nascent, EdU-labeled DNA segment away from the replication fork. The chase sample provides a control to distinguish replisome components from general chromatin-binding factors. (**b**) To study proteins and modifications associated with damaged replication forks, an agent that stalls replication forks, such as HU, is added after the EdU-labeling period.

Comparison with other methods

Compared with conventional indirect immunofluorescence, iPOND has an improved sensitivity of detection because even low-abundance replisome proteins such as polymerases are isolated[5]. It also provides improved spatial and temporal resolution. An improved imaging technique permits single-molecule detection of replisome proteins in bacteria[12]; however, unlike imaging, iPOND is compatible with unbiased approaches for protein identification such as MS.

ChIP is a powerful substitute for several iPOND capabilities in organisms such as *S. cerevisiae* that have highly efficient, sequence-defined origins of replication and cell cycle synchronization is easily achieved. ChIP has the advantage of being more sensitive than iPOND as it detects DNA sequences after PCR amplification. However, ChIP requires highly specific, often unavailable antibodies and is not compatible with unbiased approaches such as MS. Moreover, although ChIP has been used in mammalian systems to examine protein recruitment to origins of replication[13], it is generally not useful for studying the dynamic processes associated with fork elongation and chromatin maturation. Finally, adapting ChIP to studying damaged replication forks in mammalian cell culture awaits the development of ways to engineer site-specific DNA lesions that stall forks with high efficiency as has been done using *Xenopus* egg extracts to study interstrand cross-link repair[14,15].

The most comparable technology to iPOND is the immunoprecipitation of nascent DNA-protein complexes with antibodies to halogenated nucleoside analogs, which was used to examine the recruitment of the homologous recombination factor RAD51 to sites of replication fork stalling[16]. However, the relatively low affinity of this antibody-epitope interaction and the requirement for DNA denaturation for antibody access necessitated a very long chlorodeoxyuridine (CldU)-labeling period (40 min), providing little advantage over biochemical fractionation of chromatin. In principle, biotin-dUTP could be used directly to label the nascent DNA, thus avoiding the need to perform the click chemistry reaction. However, biotin-dUTP is not cell permeable, thus necessitating some cellular manipulation to introduce it into cells, and the large biotin tag may interfere with DNA structure and protein associations with DNA.

Experimental design

Several parameters can be varied within the iPOND protocol depending on the specific experimental purpose. As outlined above, the EdU pulse and chase combinations yield different types of information. In addition, it may be useful to omit the formaldehyde cross-linking step. In particular, formaldehyde cross-linking may complicate analysis of proteins by MS if the cross-links are not fully reversed. Chromatin can be captured with iPOND without cross-linking, provided that Igepal or another nondenaturing detergent is used in the lysis step and that the salt concentration in the wash step is reduced (**Box 1**).

A second experimental design option is to change the elution methodology. For most applications we found that boiling in SDS sample buffer is sufficient to reverse cross-links and solubilize proteins after purification (**Fig. 2**, elution option A). However, this method also releases any proteins that bind to the bead matrix nonspecifically and does not release the DNA from the beads. The use of a cleavable biotin azide in the click reaction facilitates elution in milder conditions to improve specificity and recovery of the DNA (**Fig. 2**, elution option B). Several cleavable biotin azides have been described[17]. We successfully use a UV-photocleavable biotin-azide synthesized by Ned Porter's group at Vanderbilt[18]. This elution option may also be useful in experimental systems where biotinylation of endogenous proteins is a concern.

Controls

Control samples are essential for interpreting the results. Most importantly, a control for the specificity of the purification is needed. This control is analogous to the preimmune control for coimmunoprecipitation experiments. We typically use a sample that omits the biotin azide during the click reaction (Steps 29 and 30). Alternatively, a sample in which the cells were not incubated with EdU can be used as the control. No DNA-protein complexes should be purified in this control sample. If any protein is detected, it is likely to come from nonspecific interactions with the streptavidin matrix or precipitation of protein during the manipulations.

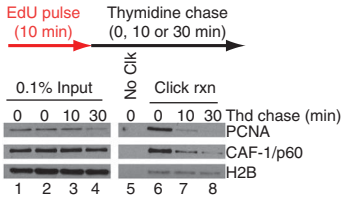

Figure 4 | Example of results obtainable with iPOND. Cells were pulsed with EdU for 10 min and then incubated with thymidine (Thd) for 0, 10 or 30 min as indicated. iPOND was performed as described in the protocol. Eluted proteins were analyzed by SDS-PAGE followed by immunoblotting for the replication proteins PCNA, chromatin assembly factor 1 (CAF-1/p60) and histone H2B. As expected, proteins are detectable in every sample of the input (lanes 1–4). In the absence of click chemistry (No Clk, lane 5, negative control), no proteins are isolated from nascent DNA. PCNA and CAF-1 are enriched specifically at the replication fork (Click rxn, lane 6), but not on nascent DNA that is thymidine chased away from the replication fork (Click rxn, lanes 7 and 8). In contrast, a chromatin-bound protein such as H2B is detectable both at the replication fork (Click rxn, lane 6) and in thymidine-chased samples (Click rxn, lanes 7 and 8).

Box 1 | Native iPOND

iPOND performed without formaldehyde cross-linking (native iPOND) may simplify mass spectrometry analyses of purified histones.

1. Culture 5 × 10^7 cells in one 150-mm dish per sample.
2. Label the samples with 10 µM EdU for 60 min.
3. Collect the cells by scraping on ice.
4. Collect the pellets by centrifuging at 100*g* for 5 min at 4 °C.
5. Discard the supernatant and wash the cells with 5 ml of ice-cold PBS. Collect the cells by centrifuging at 100*g* for 5 min at 4 °C.
6. Discard the supernatant and lyse the cells by resuspension in ice-cold cell lysis buffer with Igepal CA-630 at 1 × 10^7 cells per ml.
7. Vortex five times for 5 s with 5 s between pulses.
8. Collect nuclei by centrifugation at 100*g* for 5 min at 4 °C.
9. Discard the supernatant and wash twice in 5 ml cell lysis buffer without Igepal CA-630.
10. Collect nuclei by centrifugation at 100*g* for 5 min at 4 °C.
11. Discard the supernatant and resuspend the cells in ice-cold nuclei buffer at 2.5 × 10^7 cells per ml.
12. Set up click reactions using the formula in **Table 1**.
13. Incubate for 1 h on a shaker at 4 °C and protect from light.
14. Collect the nuclei by centrifugation at 100*g* for 5 min at 4 °C.
15. Discard the supernatant and resuspend in ice-cold nuclei buffer at 2 × 10^7 cells per ml.
16. Add EDTA to a final concentration of 1 mM and $CaCl_2$ to 2 mM.
17. Warm to 37 °C in a water bath and add micrococcal nuclease to 20 Kurntz units per 1 × 10^7 cells.
18. Incubate the cells at 37 °C for 3.5 min.
19. Add EDTA to a final concentration of 2 mM to quench the reactions. Collect nuclei by centrifugation at 100*g* for 5 min at 4 °C.
20. Extract chromatin by discarding the supernatant and resuspending the nuclei in ice-cold extraction buffer at 5 × 10^7 cells per 3 ml. Rotate for 2 h to overnight at 4 °C, protected from light.
21. Centrifuge at 16,100*g* for 5 min at 4 °C to remove all insoluble material. Transfer the supernatant to a fresh tube and discard the pellet.
22. Remove 0.5% of the total volume and save it as the 'input' sample. To the remaining lysate, add 20 µl of streptavidin-agarose beads per 1 × 10^7 cells. Rotate for 1.5 h to overnight at 4 °C, protected from light.
23. Collect the beads by centrifugation at 1,800*g* for 1 min. Let the beads stand for another minute to settle completely. Aspirate and discard the supernatant.
24. Transfer the beads to a 1.5-ml centrifuge tube.
25. Wash the beads twice with 1 ml of extraction buffer for 5 min at 4 °C.
26. Add an equal volume of 2× SB and heat to 95 °C for 10 min.
27. Separate the recovered proteins with SDS-PAGE and analyze them by immunoblotting or mass spectrometry.

A second control is needed to ensure that a purified protein is actually enriched at replication forks, as opposed to simply being an abundant chromatin-associated protein. This control is a sample in which the EdU is removed and cells are incubated with thymidine for several minutes before collecting (a chase sample). Proteins that travel with the replication fork will only be detected before this thymidine chase. If a protein is detected in the chase sample, this indicates that it is a chromatin-bound protein but not specifically part of the replisome.

Finally, control immunoblots to examine known replisome components, such as proliferating cell nuclear antigen (PCNA), should be performed within each experiment to ensure that the procedure worked as expected.

iPOND limitations and other considerations

Currently, the major limitation of iPOND is the large amount of starting material needed. Each sample requires approximately 1 × 10^8 cells for efficient iPOND capture of replisome proteins with a 10-min EdU incubation. The large number of cells needed for the procedure is dictated by the sensitivity of the immunoblotting and MS detection methods. This cell number is based on unsynchronized cultures of 293T cells in which about 50% of the cells are in S-phase at the time of the experiment. Synchronizing cells such that 100% are in S-phase would reduce the cells needed, whereas the use of cell types with fewer replicating cells would increase it. Although these cell numbers are large, they are obtainable by using standard cell culture methods.

iPOND is an ensemble methodology, meaning that the data comes from hundreds of replication forks in millions of cells. It provides a picture of an average replication fork and cannot distinguish the significant heterogeneity between cells in the population or between forks within different genomic regions. Thus, identification of two proteins by iPOND does not mean that those two proteins are necessarily recruited to the same nascent DNA segment. Furthermore, distinguishing the relative distribution of proteins within the chromosomal space at the replication fork is currently not possible with iPOND. Such high-resolution mapping has been achieved with *in vitro* replication systems by using T4 DNA polymerase and primer template DNA that contains a position-specific cross-linkable aryl azide[19]. This elegant study provided topographical information about the location of binding of accessory proteins respective to polymerase interaction with and movement along the DNA template. Finally, iPOND resolution may be improved in a system in which EdU exists as the sole nucleoside to pair with adenosine. This could be achieved in a cellular system such as *Xenopus*, in which dNTPs are added in a controlled manner for incorporation into nascent DNA.

MATERIALS

REAGENTS

- EdU (Invitrogen, cat. no. E10187)
- Thymidine (Sigma, cat. no. T1895)
- Formaldehyde solution (37% (wt/vol); Sigma, cat. no. F1635) ! CAUTION Formaldehyde is very toxic if inhaled, ingested or absorbed through skin.
- PBS, pH 7.2 (10×; Gibco, cat. no. 70013)
- Glycine (Fisher, cat. no. BP 381)
- Cell lifter (Corning, cat. no. 3008)
- Triton X-100 (Sigma, cat. no. T8787) ! CAUTION Hazardous in case of eye contact, ingestion or inhalation.
- BSA (Sigma, cat. no. A7030)
- Dimethyl sulfoxide (DMSO; Fisher, cat. no. A4034) ! CAUTION It readily permeates skin, is a combustible liquid and vapor, and is hygroscopic.
- Copper (II) sulfate pentahydrate ($CuSO_4 \cdot 5H_2O$; Fisher, cat. no. C489) ! CAUTION It is toxic if swallowed and causes skin and eye irritation.
- (+) Sodium L-ascorbate (Sigma, cat. no. A4034)
- Biotin azide (Invitrogen, cat. no. B10184)
- SDS (Sigma, cat. no. L4390) ! CAUTION SDS is toxic on contact with skin, harmful if swallowed, and causes skin, eye and respiratory irritation.
- Tris, pH 8.0 and 6.7
- Sodium chloride (NaCl)
- RNase A solution (Sigma, cat. no. R6148)
- Proteinase K (Sigma, cat. no. P5568)
- Glycerol
- Bromophenol blue
- EDTA
- Agarose (Bio-Rad Laboratories, cat. no. 161-3101)
- Dithioerythritol (DTT; Sigma, cat. no. D-8255)
- Aprotinin (Sigma, cat. no. A6279)
- Leupeptin (Sigma, cat. no. L2884)
- Streptavidin agarose (Novagen, cat. no. 69203-3) ▲ CRITICAL Different bead surfaces and binding capacities will alter iPOND efficiency.
- Trichloroacetic acid (TCA) ! CAUTION TCA is corrosive.
- Acetone ! CAUTION It is highly flammable.
- Western Lightning Plus enhanced chemilluminescence substrate (PerkinElmer, cat. no. NEL103001EA)
- Igepal CA-630
- Odyssey infrared imaging system (Li-Cor Biosciences)
- Click reaction stock solutions (biotin azide, $CuSO_4$ and sodium L-ascorbate; see REAGENT SETUP)

EQUIPMENT

- Nylon mesh (90 µm; Small Parts, cat. no. B000FN0PGQ)
- Glass vial screw thread with cap attached for UV photocleavage (Fisher, cat. no. 03-338AA) ▲ CRITICAL Other vial surfaces may perturb penetration of UV light, necessitating different elution times or conditions.
- Magnetic micro-stirring bar (2 mm diameter × 7 mm length; Fisher, cat. no. 1451363)
- Microtip sonicator for cell lysis and chromatin fragmentation (Misonix 4000 or Fisher Scientific Sonic Dismembrator, model 500)
- Rotating platform for biotin captures
- UV lamp (UVP, cat. no. UVLMS-38 EL Series 3UV lamp, 365/302/254 nm UV 8 Watt)
- Magnetic stir plate
- Microcentrifuge for 1.5-ml microcentrifuge tubes
- Tabletop centrifuge for 15-ml and 50-ml conical tubes
- Cell culture incubator
- Biological safety cabinet

REAGENT SETUP

EdU Dissolve EdU in DMSO to obtain a final concentration of 10 mM. Protect from light. Store in aliquots at −20 °C for up to 1 year. Before use, thaw at 37 °C. To EdU-label cells, pipette 1:1,000 of EdU directly into medium for a final concentration of 10 µM.

Thymidine Dissolve in water to a final concentration of 10 mM. Store in aliquots at –20 °C for up to 1 year. Thaw the solution before use. Use at a final concentration of 10 µM.

PBS, 1× Prepare 1× PBS from 10× PBS stock by diluting 1:10 with water; store at room temperature (RT, 25 °C) for up to 1 year.

Formaldehyde/PBS, 1% (wt/vol) Dilute 37% (wt/vol) formaldehyde 1:37 with PBS. Freshly prepare this reagent and keep it at RT until cell fixation (PROCEDURE, Step 12).

Glycine, 1.25 M Prepare 1.25 M glycine stock in water and store at RT for up to 1 year. Use at 1:10 dilution for a final concentration of 0.125 M glycine.

Permeabilization buffer Prepare a 20% (vol/vol) stock of Triton X-100 in water and keep it at RT. Dilute to 0.25% (vol/vol) Triton X-100 in PBS. Store at 4 °C for several months.

BSA in PBS wash buffer, 0.5% (wt/vol) Prepare 0.5% (wt/vol) BSA in PBS. Filter-sterilize the solution and store it at 4 °C for a couple of weeks.

Biotin azide (1 mM) Dissolve biotin azide in DMSO to a final concentration of 1 mM. Aliquot and store at −20 °C for up to 1 year.

$CuSO_4$ (100 mM) Prepare a stock of 100 mM $CuSO_4$ in H_2O; store at RT for several months.

Sodium L-ascorbate Freshly prepare 20 mg ml^{-1} of (+) sodium L-ascorbate (reducing agent) in H_2O; limit exposure to air and store on ice until needed.

Click reaction mixes To prepare click reaction cocktails, please see **Table 1** for details. Cocktails are freshly prepared for each experiment before the click reaction (PROCEDURE, Step 28).

Lysis buffer Prepare 1% (wt/vol) SDS in 50 mM Tris (pH 8.0). Store at RT for several months. Before use, add protease inhibitors aprotinin and leupeptin to a final concentration of 1 µg ml^{-1}.

Salt wash Prepare 5 M NaCl in water. Dilute to 1 M NaCl with water before use. Store at RT for 1 year.

SDS Laemmli sample buffer (2× SB) Mix 0.4 g of SDS, 2 ml of 100% glycerol, 1.25 ml of 1 M Tris (pH 6.8), and 0.01 g of bromophenol blue in 8 ml of H_2O. Store at −20 °C for up to 1 year. Before use, add 1 M DTT to a final concentration of 0.2 M.

Cross-link reversal solution Mix 2 µl of 0.5 M EDTA, 4 µl of 1 M Tris (pH 6.7) and 1 µl of Proteinase K. Freshly prepare this solution.

TABLE 1 | Click reaction cocktails for a sample with 1 × 10^8 cells.

Reagent	Stock	Final	Control reaction volume (ml)	Experimental reaction volume (ml)
PBS, 1×			4.35	4.35
DMSO			0.05	
Biotin azide	1 mM	10 µM		0.05
Sodium ascorbate	100 mM	10 mM	0.5	0.5
$CuSO_4$	100 mM	2 mM	0.1	0.1
Total volume			5.0	5.0

Adjust volumes proportionally for actual cell numbers.

Box 2 | Cross-link reversal and DNA analysis

To examine DNA fragmentation size, cross-links are reversed from lysates collected before and after DNA sonication, bound proteins are digested, DNA fragments are separated on an agarose gel and analyzed under UV light.

1. Before sonication (PROCEDURE, Step 39), remove 5 µl of lysate and place it on ice. This is the presonication sample.
2. After sonication and sample filtration (Step 44), remove 5 µl of lysate and place it on ice. This represents the postsonication sample.
3. To all samples, add 90 µl of H_2O and 4 µl of 5 M NaCl.
4. Incubate the samples at 65 °C for 4–16 h.
5. Add 1 µl of RNase A (20 mg ml^{-1}) to each sample.
6. Incubate the samples in a 37 °C water bath for 30 min.
7. Prepare the cross-link reversal solution (see REAGENT SETUP).
8. Add 7 µl of cross-link reversal solution to each sample.
9. Incubate the samples at 45 °C for 1–2 h.
10. During the incubation time, pour a 1.5% (wt/vol) agarose/TAE gel without ethidium bromide.
11. Add DNA loading dye to 20 µl of sample and load it on a 1.5% (wt/vol) agarose gel.
12. Perform electrophoresis at 75 V for 3 h in 1× TAE buffer to resolve DNA fragments.
13. Stain the gel with ethidium bromide.
14. Visualize DNA fragments under UV light.

Prepare sufficient cross-link reversal solution mix to add 7 µl to each sample in step 8 of **Box 2**.

Cell lysis buffer Mix 10 mM Tris (pH 8.0), 2 mM $MgCl_2$ and 1% (vol/vol) Igepal CA-630. Before use, add protease inhibitors aprotinin and leupeptin to a final concentration of 1 µg ml^{-1}. Freshly prepare this buffer.

Nuclei buffer Mix 15 mM Tris (pH 8.0), 0.125 M sucrose, 15 mM NaCl, 40 mM KCl, 0.5 mM spermidine and 0.15 M spermine. Freshly prepare this buffer.

Extraction buffer Mix 1× PBS with 350 mM NaCl, 2 mM EDTA and 0.1% (vol/vol) Triton X-100. Freshly prepare this buffer.

PROCEDURE

Cell culture preparation ● TIMING 1–7 d

1| Calculate the number of dishes of cells needed for the experiment. Each sample requires at least 1.0 × 10^8 cells at the time of the EdU pulse. We typically use three 150 mm dishes of HEK293T cells per sample. The number of cells may need to be increased depending on the application and cell type.

2| Expand cell cultures 1 d before EdU incubation (Step 3) to ensure that the cells are growing optimally. Include one extra dish of cells for counting the cell number in Step 3.

▲ **CRITICAL STEP** For HEK293T cells, the experiment works best when cell confluence is between 4 and 6 × 10^7 cells per dish on the day of the EdU pulse. Cells must be in log phase of growth and should not be overgrown. Monitor proper incubator temperature and CO_2 content. EdU incorporation is not maximal unless these crucial parameters are met. If you are performing chases, equilibrate the medium to 37 °C and the proper CO_2 content overnight.

EdU labeling of nascent DNA ● TIMING 10 min–8 h

3| Determine the cell number in the extra dish of cells from Step 2. This cell number will be used to calculate the amount of the reagents used for each sample in Step 29.

4| Plan out times to pulse, chase, fix, quench, collect and wash the samples.

▲ **CRITICAL STEP** Stagger the samples to ensure that each is treated equally throughout the processing steps.

5| To pulse cells with EdU, remove the dishes from the incubator and place them in a biological safety cabinet.

6| Add 23 µl of the 10 mM EdU stock into 23 ml of cell culture medium in each dish to achieve a final EdU concentration of 10 µM. Return the dishes to the incubator for the desired pulse time (e.g., 10 min).

7| If thymidine chases or drug treatments are not being performed, skip to Step 11.

8| To perform thymidine chase or addition of drug, remove the dishes from the incubator and decant the medium.

9| Carefully wash the cells with 5 ml of chase medium and decant. The chase medium should have been pre-equilibrated to 37 °C and the proper CO_2 content.

10| Add 20 ml of chase medium containing 10 μM thymidine or the desired concentration of DNA damaging drug. Return the dishes to the incubator for the desired length of time.
▲ **CRITICAL STEP** It is important to perform Steps 5–10 as quickly as possible to prevent pH and temperature changes in the medium, which can affect replication rates.

Formaldehyde cross-linking and collection of cells ● TIMING 1 h
11| After EdU pulse and/or chase, decant the medium.

12| Immediately fix the cells on a dish by adding 10 ml of 1% (wt/vol) formaldehyde in PBS and incubating for 20 min at RT.

13| Quench cross-linking by adding 1 ml of 1.25 M glycine.

14| Collect the sample by scraping with a cell lifter and transfer it to a 50-ml conical tube. Note the volume. This is the same volume that should be used for PBS washes in Step 17.

15| Centrifuge for 5 min at 900*g*, 4 °C.

16| Decant the supernatant.

17| Wash pellets three times with 1× PBS and centrifuge for 5 min at 900*g*, 4 °C. PBS wash volume is same as fixation volume noted in Step 14. Vortex to resuspend pellets in PBS.

18| After the last wash, decant PBS.
■ **PAUSE POINT** The samples can be flash-frozen and stored at −80 °C for several weeks.

Cell permeabilization ● TIMING 1 h
19| Resuspend the cells in permeabilization buffer at a concentration of 1×10^7 cells per ml.

20| Incubate the cells at RT for 30 min. During incubation, thaw and prepare the reagents necessary for the click reaction cocktail (see Steps 28 and 29).

21| Spin down for 5 min at 900*g*, 4 °C.

22| Carefully decant the supernatant.

23| Wash the cells once with cold 0.5% (wt/vol) BSA in PBS, using the same volume as used for permeabilization in Step 19.
▲ **CRITICAL STEP** BSA prevents the cell pellet from detaching from the wall of a 50-ml conical flask. A loose pellet will lead to the loss of cells in this step.

24| Centrifuge the cells for 5 min at 900*g*, 4 °C, and then decant the supernatant.
? TROUBLESHOOTING

25| Wash the cells once with PBS using the same volume as used for permeabilization in Step 19.

26| Spin down for 5 min at 900*g*, 4 °C.

27| Decant the supernatant and place the pellets on ice while completing the preparation for the click reaction cocktail.

Click reaction ● TIMING 2 h
28| Thaw an aliquot of stock biotin azide by placing it on a 37 °C heat block.
▲ **CRITICAL STEP** If you are using photocleavable biotin azide, keep the reagent protected from light and prepare the click reaction cocktail in the dark.

29| To calculate click reaction cocktail volumes, **Table 1** lists the amounts of each reagent needed per reaction with an example sample size of 1×10^8 cells. The actual volumes should be adjusted on the basis of the cell number measured per sample (Step 3). Note that two click reaction cocktails need to be prepared: one for the control, which contains DMSO, and one for the experimental samples, which contains the biotin azide.

30| Combine the click reaction cocktail reagents on ice in the order listed in **Table 1**.

31| Resuspend the cell pellets from Step 27 in the click reaction cocktail from Step 30 by vortexing.

32| Rotate the reactions at RT for 1–2 h.

33| Centrifuge the samples for 5 min at 900*g*, 4 °C, and decant the supernatants.

34| Wash the cells once with cold 0.5% (wt/vol) BSA in PBS, using the same volume as used in click reaction for one sample.

35| Centrifuge for 5 min at 900*g*, 4 °C and decant supernatant.

36| Wash the cells once with PBS, using the same volume as used in click reaction for one sample.

37| Decant the PBS and invert the tubes on a paper towel to remove all PBS.
■ **PAUSE POINT** The samples can be flash-frozen and stored at −80 °C for a few days.

Cell lysis and sonication ● TIMING 1 h

38| Prepare the lysis buffer by adding aprotinin and leupeptin before use (see REAGENT SETUP) and place on ice.

39| Resuspend the samples from Step 37 at a concentration of 1.5×10^7 cells per 100 µl of lysis buffer and transfer them to 1.5-ml centrifuge tubes on ice. To examine DNA fragment size at this step, see **Box 2**.

40| Sonicate the cells by using a microtip sonicator and the following settings: pulse: 20 s constant pulse, 40 s pause; power: 13–16 Watts; repeat pulse 1× for every 200 µl of cell lysate; total pulse time: 4–5 min per sample.
▲ **CRITICAL STEP** Lysates should appear translucent after sonication and not cloudy. Cloudiness is an indicator of an improper ratio of SDS to protein in the lysate or of insufficient sonication. Keep the samples on an ice slurry during sonication to prevent overheating.
? TROUBLESHOOTING

41| Centrifuge the samples for 10 min at 16,100*g*, RT in a tabletop centrifuge.
▲ **CRITICAL STEP** Lysate should appear clear after centrifugation. The presence of a white precipitate or a white film on top of the lysate is indicative of insufficient clearing of the lysate.

42| Filter the supernatant through a 90-µm nylon mesh into a new tube. Place the tube on ice.

43| Note the lysate volume.

44| To examine DNA fragment size at this step, see **Box 2** for cross-link reversal and DNA analysis.

45| Dilute the lysate 1:1 (vol/vol) with cold PBS containing 1 µg ml^{-1} of aprotinin and leupeptin.
▲ **CRITICAL STEP** Samples have been diluted to contain 0.5% (wt/vol) SDS and 25 mM Tris because less efficient biotin capture is observed in lysates containing 1% (wt/vol) SDS.

46| Note the final capture volume.

47| Remove 15 µl of the lysate to save as the input sample for use in Step 64 and place it on ice. Immediately add 15 µl of 2× SB to this input sample and store at −80 °C. The remaining lysate is used for the streptavidin capture, which is described below.

Streptavidin capture of biotin-tagged nascent DNA and associated proteins ● TIMING 16–20 h

48| To capture biotin-tagged nascent DNA, each sample from Step 47 is incubated with streptavidin-agarose beads at a concentration of 100 µl of bead slurry (50 µl packed volume) per 1 × 10^8 cells. First, wash sufficient beads for all samples together by centrifuging the bead slurry at 1,800*g* for 1 min at RT.

49| Slowly and carefully aspirate the storage buffer from the beads.

50| Wash the beads twice with 1:1 (vol/vol) lysis buffer containing aprotinin and leupeptin.

51| Carefully and slowly aspirate the supernatant after each wash in Step 50.

52| Wash the beads once with 1:1 (vol/vol) PBS containing aprotinin and leupeptin; carefully aspirate the supernatant.

53| Resuspend the beads in 1:1 (vol/vol) PBS containing protease inhibitors.

54| Add an equal volume of beads to each sample from Step 47 with a pipette tip that is cut at the end.

55| Rotate the biotin captures in a cold room for 16–20 h (in the dark if photocleavable biotin azide is used).

56| Centrifuge the streptavidin-agarose beads with the captured DNA and associated proteins for 3 min at 1,800*g*, RT.

57| Very slowly and carefully aspirate most of the supernatant.
▲ **CRITICAL STEP** The supernatant should be light blue/clear with no precipitate.
? TROUBLESHOOTING

58| Add 1 ml of cold lysis buffer (no additives needed) to wash the beads.

59| Rotate at RT for 5 min.

60| Centrifuge for 1 min at 1,800*g* at RT and carefully aspirate and discard the supernatant.

61| Wash the beads once with 1 ml of 1 M NaCl.

62| Rotate and pellet the beads by repeating Steps 59 and 60.

63| Repeat the lysis buffer washes (Steps 58–60) two more times.

Elution of proteins bound to nascent DNA ● TIMING 1–4 h

64| Protein elution can be performed using option A (boiling in 2× SB) or option B (UV photocleavage), depending on the amount of background observed in the negative control. Option B is best suited for proteins that show substantial background and require larger amounts of starting material for detection.

(A) Boiling in 2× SB

(i) After the last wash in Step 63, aspirate all of the supernatant. Protein-DNA complexes isolated on the beads are called the capture sample.

(ii) To elute proteins bound to nascent DNA, add 2× SB to packed beads from Step 64A(i) (1:1, vol/vol of packed beads; e.g., 100 µl 2× SB/100 µl packed beads).

(iii) Incubate the capture sample from Step 64A(ii) and the input sample from Step 47 for 25 min at 95 °C to reverse cross-links.
▲ **CRITICAL STEP** Typically, both the input and iPOND-purified capture samples should be examined concurrently.

(iv) Centrifuge the boiled samples for 1 min at 1,800*g*, RT. The supernatant is the '2× eluted capture' sample and is ready to use in standard SDS-PAGE and immunoblotting procedures (see Step 65).

(B) UV photocleavage, TCA concentration and boiling in 2× SB

(i) After the last wash in Step 63, wash one additional time with 1× PBS containing leupeptin and aprotinin as in Steps 59 and 60.

(ii) Centrifuge for 1 min at 1,800*g*, RT, and carefully aspirate the supernatant.
(iii) Add 1:1 (vol/vol) of 1× PBS containing protease inhibitors to the packed beads and resuspend by pipetting.
(iv) Transfer the resuspended beads into a glass vial with a mini magnetic stir bar.
(v) Place the glass vial containing the sample on a magnetic stir plate and adjust to stir on the lowest possible speed.
(vi) Position a UV lamp as close to the glass vial as possible. UV-photoelute at 365 nm for 1–2 h at RT.
(vii) Transfer the bead slurry from the glass vial into a 1.5-ml centrifuge tube.
(viii) Centrifuge the tube for 1 min at 1,800*g*, RT to pellet the beads.
(ix) Carefully remove the supernatant into a fresh tube. This is the 'UV-photoeluted capture' sample in PBS.
(x) Optionally, to concentrate the sample using TCA precipitation, proceed to the next step. Otherwise, add 1:1 (vol/vol) of 2× SB to the UV-photoeluted capture sample, boil at 95 °C for 25 min to reverse cross-links, and then proceed to analysis of proteins (Step 65).
(xi) Add ice-cold 100% TCA to the UV photoeluted capture sample from Step 64B(ix) to achieve a final concentration of 15% (vol/vol) TCA.
(xii) Incubate the sample on ice for 30 min.
(xiii) Centrifuge at 16,100*g* for 30 min in a cold room.
(xiv) Carefully remove the supernatant and save it for troubleshooting.
(xv) Wash the pellet with 1 ml of ice-cold acetone.
(xvi) Centrifuge for 10 min at 16,100*g* in cold room.
(xvii) Carefully remove the supernatant and save it for troubleshooting.
(xviii) Air-dry the pellet for 2–3 min until the smell of acetone is undetectable.
▲ **CRITICAL STEP** If the pellet is not visible at this step, spin down the supernatant saved from Step 64B(xiv), and then repeat Step 64B(xv–xviii). If no pellet is observed, spin down the supernatant previously saved from Step 64B(xvii) and repeat Step 64B(xviii).
? TROUBLESHOOTING
(xix) Add 30 µl of 2× SB to the protein pellet to resuspend the sample.
(xx) Incubate the capture sample (from Step 64B(x) if it is not TCA precipitated or from Step 64B(xix) if it is TCA precipitated) and the input sample (from Step 47) for 25 min at 95 °C. The samples are ready for use in standard SDS-PAGE and immunoblotting procedures.

Analysis of eluted proteins using western blotting ● TIMING 2–3 d

65| Prepare a standard SDS-PAGE gel[20]. To examine purification of positive controls concurrently (a replication protein and a histone, e.g., PCNA and H3, respectively), it is useful to prepare a 15% (wt/vol) gel.

66| To detect purified proteins from input and capture samples (from Step 64A(iv) or Step 64B(xx)), load the equivalent of 3 to 6 × 10^7 cells per well from the total protein capture (e.g., 3 to 6 × 10^7 of 1 × 10^8). This means that each sample of 1 × 10^8 cells yields sufficient sample for analysis of 2–3 immunoblots. For input samples, load the equivalent of 0.1% (vol/vol) input per well.
▲ **CRITICAL STEP** Depending on antibody quality, different proteins may require more cells for detection than others. This will require empirical determination.

67| Perform electrophoresis to resolve proteins on the basis of molecular weight, and then proceed with standard immunoblotting with desired antibodies according to supplier instructions or with MS analysis[21].

68| Proteins can be detected by using chemiluminescence (e.g., Western Lightning Plus) or quantitative immunoblotting with the Odyssey infrared imaging system.
? TROUBLESHOOTING

? TROUBLESHOOTING
Troubleshooting advice can be found in **Table 2**.

TABLE 2 | Troubleshooting table.

Step	Problem	Reason	Solution
24	Poor cell recovery	The cells were not pelleted sufficiently during the centrifugation	Increase the time or speed of the centrifugation. Be sure that the wash solution contains BSA
40	Cell lysate is cloudy after sonication	Sonication did not completely lyse cells or SDS-protein complexes precipitate from solution	Increase sonication times and be sure to avoid foaming of samples. Ensure that the proper volume of lysis buffer was used in Step 39
57	White precipitate layer is observed above beads after centrifugation of biotin captures	Lipids from cell membranes were not properly pelleted after sonication	Make certain that lysate is clear after sonication and centrifugation. If a white layer is observed on top of the cell lysate, remove the lysate and clear again by centrifugation
64B(xviii)	No pellet is observed after air-drying the TCA-concentrated iPOND eluate	Sample was lost during TCA precipitation	Centrifuge the supernatant saved in Step 64B(xiv). Proceed with Step 64B(xv–xviii). If no pellet is observed, centrifuge supernatant previously saved in Step 64B(xvii). Continue with Step 64B(xviii)
68	High background signal in the control sample	Protein binds to streptavidin beads nonspecifically	Use elution option B; increase the number of washes in Steps 62 and 63
	Poor signal for control proteins such as PCNA in the experimental sample	Poor EdU incorporation	Increase the number of cells used in each sample and ensure that the cells are growing well prior to experiment
	Poor detection of the protein of interest in the input samples	Poor antibody or formaldehyde cross-linking interferes with epitope detection	Optimize immunoblotting conditions or change antibody. Consider increasing the boiling time in Step 65A(iii) or Step 65B(xx) to completely reverse the formaldehyde cross-links

● **TIMING**

Steps 1 and 2, preparation of cell cultures: 1–7 d
Steps 3–10, EdU labeling and thymidine/HU chase: variable, typically 10 min–8 h
Steps 11–18, cell fixation/collection: 1 h
Steps 19–27, cell permeabilization: 1 h
Steps 28–37, click reaction: 2 h
Steps 38–47, cell lysis and sonication: 1 h
Steps 48–55, biotin capture: 16–20 h
Steps 56–64, washes and protein elution: variable, typically 1–4 h
Steps 65–68, analysis of eluted proteins: variable, typically 2–3 d

ANTICIPATED RESULTS

Typically, 1×10^8 cells are EdU labeled and processed by using iPOND to yield sufficient material for immunoblotting with 2–3 antibodies. A protein is interpreted to be enriched at the replication fork if the following conditions are met: the protein is detected in a click reaction sample that has been EdU labeled (**Fig. 4**, lane 6); the protein is not detected in a sample that omits the click reaction (**Fig. 4**, lane 5); and the protein level is progressively decreased in the thymidine chase samples (**Fig. 4**, lanes 7–8). Chromatin-bound proteins will appear to be enriched specifically after the click reaction, but they will also be detected in the thymidine chase sample (**Fig. 4**, e.g., histone H2B). Replication stress proteins recruited to damaged forks will be detected only after a chase into a replication stress reagent (**Fig. 3b**).

ACKNOWLEDGMENTS This work was supported by the US National Cancer Institute grants R01CA136933 and R01CA102729 to D.C. B.M.S. is supported by a Department of Defense Breast Cancer Research Program predoctoral fellowship (W81XWH-10-1-0226). We thank N. Porter, K. Tallman, D. Liebler and S. Codreanu, who developed the UV-photocleavable biotin azide and optimized methods of photoelution. We also thank L. Marnett, K. Gould, J. McLean and M. Chandrasekharan for helpful advice and discussions.

AUTHOR CONTRIBUTIONS B.M.S. developed the protocol and F.B.C. made modifications to omit the formaldehyde cross-linking step. D.C. conceived and supervised the project. B.M.S. and D.C. wrote the manuscript.

COMPETING FINANCIAL INTERESTS The authors declare no competing financial interests.

Published online at http://www.natureprotocols.com/.
Reprints and permissions information is available online at http://www.nature.com/reprints/index.html.

1. Cimprich, K.A. & Cortez, D. ATR: an essential regulator of genome integrity. *Nat. Rev. Mol. Cell Biol.* **9**, 616–627 (2008).
2. Hoeijmakers, J.H. Genome maintenance mechanisms for preventing cancer. *Nature* **411**, 366–374 (2001).
3. Berkovich, E., Monnat, R.J. Jr. & Kastan, M.B. Assessment of protein dynamics and DNA repair following generation of DNA double-strand breaks at defined genomic sites. *Nat. Protoc.* **3**, 915–922 (2008).
4. Bell, S.P. & Dutta, A. DNA replication in eukaryotic cells. *Annu. Rev. Biochem.* **71**, 333–374 (2002).
5. Sirbu, B.M. *et al.* Analysis of protein dynamics at active, stalled, and collapsed replication forks. *Genes Dev.* **25**, 1320–1327 (2011).
6. Salic, A. & Mitchison, T.J. A chemical method for fast and sensitive detection of DNA synthesis *in vivo*. *Proc. Natl. Acad. Sci. USA* **105**, 2415–2420 (2008).
7. Moses, J.E. & Moorhouse, A.D. The growing applications of click chemistry. *Chem. Soc. Rev.* **36**, 1249–1262 (2007).
8. Herrick, J. & Bensimon, A. Global regulation of genome duplication in eukaryotes: an overview from the epifluorescence microscope. *Chromosoma* **117**, 243–260 (2008).
9. Probst, A.V., Dunleavy, E. & Almouzni, G. Epigenetic inheritance during the cell cycle. *Nat. Rev. Mol. Cell Biol.* **10**, 192–206 (2009).
10. Kliszczak, A., Rainey, M., Harhen, B., Boisvert, F. & Santaocanale, C. DNA-mediated chromatin pull-down for the study of chromatin replication. *Scientific Rep.* **1**, 1–7 (2011).
11. Jao, C.Y. & Salic, A. Exploring RNA transcription and turnover in vivo by using click chemistry. *Proc. Natl. Acad. Sci. USA* **105**, 15779–15784 (2008).
12. Reyes-Lamothe, R., Sherratt, D.J. & Leake, M.C. Stoichiometry and architecture of active DNA replication machinery in *Escherichia coli*. *Science* **328**, 498–501 (2010).
13. Aladjem, M.I. Replication in context: dynamic regulation of DNA replication patterns in metazoans. *Nat. Rev. Genet.* **8**, 588–600 (2007).
14. Raschle, M. *et al.* Mechanism of replication-coupled DNA interstrand crosslink repair. *Cell* **134**, 969–980 (2008).
15. Ben-Yehoyada, M. *et al.* Checkpoint signaling from a single DNA interstrand crosslink. *Mol. Cell* **35**, 704–715 (2009).
16. Petermann, E., Orta, M.L., Issaeva, N., Schultz, N. & Helleday, T. Hydroxyurea-stalled replication forks become progressively inactivated and require two different RAD51-mediated pathways for restart and repair. *Mol. Cell* **37**, 492–502 (2010).
17. Szychowski, J. *et al.* Cleavable biotin probes for labeling of biomolecules via azide-alkyne cycloaddition. *J. Am, Chem. Soc.* **132**, 18351–18360 (2010).
18. Kim, H.Y., Tallman, K.A., Liebler, D.C. & Porter, N.A. An azido-biotin reagent for use in the isolation of protein adducts of lipid-derived electrophiles by streptavidin catch and photorelease. *Mol. Cell Proteomics* **8**, 2080–2089 (2009).
19. Capson, T.L., Benkovic, S.J. & Nossal, N.G. Protein-DNA cross-linking demonstrates stepwise ATP-dependent assembly of T4 DNA polymerase and its accessory proteins on the primer-template. *Cell* **65**, 249–258 (1991).
20. Gallagher, S.R. One-dimensional SDS gel electrophoresis of proteins. *Curr. Prot. Mol. Biol.* 10.2A.1–10.2A.34 (1999).
21. Shevchenko, A., Tomas, H., Havlis, J., Olsen, J.V. & Mann, M. In-gel digestion for mass spectrometric characterization of proteins and proteomes. *Nat. Protoc.* **1**, 2856–2860 (2006).

SMARCAL1 catalyzes fork regression and Holliday junction migration to maintain genome stability during DNA replication

Rémy Bétous,[1] Aaron C. Mason,[2] Robert P. Rambo,[3] Carol E. Bansbach,[1] Akosua Badu-Nkansah,[1] Bianca M. Sirbu,[1] Brandt F. Eichman,[1,2] and David Cortez[1,4]

[1]Department of Biochemistry, Vanderbilt University School of Medicine, Nashville, Tennessee 37232, USA; [2]Department of Biological Sciences, Vanderbilt University, Nashville, Tennessee 37240, USA; [3]Life Sciences Division, Advanced Light Source, Lawrence Berkeley National Laboratory, Berkeley, California 94720, USA

SMARCAL1 (SWI/SNF-related, matrix-associated, actin-dependent regulator of chromatin, subfamily A-like1) maintains genome integrity during DNA replication. Here we investigated its mechanism of action. We found that SMARCAL1 travels with elongating replication forks, and its absence leads to MUS81-dependent double-strand break formation. Binding to specific nucleic acid substrates activates SMARCAL1 activity in a reaction that requires its HARP2 (Hep-A-related protein 2) domain. Homology modeling indicates that the HARP domain is similar in structure to the DNA-binding domain of the PUR proteins. Limited proteolysis, small-angle X-ray scattering, and functional assays indicate that the core enzymatic unit consists of the HARP2 and ATPase domains that fold into a stable structure. Surprisingly, SMARCAL1 is capable of binding three-way and four-way Holliday junctions and model replication forks that lack a designed ssDNA region. Furthermore, SMARCAL1 remodels these DNA substrates by promoting branch migration and fork regression. *SMARCAL1* mutations that cause Schimke immunoosseous dysplasia or that inactivate the HARP2 domain abrogate these activities. These results suggest that SMARCAL1 continuously surveys replication forks for damage. If damage is present, it remodels the fork to promote repair and restart. Failures in the process lead to activation of an alternative repair mechanism that depends on MUS81-catalyzed cleavage of the damaged fork.

[*Keywords*: DNA repair; HARP; Holliday junction; fork reversal; SIOD; SAXS]

Supplemental material is available for this article.

Received September 3, 2011; revised version accepted December 12, 2011.

SMARCAL1 (SWI/SNF-related, matrix-associated, actin-dependent regulator of chromatin, subfamily A-like1), also known as DNA-dependent ATPase A and HARP (Hep-A-related protein), is a member of the SNF2 family of ATPases (Flaus et al. 2006). Many of these proteins use the energy of ATP hydrolysis to translocate along DNA and thereby remodel DNA structures or DNA–protein interactions. They function in many cellular processes, including transcription, DNA replication, and DNA repair.

Biallelic mutations in *SMARCAL1* cause the human disease Schimke immunoosseous dysplasia (SIOD) (Boerkoel et al. 2002). SIOD symptoms commonly include skeletal dysplasia, T-cell immunodeficiency, and kidney failure (Boerkoel et al. 2000). At the cellular level, SMARCAL1 deficiency causes increased DNA replication-associated damage (Bansbach et al. 2009, 2010; Postow et al. 2009; Yuan et al. 2009) and sensitizes cells to DNA-damaging agents that inhibit DNA replication (Bansbach et al. 2009; Ciccia et al. 2009; Yuan et al. 2009). SMARCAL1 localizes to damaged replication factories via an interaction with the ssDNA-binding protein replication protein A (RPA) (Bansbach et al. 2009; Ciccia et al. 2009; Yuan et al. 2009; Yusufzai et al. 2009), and this interaction is essential for its genome maintenance function (Bansbach et al. 2009; Yuan et al. 2009). SMARCAL1 is phosphorylated by checkpoint kinases in response to DNA damage (Bansbach et al. 2009; Postow et al. 2009). *SMARCAL1* mutants derived from SIOD patients fail to rescue the genome maintenance defects caused by *SMARCAL1* deficiency (Bansbach et al. 2009, 2010; Yuan et al. 2009). Thus, SMARCAL1 acts at damaged replication forks to maintain genome stability, and defects in this activity may underlie at least some of the phenotypes associated with SIOD (Bansbach et al. 2010).

[4]Corresponding author.
E-mail david.cortez@vanderbilt.edu.
Article is online at http://www.genesdev.org/cgi/doi/10.1101/gad.178459.111.

The mechanism of how SMARCAL1 acts to repair damaged forks remains largely unknown. Biochemically, SMARCAL1 can bind to DNA that contains single- and double-stranded regions such as forks and DNA hairpins (Muthuswami et al. 2000; Yusufzai and Kadonaga 2008). DNA binding activates its ATPase activity, and this activity promotes DNA single-strand annealing even in the presence of RPA (Yusufzai and Kadonaga 2008). The N-terminal RPA-binding domain of SMARCAL1 is not necessary for this DNA strand-annealing activity (Bansbach et al. 2009; Yusufzai et al. 2009), but patient-derived mutants lack this function. The molecular basis for this activity may not be simply translocation along dsDNA, since the related protein RAD54 cannot perform this function despite being a robust translocase (Yusufzai and Kadonaga 2008).

SMARCAL1 is a multidomain protein. The ATPase domain, which lies in the C-terminal half of the protein, is split into two regions of primary amino acid sequence by a 115-amino-acid linker sequence. The N-terminal half of the protein contains a highly sequence conserved RPA-binding domain (Bansbach et al. 2009; Ciccia et al. 2009; Postow et al. 2009; Yuan et al. 2009; Yusufzai et al. 2009), a 200-amino-acid region of low sequence conservation without predicted domain structure, and two HARP domains. The HARP domains are 55 amino acids in length with high sequence similarity but unknown function and structure. They are separated by 40 amino acids, and the second HARP domain is linked to the ATPase domain by an additional 47 amino acids.

Fusing the HARP domains to the ATPase domain of the SNF2 proteins BRG1 or HELLS is sufficient to reconstitute DNA-dependent ATPase and annealing helicase activities, suggesting that the HARP domains are important determinants of the SMARCAL1 enzyme specificity (Ghosal et al. 2011). Paradoxically, the closest homolog of SMARCAL1 in humans, annealing helicase 2 (AH2, also known as ZRANB3), also has annealing helicase activity despite a different domain structure and no unambiguous HARP domains (Yusufzai and Kadonaga 2010).

In this study, we took genetic, biochemical, and biophysical approaches to understand how SMARCAL1 functions to maintain genome integrity. We found that SMARCAL1 travels with at least some elongating replication forks, and the MUS81 structure-specific endonuclease cleaves damaged forks in SMARCAL1-deficient cells. The HARP2 domain is essential for DNA binding, and both biochemical and small-angle X-ray scattering (SAXS) data indicate that the HARP2+SNF2 domains provide the minimal enzymatic unit. The HARP domain resembles the DNA-binding domain of the PUR-α protein and has limited ability to bind DNA on its own. Surprisingly, we found that SMARCAL1 can bind three-way and four-way DNA structures and model replication forks. Furthermore, SMARCAL1 branch-migrates the four-way junction and catalyzes extensive fork regression of model replication forks. These data provide mechanistic insight into how SMARCAL1 functions and suggest that it remodels stalled replication forks through fork regression and branch migration to promote replication fork restart and prevent replication-associated DNA double-strand breaks.

Results

SMARCAL1 is present at DNA replication forks during an unperturbed S phase and prevents MUS81-dependent double-strand breaks

Previous analyses indicated that SMARCAL1 localizes to nuclear foci that colocalize with replisomes in response to agents that induce replication stress (Bansbach et al. 2009; Ciccia et al. 2009; Postow et al. 2009; Yuan et al. 2009; Yusufzai et al. 2009). This localization is dependent on an interaction with the replisome protein RPA. Silencing SMARCAL1 using RNAi causes elevated levels of γH2AX in replicating cells (Bansbach et al. 2009; Postow et al. 2009; Yuan et al. 2009). To determine whether SMARCAL1 actually is a component of active replisomes, we used the iPOND procedure (Sirbu et al. 2011) to purify active and stalled replication forks. SMARCAL1 is purified with nascent, 5-ethynyl-2′-deoxyuridin (EdU)-labeled DNA at elongating replication forks even when replication is not perturbed (Fig. 1A). It is not purified with

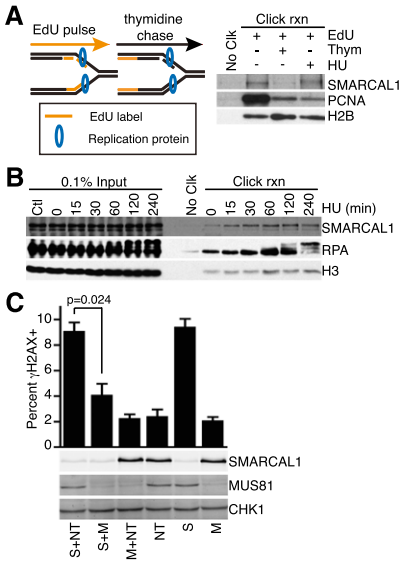

Figure 1. SMARCAL1 acts at replication forks to prevent MUS81-catalyzed double-strand breaks. (*A*) Cells were labeled with EdU for 10 min, the EdU was removed, and thymidine was added for 20 min or HU was added for 3 h prior to purifying the nascent DNA–protein complexes using the iPOND procedure. (*B*) EdU-labeled cells were treated with 2 mM HU for the indicated lengths of time prior to performing iPOND. The "No Clk" controls in *A* and *B* are samples treated with EdU only, but no biotin-azide was added during the click reaction. (*C*) U2OS cells were transfected with siRNAs targeting SMARCAL1 (S), MUS81 (M), or nontargeting (NT) as indicated. Three days after transfection, the cells were either stained with antibodies to γH2AX or harvested for immunoblotting with the indicated antibodies. The percentage of cells staining positive for γH2AX was determined by immunofluorescent imaging from three independent experiments. Cells with >10 foci were counted as positive. Error bars are the standard deviation (SD; $n = 3$).

the EdU-labeled DNA once the labeled DNA segment is no longer adjacent to the fork (after a chase in medium lacking EdU), indicating that it travels with at least some moving replisomes. As expected, SMARCAL1 is also found at forks stalled with hydroxyurea (HU) (Fig. 1A,B), and its mobility on SDS-PAGE gels is altered in these circumstances due to phosphorylation by checkpoint kinases (Bansbach et al. 2009).

The MUS81 endonuclease cleaves some blocked and damaged replication forks, generating a double-strand break and initiating recombination-based repair mechanisms (Osman and Whitby 2007). Therefore, we hypothesized that the high level of γH2AX found in *SMARCAL1* silenced cells could be due to double-strand breaks catalyzed by MUS81. To address this question, we measured the proportion of cells containing γH2AX after SMARCAL1 and/or MUS81 depletion. As expected, silencing *SMARCAL1* caused an induction of γH2AX, while silencing *MUS81* had no effect (Fig. 1C). *MUS81* silencing prevented γH2AX induction in *SMARCAL1* silenced cells without significantly altering the efficiency of *SMARCAL1* silencing (Fig. 1C). Thus, γH2AX induction after SMARCAL1 depletion is MUS81-dependent.

SMARCAL1 binds a wide variety of DNA substrates that combine ssDNA and dsDNA

Our results suggest that SMARCAL1 either processes or prevents the formation of MUS81 substrates. Little is known about SMARCAL1 substrate specificity other than it prefers to bind DNA with both single- and double-stranded characteristics rather than ssDNA or dsDNA (Supplemental Fig. 1A; Muthuswami et al. 2000; Yusufzai and Kadonaga 2008), and its ATPase activity is activated upon DNA binding. To clarify the DNA determinants that mediate SMARCAL1 DNA binding and activation, we investigated a broad range of possible DNA substrates. We first evaluated how long the ssDNA arms of a fork need to be and found that significant SMARCAL1 binding is observable even with a fork length of only 5 nucleotides (nt) per arm (Supplemental Fig. 1B,C). Increasing the arm lengths beyond 5 nt increases the binding affinity. We also observe a second DNA–protein complex forming when the ssDNA region is lengthened to 20 nt or more. The second, higher-molecular-weight complex may contain more than one SMARCAL1 molecule.

We next varied the length of one of the ssDNA arms while keeping the other constant and found that the length of the second arm did not influence binding affinity (Supplemental Fig. 1D,E). In fact, SMARCAL1 bound equivalently to a fork and an ssDNA overhang substrate. Both DNA substrates stimulated SMARCAL1 ATPase activity as well (Supplemental Fig. 1F). Furthermore, DNA substrates with either a 5′ or 3′ recessed end bind and stimulate SMARCAL1 ATPase activity equivalently (Fig. 2A–C).

At a replication fork, the free 5′ end of the nascent nucleic acid on the lagging stand template would consist of a short RNA primer rather than DNA. To test whether SMARCAL1 can bind and be activated on the lagging strand, we examined a nucleic acid substrate that mimics this chimeric nucleic acid structure. A RNA–DNA primer substrate bound and stimulated SMARCAL1 equivalently to the DNA–DNA substrate (Supplemental Fig. 1G–I).

Next, we assessed how the length of ssDNA alters SMARCAL1-binding affinity. Five nucleotides are suffi-

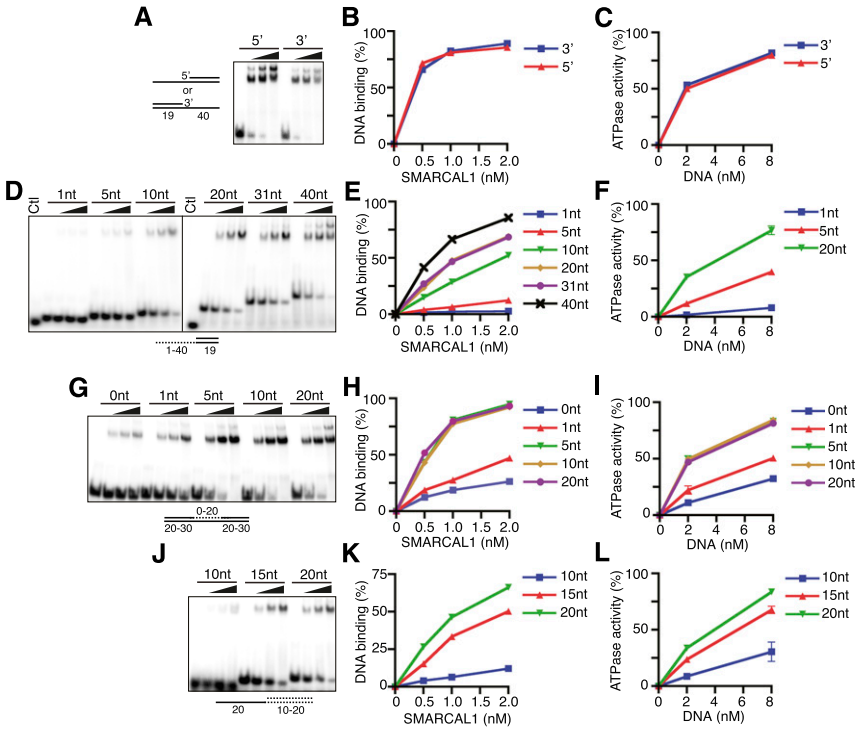

Figure 2. Characterization of the DNA-binding and DNA-stimulated ATPase activities of full-length SMARCAL1. (*A*,*D*,*G*,*J*) Increasing amounts of SMARCAL1 were incubated with the indicated oligonucleotide substrates prior to polyacrylamide gel electrophoresis. The control (Ctl) in *D* is an unhybridized single-stranded oligonucleotide. (*B*,*E*,*H*,*K*) Quantitation of a representative DNA-binding experiment. (*C*,*F*,*I*,*L*) Increasing amounts of DNA substrate were added to SMARCAL1, and ATPase activity was measured as the percentage of ATP hydrolyzed. Error bars represent the mean ± SD from three independent experiments. In cases in which no error bars are visible, the SD is smaller than the symbol size. The sequences of the oligonucleotides are listed in Supplemental Table 1, and a description of which oligonucleotides were used in each experiment is presented in Supplemental Table 2.

cient to allow some binding and elicit significant ATPase activity (Fig. 2D–F). SMARCAL1 binding and ATPase activity increase as the length of the ssDNA increases. SMARCAL1 also binds and is stimulated efficiently by a gapped DNA substrate. Maximum binding and activation require only a five single-stranded nucleotide gap, and even a nick can elicit some activity (Fig. 2G–I; Supplemental Fig. 1J,K). When a bubble replaces the gap, increasing the length of the mismatched nucleotides to 16 significantly increases affinity (Supplemental Fig. 1L,M). Thus, the length of ssDNA needed for optimal binding and activation of SMARCAL1 is shortest when it is presented in the context of a gap.

We also investigated how the length of dsDNA affects binding and ATPase stimulation of SMARCAL1. Optimal SMARCAL1 binding and ATPase activation requires 20 dsDNA nucleotides (Fig. 2J–L). Greater dsDNA lengths yield no further improvement in SMARCAL1 affinity (data not shown). Fifteen nucleotides of dsDNA on either side of a 5-nt gap are sufficient to elicit maximal SMARCAL1 binding (Supplemental Fig. 1N,O).

Taken together, these results show that SMARCAL1 binds and is activated by any nucleic acid structure that contains both single- and double-stranded regions, including an RNA–primer template. The optimal length of ssDNA that elicits binding depends on the structural context of the DNA, with 5 nt being sufficient for a gap and longer lengths promoting better binding to a forked or single-stranded overhang substrate. The optimal length of dsDNA is ~15 nt. Finally, the dsDNA and ssDNA must be within the same molecule, since adding these separately to SMARCAL1 does not elicit any binding (Supplemental Fig. 1A).

HARP2 but not HARP1 is required for SMARCAL1 DNA-binding, ATPase, and annealing helicase activities

To understand how SMARCAL1 binds DNA, we examined the affinity of a series of truncated SMARCAL1 proteins for a forked DNA substrate (Fig. 3A). While deletion of the first 198 and the last 84 amino acids had no effect on SMARCAL1 DNA binding, deletion of the first 424 amino acids containing the HARP domains severely compromises the DNA-binding and ATPase activities of SMARCAL1 (Fig. 3B–E).

These results led us to hypothesize that the HARP domains may be essential for SMARCAL1 DNA binding. To test this hypothesis, we assessed the behavior of a series of HARP domain mutants (Fig. 4A). SMARCAL1 lacking the first HARP domain (ΔHARP1) binds to and is activated by a forked DNA substrate, although with slightly reduced affinity compared with wild-type SMARCAL1 (Fig. 4B,C; Supplemental Fig. 2A). In contrast, deleting the second HARP domain alone or in combination with the first HARP domain (SMARCAL1-ΔHARP2 and ΔHARP1+2) severely attenuated both DNA binding and ATPase activation. The effects of the deletions were even more severe when assayed with a 5-nt, single-stranded gap substrate (Fig. 4D,E).

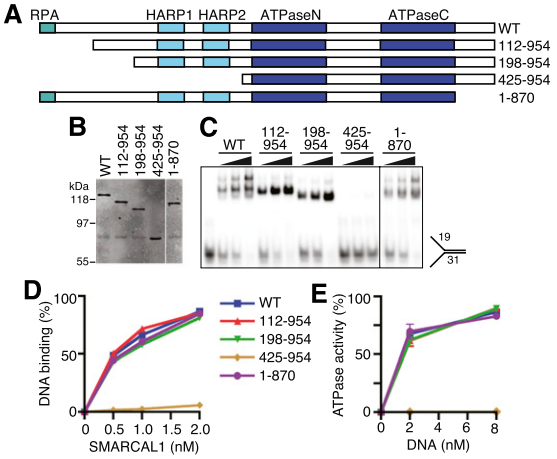

Figure 3. The SMARCAL1 N terminus containing the HARP domains is necessary for DNA-binding and ATPase activity. (*A*) Diagram of the SMARCAL1 proteins used to identify domains required for function. Wild type (WT) in all figures is full-length SMARCAL1. (*B*) Overexpressed SMARCAL1 proteins were purified from HEK-293T cells and examined on an SDS-PAGE gel by immunoblotting. (*C*,*D*) Increasing amounts of purified SMARCAL1 proteins were incubated with the forked DNA substrate to measure DNA binding. (*E*) Increasing amounts of forked DNA were added to the SMARCAL1 fragments to measure DNA-stimulated ATPase activity. Error bars represent the mean ± SD from three independent experiments. In cases in which no error bars are visible, the SD is smaller than the symbol size. The DNA substrates corresponding to each symbol and line color are the same in *D* and *E*.

To confirm the deletion results, we generated point mutants in HARP1 and HARP2. The HARP domains are evolutionarily conserved (Fig. 4F). We mutated two of the invariant residues within each domain to alanine (HARP1 W277A/F279A and HARP2 W372A/F379A). These mutants exhibit DNA-binding and ATPase activity similar to the corresponding complete deletion of the domain (Fig. 4G–I). Interestingly, we found that the decreased DNA-binding and ATPase activity of the HARP1-WF mutant yielded only a slight impairment of SMARCAL1 annealing helicase activity, while mutation of the HARP2 domain completely abolished the ability of SMARCAL1 to anneal an RPA-coated plasmid substrate (Fig. 4J). The complete deletion of HARP1 also had no effect on the SMARCAL1 annealing helicase activity (Supplemental Fig. 2B). These results suggest that HARP2 is critical for the DNA-binding, ATPase, and annealing helicase activities of SMARCAL1. HARP1 may have a supporting role in facilitating SMARCAL1 function.

Finally, we asked whether the HARP domains themselves have any DNA-binding activity. We found that a SMARCAL1 fragment encompassing both HARP domains (amino acids 198–425) is sufficient to bind forked DNA, albeit with much lower affinity than the full-length protein (Supplemental Fig. 3A–C). The HARP domain–DNA complex did not migrate as a discrete band in the electrophoretic mobility shift assay; however, we were able to supershift the DNA–protein

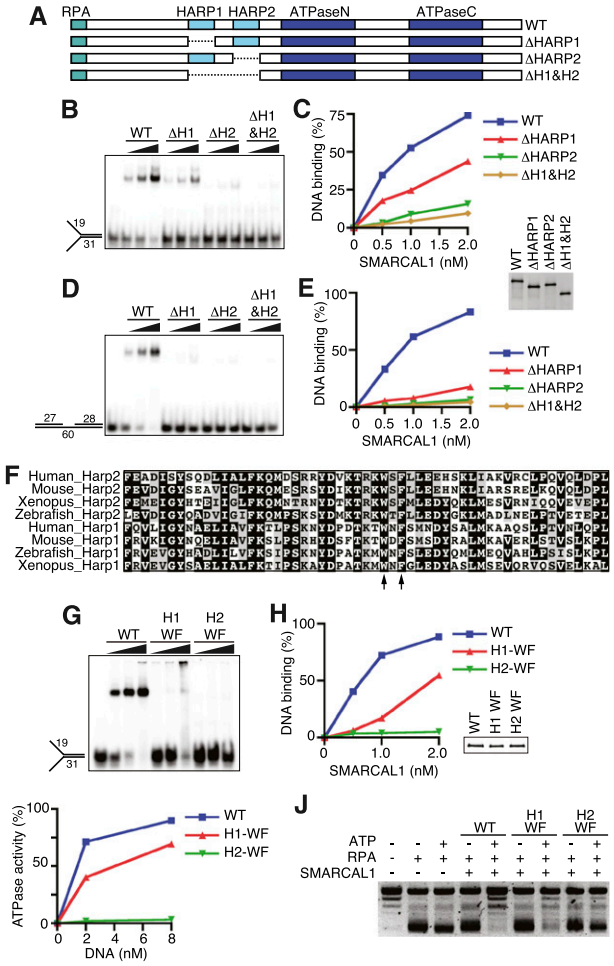

Figure 4. The HARP2 domain of SMARCAL1 is required for annealing helicase activity. (*A*) Diagram of the SMARCAL1 HARP domain deletion mutants purified after overexpression in HEK-293T cells. DNA binding was measured with increasing concentrations of a forked DNA substrate (*B*,*C*) or 5-nt gap DNA substrate (*D*,*E*). (*F*) Sequence alignment of the HARP1 and HARP2 domains of human, mouse, *Xenopus laevis*, and zebrafish SMARCAL1. The arrows point to the two residues mutated in the WF mutants used in *G*–*J*. (*G*,*H*) Forked DNA binding of the wild type and SMARCAL1 HARP-WF mutants purified from baculovirus-infected insect cells. Note that the HARP1-WF mutant reproducibly shifted much of the DNA substrate into the well of the gel at higher concentrations of protein. (*I*) Increasing amounts of forked DNA were added to the SMARCAL1 mutants to measure DNA-stimulated ATPase activity. Error bars represent the mean ± SD from three independent experiments. In cases in which no error bars are visible, the SD is smaller than the symbol size. (*J*) Annealing helicase activities of SMARCAL1 wild-type and mutant proteins. The concentration of the SMARCAL1 proteins in this assay is 15 nM. The *insets* in *C* and *H* are immunoblots confirming that equal concentrations of SMARCAL1 proteins were used.

complex with an antibody that recognizes the recombinant HARP1+2 protein fragment, confirming the complex was not due to a contaminant in the protein purification.

The HARP2-ATPase constitutes a structural core motor domain

Our biochemical results demonstrate the importance of the HARP2 domain in SMARCAL1 function. To gain mechanistic insight into how SMARCAL1 might use this novel domain, SAXS experiments were performed to determine the spatial arrangement of the HARP2 and ATPase domains in solution (Fig. 5A). Limited proteolysis of the full-length protein purified from insect cells revealed a proteolytically resistant fragment consisting of the HARP2-ATPase regions (Supplemental Fig. 4A). Kratky analysis of SMARCAL1(325–954) revealed parabolic features, suggesting that the protein is globular with distinct domains (Supplemental Fig. 4B,C). The radius of gyration (r_g) obtained from the Guinier region was 33.0 ± 0.3 Å (Supplemental Fig. 4D), indicating that the 75-kDa protein is elongated when compared with glucose isomerase, a spherical protein at 173 kDa with a similar R_g of 32 Å.

SAXS data provide complete structural information and can be used to distinguish between different conformations of a high-resolution model or build a complete atomistic model from known domains (Rambo and Tainer 2010). Therefore, we used the SAXS data of SMARCAL1 and homology models of both the HARP2 and ATPase domains to determine the solution state of the protein. To date, there are no known structural homologs of the HARP domain. However, we discovered by sequence–structure comparison (Shi et al. 2001) that there is good agreement between the predicted secondary structural elements of the HARP domains with tandem PUR repeats observed in the structure of the purine-rich element-binding protein PUR-α (Supplemental Fig. 5; Graebsch et al. 2009). PUR repeats are ~140-residue motifs consisting of anti-parallel β-β-β-β-α topology that bind ssDNA and dsDNA and thus provide a reasonable structural model for the HARP domains. A model of the core ATPase domain was also created based on the crystal structure of *Sulfolobus sulfotaricus* (Sso) Rad54, which shares 23% sequence identity and 58% overall similarity with SMARCAL1 (Supplemental Fig. 6).

Preliminary normal mode analysis (Suhre and Sanejouand 2004) was performed on the core ATPase domain to produce a family of alternative conformations. Each conformation was then combined with the HARP2 model for partial ab initio modeling using a simulated annealing search algorithm. The models converged into an elongated structure that was independently validated by the close resemblance to the three-dimensional (3D) molecular envelope generated from the SAXS data using GASBOR (Fig. 5B), and the remarkable agreement between the experimental scattering curve and the theoretical curve calculated from the docking model (Fig. 5C). The resulting HARP2-ATPase model revealed that the HARP2 and ATPase motifs form one continuous domain in the absence of DNA, suggesting that their association constitutes a structural and functional core domain necessary to drive translocation. To test this idea, we assayed whether the HARP2-ATPase protein is sufficient to

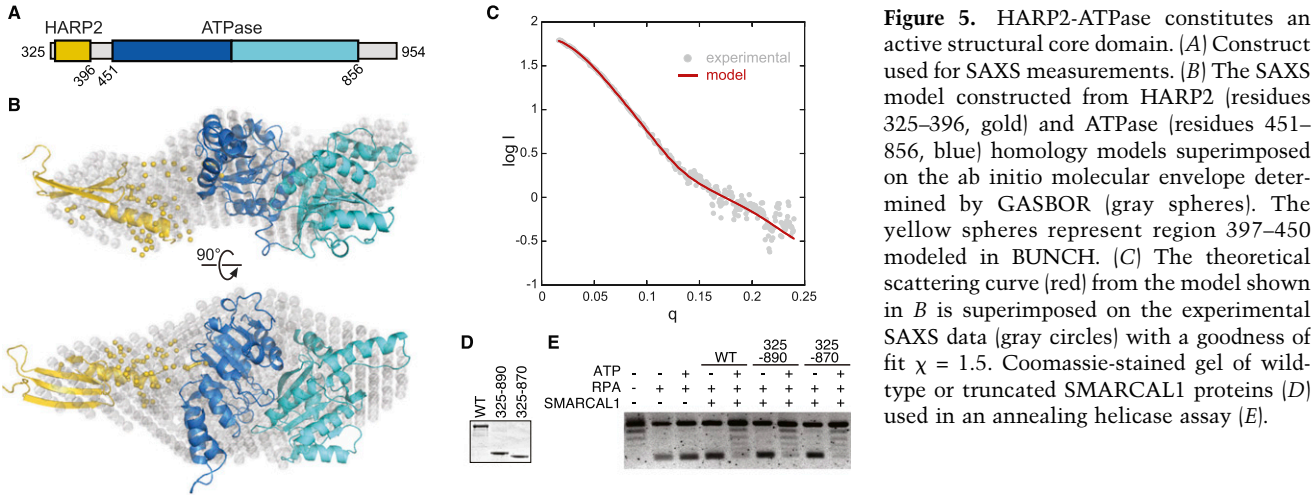

Figure 5. HARP2-ATPase constitutes an active structural core domain. (*A*) Construct used for SAXS measurements. (*B*) The SAXS model constructed from HARP2 (residues 325–396, gold) and ATPase (residues 451–856, blue) homology models superimposed on the ab initio molecular envelope determined by GASBOR (gray spheres). The yellow spheres represent region 397–450 modeled in BUNCH. (*C*) The theoretical scattering curve (red) from the model shown in *B* is superimposed on the experimental SAXS data (gray circles) with a goodness of fit χ = 1.5. Coomassie-stained gel of wild-type or truncated SMARCAL1 proteins (*D*) used in an annealing helicase assay (*E*).

catalyze strand annealing. Indeed, SMARCAL1(325–870) and SMARCAL1(325–890) are both efficient ATP-dependent annealing helicases (Fig. 5D,E).

SMARCAL1 can bind and branch-migrate a four-way junction

The DNA-binding activities of SMARCAL1 characterized thus far suggest that SMARCAL1 may have dsDNA- and ssDNA-binding surfaces. Combined with the energy of ATP hydrolysis, SMARCAL1 may translocate along the DNA in a way that leads to single-strand annealing. To determine whether these properties could yield any other enzymatic consequences, we expanded our search for SMARCAL1 substrates to more complex DNA structures, including three-way and four-way Holliday junctions. Surprisingly, despite lacking any designed ssDNA regions, SMARCAL1 could bind these DNA substrates with only slightly reduced affinity compared with a fork substrate (Fig. 6A,B). Furthermore, both DNA substrates activated the SMARCAL1 ATPase (Fig. 6C).

Given that these structures bind SMARCAL1 and stimulate its ATPase activity, we asked whether SMARCAL1 could also induce branch migration like Rad54 (Bugreev et al. 2006). We prepared a synthetic Holliday junction consisting of two homologous and two heterologous arms, similar to those used in previous branch migration studies (Fig. 6D; Gari et al. 2008b). Indeed, SMARCAL1 catalyzed branch migration in an ATP-dependent manner (Fig. 6E,F). As expected, the SIOD patient-derived ATPase-defective mutant (R764Q) failed to promote branch migration despite having the ability to bind DNA (Fig. 6G,H; Yusufzai and Kadonaga 2008). To test the importance of the HARP domains in this process, we examined the branch migration properties of HARP1-WF and HARP2-WF SMARCAL1 mutants. While the HARP1 mutant was able to branch-migrate the Holliday junction as efficiently as the wild-type protein, the HARP2 mutant had severely attenuated activity (Fig. 6I,J).

SMARCAL1 can bind and branch-migrate a replication fork

Previous studies indicate that SMARCAL1 acts at stalled replication forks but may not have an essential function in homology-directed double-strand break repair. Double-strand breaks are only thought to form in normal cells at persistently stalled forks (Petermann et al. 2010; Sirbu et al. 2011). Thus, we investigated whether SMARCAL1 could bind and process other branched structures that might exist at a transiently stalled fork. Specifically, we compared SMARCAL1 affinity to model forks with no nascent DNA strands, a leading strand, a lagging strand, or both. Strikingly, we found that SMARCAL1 binds to and is activated by each of these structures (Fig. 7A–C). To determine whether SMARCAL1 can catalyze remodeling of these replication fork structures, we prepared a substrate to monitor fork regression (Fig. 7D; Gari et al. 2008b). SMARCAL1 catalyzed displacement of the two "nascent" DNA strands and annealing of the parental strands (Fig. 7E,F). Again, the SIOD patient-derived R764Q mutation eliminated this activity.

SMARCAL1 does not possess any helicase activity (Yusufzai and Kadonaga 2008), so it is unlikely that it could unwind the nascent strands before annealing both parental and both nascent strands together. To confirm that the SMARCAL1 fork reversal activity is coordinated without the formation of ssDNA intermediates, we labeled the model nascent leading strand of the synthetic replication fork and performed a time-course assay. We found that only a double-stranded product consisting of the two nascent strands is formed without the appearance of any ssDNA intermediates (Supplemental Fig. 7A–C). We conclude that SMARCAL1 processes replication fork structures by coupling unwinding and annealing in a concerted manner to yield fork regression. As expected, the SMARCAL1 HARP1-WF mutant is able to regress the replication fork as efficiently as the wild-type protein, whereas mutations in the SMARCAL1 HARP2 domain eliminate fork regression activity (Supplemental Fig. 7D–F). Thus, HARP2 but not HARP1 is critical for SMARCAL1 fork regression activity.

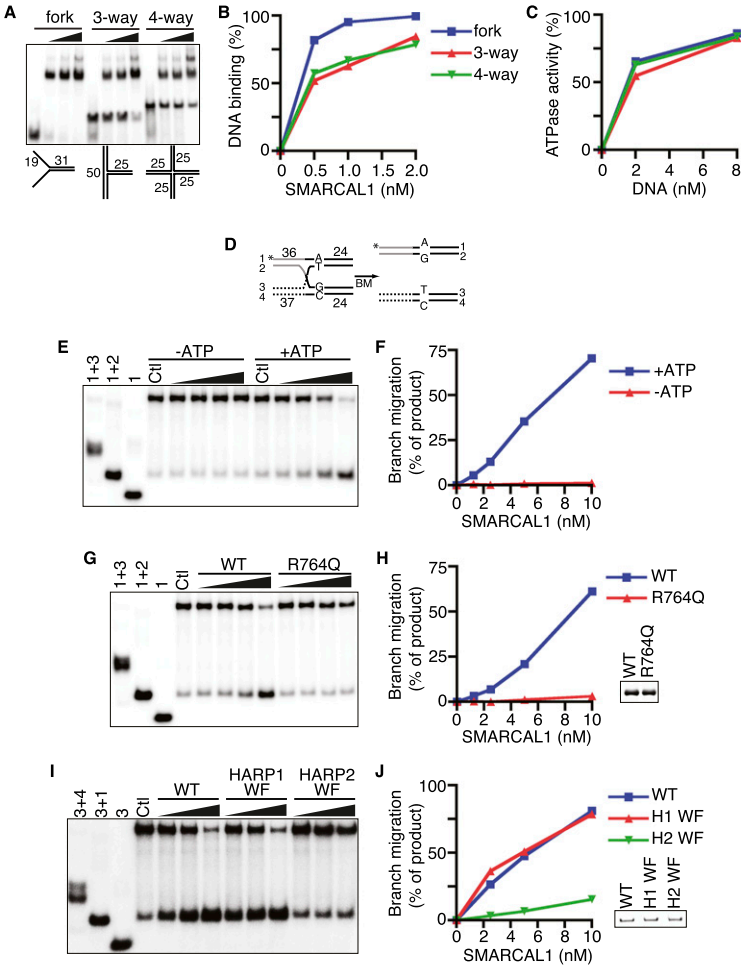

Figure 6. SMARCAL1 binds and branch-migrates Holliday junctions. The ability of SMARCAL1 to bind (*A*,*B*) and be activated (*C*) by forked, three-way, and four-way Holiday junctions was compared. The DNA substrates corresponding to each symbol and line color are the same in *B* and *C*. (*D*) Four-way branch migration substrate used in *E*–*J*. The ^{32}P-labeled DNA strand (#1) for the experiments shown in *E*–*H* is indicated with an asterisk. Strand #3 was labeled for the experiment shown in *I* and *J*. (*E*) Increasing amounts of SMARCAL1 were incubated with the four-way branch migration substrate in the absence or presence of ATP as indicated. (*G*,*I*) Increasing amounts of wild-type (WT), R764Q, HARP1-WF, or HARP2-WF SMARCAL1 proteins were incubated with the DNA substrate in the presence of ATP. The first three lanes in *E*, *G*, and *I* are size standards generated by annealing the indicated oligonucleotides. The control (Ctl) samples are the annealed branch migration substrate in the absence of recombinant protein. (*F*,*H*,*J*) Quantitation of the reactions from *E*, *G*, and *I*, respectively. The amount of product in the control reactions (from spontaneous branch migration) was set at zero in each experiment, and all other samples are measured relative to the control sample. All reactions in *E*–*J* were performed for 20 min prior to termination and gel electrophoresis to characterize the products. The *insets* in *H* and *J* are Coomassie-stained gels confirming that equal concentrations of SMARCAL1 proteins were used.

Finally, we tested whether SMARCAL1 can catalyze fork regression and sustained migration on a plasmid-sized substrate that more closely models a stalled replication fork. We created a joint molecule by annealing gapped plasmids (Fig. 7G). This substrate mimics a stalled fork in which the lagging strand is 14 nt longer than the leading strand (Ralf et al. 2006; Blastyak et al. 2007). The extent of fork regression of this substrate was detected by restriction enzyme digestion to liberate a linear 5′-labeled lagging strand. SMARCAL1 efficiently catalyzed remodeling of this substrate, yielding substantial amounts of a regressed fork corresponding to movement of at least 836 base pairs (bp) (Fig. 7H). This reaction is dependent on the amount of SMARCAL1 added to the reaction and requires ATP hydrolysis, since ATPγS completely blocked remodeling of the substrate.

Discussion

Previous studies by our group and others defined SMARCAL1 as a replication stress response protein that acts to preserve genome integrity during DNA replication (Bansbach et al. 2009; Ciccia et al. 2009; Driscoll and Cimprich 2009; Postow et al. 2009; Yusufzai et al. 2009). Immunofluorescent imaging demonstrated that SMARCAL1 accumulates at damaged replication forks due to its interaction with RPA. We now report that SMARCAL1 associates with active, elongating replisomes, and its absence causes MUS81-dependent DNA damage. Significantly, we found that SMARCAL1 exhibits a much broader range of enzymatic activities than previously recognized, including an ability to promote branch migration of Holliday junctions and fork reversal of model replication forks. Concerted fork regression and branch migration coupled to DNA polymerization provides one mechanism to allow DNA damage bypass and replication restart (Petermann and Helleday 2010). SMARCAL1 depletion does not significantly slow the overall rate of DNA replication but is required for efficient DNA replication restart of stalled or collapsed replication forks (Ciccia et al. 2009). Thus, SMARCAL1 may continuously survey replisomes and promote efficient restart of stalled forks through its fork remodeling activity. In the absence of SMARCAL1, slowed or damaged forks are cleaved by MUS81, perhaps as an alternative mechanism of fork repair.

In addition, our results indicate that all SMARCAL1 activities require the HARP2 and SNF2-like ATPase domains. The HARP2 domain is required for DNA binding, and the HARP2-ATPase domains together form the

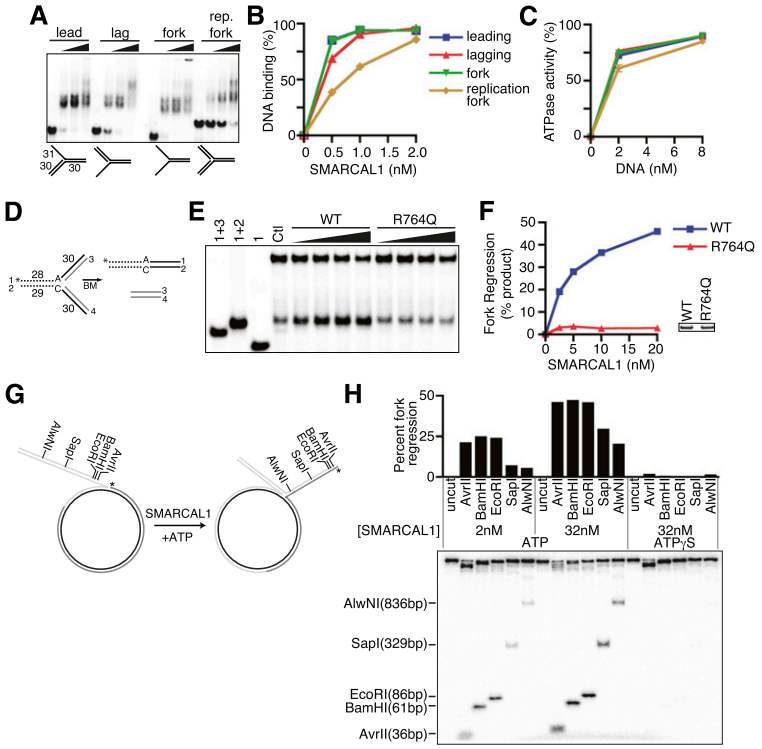

Figure 7. SMARCAL1 catalyzes fork regression of model replication forks. (*A*,*B*) Increasing amounts of SMARCAL1 were incubated with the indicated substrates to measure DNA binding. (*C*) ATPase activity of SMARCAL1 was measured in the presence of increasing amounts of leading, lagging, fork, and replication fork substrate. Symbols and line colors correspond to the same substrates as in *B*. Error bars represent the mean ± SD from three independent experiments. In cases in which no error bars are visible, the SD is smaller than the symbol size. (*D*) Diagram of the model replication fork substrates used to measure fork regression activity in *E* and *F*. A single mismatch is present at the fork junction to prevent spontaneous fork migration. The labeled strand (#1) is indicated by an asterisk. (*E*,*F*) Increasing amounts of SMARCAL1 (wild type [WT]) or R764Q SMARCAL1 were incubated with the annealed substrate for 20 min, the reaction was terminated, and products were separated by gel electrophoresis for analysis. The first three lanes in *E* are size standards generated by annealing the indicated oligonucleotides. The control (Ctl) sample is the annealed fork regression substrate in the absence of recombinant protein. The amount of product in the control reaction (from spontaneous regression of the model replication fork substrate) was set at zero in each experiment, and all other samples are measured relative to the control sample. The *inset* in *F* is a Coomassie-stained gel confirming that equal concentrations of SMARCAL1 proteins were used. (*G*) Diagram of the annealed gapped plasmid substrate used to measure SMARCAL1-catalyzed fork regression in *H*. The ^{32}P-labeled DNA end is indicated with an asterisk. (*H*) Restriction digests with the indicated enzymes were completed following incubation of the plasmid substrate with the indicated concentrations of SMARCAL1 in the presence of ATP or ATPγS. The liberated, ^{32}P-labeled DNA fragment was visualized on a polyacrylamide gel. The extent of fork regression was calculated as the amount of liberated fragment compared with the total radioactivity in the reaction. A representative experiment is shown.

functional enzymatic unit of SMARCAL1. Significant sequence similarity between the HARP domain and the DNA-binding domain of the PUR proteins combined with our SAXS data allowed us to derive a model of the solution state structure of the SMARCAL1 core enzyme. The HARP2 and ATPase motifs dock together and constitute a structural and functional core necessary to drive ATP-dependent translocation.

The HARP2 domain likely provides specificity to the action of the ATPase motor domain, thereby converting the energy of ATP hydrolysis into functional strand annealing, branch migration, and fork reversal. This type of activity could be facilitated by insertion of the HARP domain as a kind of wedge at the branch point within these structures (Fig. 8). One possibility supported by our data is that the compact HARP2-ATPase core enzyme contains both dsDNA- and ssDNA-binding surfaces encoded in the ATPase and HARP2 domains, respectively. DNA binding induces a conformational change, promoting ATP hydrolysis and protein translocation. A model for how this could function to promote fork regression is provided by the bacterial RecG protein, which shares some enzymatic activities with SMARCAL1 (Atkinson and McGlynn 2009). Further structural data, including high-resolution structures of SMARCAL1 with a bound DNA substrate, will be required to fully test this hypothesis.

In contrast to the HARP2 domain, the HARP1 domain makes a modest contribution to the DNA-binding and ATPase activities of SMARCAL1 and is largely dispensable for its annealing, branch migration, and fork regression functions. While vertebrate SMARCAL1 proteins contain two HARP domains, invertebrate SMARCAL1 proteins contain only a single HARP domain adjacent to the ATPase domain, suggesting that only a single HARP domain is essential for its evolutionarily conserved functions.

Our conclusions about the important function of the HARP2 domain are generally consistent with a recent report that found that the HARP domains are important for the annealing helicase activity of SMARCAL1 (Ghosal et al. 2011). However, the Chen group (Ghosal et al. 2011) reported that deleting both HARP1 and HARP2 together did not impair either DNA-binding or ATPase activity despite eliminating the annealing helicase activity. In contrast, our data with both deletion and point mutants clearly point to a requirement for the HARP2 domain for all SMARCAL1 enzymatic functions. We tested multiple proteins purified from both insect and human cells using several different DNA substrates and always found that the HARP2 domain was critical for DNA binding, ATPase activity, strand annealing, and branch migration. We do not have an explanation for this discrepancy.

The ability of SMARCAL1 to efficiently bind to Holliday junctions and model replication forks that lack ssDNA

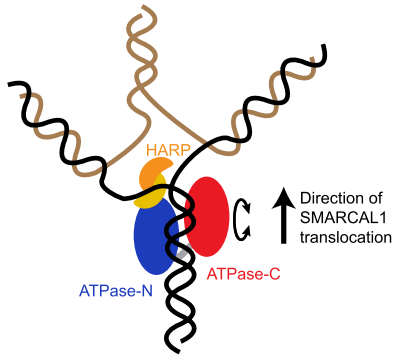

Figure 8. Model for how the translocase activity of the SMARCAL1 HARP2-ATPase core catalyzes fork regression. Existing structures of SNF2 translocases demonstrate that ATPase-N and ATPase-C lobes are capable of adopting different relative conformations and suggest that such conformational changes (depicted as a circular arrow) in response to the ATPase-binding and hydrolysis cycle may drive translocation along dsDNA (Durr et al. 2005; Thoma et al. 2005; Lewis et al. 2008). The SAXS model shows that the HARP2 domain in SMARCAL1 is physically associated with the ATPase-N lobe and may aid in the specialized annealing activity through ssDNA or junction binding. Translocation displaces the nascent DNA strands, induces fork regression, and promotes junction migration.

regions was unexpected, since SMARCAL1 has very little affinity to dsDNA compared with the optimal substrates containing at least 15 nt of dsDNA and 5 nt of ssDNA. One possibility is that SMARCAL1 captures a small amount of these structures as the dsDNA regions near the junction or fork breath to expose ssDNA. Our data indicate that only a small amount of ssDNA or even just a nick is necessary for SMARCAL1 DNA binding when it is in the context of a gap. Likewise, only a small amount may be needed in the context of these more complicated structures. We also observed no significant specificity of human SMARCAL1 for 3′ or 5′ recessed junctions. Furthermore, a 5′ recessed junction containing a model RNA–DNA primer, as would be found during lagging strand replication, efficiently binds and activates SMARCAL1. This contrasts with a previous report that found a preference for a 3′-hydroxyl recessed end (Muthuswami et al. 2000). The origin of this difference may be because the previous report used a fragment of bovine SMARCAL1, whereas we used full-length human SMARCAL1 in our studies.

The ATP-dependent activity of SMARCAL1 to remodel Holliday junctions and replication forks and prevent DNA damage during S phase is reminiscent of the activities of other proteins, including FANCM, WRN, RAD5, BLM, and HLTF (Constantinou et al. 2000; Ralf et al. 2006; Blastyak et al. 2007; Franchitto et al. 2008; Gari et al. 2008a,b; Opresko et al. 2009; Achar et al. 2011). All of these proteins are thought to be recruited to damaged replication forks, but it is unclear whether any travel with active forks like SMARCAL1. In contrast to SMARCAL1, none of these proteins contain a HARP domain or exhibit annealing helicase activity. Instead, most are DNA helicases. Thus, the enzymatic mechanisms by which they remodel replication fork structures are likely to be different. Why there are so many different enzymes that can catalyze similar reactions on DNA is unclear. It is possible that some of these enzymes work coordinately at the same damaged fork. In this regard, it is interesting that the loss of WRN, like SMARCAL1, also causes MUS81-dependent fork cleavage (Franchitto et al. 2008), and we and others have found WRN in SMARCAL1 purifications, suggesting a possible physical interaction (Ciccia et al. 2009; data not shown). Coordination of their enzymatic activities might help remodel damaged forks in cells where many other replisome and repair proteins may be present. However, these proteins must also have distinct functions, since inactivating mutations cause different human diseases.

In summary, our data suggest that SMARCAL1 surveys DNA replication forks. When it detects a problem, it uses its DNA-stimulated ATPase motor to remodel the fork by catalyzing strand annealing, branch migration, and fork reversal to promote efficient fork repair. These activities are encoded within the HARP2-SNF2 ATPase domains, which form a functional enzyme flanked by regulatory sequences. Absence of SMARCAL1 forces the use of alternative fork repair mechanisms that involve MUS81-dependent DNA double-strand breaks.

Materials and methods

Cell culture

HEK-293T and U2OS cells were cultured in DMEM supplemented with 7.5% FBS. Sf9 cells were cultured in Insect XPRESS medium with 7.5% FBS at 27°C.

Antibodies

The antibodies used were as follows: Flag-M2 (Sigma), γH2AX and GAPDH (Millipore), RPA (Bethyl Laboratories), H3 (Abcam), and MUS81 (Novus). The SMARCAL1 antibody was described previously (Bansbach et al. 2009).

Detection of γH2AX

γH2AX foci were detected by indirect immunofluorescent imaging of fixed U2OS cells 72 h after transfection with siRNA as previously described (Lovejoy et al. 2009).

iPOND

The iPOND technique was performed as described previously (Sirbu et al. 2011). Briefly, cells were labeled for 10 min with EdU, then treated with 2 mM HU for increasing amounts of time. Alternatively, after the EdU labeling period, 10 μM thymidine was added to the growth medium for 20 min as a "chase" sample. This concentration of thymidine does not block replication but is sufficient to ensure that no additional EdU is incorporated. After cross-linking with formaldehyde and a click reaction to conjugate biotin to the EdU-labeled nascent DNA, protein–DNA complexes were isolated with streptavidin beads, cross-links were reversed, and the eluted proteins were analyzed by immunoblotting. The "no click" control omitted the biotin-azide during the click reaction.

Protein purification

Flag-SMARCAL1, His-SMARCAL1(325-954), HARP1-WF, and HARP2-WF were purified from baculovirus-infected cells essentially as described previously (Yusufzai and Kadonaga 2008) except that cells were lysed in TNT buffer containing 20 mM Tris (pH 7.5), 150 mM NaCl, 0.1 mM EDTA, 1 mM DTT, 0.2 mM PMSF, 1 mg/mL leupeptin, 1 mg/mL aprotinin, and 0.1% Triton X-100. Proteins for structural studies were purified by Ni-NTA affinity, ion exchange, and gel filtration chromatography. To purify SMARCAL1 proteins from human cells, HEK-293T cells were transfected with pLPCX-Flag-HA-SMARCAL1 plasmids using Lipofectamine 2000 (Invitrogen). Seventy-two hours after transfection, the cells were lysed in TNT buffer for 30 min on ice. After high-speed centrifugation, the cleared lysates were incubated with Flag-M2 beads (Sigma) for 3 h at 4°C. The beads were washed three times in wash buffer (TNT buffer containing 0.3 M LiCl) and twice in SMARCAL1 buffer (20 mM HEPES at pH 7.6, 20% glycerol, 0.1 M KCl, 1.5 mM $MgCl_2$, 0.2 mM EDTA, 1 mM DTT, 0.2 mM PMSF, 0.01% IGEPAL CA-630). The bound proteins were eluted in SMARCAL1 buffer containing 0.25 mg/mL Flag peptide on ice, flash-frozen, and stored at −80°C.

DNA-binding, annealing helicase, and ATPase assays

The gel mobility shift assays for DNA-binding, annealing helicase, and SMARCAL1 ATPase assays were performed as described previously (Yusufzai and Kadonaga 2008) with the following modifications. For the gel mobility shift assay, increasing concentrations of purified SMARCAL1 (0, 0.5, 1, 2 nM final concentrations) were combined with radiolabeled oligonucleotide probe (1 nM final concentration) in binding buffer supplemented with 0.2% IGEPAL CA-630. The samples were loaded into a 5% polyacrylamide 0.5× TBE gel (82 × 28.5 cm, 1 mm thick), and subjected to electrophoresis in 0.5× TBE for 2 h and 30 min at 50 V at 4°C. The gels were dried and quantified using a Molecular Imager FX (Bio-Rad). DNA-binding reactions were performed at least twice, and a representative experiment is shown with quantitation. For the annealing helicase assay, the topoisomerase I was purchased (Invitrogen), and pBluescript was used as the plasmid substrate. For the ATPase assay, increasing concentrations of oligonucleotides (0, 2, or 8 nM final concentration) were incubated with purified SMARCAL1 (8 nM final concentration) in a final volume of 10 μL, and the reactions were incubated for 30 min at 30°C. The results are presented as the percent of ATP hydrolyzed to ADP during the reaction. ATPase assays were performed a minimum of three times each, and graphs depict means and standard deviation error bars. All oligonucleotide sequences are described in Supplemental Table 1, and all DNA substrates are described in Supplemental Table 2. All figures show a representative experiment from at least two replicates.

Homology modeling

The HARP repeats were identified as evolutionary structural homologs to PUR-α repeats using the FUGUE sequence–structure homology recognition server (Shi et al. 2001). The HARP2 (amino acids 325–396) homology model was constructed using the crystal structure of PUR-α (Protein Data Bank [PDB] ID 3K44) (Graebsch et al. 2009) residues 41–185 as a template. The ATPase model (SMARCAL1 residues 451–856) was generated from residues 455–891 of the SsoRad54 crystal structure (PDB ID 1Z63) (Durr et al. 2005). In both cases, the SMARCAL1 sequences were threaded onto the crystal structure using Swiss PDB Viewer, and the model was optimized using Swiss Model (http://swissmodel.expasy.org).

SAXS data collection and model building

SAXS data were collected at the SIBYLS beamline at the Advanced Light Source and prepared as described (Hura et al. 2009). Specifically, SAXS data were collected on SMARCAL1(325–954) in buffer containing 20 mM HEPES (pH 7.6), 200 mM NaCl, 2 mM $MgCl_2$, 0.5 mM TCEP, 5% glycerol, and 1% sucrose. The protein sample was prepared for SAXS as described (Kazantsev et al. 2011) using a Shodex KW402.5 size exclusion column. The peak fraction was analyzed for SAXS as a 2/3 dilution series starting from 3 mg/mL. Three exposure times (0.5, 1, and 6 sec) were taken at 25°C and 12 keV. Guinier and Kratky analysis was performed as described (Putnam et al. 2007; Rambo and Tainer 2011). Linearity of the Guinier region for each exposure demonstrated a lack of radiation damage and aggregation (Supplemental Fig. 4D). SAXS profiles were overlaid, inspected for concentration-dependent scattering, and merged (Hura et al. 2009). For modeling, the composite scattering curve was generated from data from 1-sec exposures of 2 and 3 mg/mL samples. The maximum dimension (116 Å) was determined using GNOM (Svergun 1992). Atomistic-based modeling of the SAXS data was achieved with the program BUNCH (Petoukhov and Svergun 2005) using HARP and ATPase homology models. The models were treated as independent domains in a simulated annealing algorithm to determine their relative spatial arrangements. Missing residues between the HARP and ATPase domains (397–450) were modeled as dummy residues as described (Petoukhov and Svergun 2005). Ab initio modeling was performed with GASBOR using 630 dummy residues. Ten independent modeling runs were performed and averaged (Volkov and Svergun 2003) to produce a final macromolecular envelope. The final model targeted residues 325–856, consistent with a Porod volume of 91,148 $Å^3$ calculated from the SAXS data. The missing C-terminal 99 residues were not included in the modeling based on proteolytic sensitivity of the C terminus (Supplemental Fig. 4A).

Branch migration and fork regression assays

Oligonucleotide #48 was end-labeled with [γ-^{32}]ATP and T4 polynucleotide kinase (New England Biolabs) and purified through a G25 column (GE Healthcare). To prepare tailed or forked intermediates, 250 nM complementary ssDNA oligonucleotides (#48/#54 and #55/#56 for the branch migration, and #48/#50 and #53/#54 for the fork regression) were annealed in 20 μL of SSC buffer (15 mM NaCitrate at pH 7.0, 150 mM NaCl) in a PCR machine. To prepare the branch migration and the fork regression substrate, 32 nM ^{32}P-labeled and 48 nM nonlabeled DNA intermediates were incubated in reaction buffer (40 mM Tris at pH 7.5, 20 mM KCl, 5 mM $MgCl_2$, 100 μg/mL BSA, 2 mM ATP, 2 mM DTT) for 30 min at 37°C. The DNA substrates were diluted threefold in reaction buffer and mixed with increasing amounts of SMARCAL1 in a 20-μL reaction volume. The reaction was completed for 20 min at 37°C and terminated by the addition of 3× stop buffer (0.9% SDS, 50 mM EDTA, 40% glycerol, 0.1% bromophenol blue, 0.1% xylene cyanol). Samples were loaded into 8% polyacrylamide 1× TBE gels (82 × 28.5 cm, 1 mm thick) and subjected to electrophoresis in 1× TBE for 90 min at 80 V at room temperature. The gels were dried and quantified using a Molecular Imager FX (Bio-Rad).

The plasmid-sized replication fork model substrate was generated and purified as described (Blastyak et al. 2007). Recombinant SMARCAL1 purified from insect cells was incubated with 0.5 nM substrate for 20 min at 37°C in reaction buffer (20 mM Tris at pH 7.5, 50 mM KCl, 5 mM $MgCl_2$, 100 μg/mL BSA, 2 mM ATP or ATPγS, 1 mM DTT). The reaction was quenched by the addition of 10 mM ATPγS and 10 mM $MgCl_2$. One microliter

(2–20 U, depending on the enzyme) of the indicated restriction enzymes was added to the reaction and further incubated for 30 min at 37°C. The reaction products were then separated on a 6% polyacrylamide gel. The gel was dried and quantified using a Molecular Imager FX (Bio-Rad).

Acknowledgments

This work was supported by NIH grant R01CA136933 to D.C. R.B. is supported in part by a Department of Defense Breast Cancer Research Program post-doctoral fellowship (W81XWH-10-1-0581). A.C.M. and C.B. are supported in part by the Vanderbilt Training Program in Environmental Toxicology (T32 ES07028). The SAXS analysis was made possible by the core facilities supported by the SBDR NIH grant P01CA092584 and a Center in Molecular Toxicology (P30 ES000267) pilot project grant to B.F.E.

References

Achar YJ, Balogh D, Haracska L. 2011. Coordinated protein and DNA remodeling by human HLTF on stalled replication fork. *Proc Natl Acad Sci* **108:** 14073–14078.

Atkinson J, McGlynn P. 2009. Replication fork reversal and the maintenance of genome stability. *Nucleic Acids Res* **37:** 3475–3492.

Bansbach CE, Betous R, Lovejoy CA, Glick GG, Cortez D. 2009. The annealing helicase SMARCAL1 maintains genome integrity at stalled replication forks. *Genes Dev* **23:** 2405–2414.

Bansbach CE, Boerkoel CF, Cortez D. 2010. SMARCAL1 and replication stress: An explanation for SIOD? *Nucleus* **1:** 245–248.

Blastyak A, Pinter L, Unk I, Prakash L, Prakash S, Haracska L. 2007. Yeast Rad5 protein required for postreplication repair has a DNA helicase activity specific for replication fork regression. *Mol Cell* **28:** 167–175.

Boerkoel CF, O'Neill S, Andre JL, Benke PJ, Bogdanovic R, Bulla M, Burguet A, Cockfield S, Cordeiro I, Ehrich JH, et al. 2000. Manifestations and treatment of Schimke immuno-osseous dysplasia: 14 new cases and a review of the literature. *Eur J Pediatr* **159:** 1–7.

Boerkoel CF, Takashima H, John J, Yan J, Stankiewicz P, Rosenbarker L, Andre JL, Bogdanovic R, Burguet A, Cockfield S, et al. 2002. Mutant chromatin remodeling protein SMARCAL1 causes Schimke immuno-osseous dysplasia. *Nat Genet* **30:** 215–220.

Bugreev DV, Mazina OM, Mazin AV. 2006. Rad54 protein promotes branch migration of Holliday junctions. *Nature* **442:** 590–593.

Ciccia A, Bredemeyer AL, Sowa ME, Terret ME, Jallepalli PV, Harper JW, Elledge SJ. 2009. The SIOD disorder protein SMARCAL1 is an RPA-interacting protein involved in replication fork restart. *Genes Dev* **23:** 2415–2425.

Constantinou A, Tarsounas M, Karow JK, Brosh RM, Bohr VA, Hickson ID, West SC. 2000. Werner's syndrome protein (WRN) migrates Holliday junctions and co-localizes with RPA upon replication arrest. *EMBO Rep* **1:** 80–84.

Driscoll R, Cimprich KA. 2009. HARPing on about the DNA damage response during replication. *Genes Dev* **23:** 2359–2365.

Durr H, Korner C, Muller M, Hickmann V, Hopfner KP. 2005. X-ray structures of the *Sulfolobus solfataricus* SWI2/SNF2 ATPase core and its complex with DNA. *Cell* **121:** 363–373.

Flaus A, Martin DM, Barton GJ, Owen-Hughes T. 2006. Identification of multiple distinct Snf2 subfamilies with conserved structural motifs. *Nucleic Acids Res* **34:** 2887–2905.

Franchitto A, Pirzio LM, Prosperi E, Sapora O, Bignami M, Pichierri P. 2008. Replication fork stalling in WRN-deficient cells is overcome by prompt activation of a MUS81-dependent pathway. *J Cell Biol* **183:** 241–252.

Gari K, Decaillet C, Delannoy M, Wu L, Constantinou A. 2008a. Remodeling of DNA replication structures by the branch point translocase FANCM. *Proc Natl Acad Sci* **105:** 16107–16112.

Gari K, Decaillet C, Stasiak AZ, Stasiak A, Constantinou A. 2008b. The Fanconi anemia protein FANCM can promote branch migration of Holliday junctions and replication forks. *Mol Cell* **29:** 141–148.

Ghosal G, Yuan J, Chen J. 2011. The HARP domain dictates the annealing helicase activity of HARP/SMARCAL1. *EMBO Rep* **12:** 574–580.

Graebsch A, Roche S, Niessing D. 2009. X-ray structure of Pur-α reveals a Whirly-like fold and an unusual nucleic-acid binding surface. *Proc Natl Acad Sci* **106:** 18521–18526.

Hura GL, Menon AL, Hammel M, Rambo RP, Poole FL II, Tsutakawa SE, Jenney FE Jr, Classen S, Frankel KA, Hopkins RC, et al. 2009. Robust, high-throughput solution structural analyses by small angle X-ray scattering (SAXS). *Nat Methods* **6:** 606–612.

Kazantsev AV, Rambo RP, Karimpour S, Santalucia J Jr, Tainer JA, Pace NR. 2011. Solution structure of RNase P RNA. *RNA* **17:** 1159–1171.

Lewis R, Durr H, Hopfner KP, Michaelis J. 2008. Conformational changes of a Swi2/Snf2 ATPase during its mechano-chemical cycle. *Nucleic Acids Res* **36:** 1881–1890.

Lovejoy CA, Xu X, Bansbach CE, Glick GG, Zhao R, Ye F, Sirbu BM, Titus LC, Shyr Y, Cortez D. 2009. Functional genomic screens identify CINP as a genome maintenance protein. *Proc Natl Acad Sci* **106:** 19304–19309.

Muthuswami R, Truman PA, Mesner LD, Hockensmith JW. 2000. A eukaryotic SWI2/SNF2 domain, an exquisite detector of double-stranded to single-stranded DNA transition elements. *J Biol Chem* **275:** 7648–7655.

Opresko PL, Sowd G, Wang H. 2009. The Werner syndrome helicase/exonuclease processes mobile D-loops through branch migration and degradation. *PLoS ONE* **4:** e4825. doi: 10.1371/journal.pone.0004825.

Osman F, Whitby MC. 2007. Exploring the roles of Mus81-Eme1/Mms4 at perturbed replication forks. *DNA Repair (Amst)* **6:** 1004–1017.

Petermann E, Helleday T. 2010. Pathways of mammalian replication fork restart. *Nat Rev Mol Cell Biol* **11:** 683–687.

Petermann E, Orta ML, Issaeva N, Schultz N, Helleday T. 2010. Hydroxyurea-stalled replication forks become progressively inactivated and require two different RAD51-mediated pathways for restart and repair. *Mol Cell* **37:** 492–502.

Petoukhov MV, Svergun DI. 2005. Global rigid body modeling of macromolecular complexes against small-angle scattering data. *Biophys J* **89:** 1237–1250.

Postow L, Woo EM, Chait BT, Funabiki H. 2009. Identification of SMARCAL1 as a component of the DNA damage response. *J Biol Chem* **284:** 35951–35961.

Putnam CD, Hammel M, Hura GL, Tainer JA. 2007. X-ray solution scattering (SAXS) combined with crystallography and computation: Defining accurate macromolecular structures, conformations and assemblies in solution. *Q Rev Biophys* **40:** 191–285.

Ralf C, Hickson ID, Wu L. 2006. The Bloom's syndrome helicase can promote the regression of a model replication fork. *J Biol Chem* **281:** 22839–22846.

Rambo RP, Tainer JA. 2010. Bridging the solution divide: Comprehensive structural analyses of dynamic RNA, DNA, and

protein assemblies by small-angle X-ray scattering. *Curr Opin Struct Biol* **20:** 128–137.

Rambo RP, Tainer JA. 2011. Characterizing flexible and intrinsically unstructured biological macromolecules by SAS using the Porod-Debye law. *Biopolymers* **95:** 559–571.

Shi J, Blundell TL, Mizuguchi K. 2001. FUGUE: Sequence–structure homology recognition using environment-specific substitution tables and structure-dependent gap penalties. *J Mol Biol* **310:** 243–257.

Sirbu BM, Couch FB, Feigerle JT, Bhaskara S, Hiebert SW, Cortez D. 2011. Analysis of protein dynamics at active, stalled, and collapsed replication forks. *Genes Dev* **25:** 1320–1327.

Suhre K, Sanejouand YH. 2004. ElNemo: A normal mode Web server for protein movement analysis and the generation of templates for molecular replacement. *Nucleic Acids Res* **32:** W610–W614. doi: 10.1093/nar/gkh368.

Svergun DI. 1992. Determination of the regularization parameter in indirect-transform methods using perceptual criteria. *J Appl Crystallogr* **25:** 495–503.

Thoma NH, Czyzewski BK, Alexeev AA, Mazin AV, Kowalczykowski SC, Pavletich NP. 2005. Structure of the SWI2/SNF2 chromatin-remodeling domain of eukaryotic Rad54. *Nat Struct Mol Biol* **12:** 350–356.

Volkov VV, Svergun DI. 2003. Uniqueness of ab initio shape determination in small-angle scattering. *J Appl Crystallogr* **36:** 860–864.

Yuan J, Ghosal G, Chen J. 2009. The annealing helicase HARP protects stalled replication forks. *Genes Dev* **23:** 2394–2399.

Yusufzai T, Kadonaga JT. 2008. HARP is an ATP-driven annealing helicase. *Science* **322:** 748–750.

Yusufzai T, Kadonaga JT. 2010. Annealing helicase 2 (AH2), a DNA-rewinding motor with an HNH motif. *Proc Natl Acad Sci* **107:** 20970–20973.

Yusufzai T, Kong X, Yokomori K, Kadonaga JT. 2009. The annealing helicase HARP is recruited to DNA repair sites via an interaction with RPA. *Genes Dev* **23:** 2400–2404.

OPEN ACCESS Freely available online

PLOS | GENETICS

Histone Acetyl Transferase 1 Is Essential for Mammalian Development, Genome Stability, and the Processing of Newly Synthesized Histones H3 and H4

Prabakaran Nagarajan[1], Zhongqi Ge[1], Bianca Sirbu[2], Cheryl Doughty[3], Paula A. Agudelo Garcia[1], Michaela Schlederer[4], Anthony T. Annunziato[3], David Cortez[2], Lukas Kenner[4,5], Mark R. Parthun[1]*

1 Department of Molecular and Cellular Biochemistry, The Ohio State University, Columbus, Ohio, United States of America, **2** Department of Biochemistry, Vanderbilt University School of Medicine, Nashville, Tennessee, United States of America, **3** Department of Biology, Boston College, Chestnut Hill, Massachusetts, United States of America, **4** Ludwig Boltzmann Institute for Cancer Research (LBI-CR), Vienna, Austria, **5** Clinical Institute of Pathology, Medical University of Vienna, Vienna, Austria

Abstract

Histone acetyltransferase 1 is an evolutionarily conserved type B histone acetyltransferase that is thought to be responsible for the diacetylation of newly synthesized histone H4 on lysines 5 and 12 during chromatin assembly. To understand the function of this enzyme in a complex organism, we have constructed a conditional mouse knockout model of Hat1. Murine Hat1 is essential for viability, as homozygous deletion of Hat1 results in neonatal lethality. The lungs of embryos and pups genetically deficient in Hat1 were much less mature upon histological evaluation. The neonatal lethality is due to severe defects in lung development that result in less aeration and respiratory distress. Many of the Hat1$^{-/-}$ neonates also display significant craniofacial defects with abnormalities in the bones of the skull and jaw. Hat1$^{-/-}$ mouse embryonic fibroblasts (MEFs) are defective in cell proliferation and are sensitive to DNA damaging agents. In addition, the Hat1$^{-/-}$ MEFs display a marked increase in genome instability. Analysis of histone dynamics at sites of replication-coupled chromatin assembly demonstrates that Hat1 is not only responsible for the acetylation of newly synthesized histone H4 but is also required to maintain the acetylation of histone H3 on lysines 9, 18, and 27 during replication-coupled chromatin assembly.

Citation: Nagarajan P, Ge Z, Sirbu B, Doughty C, Agudelo Garcia PA, et al. (2013) Histone Acetyl Transferase 1 Is Essential for Mammalian Development, Genome Stability, and the Processing of Newly Synthesized Histones H3 and H4. PLoS Genet 9(6): e1003518. doi:10.1371/journal.pgen.1003518

Editor: Paul D. Kaufman, University of Massachusetts Medical School, United States of America

Received December 18, 2012; **Accepted** April 4, 2013; **Published** June 6, 2013

Funding: This work was supported by grants from the National Institutes of Health (GM62970 to MRP, CA136933 to DC) and by a Pelotonia Predoctoral Fellowship from the Ohio State University Comprehensive Cancer Center (to ZG). The funders had no role in study design, data collection and analysis, decision to publish, or preparation of the manuscript.

Competing Interests: The authors have declared that no competing interests exist.

* E-mail: Parthun.1@osu.edu

Introduction

The packaging of genomic DNA during replication is a highly orchestrated process that ensures both the necessary compaction of the DNA and the proper transmission of the epigenetic landscape [1,2,3,4,5]. An important aspect of chromatin assembly is the processing of newly synthesized histones for their incorporation into chromatin. The transient acetylation of histone H3 and H4 NH_2-terminal tails is a hallmark of this processing. Newly synthesized molecules of histone H4 are predominantly diacetylated. This diacetylation occurs specifically on lysine residues 5 and 12 and this precise pattern is widely conserved throughout eukaryotic evolution. The acetylation of histone H3 occurs on a smaller fraction of the newly synthesized molecules and does not occur in a consistent pattern across eukaryotes. A role for this acetylation in histone deposition was first suggested by the correlation between the presence of these histone marks and active chromatin assembly as H3 and H4 are rapidly modified after their synthesis and then deacetylated following their incorporation into chromatin [6]. However, despite this long-standing correlation, an understanding of the function of histone NH_2-terminal tail domain acetylation in chromatin assembly remains elusive.

In addition to their NH_2-terminal tail domains, evidence from *S. cerevisiae* indicates that newly synthesized histones are also acetylated in their core domains with H3 acetylated on lysine 56 and H4 acetylated on lysine 91 [7,8,9,10]. H3 lysine 56 lies near the entry/exit point of the nucleosome in close proximity to the DNA. The acetylation of this site occurs specifically in S phase and has been linked to chromatin assembly by a number of observations. First, mutations in yeast that alter H3 lysine 56 cause defects in the reassembly of chromatin structure that accompanies the recombinational repair of a DNA double strand break. Second, H3 lysine 56 mutations influence the binding of histone H3 to the CAF-1 histone chaperone complex that plays a key role in replication coupled chromatin assembly [7,11,12,13, 14,15,16,17]. Histone H4 lysine 91 lies in the interface between H3/H4 tetramers and H2A/H2B dimers where it forms a salt bridge with an aspartic acid residue in histone H2B. Hence, the acetylation of H4 lysine 91 may regulate tetramer-dimer interactions and genetic results are consistent with a role for this modification in chromatin assembly [10,18].

Enzymes known as type B histone acetyltransferases (HATs) catalyze the acetylation of newly synthesized histones. Type B HATs are primarily distinguished from type A HATs by their substrate specificity. As expected for enzymes that modify histones

Author Summary

The packaging of genomic DNA during replication is a highly orchestrated process. An important aspect of chromatin assembly is the processing of newly synthesized histones prior to their incorporation into chromatin. The transient acetylation of histone H3 and H4 NH_2-terminal tails is a hallmark of this processing with newly synthesized molecules of histone H4 being predominantly diacetylated. This diacetylation occurs specifically on lysine residues 5 and 12 and this precise pattern is widely conserved throughout eukaryotic evolution. The acetylation of newly synthesized histones is catalyzed by type B histone acetyltransferases. Hat1 is the founding member of this class of enzymes and has been proposed to be responsible for the diacetylation of newly synthesized histone H4. Here we describe the development of a mouse knockout model of Hat1. The absence of Hat1 results in neonatal lethality due to developmental defects in the lung. Mouse embryonic fibroblasts derived from $Hat1^{-/-}$ mice are sensitive to DNA damaging agents and display a high level of genome instability. Biochemical analyses provide definitive evidence that Hat1 is the sole enzyme responsible for the acetylation of newly synthesized histone H4. Surprisingly, Hat1 is also necessary for the normal processing of newly synthesized histone H3.

prior to their assembly into chromatin, type B HATs are highly specific for free histones. Type B HATs may also function outside of the nucleus [19]. A number of type B HATs have now been identified. The first was Hat1p, which acetylates free histone H4 on lysine residues 5 and 12 [20,21]. In addition, the yeast enzyme Rtt109p acetylates free histone H3 on lysine 56 and lysine 9 [22,23,24]. Interestingly, the original type A HAT, Gcn5p, may also possess type B HAT activity in *S. cerevisiae* as it has been shown to be involved in the acetylation of the NH_2-terminal tail of newly synthesized histone H3 [25,26]. Finally, the mammalian enzyme HAT4 may also be a type B HAT as it resides in the Golgi and is capable of acetylating histone H4 lysine 91 [27].

Originally isolated from budding yeast, Hat1p was found to exist in at least 2 complexes. The first is a cytoplasmic complex that also contains Hat2p, which is a homolog of the Rbap46 histone chaperone in mammalian cells [21,28]. Hat1p is also found in a nuclear complex that, in addition to Hat2p, contains another histone chaperone, Hif1p (a homolog of the mammalian protein NASP) [29]. Not only the Hat1p protein itself but also the Hat1p-containing complexes are highly conserved in eukaryotes. Complexes with similar compositions have been isolated from human, frog, chicken and corn. As expected from their high degree of similarity, these enzymes specifically acetylate free histone H4 on lysines 5 and 12 [30,31,32,33].

Despite its widespread conservation, initial genetic analyses in yeast showed that loss of Hat1p had no detrimental effects on either chromatin assembly or cell viability [20,21,34]. This lack of phenotypic effect was, at least partly, due to functional redundancy as combining the deletion of *HAT1* with mutations in specific sets of lysine residues in the histone H3 NH_2-terminal tail resulted in defects in telomeric silencing and DNA damage sensitivity [35,36]. DNA damage sensitivity has also been observed in *S. pombe* and chicken DT40 cells lacking Hat1 [37,38]. Importantly, direct evidence linking yeast Hat1p to chromatin assembly in the contexts of DNA damage repair and histone exchange has recently been reported [39,40].

Despite the minor effects on cell viability observed in the absence of Hat1, biochemical analyses have implied that Hat1 may play a critical role in histone processing and dynamics. This is suggested by an intriguing property of Hat1p. Unlike most enzymes, Hat1 appears to remain stably associated with its histone substrates following acetylation [41]. This property of Hat1p also appears to be widely conserved. In yeast, both the cytoplasmic and nuclear Hat1p-containing complexes are stably associated with histones H3 and H4 [29]. In mammalian cells, Hat1p appears to be one of the primary proteins physically associated with soluble histones [42,43,44,45,46,47]. Therefore, Hat1p has the potential to function both catalytically and stoichiometrically in the chromatin assembly process.

To explore the function of Hat1 and the acetylation of newly synthesized histones in mammals, we have generated a conditional Hat1 knockout mouse model. $Hat1^{-/-}$ animals are neonatal lethal with developmental lung defects. These result from hyper proliferation of mesenchymal cells leading to severe atelectasis, less aeration and death upon respiratory failure. In addition, a significant fraction of the $Hat1^{-/-}$ animals display severe craniofacial defects. Mouse embryonic fibroblasts (MEFs) derived from $Hat1^{-/-}$ embryos show multiple defects including slow growth, DNA damage sensitivity and genome instability. Analysis of proteins present on newly replicated DNA by iPond (isolation of proteins on nascent DNA) indicates that histones H3 and H4 deposited during replication-coupled chromatin assembly are hypo-acetylated in the absence of Hat1 [48]. Consistent with these observations, analysis of newly synthesized histones indicates that Hat1 is the sole HAT responsible for the acetylation of newly synthesized histone H4. Surprisingly, loss of Hat1 also leads to a decrease in the modification of newly synthesized histone H3. These results demonstrate that Hat1 is essential in mammals and that it plays an integral role in the processing of newly synthesized histones during the process of chromatin assembly.

Results

Generation of a conditional Hat1 knockout mouse model

There is a single homolog of Hat1 in the murine genome that is highly similar to human and yeast Hat1. The murine Hat1 gene consists of 11 exons (Figure 1A). A construct was generated to target the integration of loxP sites to flank Hat1 exon 3. In the presence of cre recombinase, exon 3 can be deleted with the subsequent introduction of a stop codon (Figure 1A). This will create a truncation mutant of Hat1 that produces a product less 50 amino acids long. In the event that alternate splicing occurs in the Hat1 gene that could skip exon 3, only exon 9 can be spliced to exon 2 and retain the proper reading frame. In this case, the protein that would be produced would lack the entire Hat1 active site.

The targeting construct was transfected into mouse embryonic stem (ES) cells and cells grown with antibiotic selection. Cell lines in which the targeting construct was properly integrated were identified (data not shown). These cells were then injected into blastocysts to generate chimeric mice. The chimeras were then mated with wild type mice (C57/Bl6) and the pups were screened by Southern blot to determine whether germline transmission of the $Hat1^{flox}$ allele had been achieved. Several animals with a $Hat1^{flox}/Hat1^{+}$ genotype were identified (Figure 1B).

To generate a complete Hat1 mouse knockout, the $Hat1^{flox}/Hat1^{+}$ mice were mated to mice that ubiquitously express the Cre recombinase. The litters from these matings were screened to identify offspring in which Hat1 exon 3 had been deleted ($Hat1^{\Delta 3}$). As seen in Figure 1C, several mice were obtained with the genotype $Hat1^{\Delta 3}/Hat1^{+}$. These mice also carried a copy of the Cre recombinase gene. We backcrossed these mice with C57/Bl6

A

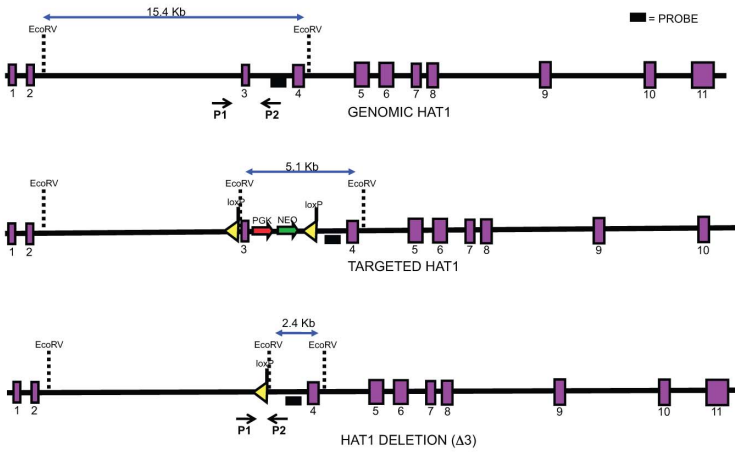

B

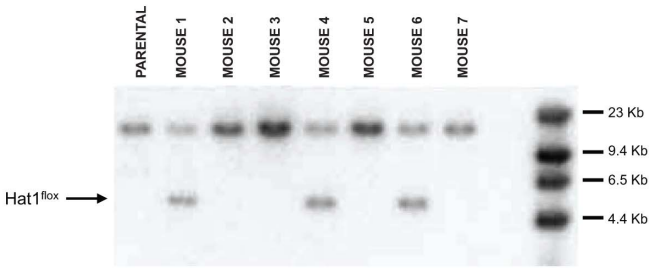

C

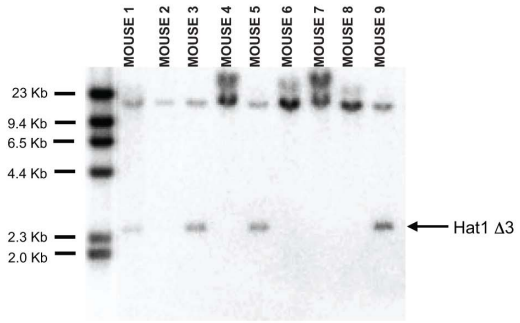

D

HAT1$^{+/-}$ X HAT1$^{+/-}$ (36 MATINGS)				
GENOTYPE	**HAT1$^{+/+}$**	**HAT1$^{+/-}$**	**HAT1$^{-/-}$**	**TOTAL**
PUPS EXPECTED	77	154	77	308
PUPS OBTAINED	77	137	26	240
PUPS VIABLE	77	108	0	185

!

E

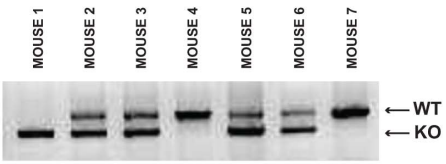

F

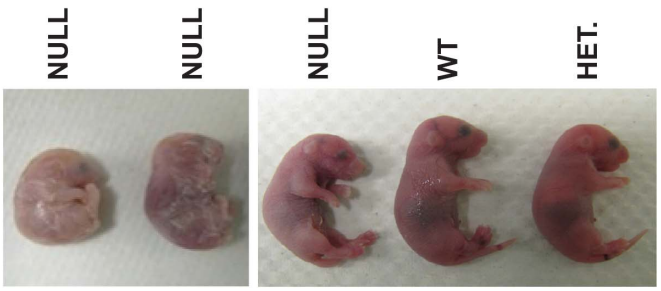

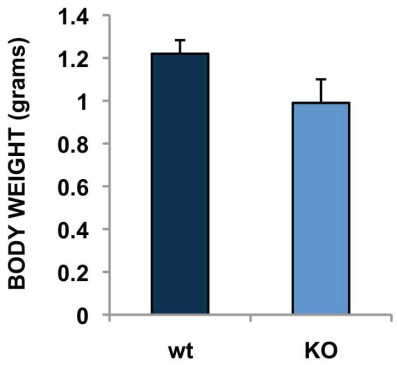

Figure 1. Histone acetyltransferase 1 is essential for viability in mice. A) Schematic diagram of the wild type mouse Hat1 locus (top), the Hat1 locus following integration of loxP sequences flanking intron three (middle) and the Hat1 locus following Cre mediated deletion of exon 3. Exons are represented by purple rectangles. Locations of probes and PCR primers are indicated. (B) Genomic DNA isolated from a parental (C57/bl6) mouse and mice generated from a cross between a chimeric mouse and a wild type mouse was digested with EcoRV and analyzed by Southern blot using the indicated probe. Mice 1, 4 and 6 are $Hat1^{flox/WT}$. C) A $Hat1^{flox/WT}$ mouse was crossed with a mouse that ubiquitously expresses the cre recombinase. Genomic DNA was isolated from mice generated by this cross, digested with EcoRV and analyzed by Southern blot with the indicated probe. Mice 3, 5 and 9 are WT/KO/Cre. D) Table lists the number of expected, obtained and viable pups of the indicated genomes derived from matings of $Hat1^{+/-}$ mice. E) PCR genotyping of a representative litter from a $Hat1^{+/-}$ X $Hat1^{+/-}$ mating. Primers P1 and P2 (see above) were used for amplification. Arrows indicate specific PCR products. F) Representative neonatal pups from $Hat1^{+/-}$ X $Hat1^{+/-}$ matings with the indicated genotype. F) Body weight of pups was measured immediately following birth. Data are derived from 10 pups of each genotype.
doi:10.1371/journal.pgen.1003518.g001

mice to obtain animals that no longer expressed Cre to avoid any undesired phenotypic consequences that could arise from expression of this recombinase. Following backcrossing to remove cre from the genome, $Hat1^{+}/Hat1^{\Delta 3}$ mice were mated and the genotypes of the resulting pups were determined (Figure 1D,E). For simplicity, $Hat1^{\Delta 3}$ mice will be referred to as $Hat1^{-}$. As seen in Figure 1D, based on the number of $Hat1^{+/+}$ pups born, there were slightly fewer than expected $Hat1^{+/-}$ pups and a marked decrease in the number of $Hat1^{-/-}$ pups born. Importantly, all of the $Hat1^{-/-}$ pups were either born dead or died shortly after birth (Figure 1F). In addition, the $Hat1^{-/-}$ pups were approximately 20% smaller than their $Hat1^{+/+}$ counterparts (Figure 1F).

Hat1 is necessary for proper mammalian development

Contrary to what is observed in the other model organisms that have been examined, Hat1 is necessary for viability in mice as the loss of this enzyme results in neonatal lethality. To determine the cause of this lethality, $Hat1^{+/+}$ and $Hat1^{-/-}$ neonates were subjected to pathological examination. Significantly more cells per alveolar septum, which is a measure of fetal lung immaturity, were observed in the $Hat1^{-/-}$ neonates compared to the WT mouse lung (Figure 2A). The lungs from the neonatal $Hat1^{-/-}$ pups also showed a lower overall lung maturation, which was compiled by an assessment of vascularity, aerated lung tissue and septum thickness. These defects in lung development resulted in atelectasis, less aeration and finally lead to respiratory failure (Figure 2A). Lungs of $Hat1^{+/+}$ controls were completely normal (Figure 2A). Hat1 is highly expressed in alveolar as well as lung interstitial cells of $Hat1^{+/+}$ mice (Figure 2B). A highly significant increase in Ki67+ proliferation rates was observed in $Hat1^{-}/^{-}$ compared to $Hat1^{+/+}$ neonates. However cleaved Caspases 3 expression was not altered suggesting that the developmental defect was the result of inappropriate proliferation rather than a defect in apoptosis (Figure 2C,D). The inappropriate proliferation begins early in development and is apparent by 11.5 d.p.c. (Figure S1).

There was another more obvious, but less penetrant, phenotype observed in the $Hat1^{-/-}$ mice. Approximately 25% of the $Hat1^{-/-}$ neonates were born with craniofacial abnormalities. The skeletal structures of $Hat1^{+/+}$ and $Hat1^{-/-}$ neonates were examined by microCT scanning. As seen in Figure 3A, the structure of the skulls from a number of the neonates is highly abnormal. For example, the nasal passages were often missing, having been overgrown with bone. In addition, there were severe defects in the development of the lower jaw structure. These defects included several neonates where the lower jaw was missing in its entirety (Figure 3A, right-hand panels) or examples where the lower jaw bones were fused into a single bone (Figure 3A, middle panel). Defects to the remainder of the skeletal system were less severe. As shown in Figure 3B, while the upper areas of the spine are relatively normal, the structure of the vertebrae in the $Hat1^{-/-}$ neonates degenerate near the base of the spinal column.

To characterize the skeletal defects in more detail, WT and $Hat1^{-/-}$ neonates were stained with Alcian blue and Alizarin red. Alcian blue stains cartilage blue and Alizarin red stains bone purple. Consistent with the microCT results, bone and cartilage staining is similar for the majority of the skeletal system in the WT and $Hat1^{-/-}$ neonates (Figure 3C). However, there are differences in the head. The $Hat1^{-/-}$ neonates showed a marked increase in bone density in the skull and a decrease in the amount of cartilage staining. These results are consistent with the defects seen in lung development as the increased bone density may be the result of osteoblast hyper-proliferation in the absence of Hat1.

To correlate embryonic expression of Hat1 with the skeletal defects observed in the $Hat1^{-/-}$ neonates, whole embryos were stained with α-Hat1 antibodies. As seen in Figure 3D, there is widespread expression of Hat1 protein in the head of embryos. There is also a high level of staining in the abdominal region. Closer examination of Hat1 in the head by immunohistochemistry showed that Hat1 is widely expressed in most tissue types (Figure 3E). Therefore, the phenotypes observed in the $Hat1^{-/-}$ neonates are not strictly linked sites of Hat1 protein expression.

Hat1 is necessary for DNA damage repair and genome stability

The fact that $Hat1^{-/-}$ offspring survive to at least late embryogenesis facilitated the generation of $Hat1^{-/-}$ embryonic fibroblast cell lines to address specific questions about the function of Hat1 in mammalian cells. Mouse embryonic fibroblasts (MEFs) were generated from $Hat1^{+/+}$, $Hat1^{+/-}$ and $Hat1^{-/-}$ embryos (Figure 4A). Western blot analysis using α-Hat1 antibodies confirmed that the MEFs isolated from the $Hat1^{-/-}$ embryos were completely devoid of Hat1 protein (Figure 4A). In addition, heterozygous MEFs (isolated from $Hat1^{+}/Hat1^{-}$ embryos) showed an ~2-fold decrease in Hat1 protein levels.

The loss of Hat1 protein does not influence cell proliferation in any of the model organisms in which it has been genetically deleted (yeast and avian cells). To determine whether Hat1 was important for mammalian cell proliferation, growth curves were measured for the WT, heterozygous and Hat1 null MEFs. As seen in Figure 4B, only minor differences in proliferation between the WT and heterozygous cells were observed. However, Hat1 null cells showed an ~50% decrease in cell proliferation.

To determine whether the decrease in cell proliferation seen with the $Hat1^{-/-}$ MEFs was the result of a specific defect in cell cycle progression, FACS analysis was used to monitor cell cycle distribution. As seen in Figure 4C, $Hat1^{-/-}$ MEFs displayed a moderate accumulation of cells in G2/M suggesting that the decrease in cell proliferation seen in the absence of Hat1 may be, at least in part, due to a G2/M delay in these cells. Taken together, these results indicate that Hat1 protein is not essential for the proliferation of mammalian cells but that cell cycle progression is defective in the absence of this enzyme.

Loss of Hat1 in budding yeast, fission yeast and chicken DT40 cells results in the sensitivity to DNA damaging agents [36,37,38]. To determine whether a role for Hat1 in DNA damage repair is conserved in mammalian cells, WT and $Hat1^{-/-}$ MEFs were

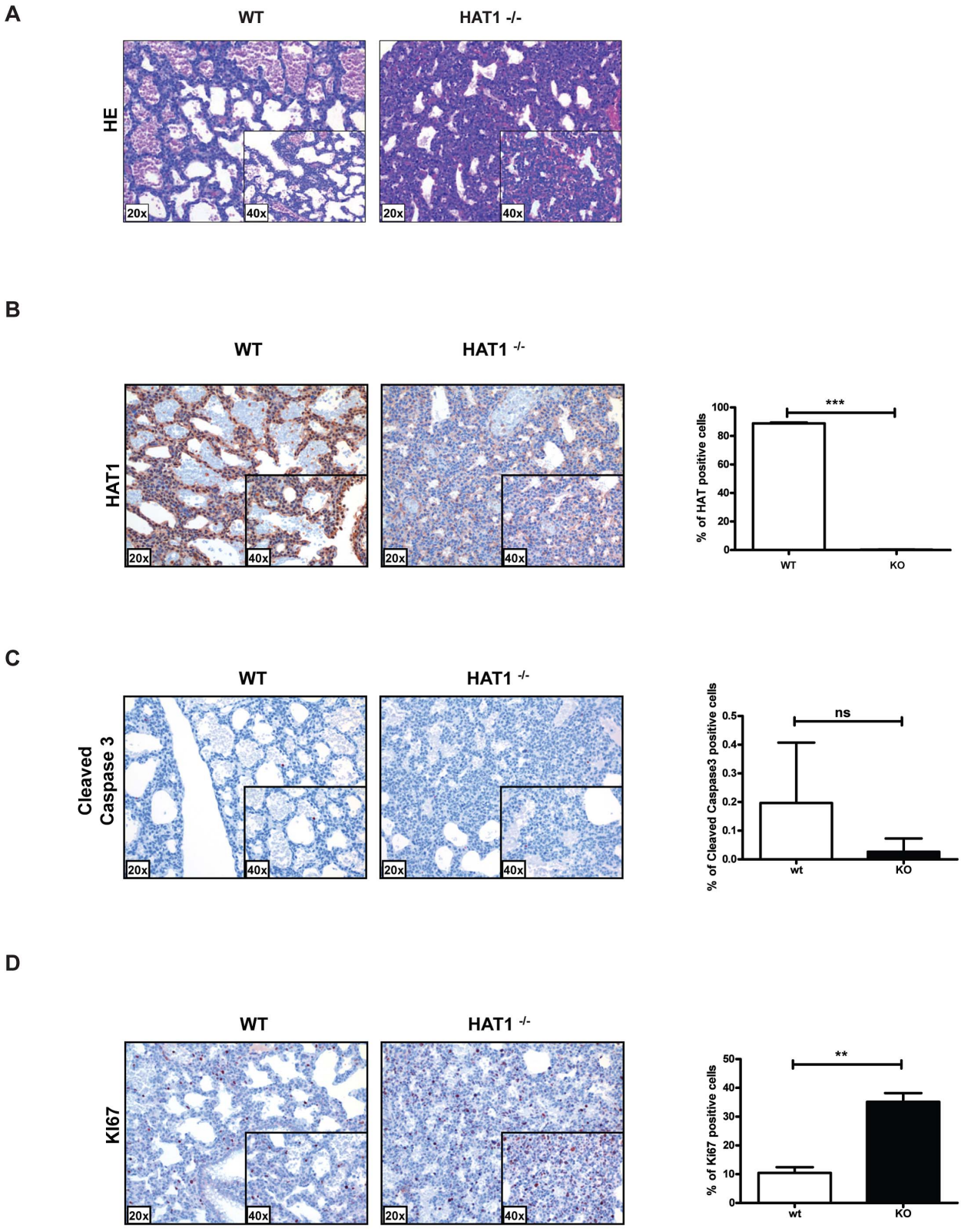

Figure 2. Developmental lung defects result in neonatal death in the absence of Hat1. A) Histologic appearance of lungs from newborn pups obtained from a $Hat1^{+/-+}$ and $Hat1^{-/-}$ mice. Staining was with hematoxylin-eosin; magnification 20×, (inlets ×40). The lungs of $Hat1^{-/-}$ show less aeration, due to thickened mesenchyme resulting in death due to respiratory failure. B) Hat1 is highly expressed in lungs of $Hat1^{+/+}$ but not in $Hat1^{-/-}$ mice; magnification 20×, (inlets ×40) C) Cleaved Caspase3 stained by IHC showed no difference between lungs of $Hat1^{++}$ and $Hat1^{-/-}$ mice; magnification 20×, (inlets ×40) D) Ki67 stained by IHC shows significantly higher proliferation rates in lungs of $Hat1^{-/-}$ mice compared to controls; magnification 20×, (inlets ×40). Quantification was done by HistoQuest software.
doi:10.1371/journal.pgen.1003518.g002

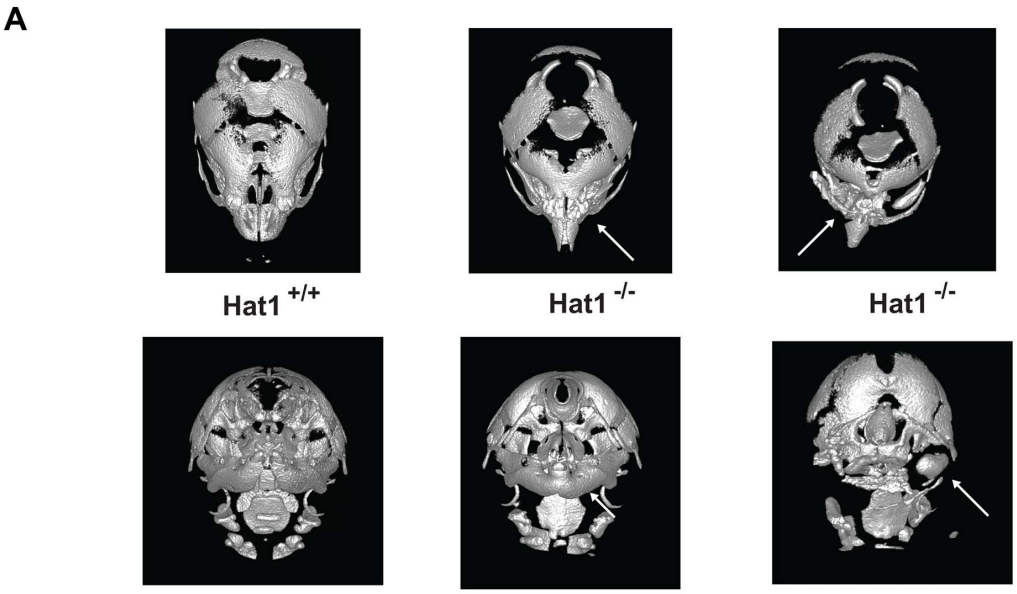
A
Hat1 +/+
Hat1 -/-
Hat1 -/-
B
Hat1 +/+
Hat1 -/-
Hat1 -/-
C
Hat1 +/+
Hat1 -/-
D
Hat1 +/+
Hat1 -/-
E
Hat1+/+
Hat1-/-

Figure 3. Skeletal defects associated with the loss of Hat1. A) Micro CT scans of the heads of neonates with the indicated genotype. Top row shows a dorsal view and bottom row shows a ventral view. Arrows indicate defects in the nasal cavity (top) and jaw structures (bottom). B) Micro CT scans of $Hat1^{+/+}$ and $Hat1^{-/-}$ neonates (as indicated) showing a dorsal view of the entire animal. C) Acian blue and Alizarin red stained $Hat1^{+/+}$ and $Hat1^{-/-}$ neonates. D) $Hat1^{+/+}$ and $Hat1^{-/-}$ embryos (12.5 dpc) were stained with α-Hat1 antibodies. E) Cross section of the head and neck of 11.5 dpc $Hat1^{+/+}$ and (WT) and $Hat1^{-/-}$ embryos stained with α-Hat1 antibody. 2.5× magnification.
doi:10.1371/journal.pgen.1003518.g003

assayed for their sensitivity to a variety of DNA damaging agents. To avoid complications arising from the limited proliferation potential of primary MEFs, immortalized cells lines from $Hat1^{+/+}$ and $Hat1^{-/-}$ primary MEFs were generated via transfection with SV40 large T antigen (proliferation rates of immortalized MEFs are shown in Figure S2). Equal numbers of Hat1 WT and Hat1 null cells were plated and allowed to grow in normal serum containing either methyl methane sulfonate (MMS) or hydroxyurea (HU) or following exposure to ultraviolet radiation (UV) (Figure 4D). The $Hat1^{-/-}$ cells showed a pronounced sensitivity to each of these DNA damaging agents. Hence, Hat1 plays a critical role in DNA damage repair in mammalian cells. Interestingly, the $Hat1^{-/-}$ mammalian cells were sensitive to a broader range of DNA damaging agents. Both yeast and avian cells lacking Hat1 are sensitive to MMS but not UV radiation, suggesting that these $Hat1^{-/-}$ mutants are specifically sensitive to DNA double strand breaks [36,37,38]. However, the $Hat1^{-/-}$ MEF cell lines sensitivity to both types of DNA damage indicating that Hat1 is important for multiple pathways of DNA repair.

As loss of Hat1 resulted in sensitivity to DNA damage, we next explored whether Hat1 was also necessary for proper genome stability. One hallmark of genome instability is the presence of DNA damage in the absence of treatment with DNA damaging agents. $Hat1^{+/+}$ cells showed undetectable levels of endogenous DNA damage, as measured by the presence of γ-H2AX foci (Figure 5A). In contrast, untreated $Hat1^{-/-}$ cells showed numerous γ-H2AX foci. An increase in γ-H2AX levels, both before and after DNA damage, in $Hat1^{-/-}$ MEFs was confirmed by Western blot analysis of whole cell extracts (Figure S3).

To directly visualize genome structure, we generated metaphase spreads from Hat1 WT and Hat1 null cells. Genomic abnormalities that were more frequently observed in the $Hat1^{-/-}$ cells than in the $Hat1^{+/+}$ cells were of several different types (Figure 5B). First, there was a significant increase in chromatid breaks and chromosome fusions. Representative examples are shown in Figure 5C (additional metaphase spreads are shown in Supplemental Figure S4). In this figure, black arrows indicate examples of chromatid breaks or gaps. Red arrows indicate examples of chromosomal fusions. These included both "end-to-end" fusions and unusual "bridge-like" structures where the ends of one chromosome were fused to internal regions of another chromosome. We also observed changes in chromosome number. There was an increase in the number of aneuploid cells that contained a smaller than normal number of chromosomes in the $Hat1^{-/-}$ cells. In addition, there were high numbers of $Hat1^{-/-}$ cells with a 4n DNA content (Figure 5C). In summary, the absence of Hat1 resulted in the presence of high levels of endogenous DNA damage and chromosomal abnormalities, indicating that Hat1 plays an essential role in maintaining genome stability.

Hat1 is essential for the processing of histones H3 and H4 during replication-coupled chromatin assembly

Since its initial discovery and biochemical characterization, Hat1 has been presumed to be involved replication-coupled chromatin assembly through the conserved diacetylation of newly synthesized histone H4. However, evidence to support this hypothesis has been circumstantial [41,49]. The availability of mammalian cells genetically deleted for Hat1 allowed us to definitively address this issue. To directly determine whether Hat1 is involved in the acetylation of histones that are incorporated during replication coupled chromatin assembly, we used iPond to monitor histone modification dynamics on newly replicated DNA [48]. The iPond technique involves pulse-labeling cells with the thymidine analog EdU. The EdU will then be incorporated into DNA that is synthesized during the pulse phase. Following cross-linking, Click chemistry can then be used to covalently attach biotin to the EdU moieties, which allows for the affinity purification of the nascent DNA using streptavidin beads. Western blot analysis of the fractions that elute from the streptavidin beads can then be used to monitor the presence of specific proteins or their modified isoforms on the newly synthesized DNA.

Immortalized $Hat1^{+/+}$ and $Hat1^{-/-}$ MEFs were pulsed with EdU for 15 minutes and then chased with thymidine for 90 minutes. The 90 minute thymidine chase allowed us to distinguish between stably associated chromatin proteins and proteins that associate with newly replicated DNA but then are removed from chromatin after replication. For example, the DNA replication factor PCNA is found associated with nascent DNA immediately following the EdU pulse but is largely absent following the 90 minute thymidine chase while the levels of histone H3 and H4 remain constant (Figure 6A, right panel). It is important to note that the levels of PCNA and histones H3 and H4 do not vary between the $Hat1^{+/+}$ and $Hat1^{-/-}$ MEFs indicating that the rate of EdU incorporation is not altered by the loss of Hat1. As previously reported, the levels of histone H4 lysine 5 and lysine 12 acetylation are high on nascent DNA and then decrease over the 90 minute thymidine chase in the $Hat1^{+/+}$ MEFs [48]. In the $Hat1^{-/-}$ cells there is a striking decrease in the levels of H4 lysine 5 and 12 acetylation on the nascent DNA. The low level of acetylation that remains does not decay over time and is consistent with the observation that parental histones can remain acetylated during their reassembly during DNA replication [50]. These results indicate that Hat1 is likely to be the sole histone acetyltransferase involved in the acetylation of histone H4 lysines 5 and 12 during replication coupled chromatin assembly.

We also examined the dynamics of histone H3 modification during replication-coupled chromatin assembly. In these experiments cells were given either 10 or 30 minute pulses of EdU. Following the 30-minute EdU pulse, the cells were given a thymidine chase for 10, 60 or 120 minutes. Surprisingly, examination of the input samples indicated that loss of Hat1 impacted the steady state levels of acetylation at specific H3 lysine residues (Figure 6B, left panel). When normalized to unmodified histone H3, there was a marked decrease in the overall abundance of acetylated H3 lysine 9 (>2-fold)and a moderate decrease in the acetylation of lysines 18 and 27 (<2-fold). In addition, there was an increase in the level of H3 lysine 14 acetylation (~2-fold).

Importantly, Hat1 also had a significant influence on the dynamics of histone H3 acetylation on nascent DNA. In both $Hat1^{+/+}$ and $Hat1^{-/-}$ cells, total histone H3 levels increased during the pulse, as more nascent DNA was labeled, and then remained constant throughout the chase (Figure 6B, right panel). As expected, PCNA levels increased during the EdU pulseand then decreased during the thymidine chase [48]. Interestingly,

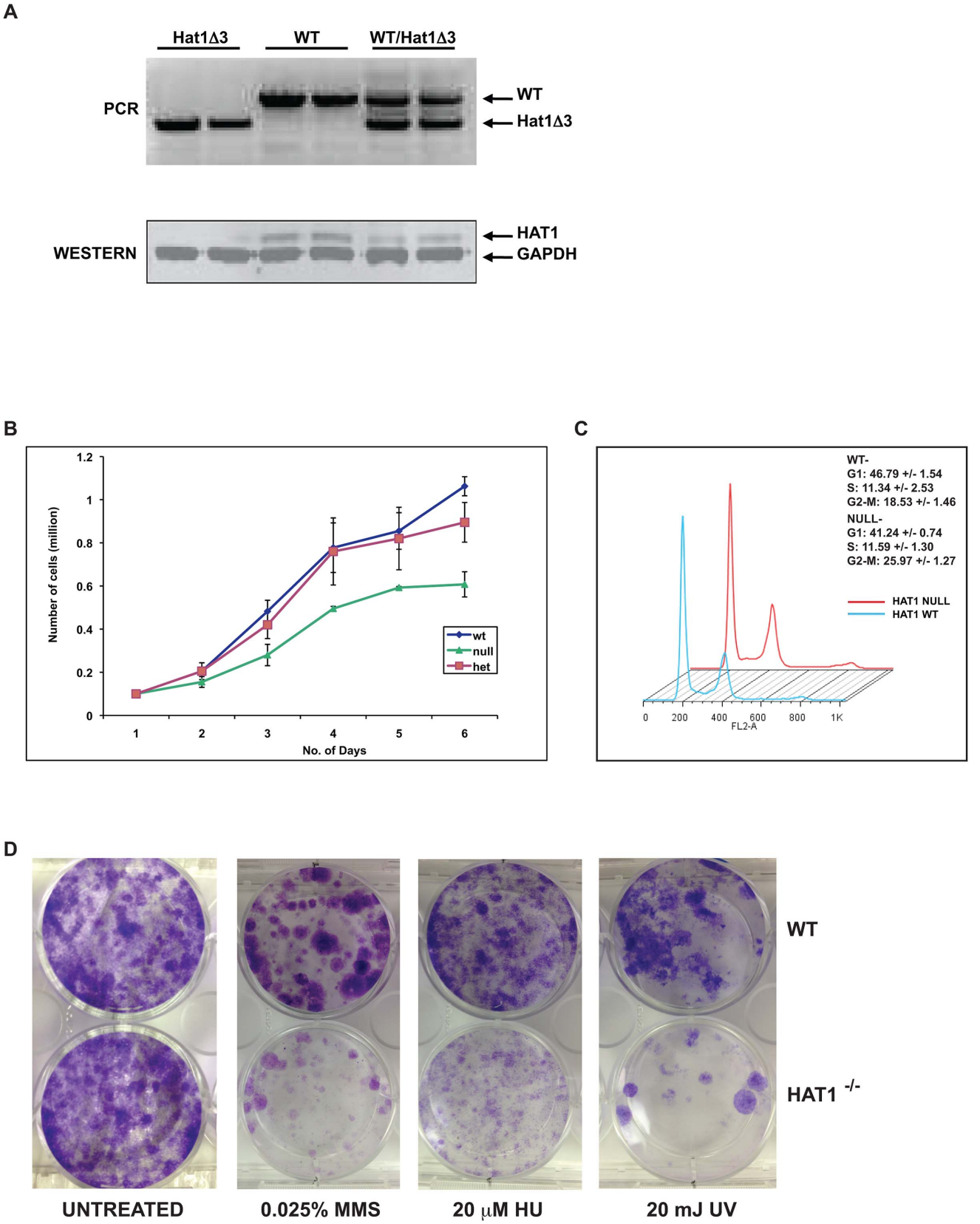

Figure 4. Hat1$^{-/-}$ MEFs display cell proliferation and DNA damage repair defects. A) Hat1$^{+/+}$, Hat1$^{+/-}$ and Hat1$^{-/-}$ primary MEFs were genotyped by PCR as described in the legend to Figure 1. Whole cell extracts from the indicated MEFs were analyzed by Western blots probed with the indicated antibodies. B) Equal numbers of primary MEFs of the indicated genotype were seeded at time zero. Cell numbers were counted at the indicated time points. C) Primary Hat1$^{+/+}$ and Hat1$^{-/-}$ MEFs were stained with propidium iodide and analyzed by FACS. Fraction of cells in each phase of the cell cycle is indicated. D) Immortalized Hat1$^{+/+}$ and Hat1$^{-/-}$ MEFs were grown under the indicated conditions. Plates were photographed after crystal violet staining.
doi:10.1371/journal.pgen.1003518.g004

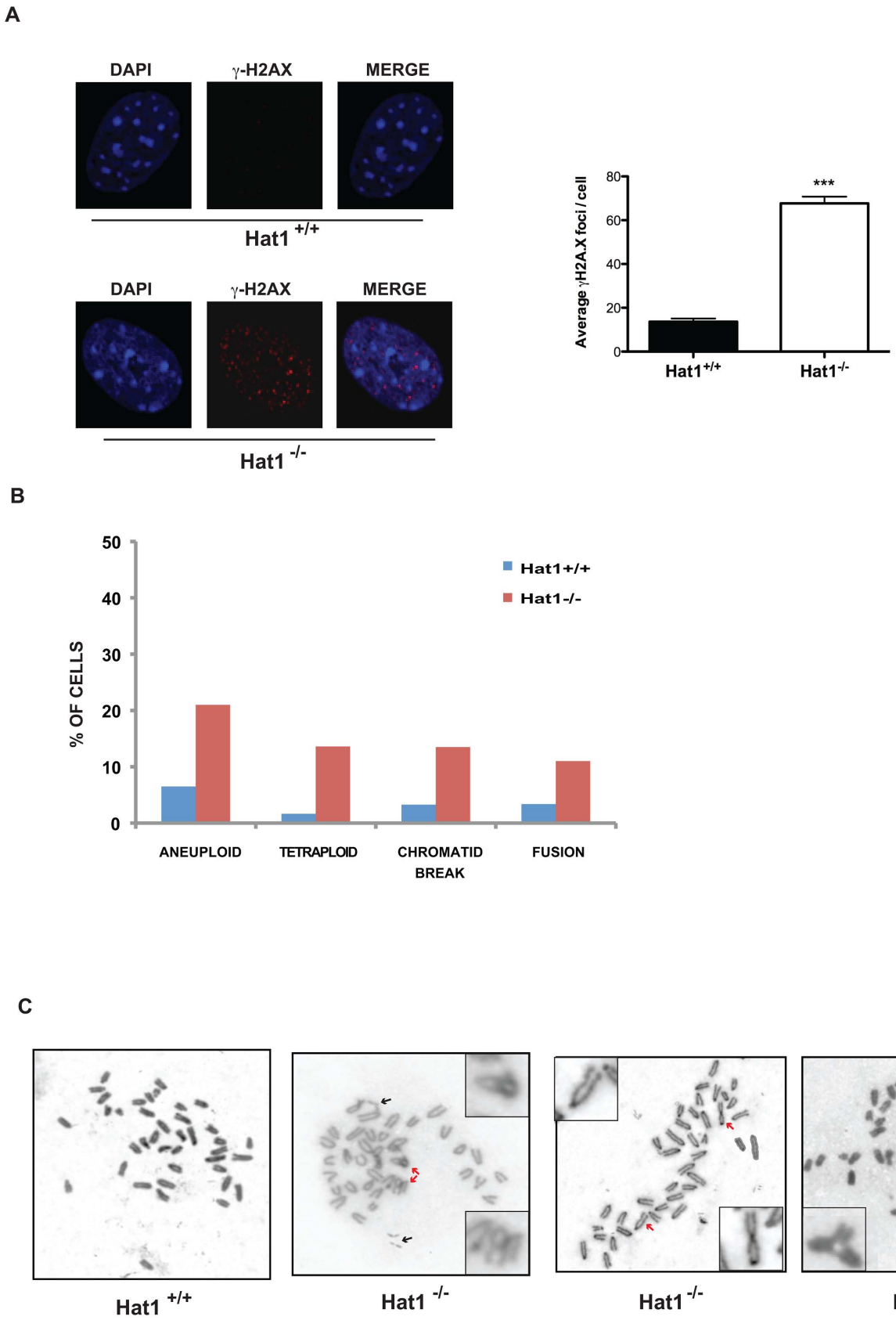

Figure 5. Hat1 is essential for maintaining genome stability. A) Hat1$^{+/+}$ and Hat1$^{-/-}$ MEFs were stained with either DAPI or α-γH2AX antibodies as indicated (left). Visible γH2AX foci were counted in 12 cells of each genotype (right). B) Metaphase spreads from Hat1$^{+/+}$ and Hat1$^{-/-}$ MEFs were analyzed for chromosome number and the presence of breaks and fusions. The percentage of cells containing the indicated chromosomal abnormality is given. The number of spreads analyzed was 56 (Hat1$^{+/+}$) and 112 (Hat1$^{-/-}$). C) Metaphase spreads were generated from Hat1$^{+/+}$ and Hat1$^{-/-}$ MEFs. Insets show enlarged views of selected abnormal chromosomes. Red arrows indicate examples of chromosome fusions and blue arrows indicate chromosome breaks.
doi:10.1371/journal.pgen.1003518.g005

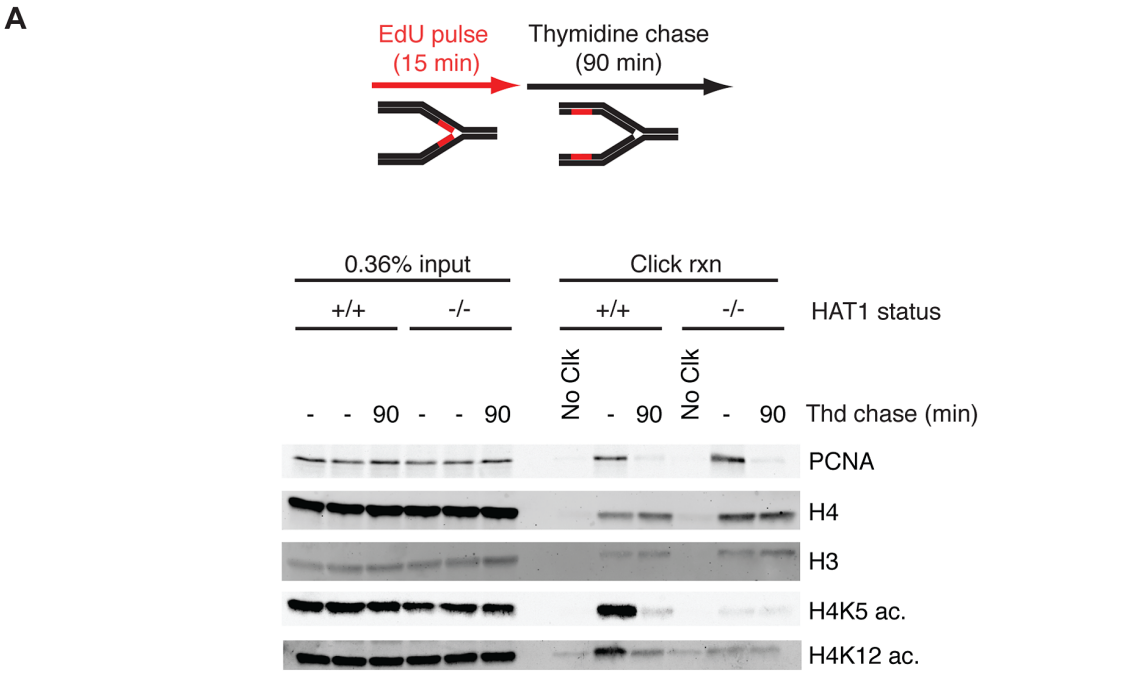
A
EdU pulse
(15 min)
Thymidine chase
(90 min)
0.36% input
Click rxn
+/+
-/-
+/+
-/-
HAT1 status
No Clk
No Clk
- - 90 - - 90
- 90
- 90
Thd chase (min)
PCNA
H4
H3
H4K5 ac.
H4K12 ac.

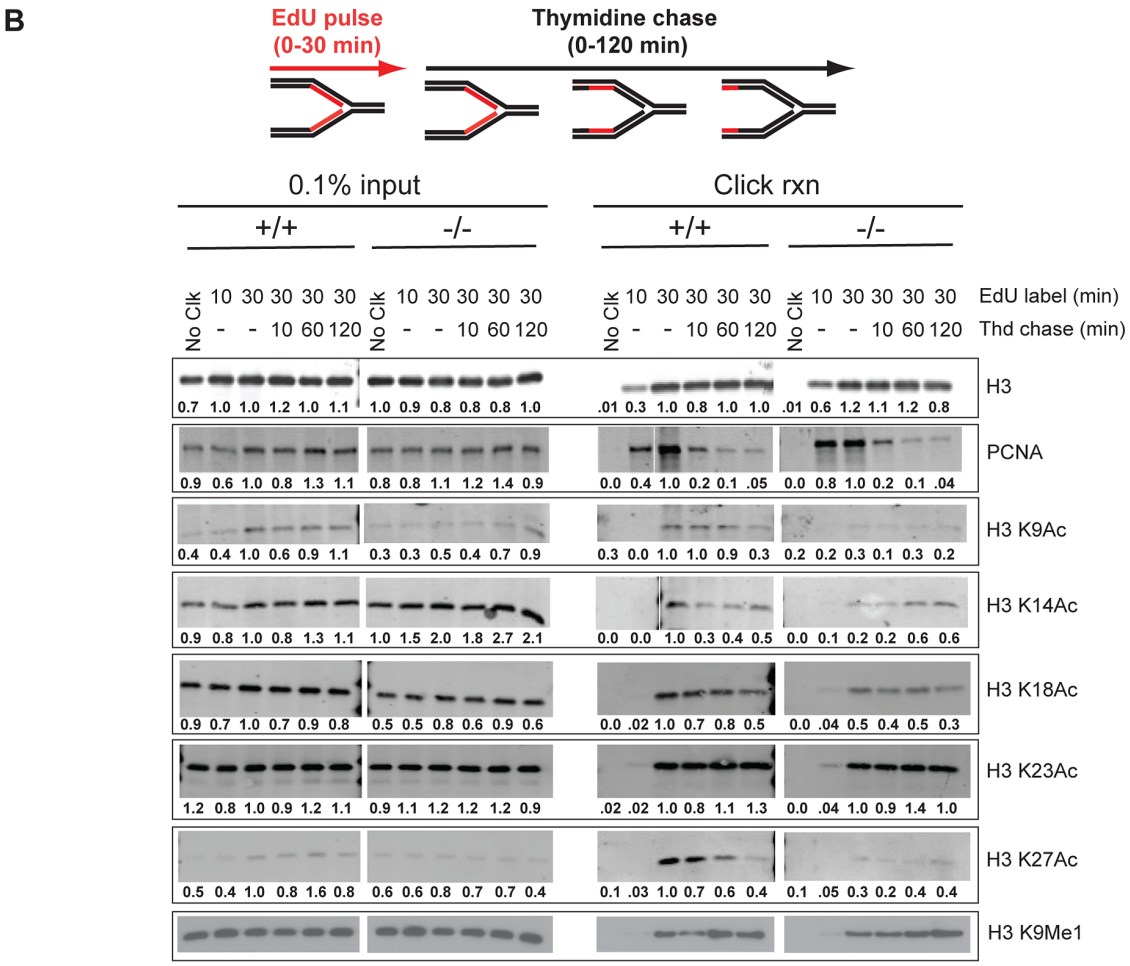
B
EdU pulse
(0-30 min)
Thymidine chase
(0-120 min)
0.1% input
Click rxn
+/+
-/-
+/+
-/-
No Clk 10 30 30 30 30
- - 10 60 120
EdU label (min)
Thd chase (min)
H3
PCNA
H3 K9Ac
H3 K14Ac
H3 K18Ac
H3 K23Ac
H3 K27Ac
H3 K9Me1

Figure 6. Hat1 is required for the acetylation of histones H3 and H4 deposited during replication-coupled chromatin assembly. A and B) Hat1$^{+/+}$ and Hat1$^{-/-}$ MEFs were pulse-labeled with EdU and chased with thymidine as schematically depicted at the top of each panel. Samples were isolated at the indicated time points and proteins associated with nascent DNA were resolved by SDS-PAGE following affinity purification of EdU-labeled DNA (iPond). The indicated amounts of the input fractions (prior to affinity purification) are on the left-hand side of each panel. Samples eluted from the affinity purification resin are on the right-hand side of each panel. In all cases, the respective Hat1$^{+/+}$ and Hat1$^{-/-}$ samples were analyzed on the same gel (separated by a MW standard lane that has been removed). Western blots were probed with the antibodies indicated on the right. Numbers below each lane indicate the normalized intensity of the band as determined using Licor software. Each sample was normalized to the level of unmodified histone H3. The intensity observed in the 30′ pulse sample was arbitrarily set to 1.0. No Clck indicates control samples that were not biotin labeled.
doi:10.1371/journal.pgen.1003518.g006

distinct patterns of acetylation dynamics were observed for subsets of the lysine residues on the NH_2-terminal tail of histone H3. The acetylation of H3 lysines 14 and 23 largely mirrored that of bulk H3 where the levels remained relatively stable during the thymidine chase. This acetylation was not significantly influenced by the loss of Hat1. A second pattern, seen for lysines 9, 18 and 27, displayed kinetics similar to those seen for H4 lysine 5 and 12 acetylation where acetylation increased during the EdU pulse and then decayed to a basal level during the thymidine chase. Surprisingly, the acetylation of lysines 9, 18 and 27 was sensitive to the loss of Hat1 and showed only a basal level of acetylation that did not decay during chromatin maturation. Therefore, in addition to its expected effects on histone H4, the presence of Hat1 is also essential for acetylation of histone H3 deposited during replication-coupled chromatin assembly.

In addition to acetylation, newly synthesized histone H3 is also monomethylated on lysine 9. In fact, H3 lysine 9 monomethylation appears to be precede any other modifications on H3 and H4 [43,51]. H3 lysine 9 monomethylation was apparent on nascent DNA and then increased during the course of the thymidine chase (Figure 6B). The levels and kinetics of H3 lysine 9 monomethylation were not influenced by the absence of Hat1. Hence, the mono-methylation of newly synthesized histone H3, which is thought to occur prior to its association with the Hat1 complex, is not dependent on Hat1.

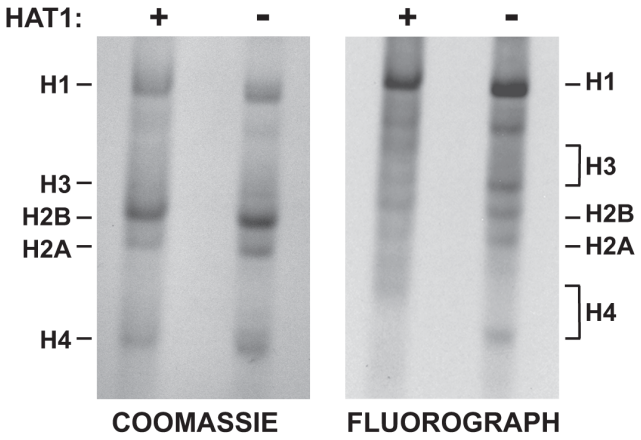

Figure 7. Hat1 is essential for the acetylation of newly synthesized histones. Hat1$^{+/+}$ and Hat1$^{-/-}$ MEFs were pulse-labeled with ^{3}H-lysine for 12 minutes. Histones were then isolated and resolved by Acid-Urea (AU) gel electrophoresis. Total protein was visualized with Coomassie blue staining and radio-labeled proteins visualized by fluorography (as indicated). The mobility of each histone is indicated. The brackets indicate the regions of mobility for the acetylated isoforms of histone H4 and histone H3.
doi:10.1371/journal.pgen.1003518.g007

Hat1 is essential for the acetylation of newly synthesized histones

The effect of Hat1 on the acetylation state of histones incorporated during replication-coupled chromatin assembly suggested that Hat1 is modifying newly synthesized molecules. To test this, Hat1$^{+/+}$ and Hat1$^{-/-}$ MEFs were briefly pulsed with ^{3}H-lysine to radiolabel newly synthesized proteins. Histones were then purified from these cells by acid extraction and resolved by acid-urea (AU) gel electrophoresis. AU gels are capable of resolving the acetylated isoforms of histones where the addition of each acetyl groups causes a successive decrease in electrophoretic mobility. The AU gels were stained with coomassie blue and then processed for fluorography (Figure 7). The coomassie blue stained gel shows the mobility and distribution of bulk histones. The absence of Hat1 had little effect on the bulk histones. Examining the radiolabeled histones provides specific information on the distribution of acetylated isoforms of the newly synthesized histones. In Hat1 WT cells, essentially all of the newly synthesized histone H4 migrated at a position consistent with the diacetylated state, in agreement with previous reports. However, in the absence of Hat1, it appeared that nearly all of the newly synthesized histone H4 was found to be unacetylated. This conclusively demonstrates that Hat1 is involved in the acetylation of newly synthesized histone H4 and appears to be the only enzyme responsible for this pattern of acetylation.

Surprisingly, loss of Hat1 also altered the distribution of newly synthesized histone H3. While histone H3 is more difficult to resolve in AU gels, newly synthesized histone H3 isolated from Hat1 WT cells showed a distribution of isoforms. In the absence of Hat1, there was a decrease in the modified isoforms and a marked increase in unacetylated newly synthesized histone H3. This is consistent with the effect of Hat1 on the acetylation state of H3 deposited during replication-coupled chromatin assembly and suggests the possibility that the proper processing of newly synthesized histone H3 is linked to processing and acetylation of newly synthesized histone H4.

Discussion

The results presented here provide definitive evidence for the role of mammalian Hat1 in the diacetylation of newly synthesized histone H4 during replication-coupled chromatin assembly. Surprisingly, Hat1 is also essential for the acetylation state of histone H3 incorporated during replication-coupled chromatin assembly. This processing of newly synthesized histones H3 and H4 may be a critical aspect of the regulation of cell proliferation as the absence Hat1 results in defects in lung and cranio-facial development. Further, the absence of Hat1 causes pronounced defects in DNA damage repair and genome stability. Therefore, type B histone acetyltransferases and the acetylation of newly synthesized histones play a fundamentally important role in mammalian cell growth and development.

In vivo functions of Hat1

Hat1 function has been studied in a number of model organisms, including *S. cerevisiae*, *S. pombe* and chicken DT40 cells. The absence of Hat1 in these organisms did not have any significant impact on overall cell proliferation [20,21,34,37,38]. Combined with the absence of a significant phenotype arising from mutating histone H4 lysine 5 and 12 in budding yeast had led to the idea that the evolutionarily conserved diacetylation pattern on newly synthesized histone H4 is either not involved in chromatin assembly or plays only an accessory or specialized role in this process [52,53,54]. The current analysis of mammalian Hat1 indicates that, while Hat1 is essential for viability in the mouse, it is not essential for cell proliferation. Indeed, the loss of viability seen in the $Hat1^{-/-}$ neonates appears to be the result of specific developmental defects that result in cellular hyperproliferation. It should be stressed that the direct cause of the morphological defects observed in the $Hat1^{-/-}$ neonates is not known. However, potential effects on development due to alterations in chromatin assembly are consistent with the recent report that a mutation in the replication-coupled histone H3 variant, H3.1, or mutations in the histone chaperone CAF-1 cause specific neural development defects in *C. elegans* [55]. Hence, while the current study does not address whether the essential function of Hat1 is related to its impact on histone deposition or through an as yet unidentified cellular role, the use of developmentally complex organisms may facilitate our understanding of the *in vivo* consequences of manipulating chromatin assembly pathways.

A function for Hat1 in DNA damage repair appears to be evolutionarily conserved. However, Hat1 appears to play a more extensive role in mammalian cells than in the other organisms examined. For example, deletion of *HAT1* in S. cerevisiae (when combined with specific mutations in histone H3) results in sensitivity to MMS and to the exogenous expression of restriction endonucleases [36]. Likewise, loss of Hat1 in S. pombe and chicken DT40 cells increases sensitivity to MMS. However, loss of Hat1 in these organisms does not increase sensitivity to UV exposure suggesting that the role of Hat1 is limited to double strand break repair [37,38]. However, the $Hat1^{-/-}$ MEFs display sensitivity to both double strand and single strand damaging agents. Importantly, mammalian Hat1 mutants also display profound defects in genome instability, which has not been observed elsewhere. These observations suggest that mammalian DNA repair-linked chromatin assembly pathways may be more dependant on the proper modification state of newly synthesized histones or that Hat1 may play a more direct and integral role in DNA repair mechanisms in mammalian cells. In addition, the observation of chromosomal fusions in the absence of Hat1 may reflect a disruption of telomere structure, which is another property of Hat1 mutants that is evolutionarily conserved [56,57].

The process of chromatin assembly is both spatially and temporally dynamic, which has complicated efforts to definitively demonstrate that Hat1 is involved in histone deposition. The alterations in histone acetylation patterns observed on nascent DNA in $Hat1^{-/-}$ MEFs directly links Hat1 to replication-coupled chromatin assembly. Combined with two other recent reports, the Hat1 enzyme has now been directly linked to the process of chromatin assembly in three distinct contexts. Consistent with the DNA double strand break sensitivity of *hat1*Δ budding yeast, the absence of Hat1 resulted in defects in the reassembly of chromatin structure that is linked to the recombinational repair of DNA double strand breaks [39]. In addition, a genetic screen in yeast identified Hat1 as a factor important for replication-independent chromatin assembly (or histone exchange) [40]. These observations suggest that the acetylation of newly synthesized histones is a ubiquitous feature of all chromatin assembly pathways consistent with the presence of the lysine 5 and 12 diacetylation pattern on both histones H3.1 and H3.3 [43,50,51,58,59,60].

While it is clear that Hat1 is involved in chromatin assembly, the precise function of the lysine 5 and 12 diacetylation pattern on newly synthesized histone H4 has not been identified. Recent reports have suggested that this diacetylation pattern promotes the nuclear import of new H4 perhaps through increasing interactions with Importin 4 [42,51]. However, the analysis of histone dynamics on nascent DNA presented here suggest that in the absence of diacetylation on newly synthesized H4, the level and kinetics of H3 and H4 deposition is similar. This suggests that any impact on nuclear import is not critical for histone deposition during DNA replication in mammalian cells.

Processing of newly synthesized histone H3

The iPond analysis of the acetylation state of histone H3 during replication-coupled chromatin assembly indicated that histone deposition is accompanied by the transient acetylation of histone H3 lysines 9, 18 and 27. The fact that decay of these acetylations is similar to that of H4 lysine 5 and 12 acetylation and that these acetylations are dependent on Hat1 suggests that this acetylation pattern may be a hallmark of chromatin assembly in murine cells. However, this pattern of acetylation does not match those observed on soluble histones in other mammalian systems. For example, newly synthesized histone H3.1 in HeLa cells appears to be unacetylated while newly synthesized H3.2 and H3.3 showed low levels of acetylation on all of the lysine residues in the H3 NH_2-terminal tail [50]. In addition, soluble histones H3.1 and H3.3 from HeLa cells showed low levels of acetylation on lysine 9 and moderate levels of acetylation on either lysine 14 or 18 (lysine 27 was not examined) [58,60]. There may be a number of reasons for this discrepancy. First, acetylation patterns on newly synthesized histone H3 are not conserved across eukaryotes as is the case for histone H4 [61]. Hence, newly synthesized histones in murine cells may be acetylated in a pattern that is different from human tissue culture cells. Second, all of the newly synthesized histones in a cell may not be equivalent. There may be separate pools of soluble histones that have specific modification patterns and these separate pools may be directed to specific chromatin assembly pathways. Finally, soluble histones may not be entirely representative of newly synthesized histones as these pools are likely to contain histones that have been removed from chromatin and, thus, will contain patterns of modification based on their previous location in chromatin.

Hat1 and the processing of newly synthesized histones

Soluble (and likely cytosolic) histones H3 and H4 are found in multiple discreet complexes [43,44,45,46,51,62]. These complexes contain different sets of associated factors and specific post-translational modification patterns on the histones. This has led to the suggestion that newly synthesized histones H3 and H4 are processed in a sequential pathway that ultimately leads to their deposition on nascent DNA [1,43,51,63]. These analyses also suggest that Hat1 plays an early role in this processing pathway. However, a number of steps in the processing of new H3 and H4 appear to occur before its association with Hat1 based on the fact that histone H4 can be found in complexes before it is acetylated on lysines 5 and 12. For example, cytosolic histones H3 and H4 can be found in separate complexes that contain heat shock factors containing heat shock factors (HSC70 and HSP90, respectively).

In fact, the first post-translational modifications on new H3 and H4 occur before these complexes are formed as the H3 associated with HSC70 contains monmethylation on lysine 9 and both H3 and H4 contain poly-ADP-ribosylation. Subsequent complexes, which contain H3 and H4 in association with histone chaperones or nuclear import factors, contain histone H4 that is diacetylated on lysines 5 and 12 indicating that association of the newly synthesized histones with Hat1 occurs upstream of these factors [43,51].

Our data support many aspects of this model. For example, the monomethylation of newly synthesized histone H3 lysine 9 is independent of Hat1 consistent with the occurrence of this modification on H3 molecules prior to their association with Hat1. In addition, acetylation of newly synthesized histone H3, which is likely to occur following nuclear import, is highly dependent on the presence of Hat1. The substrate specificity of Hat1 is highly conserved across a wide range of eukaryotic organisms. Hence, the effect of Hat1 on the acetylation of histone H3 is not likely to be due to the direct acetylation of H3 by Hat1. Rather, Hat1 may be necessary for the integrity of the newly synthesized histone processing pathway [45]. This is supported by our observation that the modification state of newly synthesized histone H3 is altered in the absence of Hat1 (Figure 7). An alternative, and not mutually exclusive, explanation for the apparent impact of Hat1 on the acetylation state of histone H3 during replication-coupled chromatin assembly is that the absence of Hat1 may have a downstream effect on the acetylation of chromatin associated histone H3. This is suggested by the significant decrease in the steady state level of acetylation on H3 lysines 9, 18 and 27 in $Hat1^{-/-}$ cells. Whether it is the presence of Hat1 or the acetylation state of histone H4 that is the key factor in promoting the downstream acetylation of newly synthesized histone H3 will be an interesting question to answer.

Materials and Methods

Generation of conditional Hat1 knockout mice

A targeting vector, WT/flox animals and $Hat1^{+/-}$ animals generated using Cre - loxP methodology with support of Ozgene Inc. (Australia). Targeting vector was designed with a 5′ homology arm (6.9 kb), a 3′ homology (6.6 kb), two loxP sites flanking exon 3 and two FRT sites flanking the PGK –neo cassette located downstream of exon 3. All fragments were generated by PCR using 129Sv/J genomic DNA and confirmed with mapping and sequencing to ensure their correct organization. The targeting vector was electroporated in Bruce 4 embryonic stem cells to generate chimeras. Chimeras were then crossed with C57Bl6/J mice to generate Wt/flox animals. To generate global deletion, Wt/flox animals were bred with Ozcre animals expressing cre recombinase to establish heterozygous mice (WT/KO/CRE).

Animals and MEFs were genotyped by either Southern blotting or PCR designed to detect both WT and Hat1Δ3 alleles. Genomic DNA was extracted by standard methods using phenol: chloroform isolation and genotypes were determined by PCR using the following pairs of primers P1: 5′-GCC TGG TGA GAT GGC TTA AAC -3′ and P2: 5′-GCA AGT AGT ATG ACA AGA GGT AGG -3′. PCR was performed under following conditions; 95°C for 50 min followed by 29 cycles at 95°C for 40 sec., 54.6°C for 30 sec. and 72°C for 60 sec. and final extension for 5 min. at 72°C. The WT and mutant alleles yielded product sizes of 916 bp and 478 bp respectively.

All animal use was performed according to the guidelines of The Ohio State University Institutional Animal Care and Use Committee (IACUC) under permit number 2007A0094.

Generation of primary and immortalized mouse embryonic fibroblasts

e12.5 to e14.5 embryos were dissected from the pregnant female, voided of their internal organs and disaggregated using an 18-gauge syringe. The embryonic tissues were then plated onto 100 mm tissue culture plates and passaged upon confluency. Passage 0 refers to the stage when the embryos were seeded on the plate and every subsequent splitting is referred to as passage 1, 2, 3, etc. These cell lines were cultured and maintained at 37°C using humidified air supplemented with 5% CO_2 in Dulbecco's modified Eagle medium (DMEM-Sigma) with 15% fetal bovine serum (FBS-Gibco) and 1X Pen/Strep antibiotics (Sigma). Genotypes were confirmed twice by PCR using yolk sac and the resultant cell lines. SV40 T ag immortalized MEFs (iMEFs) were derived from primary WT and Hat1 mutant embryonic day 13.5 embryos. To establish iMEFs, early passage cells were transformed with SV-40 T antigen containing plasmid pBSSVD2005 (ADDGENE, Cambridge, MA). Early passage cells (P>3) were seeded at 25%/well in 6 well plates and transfected with 2 ug of expression vector using Fugene reagent (Roche). Cells were harvested and seeded into 10 cm dishes after 48 hrs of transfection. The cells were split at 1 in 10 dilutions until passage 5.

Immunohistochemistry

Whole mouse embyro staining was performed by standard procedure. Briefly, Embryos (e.12.5) were fixed in PBS containing 4% Paraformaldehyde (PFA) overnight at 4°C and bleached with 5% H_2O_2 in methanol for 4 hr, blocked with PBSMT buffer (3% instant skim milk powder, 0.1% Triton X-100 in PBS) for 2 hr at room temperature and simultaneously incubated with primary antibodies against Hat1 (Abcam, 1/50 dilution) in PBSMT buffer at 4°C over night. After extensive washes in PBSMT buffer for 5 hrs at 4°C followed by incubation with HRP conjugated secondary antibody(1/100 dilution). Finally, embryos were extensively washed in blocking buffer and developed in DAB solution (0.3 mg/ml DBA, 0.5%$NiCl_2$). Immunocytochemsitry was performed by standard procedures. Hematoxylin/Eosin and PAS staining were performed with staining kits from DAKO. Slides were also stained with primary antibodies against Hat1 (Abcam, 1/50 dilution), α-Ki67 (Novocastra, NCL-KI67-P) and anti-Cleaved Caspase 3 (Cell Signaling, #9661)Images were captured with a Zeiss AxioImager Z1 microscope. The stainings were quantified with the HistoQuest and TissueQuest software (TissueGnostics GmbH, Vienna, Austria, www.tissuegnostics.com).

Colony formation assay

Immortalized MEFs (2000/well) were seeded in 6-well plates overnight to adhere and, next day, cells were exposed to either 20 mJ UV radiation, MMS (0.025%) or HU (20 μM). Cells were incubated in complete culture medium for 12 days at 37°C in a humidified 5% $C0_2$ chamber. The cells were then rinsed with PBS, fixed in methanol and stained with crystal violet. Following a 20 min. rinse with tap water, the plates were photographed.

Cytogenetic analysis of metaphase chromosomes

Metaphase chromosomes were prepared from WT and $Hat1^{-/-}$ primary mouse embryonic fibroblasts using standard cytogenetic procedures. Primary MEFs were cultured and treated with 500 ng colcemid for 4 hr to arrest the actively replicating cells in the metaphase stage. The cells were rinsed with PBS and trypsinized to collect the cell pellet. The cell pellet was exposed to hypotonic swelling with 0.056% KCl at 37°C for 15 min. followed by

fixation of nuclei with methanol/glacial acetic acid mix (3:1) and dropping nuclei on pre-warmed slides. The dried slides were stained with Giemsa and mitotic index was visualized with a light microscope. Experiments were performed with two sets of MEFs from each genotype.

Micro-computed tomography (mCT) analysis

WT and Hat1$^{-/-}$ mCT images were captured using a Siemens Inveon microCT+SPECT (Siemens Preclinical, Knoxville, TN). Each individual image comprised 400 projections/360° at 0.9 degree intervals and was captured with X-ray source energy of 80 KV, 500 mA. Estimated resolution effective pixel size was 19.40 μm. Images were analyzed by using Inveon research workplace version 2.1 software.

Bone and cartilage staining

WT and Hat1$^{-/-}$ neonatal pups were eviscerated and the skin was removed before fixing in 95% ethanol for 72 hrs. Embryos were then stained in Alcian blue 8GX solution (15 mg Alcian blue, 80 ml 98% ethanol, 20 ml acetic acid) overnight. After a 24 hour rinse in 95% ethanol, they were transferred to 1% KOH for 6 hrs. After overnight staining in Alizarin red solution (50 mg/l Alizarin red in 2% KOH), skeletons were cleared in the following ratios of 2% KOH to glycerol; 80:20, 60:40, 40:60 and indefinitely stored in 20% KOH/80% glycerol. Photographs were taken by using a dissecting microscope [64].

iPond

1.5×10^8 iMEFs were incubated with 10 μM EdU (Invitrogen) for various time periods. For thymidine chase experiments, EdU labeled cells were washed once with pre-equilibrated (temperature, pH and thymidine) medium and then incubated with 10 μM thymidine for various times. After labeling and/or pulse-chase, cells were cross-linked with 1% formaldehyde/PBS for 20 min, quenched with 1.25 M glycine and scraped off the plates and collected. After washing three times with PBS, the cell pellet was then resuspended in 0.25% Triton-X 100/PBS to permeabilize in room temperature. Cells were spun down after permeabilization and washed first with 0.5% BSA/PBS and then with PBS. Cells were incubated with either click reaction buffer (10 μM biotin azide, 10 mM sodium ascorbate, 2 μM $CuSO_4$ in PBS) or control buffer (as reaction buffer but DMSO added instead of biotin azide) at a concentration of about 3×10^7 cells/ml for 1 hr at room temperature, protected from light. After incubation, cells were again washed with 0.5% BSA/PBS and PBS. Cells were then lysed with lysis buffer (1% SDS, 50 mM Tris pH 8.0, 1 μg/ml Leupeptin, 1 μg/ml aportinin) at a concentration of 1.5×10^7 cells/μl. Samples were then sonicated using the Bioruptor (Diagenode) for 30 sec on and 60 sec off per cycle for 12 cycles. Samples were then spun down and supernatant was filtered through 90 micron nylon mesh (Small Parts) and diluted with PBS containing protease inhibitors. An aliquot of the lysate was kept as input, the rest was incubated with prewashed Streptavidin-agarose beads (Novagen) for 16 hrs at 4°C. The beads were then washed once with lysis buffer, once with 1 M NaCl, and twice with lysis buffer. Beads were boiled with 2× SDS dye for 25 min at 95°C. Proteins were resolved by SDS-PAGE and detected by western blot. Antibodies used in this study include: PCNA (Santa Cruz Biotechnology), H3 K9Ac (Abcam), H3 K14Ac (Abcam), H3 K18Ac (Upstate), H3 K23Ac (Upstate), H3 K27Ac (Upstate), H4 K5Ac (Abcam), H4 K12Ac (Abcam).

Analysis of newly synthesized histones

For the electrophoretic analysis of newly synthesized histones, cultured MEF cells were pulse-labeled with 80 μCi/ml [^{3}H]lysine (PerkinElmer Life Sciences) for 12 min, as described previously [65]. To inhibit histone deacetylation, labeling was performed in the presence of 50 mM sodium butyrate and 1 μM Trichostatin A. Acid-soluble nuclear proteins were prepared according to published protocols [66]. Fluorography of labeled histones after separation in acid-urea polyacrylamide gels was performed as described previously [67,68].

Supporting Information

Figure S1 Hat1$^{-/-}$ embryos display early defects in lung development. The histological appearance of lungs isolated from 11.5 d.p.c. Hat1$^{+/-}$ and Hat1$^{-/-}$embryos. Hat1$^{+/-}$ embryos were used because the Hat1$^{+/+}$ embryos morphology was disrupted during analysis. The Hat1$^{+/-}$ embryos do not display any viability defects at birth. Staining was with hematoxylin eosin (H+E), α-Hat1 and α-Ki67 antibodies (as indicated). Magnification was 20×. Hat1 and Ki67 staining was quantitated with Histoquest software.
(EPS)

Figure S2 Growth rates of immortalized MEFs. Immortalized Hat1+/+ and Hat1$^{-/-}$ MEFs were seeded in wells (2000 cells/well). At the indicated time points, viable cells were measured by MTT assay.
(EPS)

Figure S3 Hat1$^{-/-}$ cells display increased levels of γH2AX. Immortalized Hat1$^{+/+}$ and Hat1$^{-/-}$ MEFs were treated with 50 mJ UV and then aliquots were harvested at the indicated times. Whole cell extracts were prepared and analyzed by Western blot probed with the indicated antibodies.
(EPS)

Figure S4 Genomic instability in Hat1$^{-/-}$ MEFs. Metaphase spreads were generated from Hat1$^{-/-}$ MEFs. A) Metaphase spreads showing examples of chromatid breaks and chromosome fusions (marked by arrows). B) Metaphase spreads showing examples of aneuploidy and tetraploidy.
(EPS)

Acknowledgments

We would like to thank Dr. Nyla Hereema for helpful advice and the use of the OSU Clinical Cytogenetics Facility.

Author Contributions

Conceived and designed the experiments: PN ZG BS CD ATA DC LK MRP. Performed the experiments: PN ZG BS CD PAAG MS LK. Analyzed the data: PN ZG BS CD PAAG MS ATA DC LK MRP. Wrote the paper: PN ZG DC ATA LK MRP.

References

1. Das C, Tyler JK, Churchill ME (2010) The histone shuffle: histone chaperones in an energetic dance. Trends Biochem Sci 35: 476–489.
2. Alabert C, Groth A (2012) Chromatin replication and epigenome maintenance. Nat Rev Mol Cell Biol 13: 153–167.
3. Avvakumov N, Nourani A, Cote J (2011) Histone chaperones: modulators of chromatin marks. Mol Cell 41: 502–514.
4. Margueron R, Reinberg D (2010) Chromatin structure and the inheritance of epigenetic information. Nat Rev Genet 11: 285–296.

5. Annunziato AT (2012) Assembling chromatin: The long and winding road. Biochim Biophys Acta 1819: 196–210.
6. Annunziato AT, Hansen JC (2000) Role of histone acetylation in the assembly and modulation of chromatin structures. Gene Expr 9: 37–61.
7. Masumoto H, Hawke D, Kobayashi R, Verreault A (2005) A role for cell-cycle-regulated histone H3 lysine 56 acetylation in the DNA damage response. Nature 436: 294–298.
8. Ozdemir A, Spicuglia S, Lasonder E, Vermeulen M, Campsteijn C, et al. (2005) Characterization of lysine 56 of histone H3 as an acetylation site in Saccharomyces cerevisiae. J Biol Chem 280: 25949–25952.
9. Xu F, Zhang K, Grunstein M (2005) Acetylation in histone H3 globular domain regulates gene expression in yeast. Cell 121: 375–385.
10. Ye J, Ai X, Eugeni EE, Zhang L, Carpenter LR, et al. (2005) Histone H4 lysine 91 acetylation a core domain modification associated with chromatin assembly. Mol Cell 18: 123–130.
11. Chen CC, Carson JJ, Feser J, Tamburini B, Zabaronick S, et al. (2008) Acetylated lysine 56 on histone H3 drives chromatin assembly after repair and signals for the completion of repair. Cell 134: 231–243.
12. Recht J, Tsubota T, Tanny JC, Diaz RL, Berger JM, et al. (2006) Histone chaperone Asf1 is required for histone H3 lysine 56 acetylation, a modification associated with S phase in mitosis and meiosis. Proc Natl Acad Sci U S A 103: 6988–6993.
13. Zhou H, Madden BJ, Muddiman DC, Zhang Z (2006) Chromatin assembly factor 1 interacts with histone h3 methylated at lysine 79 in the processes of epigenetic silencing and DNA repair. Biochemistry 45: 2852–2861.
14. Maas NL, Miller KM, DeFazio LG, Toczyski DP (2006) Cell cycle and checkpoint regulation of histone H3 K56 acetylation by Hst3 and Hst4. Mol Cell 23: 109–119.
15. Yuan J, Pu M, Zhang Z, Lou Z (2009) Histone H3-K56 acetylation is important for genomic stability in mammals. Cell Cycle 8: 1747–1753.
16. Kaplan T, Liu CL, Erkmann JA, Holik J, Grunstein M, et al. (2008) Cell cycle- and chaperone-mediated regulation of H3K56ac incorporation in yeast. PLoS Genet 4: e1000270.
17. Li Q, Zhou H, Wurtele H, Davies B, Horazdovsky B, et al. (2008) Acetylation of histone H3 lysine 56 regulates replication-coupled nucleosome assembly. Cell 134: 244–255.
18. Mersfelder EL, Parthun MR (2006) The tale beyond the tail: histone core domain modifications and the regulation of chromatin structure. Nucleic Acids Res 34: 2653–2662.
19. Brownell JE, Allis CD (1996) Special HATs for special occasions: linking histone acetylation to chromatin assembly and gene activation. Current Opinion in Genetics & Development 6: 176–184.
20. Kleff S, Andrulis ED, Anderson CW, Sternglanz R (1995) Identification of a gene encoding a yeast histone H4 acetyltransferase. J Biol Chem 270: 24674–24677.
21. Parthun MR, Widom J, Gottschling DE (1996) The major cytoplasmic histone acetyltransferase in yeast: links to chromatin replication and histone metabolism. Cell 87: 85–94.
22. Driscoll R, Hudson A, Jackson SP (2007) Yeast Rtt109 promotes genome stability by acetylating histone H3 on lysine 56. Science 315: 649–652.
23. Han J, Zhou H, Horazdovsky B, Zhang K, Xu RM, et al. (2007) Rtt109 acetylates histone H3 lysine 56 and functions in DNA replication. Science 315: 653–655.
24. Schneider J, Bajwa P, Johnson FC, Bhaumik SR, Shilatifard A (2006) Rtt109 is required for proper H3K56 acetylation: a chromatin mark associated with the elongating RNA polymerase II. J Biol Chem 281: 37270–37274.
25. Sklenar AR, Parthun MR (2004) Characterization of yeast histone H3-specific type B histone acetyltransferases identifies an ADA2-independent Gcn5p activity. BMC Biochem 5: 11.
26. Burgess RJ, Zhou H, Han J, Zhang Z (2010) A role for Gcn5 in replication-coupled nucleosome assembly. Mol Cell 37: 469–480.
27. Yang X, Yu W, Shi L, Sun L, Liang J, et al. (2011) HAT4, a Golgi apparatus-anchored B-type histone acetyltransferase, acetylates free histone H4 and facilitates chromatin assembly. Mol Cell 44: 39–50.
28. Qian YW, Wang YC, Hollingsworth RE, Jr., Jones D, Ling N, et al. (1993) A retinoblastoma-binding protein related to a negative regulator of Ras in yeast. Nature 364: 648–652.
29. Ai X, Parthun MR (2004) The nuclear Hat1p/Hat2p complex: a molecular link between type B histone acetyltransferases and chromatin assembly. Mol Cell 14: 195–205.
30. Lusser A, Eberharter A, Loidl A, Goralik-Schramel M, Horngacher M, et al. (1999) Analysis of the histone acetyltransferase B complex of maize embryos. Nucleic Acids Res 27: 4427–4435.
31. Imhof A, Wolffe AP (1999) Purification and properties of the xenopus hat1 acetyltransferase: association with the 14-3-3 proteins in the oocyte nucleus. Biochemistry 38: 13085–13093.
32. Verreault A, Kaufman PD, Kobayashi R, Stillman B (1998) Nucleosomal DNA regulates the core-histone-binding subunit of the human Hat1 acetyltransferase. Curr Biol 8: 96–108.
33. Chang L, Loranger SS, Mizzen C, Ernst SG, Allis CD, et al. (1997) Histones in transit: cytosolic histone complexes and diacetylation of H4 during nucleosome assembly in human cells. Biochemistry 36: 469–480.
34. Ruiz-Garcia AB, Sendra R, Galiana M, Pamblanco M, Perez-Ortin JE, et al. (1998) HAT1 and HAT2 proteins are components of a yeast nuclear histone acetyltransferase enzyme specific for free histone H4. J Biol Chem 273: 12599–12605.
35. Kelly TJ, Qin S, Gottschling DE, Parthun MR (2000) Type B histone acetyltransferase Hat1p participates in telomeric silencing. Mol Cell Biol 20: 7051–7058.
36. Qin S, Parthun MR (2002) Histone H3 and the histone acetyltransferase Hat1p contribute to DNA double-strand break repair. Mol Cell Biol 22: 8353–8365.
37. Barman HK, Takami Y, Ono T, Nishijima H, Sanematsu F, et al. (2006) Histone acetyltransferase 1 is dispensable for replication-coupled chromatin assembly but contributes to recover DNA damages created following replication blockage in vertebrate cells. Biochem Biophys Res Commun 345: 1547–1557.
38. Benson LJ, Phillips JA, Gu Y, Parthun MR, Hoffman CS, et al. (2007) Properties of the type B histone acetyltransferase Hat1: H4 tail interaction, site preference, and involvement in DNA repair. J Biol Chem 282: 836–842.
39. Ge Z, Wang H, Parthun MR (2011) Nuclear Hat1p Complex (NuB4) Components Participate in DNA Repair-linked Chromatin Reassembly. J Biol Chem 286: 16790–16799.
40. Verzijlbergen KF, van Welsem T, Sie D, Lenstra TL, Turner DJ, et al. (2011) A barcode screen for epigenetic regulators reveals a role for the NuB4/HAT-B histone acetyltransferase complex in histone turnover. PLoS Genet 7: e1002284.
41. Parthun MR (2012) Histone acetyltransferase 1: More than just an enzyme? Biochim Biophys Acta 1819: 256–263.
42. Ejlassi-Lassallette A, Mocquard E, Arnaud MC, Thiriet C (2011) H4 replication-dependent diacetylation and Hat1 promote S-phase chromatin assembly in vivo. Mol Biol Cell 22: 245–255.
43. Campos EI, Fillingham J, Li G, Zheng H, Voigt P, et al. (2010) The program for processing newly synthesized histones H3.1 and H4. Nat Struct Mol Biol 17: 1343–1351.
44. Tagami H, Ray-Gallet D, Almouzni G, Nakatani Y (2004) Histone H3.1 and H3.3 complexes mediate nucleosome assembly pathways dependent or independent of DNA synthesis. Cell 116: 51–61.
45. Barman HK, Takami Y, Nishijima H, Shibahara K, Sanematsu F, et al. (2008) Histone acetyltransferase-1 regulates integrity of cytosolic histone H3-H4 containing complex. Biochem Biophys Res Commun 373: 624–630.
46. Drane P, Ouararhni K, Depaux A, Shuaib M, Hamiche A (2010) The death-associated protein DAXX is a novel histone chaperone involved in the replication-independent deposition of H3.3. Genes Dev 24: 1253–1265.
47. Saade E, Mechold U, Kulyyassov A, Vertut D, Lipinski M, et al. (2009) Analysis of interaction partners of H4 histone by a new proteomics approach. Proteomics 9: 4934–4943.
48. Sirbu BM, Couch FB, Feigerle JT, Bhaskara S, Hiebert SW, et al. (2011) Analysis of protein dynamics at active, stalled, and collapsed replication forks. Genes Dev 25: 1320–1327.
49. Parthun MR (2007) Hat1: the emerging cellular roles of a type B histone acetyltransferase. Oncogene 26: 5319–5328.
50. Benson LJ, Gu Y, Yakovleva T, Tong K, Barrows C, et al. (2006) Modifications of H3 and H4 during chromatin replication, nucleosome assembly, and histone exchange. J Biol Chem 281: 9287–9296.
51. Alvarez F, Munoz F, Schilcher P, Imhof A, Almozuni G, et al. (2011) Sequential establishment of marks on soluble histones H3 and H4. J Biol Chem 286: 17714–17721.
52. Megee PC, Morgan BA, Mittman BA, Smith MM (1990) Genetic analysis of histone H4: essential role of lysines subject to reversible acetylation. Science 247: 841–845.
53. Ma XJ, Wu J, Altheim BA, Schultz MC, Grunstein M (1998) Deposition-related sites K5/K12 in histone H4 are not required for nucleosome deposition in yeast. Proc Natl Acad Sci U S A 95: 6693–6698.
54. Shibahara K, Verreault A, Stillman B (2000) The N-terminal domains of histones H3 and H4 are not necessary for chromatin assembly factor-1-mediated nucleosome assembly onto replicated DNA in vitro. Proc Natl Acad Sci U S A 97: 7766–7771.
55. Nakano S, Stillman B, Horvitz HR (2011) Replication-coupled chromatin assembly generates a neuronal bilateral asymmetry in C. elegans. Cell 147: 1525–1536.
56. Tong K, Keller T, Hoffman CS, Annunziato AT (2012) Schizosaccharomyces pombe Hat1 (Kat1) is associated with Mis16, and is required for telomeric silencing. Eukaryot Cell 11: 1095–1103.
57. Kelly TJ, Qin S, Gottschling DE, Parthun MR (2000) Type B histone acetyltransferase Hat1p participates in telomeric silencing. Mol Cell Biol 20: 7051–7058.
58. Jasencakova Z, Scharf AN, Ask K, Corpet A, Imhof A, et al. (2010) Replication stress interferes with histone recycling and predeposition marking of new histones. Mol Cell 37: 736–743.
59. Loyola A, Almouzni G (2007) Marking histone H3 variants: how, when and why? Trends Biochem Sci 32: 425–433.
60. Loyola A, Bonaldi T, Roche D, Imhof A, Almouzni G (2006) PTMs on H3 variants before chromatin assembly potentiate their final epigenetic state. Mol Cell 24: 309–316.
61. Sobel RE, Cook RG, Perry CA, Annunziato AT, Allis CD (1995) Conservation of deposition-related acetylation sites in newly synthesized histones H3 and H4. Proc Natl Acad Sci U S A 92: 1237–1241.
62. Lewis PW, Elsaesser SJ, Noh KM, Stadler SC, Allis CD (2010) Daxx is an H3.3-specific histone chaperone and cooperates with ATRX in replication-independent chromatin assembly at telomeres. Proc Natl Acad Sci U S A 107: 14075–14080.

63. Corpet A, Almouzni G (2009) Making copies of chromatin: the challenge of nucleosomal organization and epigenetic information. Trends Cell Biol 19: 29–41.
64. Hogan B, Costantini F, Lacy E (1986) Manipulating the mouse embryo : a laboratory manual. Cold Spring Harbor, N.Y.: Cold Spring Harbor Laboratory. ix, 332 p. p.
65. Chang L, Ryan CA, Schneider CA, Annunziato AT (1999) Preparation/analysis of chromatin replicated in vivo and in isolated nuclei. Methods Enzymol 304: 76–99.
66. Perry CA, Allis CD, Annunziato AT (1993) Parental nucleosomes segregated to newly replicated chromatin are underacetylated relative to those assembled de novo. Biochemistry 32: 13615–13623.
67. Annunziato AT, Eason MB, Perry CA (1995) Relationship between methylation and acetylation of arginine-rich histones in cycling and arrested HeLa cells. Biochemistry 34: 2916–2924.
68. Panyim S, Chalkley R (1969) High resolution acrylamide gel electrophoresis of histones. Arch Biochem Biophys 130: 337–346.

DNA Damage Response: Three Levels of DNA Repair Regulation

Bianca M. Sirbu and David Cortez

Department of Biochemistry, Vanderbilt University School of Medicine, Nashville, Tennessee 37027

Correspondence: david.cortez@vanderbilt.edu

Cold Spring Harbor Perspectives in Biology
www.cshperspectives.org

Genome integrity is challenged by DNA damage from both endogenous and environmental sources. This damage must be repaired to allow both RNA and DNA polymerases to accurately read and duplicate the information in the genome. Multiple repair enzymes scan the DNA for problems, remove the offending damage, and restore the DNA duplex. These repair mechanisms are regulated by DNA damage response kinases including DNA-PKcs, ATM, and ATR that are activated at DNA lesions. These kinases improve the efficiency of DNA repair by phosphorylating repair proteins to modify their activities, by initiating a complex series of changes in the local chromatin structure near the damage site, and by altering the overall cellular environment to make it more conducive to repair. In this review, we focus on these three levels of regulation to illustrate how the DNA damage kinases promote efficient repair to maintain genome integrity and prevent disease.

The DNA in each of our cells accumulates thousands of lesions every day. This damaged DNA must be removed for the DNA code to be read properly. Fortunately, cells contain multiple DNA repair mechanisms including: base excision repair (BER) that removes damaged bases, mismatch repair (MMR) that recognizes base incorporation errors and base damage, nucleotide excision repair (NER) that removes bulky DNA adducts, and cross-link repair (ICL) that removes interstrand cross-links. In addition, breaks in the DNA backbone are repaired via double-strand break (DSB) repair pathways including homologous recombination (HR) and nonhomologous end joining (NHEJ). Some of these mechanisms can operate independently to repair simple lesions. However, the repair of more complex lesions involving multiple DNA processing steps is regulated by the DNA damage response (DDR). For the most difficult to repair lesions, the DDR can be essential for successful repair.

The DDR consists of multiple pathways, but for the purposes of this review we will focus on the DDR kinase signaling cascades controlled by the phosphatidylinositol 3-kinase-related kinases (PIKK). These kinases include DNA-dependent protein kinase (DNA-PKcs), ataxia telangiectasia-mutated (ATM), and ATM and Rad3-related (ATR). DNA-PKcs and ATM are primarily involved in DSB repair, whereas ATR responds to a wide range of DNA lesions, especially those associated with DNA replication (Cimprich and Cortez 2008). ATR's versatility makes it essential for the viability of replicating cells in mice and humans (Brown and Baltimore

Editors: Errol C. Friedberg, Stephen J. Elledge, Alan R. Lehmann, Tomas Lindahl, and Marco Muzi-Falconi
Additional Perspectives on DNA Repair, Mutagenesis, and Other Responses to DNA Damage available at www.cshperspectives.org

Advanced Online Article. Cite this article as *Cold Spring Harb Perspect Biol* doi: 10.1101/cshperspect.a012724

2000; de Klein et al. 2000; Cortez et al. 2001). In the case of ATM, inherited biallelic mutations cause ataxia-telangiectasia—a disorder characterized by neurodegeneration, immunodeficiency, and cancer (Shiloh 2003; Lavin 2008). *ATM* mutations are also frequently found in several types of tumors (Negrini et al. 2010).

The DDR kinases share several common regulatory mechanisms of activation (Lovejoy and Cortez 2009). All three DDR kinases sense damage through protein–protein interactions that serve to recruit the kinases to damage sites. Once localized, posttranslational modifications and other protein–protein interactions fully activate the kinases to initate a cascade of phosphorylation events. The best-studied substrate of DNA-PKcs is actually DNA-PKcs itself, and autophosphorylation is an important step in direct religation of the DSB via nonhomologous end joining (NHEJ) (Weterings and Chen 2007; Dobbs et al. 2010). ATM and ATR have both unique and shared substrates that participate in DNA repair, checkpoint signaling, and determining cell fate decisions such as apoptosis and sensescence.

THREE LEVELS OF REPAIR REGULATION BY THE DDR KINASES

DDR kinases control DNA repair at three levels (Fig. 1). First, they regulate DNA repair enzymes directly through posttranslational modifications that alter their activity. These modifications appear to be especially important in the repair of complex lesions such as ICLs and repair associated with stalled replication forks. Second, the DDR kinases modify the chromatin near the DNA lesion to create a permissive local environment for repair. This chromatin response also provides a scaffolding function for the recruitment of additional DDR factors regulating both repair and signaling. Finally, the DDR kinases act at a more global level of the nucleus or even the entire cell to provide a cellular environment conducive to repair. This global response includes changes in transcription, the cell cycle, chromosome mobility, and deoxynucleotide (dNTP) levels. Controlling these processes may be most important for repair when damage is persistent.

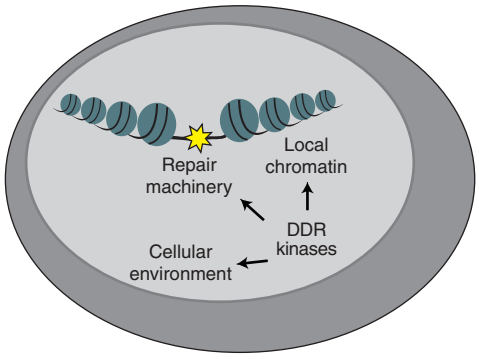

Figure 1. DDR kinases promote efficient DNA repair by directly regulating the DNA repair machinery, changing the local chromatin environment near the DNA lesion, and altering the cellular environment.

This review will highlight examples of each level of regulation. For the direct regulation of repair functions, we will discuss how DDR kinases regulate ICL repair and more general replication fork-associated repair. In discussing the local chromatin environment, we highlight the important role of chromatin modifications surrounding a DSB. Finally, at the global level, we discuss how the DDR alters nuclear architecture and maintains proper cellular dNTP pools to promote repair.

DDR KINASES DIRECTLY REGULATE THE REPLICATION-ASSOCIATED DNA REPAIR MACHINERY

DNA lesions pose an especially important problem when they interfere with DNA polymerases. Errors during DNA replication as well as mistakes in DNA repair cause mutations and chromosomal aberrations that are a source of genetic instability driving tumorigenesis. Additionally, many rare childhood diseases are the result of defects in replication-associated DNA repair. These include Seckel syndrome caused by mutations in ATR and other disorders caused by mutations in ATR substrates like BLM, WRN, and SMARCAL1 (Ciccia and Elledge 2010). Thus, the DNA damage response is particularly critical to ensure complete and accurate duplication of the genome.

ICL Repair during DNA Replication

Interstrand cross-links are perhaps the most difficult lesions to repair, requiring specialized repair mechanisms governed by genes mutated in patients with Fanconi anemia (FA), as well as components of nucleotide excision and DSB repair (Kim and D'Andrea 2012). In the context of DNA replication, interstrand cross-links are potent fork stalling lesions that activate ATR. Perhaps for these reasons, the ATR kinase has an especially critical function in initiating ICL repair (Fig. 2).

When the ICL stalls a replication fork, the DNA structure signals the recruitment of several Fanconi proteins beginning with the FANCM helicase (Meetei et al. 2005; Raschle et al. 2008; Knipscheer et al. 2009). FANCM may remodel the damaged fork to help recruit the FA core complex, a multisubunit ubiquitin ligase. An

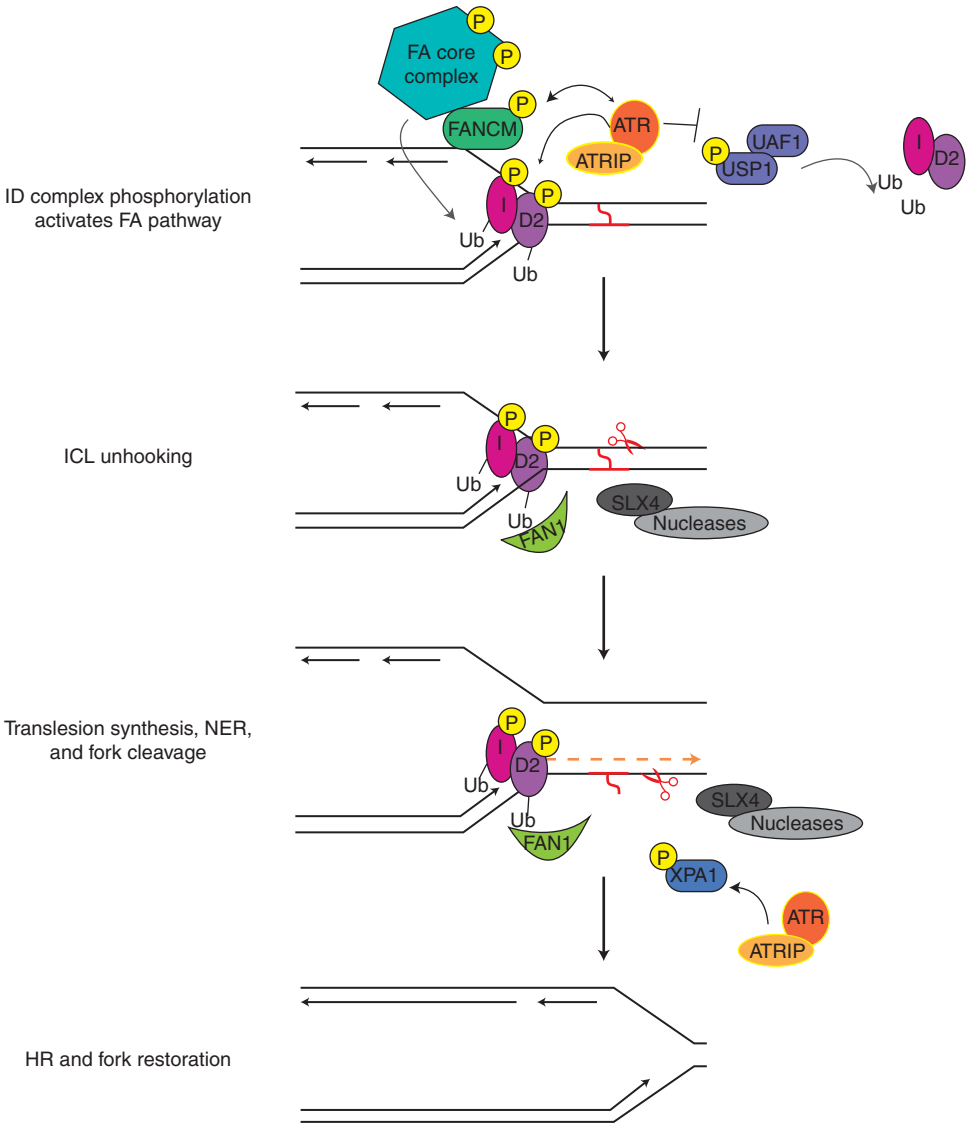

Figure 2. A simplified model of ICL repair indicating steps regulated by ATR phosphorylation.

essential activity of the core complex is monoubiquitination of FANCD2 and FANCI within the FANCI-FANCD2 (ID) complex (Garcia-Higuera et al. 2001). Repair then initiates with synchronized incision on both sides of the cross-link. Incision may be mediated by the flap endonuclease FAN1 whose ubiquitin-binding motif recognizes mono-ub FANCD2 and is essential for ICL repair (Kratz et al. 2010; Liu et al. 2010; Smogorzewska et al. 2010). Additional nucleases such as those associated with SLX4 may also participate in ICL repair given that SLX4 mutations cause FA (Kim et al. 2011). Fork cleavage results in "unhooking" of the cross-link allowing error-prone polymerases to extend past the lesion and NER to remove the cross-linked base. The unhooking reaction also generates a DSB intermediate that is processed by HR to restore the replication fork (Long et al. 2011).

ATR controls the earliest events in the FA pathway and is essential for successful repair. Thus, ATR-deficiency yields high sensitivity to DNA cross-linking agents. ATR phosphorylates several FA proteins including FANCD2, FANCI, FANCA, FANCG, and FANCM (Andreassen et al. 2004; Ishiai et al. 2008; Wilson et al. 2008; Collins et al. 2009; Sobeck et al. 2009). The phosphorylation of FANCI is a particularly critical event for FA pathway activation, as it is needed for monoubiquitination and localization of FANCD2 to sites of damage. FANCI is phosphorylated on several conserved ATR and ATM consensus sites (Matsuoka et al. 2007), and mutants that cannot be phosphorylated prevent FANCD2 mono-ub and cause hypersensitivity to cross-linking reagents (Ishiai et al. 2008). Expression of FANCI mutants that mimic phosphorylation induce FANCD2 monoubiquitination even in the absence of exogenous DNA-damaging agents. These findings suggest that FANCI phosphorylation is a necessary and perhaps sufficient step for FANCD2 monoubiquitination and FA pathway activation. The mechanism by which phosphorylation induces ubiquitylation remains unknown. However, it should be noted that FANCI has WD40 repeats, which might act analogous to F-box proteins to recruit phosphorylated substrates for ubiquitination.

Analysis of the crystal structure of the FANC ID complex has revealed that the ubiquitination sites are buried in the ID interface (Joo et al. 2011). It is possible that ATR phosphorylation of ID in *cis* may inform ID of the presence of dsDNA and ssDNA junctions. A simple model would be that once phosphorylated at the cross-link, the ID complex alters its conformation allowing core complex recognition.

ATR may also regulate FANCD2 ubiquitylation by targeting the FANCD2 deubiquitination complex USP1-UAF1. Consistent with this notion, USP1 was identified as a putative ATM/ATR substrate (Matsuoka et al. 2007), and the interaction of USP1/UAF1 with FANCI is regulated by DNA damage (Yang et al. 2011). Furthermore, in response to DNA damage, USP1 undergoes inactivating autoproteolysis, further promoting FANC ID ubiquitination.

The activities of other FA proteins including FANCA and FANCG are also under the control of the ATR kinase. FANCA is a direct ATR substrate, and mutation of the phosphorylation site creates a protein that cannot fully complement *FANCA*-deficient cells (Collins et al. 2009). FANCG is phosphorylated on multiple sites and at least one (serine 7) is ATR-dependent (Wilson et al. 2008). Phosphorylation of FANCG regulates the interactions of BRCA2 with components of the core complex and FANCD2. FANCG S7 mutants fail to rescue the cross-link sensitivity of *FANCG*-deficient cells (Qiao et al. 2004).

In addition to controlling early events in cross-link repair, the ATR pathway may also regulate later steps. For example, ATR regulates the NER-dependent unhooking reaction pathway by regulating the localization of XPA (Wu et al. 2007; Shell et al. 2009). Also, ATR regulates the HR step by promoting the recruitment of the key RAD51 recombinase (Sorensen et al. 2005).

Thus, ATR regulates nearly every step of the ICL repair process. Why is this necessary? Perhaps the answer lies in the complexity of removing an ICL. ICL repair requires the coordinated activities of multiple repair steps often at a time of maximum vulnerability for the genome (when the replication fork reaches the cross-link). Perhaps ATR signaling provides

a mechanism of ordering the repair steps to prevent undesirable DNA intermediates, which might yield aberrant repair products. In this context, it might be expected that the more difficult a DNA lesion is to repair, the more important the DDR pathways become for success.

DDR Kinase-Dependent Regulation of Replication Fork Repair Pathways

DDR regulation of ICL repair during DNA replication is a specialized version of a more general DDR response that coordinates repair of stalled forks. Base damage, dNTP depletion, and even difficult to replicate sequences that form secondary structures or RNA–DNA hybrids can cause fork damage. A stalled fork itself may not be a particularly devastating event to a cell because DNA replication will usually be completed from an adjacent origin of replication. In such cases, the DDR stabilizes the damaged fork to prevent aberrant DNA processing. In other cases, such as in replication of fragile sites that contain few replication origins, fork stabilization may be insufficient and DDR kinase-dependent restart of the stalled fork becomes essential (Casper et al. 2002).

The fork-stabilization activity of ATR is functionally defined either in terms of the ability to restart replication once a blockage is removed or by the changes in DNA or protein composition at the fork. Yeast mutants deficient in the ATR pathway lose the replicative polymerases from the fork (Cobb et al. 2003, 2005; Lucca et al. 2004) and accumulate abnormal DNA structures including long stretches of ssDNA and reversed fork structures resembling Holliday junctions (Lopes et al. 2001; Sogo et al. 2002). At least in yeast, the Exo1 nuclease is involved in generating the excess ssDNA at the stalled fork when the ATR pathway is inactivated (Cotta-Ramusino et al. 2005). Loss of ATR function in *Xenopus* extracts also causes loss of Pol epsilon and collapse of the fork into a DSB (Trenz et al. 2006).

Thus, one way ATR may stabilize a fork is by preventing dissociation of replisome proteins and thereby inhibiting aberrant enzymatic processing of the DNA. However, a recent paper by the Labib group has challenged this model (De Piccoli et al. 2012). This group monitored replisome stability in budding yeast lacking the $Mec1^{ATR}$ or $Rad53^{Chk2}$ checkpoint kinases by immunoprecipitating a subunit of the replicative helicase and immunoblotting for other replisome proteins. In contrast to expectations, they did not observe disassembly of the replisome, and chromatin immunoprecipitation assays suggested that the replisome remained near origins in cells treated with high doses of hydroxyurea to stall forks. A subset of early origins lacked replisome proteins, but the authors concluded that this was as a result of replisome movement away from the earliest origins in the absence of DDR kinase activity instead of replisome disassembly. Thus, in this case, the ATR pathway may be important for restraining fork movement. If fork movement is not accompanied by productive leading and lagging strand synthesis, it could help generate the ssDNA gaps observed by electron microscopy in $Mec1^{ATR}$-deficient yeast.

Exactly how ATR prevents replisome dissociation, movement, and aberrant fork processing is one of the least understood parts of the DDR. One DDR target is the downstream kinase CHK1, which is activated by ATR phosphorylation and needed to prevent fork collapse and regulate origin firing (Cimprich and Cortez 2008). Note that the mammalian and yeast functions of CHK1 and CHK2 have been reversed during evolution so that human CHK1 is the functional equivalent of yeast Rad53 with respect to replication fork regulation. ATR also directly phosphorylates replisome components including several Cdc45-MCM-GINS (CMG) helicase subunits (Cortez et al. 2004; Yoo et al. 2004; Matsuoka et al. 2007; Shi et al. 2007; Trenz et al. 2008; De Piccoli et al. 2012). Phosphorylation of CMG may regulate helicase activity to prevent excessive unwinding and is important to promote rescue of stalled forks from adjacent origins.

In addition, other replication fork proteins including RPA, CLASPIN, and members of the replication fork-pausing complex like TIMELESS, TIPIN, and AND1 are ATR substrates (Matsuoka et al. 2007). Deficiencies in these proteins cause hypersensitivity to replication

stress agents (Chou and Elledge 2006; Errico et al. 2007; Unsal-Kacmaz et al. 2007; Yoshizawa-Sugata and Masai 2007, 2009; Leman et al. 2010). They act in part through promoting ATR-dependent CHK1 activation but may have additional roles in regulating the repair of damaged forks.

The DDR also targets several repair enzymes that remodel damaged forks including WRN, FANCM, and SMARCAL1. The WRN and FANCM proteins are helicases capable of unwinding a variety of complex DNA structures. SMARCAL1 is an SNF2 family ATPase that is activated by complex DNA structures and uses the energy of ATP hydrolysis to reanneal DNA strands (Yusufzai and Kadonaga 2008). All three enzymes are recruited to damaged forks and can catalyze fork regression generating a Holliday junction on model replication substrates (Machwe et al. 2006; Gari et al. 2008a; Betous et al. 2012; Ciccia et al. 2012). They can also branch migrate the Holliday junction, which could restore the normal fork structure (Gari et al. 2008b; Machwe et al. 2011; Betous et al. 2012). All three are targets of ATR phosphorylation (Yannone et al. 2001; Karmakar et al. 2002; Pichierri et al. 2003; Meetei et al. 2005; Bansbach et al. 2009; Sobeck et al. 2009; Ammazzalorso et al. 2010), and deficiencies in WRN and SMARCAL1 activity lead to MUS81-dependent fork cleavage and DSB formation (Franchitto et al. 2008; Betous et al. 2012).

ATR phosphorylation of WRN and FANCM promotes their recruitment to stalled forks (Sobeck et al. 2009; Ammazzalorso et al. 2010), and cells expressing a nonphosphorylatable mutant WRN show increased fork breakage (Ammazzalorso et al. 2010). SMARCAL1 phosphorylation by DDR kinases does not regulate its localization but does regulate its enzymatic activity (D Cortez, unpubl.). The exact substrates of these fork remodeling enzymes at stalled forks and how their activities promote fork restart in cells is not yet known. Additionally, many other helicases and DNA translocases including BLM have roles at damaged forks and are regulated by ATR phosphorylation (Davalos et al. 2004; Li et al. 2004; Sengupta et al. 2004; Rao et al. 2005; Tripathi et al. 2008).

Clearly, a great deal remains to be learned about how ATR promotes replication fork stability, replication-associated DNA repair, and fork restart. These are likely the most important functions of ATR in maintaining genome stability and cell viability based on results from separation of function mutants in both yeast and human ATR (Paciotti et al. 2001; Cobb et al. 2005; Nam et al. 2011). Yet, they are also arguably the least understood. The development of new reversible ATR inhibitors (Charrier et al. 2011; Reaper et al. 2011; Toledo et al. 2011), as well as new techniques to study DNA replication such as iPOND should accelerate the mechanistic studies (Sirbu et al. 2011, 2012). Such studies will be equally critical in defining the pathways that lead to the elevated levels of replication stress observed in cancer cells (Halazonetis et al. 2008). Combined with defects in other genome-maintenance activities, this stress creates an increased dependency on ATR for successful cell division. Thus, the ATR pathway is a promising target for new cancer drug development. Defining how ATR inhibition alters replication-associated DNA repair will be important for understanding the mechanism of action of these drugs.

DDR REGULATES LOCAL CHROMATIN STRUCTURE TO PROMOTE REPAIR

DNA lesions occur in various chromosomal contexts including compacted and opened chromatin, which influences both the activation of the DDR and DNA repair efficiency. For example, in highly condensed chromatin, repairing the damaged structure is more difficult presumably because repair proteins are physically occluded from accessing the damaged structure. Independently of DDR kinases, an ATP-dependent mechanism induces rapid chromatin relaxation around a DSB, and is required for recruitment of break-sensing proteins (Kruhlak et al. 2006). However, several DDR kinase-dependent local chromatin changes also promote a local environment conducive for repair. These activities include creation of a chromatin platform for recruitment of repair and signaling factors, regulating repair factor accessibility to

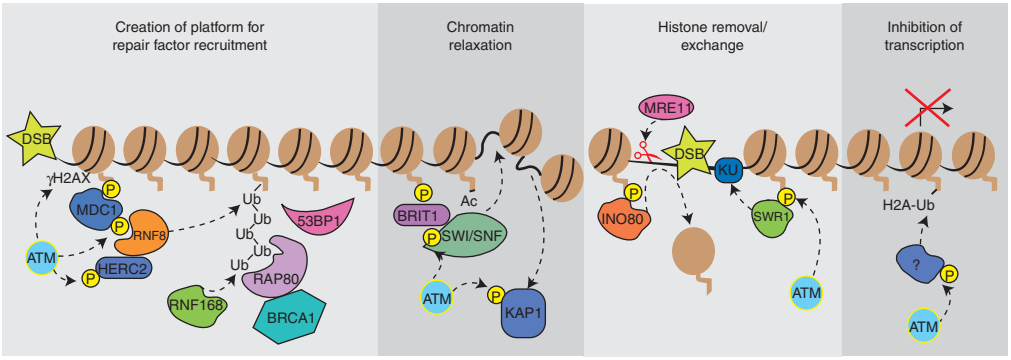

Figure 3. DDR kinases regulate the chromatin near a double-strand break to provide a scaffold for the recruitment of DNA repair proteins, promote repair protein access through nucleosome remodeling, and inhibit local transcription.

the DNA, and inhibition of nearby transcription to prevent potential interference with DNA repair (Fig. 3). Here we discuss the DDR-dependent chromatin response as it relates to DSB repair.

γH2AX as a Platform for DSB Repair

One of the earliest consequences of ATM activation at a DSB is phosphorylation of the histone variant H2AX on an evolutionarily conserved serine (S139) producing γH2AX (Fernandez-Capetillo et al. 2004; Stucki and Jackson 2006; Dickey et al. 2009). A complex of MRN, MDC1, and γH2AX recruits additional ATM to flanking regions of chromatin and facilitates propagation of γH2AX to a large chromatin domain.

γH2AX-MDC1 is a platform for the recruitment of many additional chromatin modifying, DDR signaling, and DNA repair proteins. This scaffold recruits the RING ubiquitin ligases RNF8 and RNF168 to trigger a ubiquitylation cascade surrounding the DSB (Al-Hakim et al. 2010). This recruitment is mediated by ATM-dependent phosphorylation sites on MDC1, which are recognized by the FHA domain of RNF8. Along with the E2 enzyme UBC13, RNF8 catalyzes the formation of Lys63-linked polyubiquitin chains at DSBs (Huen et al. 2007; Kolas et al. 2007; Mailand et al. 2007). Subsequently, RNF168, the protein encoded by the RIDDLIN syndrome gene recognizes and amplifies these ubiquitin chains (Doil et al. 2009; Stewart et al. 2009), whereas another ring finger protein RNF169 antagonizes the ubiquitin cascade (Chen et al. 2012; Poulsen et al. 2012). Another ATM substrate, HERC2, also regulates this process. HERC2 contains an ATM phosphorylation site that binds the RNF8 FHA domain and helps assemble the functional RNF8-UBC13 enzyme (Bekker-Jensen et al. 2010).

Ubiquitylation at the DSB regulates the recruitment of the DSB repair proteins BRCA1 and 53BP1 (Al-Hakim et al. 2010). BRCA1 is itself a ubiquitin ligase and is regulated by ATM and ATR-dependent phosphorylation (Cortez et al. 1999; Tibbetts et al. 2000). BRCA1 is recruited via an interaction with a complex of proteins containing the K63-linked ubiquitin binding protein Rap80 (Kim et al. 2007; Sobhian et al. 2007; Wang et al. 2007; Yan et al. 2007). Three distinct BRCA1 repair complexes (BRCA1-A, BRCA1-B, and BRCA1-C) are recruited, which contain different accessory proteins to regulate checkpoint activation or HR repair (Greenberg et al. 2006). 53BP1 accumulation near the DSB is also dependent on these ubiquitylation events although the mechanism is likely indirect. The overall effect of BRCA1 and 53BP1 recruitment downstream of histone phosphorylation and ubiquitylation is likely regulation of repair choice between NHEJ and HR.

In addition to recruiting repair factors to a DSB, DDR-dependent H2AX phosphorylation also induces changes to chromatin structure by recruiting ATP-dependent chromatin

Cold Spring Harbor Perspectives in Biology
www.cshperspectives.org

remodeling complexes including SWI/SNF, SWR1, and INO80. The SWI/SNF chromatin remodeling activity is targeted to DSBs through interactions with acetylated H3 (Lee et al. 2010) and BRIT1/MCPH1, a protein that binds γH2AX after damage (Wood et al. 2007; Peng et al. 2009). ATM and ATR phosphorylate a SWI/SNF subunit leading to an increased association with BRIT1 and DSBs (Peng et al. 2009). SWI/SNF presumably relaxes chromatin near the break to improve access of DNA repair enzymes to the damaged DNA.

The INO80 and SWR1 complexes are recruited to damage sites through direct interaction with γH2AX. At least in yeast, these complexes promote repair through two distinct mechanisms. INO80 catalyzes histone removal that facilitates Mre11 binding and DNA end resection to promote HR repair, whereas SWR1 promotes KU binding and NHEJ (van Attikum et al. 2007; van Attikum and Gasser 2009). INO80-dependent remodeling may also be important to promote the strand invasion step of HR through displacement of histones at the homologous donor sequences (Tsukuda et al. 2009).

H2AX-Independent but DDR Kinase-Dependent Regulation of Local Chromatin

Besides γH2AX-dependent regulation of repair, ATM controls other chromatin modifications to allow access for repair factors. H2B is monoubiquitylated near DSBs (Moyal et al. 2011). H2B-Ub is catalyzed by an RNF20-RNF40 heterodimer (the human ortholog of yeast Bre1), and this modification is typically associated with actively transcribed genes (Zhu et al. 2005). The levels of H2B-Ub increase near a DSB owing to recruitment of the RNF20-RNF40 proteins through a mechanism that may involve their interaction with ATM and NBS1 (Moyal et al. 2011). Both RNF20 and RNF40 are ATM substrates, and increased H2B-Ub surrounding the break is dependent on RNF20 phosphorylation. Both NHEJ and HR repair are impaired in cells when the damage-induced H2B-Ub is prevented (Moyal et al. 2011). The HR defect was traced to a defect in DNA end resection and could be rescued by experimentally inducing chromatin relaxation. Reduced NHEJ is associated with less XRCC4 and KU80 at the break in the absence of H2B-Ub.

In addition to modulating H2B-Ub, a second mechanism by which ATM relaxes chromatin to promote repair is through phosphorylation of KAP1 (Ziv et al. 2006). KAP1 is a transcriptional corepressor that works with histone methyltransferase and histone deacetylase complexes to promote chromatin compaction. ATM-dependent KAP1 phosphorylation disrupts an interaction between KAP1 and the CHD3 nucleosome remodeler thereby promoting chromatin relaxation (Goodarzi et al. 2011). As a result, ATM is particularly important for repair of DSBs that occur in heterochromatin (Goodarzi et al. 2008a; Noon et al. 2010).

In addition to the examples of local chromatin changes described here, there are changes in other histone modifications regulated by DDR kinases such as an ATM-dependent increase in H2A-Ub that inhibits transcription near DSBs (Shanbhag et al. 2010). There are also changes in the binding of chromatin proteins and the abundance of histone variants. Understanding how the DDR kinases regulate the local chromatin environment to promote repair of other types of DNA lesions, such as those encountered by elongating replication forks, will also be important. Some of the mechanisms may be similar. For example, γH2AX spreads away from stalled forks similarly to the spreading observed at DSBs (Sirbu et al. 2011). However, other mechanisms may be unique, adding to the complexity of the chromatin response to DNA damage.

DDR KINASES FACILITATE REPAIR BY CREATING AN OPTIMAL CELLULAR ENVIRONMENT

In addition to promoting DNA repair through direct regulation of repair proteins and changes in the chromatin near the DNA damage site, the DDR also facilitates repair through more global changes in the cellular environment (Fig. 4). The most obvious example of this mechanism is the checkpoint activity of the DDR kinases, which halts the cell cycle providing time to

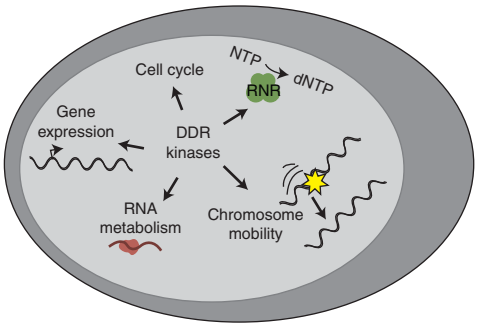

Figure 4. DDR kinases regulate several aspects of nuclear and cellular physiology to provide an environment conducive for successful DNA repair.

repair the DNA damage before DNA replication or mitosis. Checkpoint-dependent changes in cyclin-dependent kinase (CDK) activities also influence DNA repair more directly because many repair proteins are CDK substrates. A second example is the numerous DDR kinase-dependent changes in gene expression that are largely mediated through regulation of p53. In addition to inducing cell cycle arrest and apoptosis, these transcriptional changes can alter the levels of DNA repair proteins, as well as the nucleotides and histones needed for completing repair synthesis and restoring chromatin.

Furthermore, results from functional genomic screens suggest a much broader regulation of cellular physiology by the DDR. For example, proteomic screens for ATM and ATR substrates and genetic screens for new DDR factors based on the level of ATM/ATR activity in undamaged cells identified proteins involved in a wide variety of cellular functions including intracellular protein trafficking, cellular immunity, and RNA metabolism (Matsuoka et al. 2007; Lovejoy et al. 2009; Paulsen et al. 2009; Bansbach and Cortez 2011). In many cases, the connection between these processes and the DDR kinases is likely to promote a cellular environment conducive to DNA repair.

Nuclear Organization and Chromosome Movements Facilitate DNA Repair

One of the important DDR kinase-dependent changes important for repair is regulation of nuclear organization. The nucleus is a highly organized organelle with compartments devoted to specific functions. A long-standing question is whether DNA repair occurs equally well anywhere within the nucleus or whether there are specific repair centers (Misteli and Soutoglou 2009). Recent studies on DSB repair in yeast suggest that repair centers exist and indicate that DDR-dependent changes in chromosome mobility promote HR repair.

Observations of DSBs marked with fluorescent proteins revealed that unrepairable DSBs move to the nuclear periphery and cells with two DSBs merge them into a single repair focus (Nagai et al. 2008; Oza et al. 2009). More recently, the Rothstein and Gasser groups have shown increased chromosomal mobility within the yeast nucleus because of a DSB (Dion et al. 2012; Mine-Hattab and Rothstein 2012). The increased movement depends on the $Mec1^{ATR}$ kinase, resection of the DNA end, and the RAD51 recombinase. Intriguingly, the Rothstein study also showed that the dynamics of unbroken, nonhomologous chromosomes is also increased in the presence of a DSB, suggesting that DDR kinases regulate global nuclear architecture (Mine-Hattab and Rothstein 2012).

The end-result of the increased chromosome mobility is an increase in repair efficiency. Likely this results from an increase in the ability of the RAD51-coated DNA end to find a homologous sequence. Flexibility of the RAD51-coated DNA fiber is important for an efficient homology search (Forget and Kowalczykowski 2012). It is also possible that the movement to or away from a specific nuclear location promotes repair. For example, movement out of a region containing heterochromatin or the nucleolus might increase repair efficiency.

Whether similar changes in chromosome dynamics occur in higher eukaryotes is less clear. Several studies indicate that most DNA ends are largely immobile in mammalian cells (Nelms et al. 1998; Kruhlak et al. 2006; Soutoglou et al. 2007; Jakob et al. 2009). However, deprotected telomere ends have increased mobility compared with protected telomeres (Dimitrova et al. 2008). This increased mobility

depends on both ATM and 53BP1 and these ends are repaired through NHEJ. ATM and 53BP1 also control antigen receptor diversification, and chromosome movement may be needed especially in the context of long-range joining during class switch recombination (Nussenzweig and Nussenzweig 2010). DSBs induced by α particles are also mobile (Aten et al. 2004). Furthermore, breaks in heterochromatin in *Drosophila* cells cause an expansion of the heterochromatin domain followed by movement of the repair focus outside of the heterochromatin (Chiolo et al. 2011). These changes in heterochromatin are dependent on the DDR kinases and seem to be important after the resection step but before the RAD51-dependent homology search for HR repair (Chiolo et al. 2011). Thus, at least in some circumstances the increased mobility of broken chromosomes within the nucleus does occur in metazoan cells.

The mechanism by which the DDR promotes increased chromosome mobility is not known. One clue might be found in the recent observation that DNA attachments to the nuclear pore are regulated by the DDR (Bermejo et al. 2011). In this yeast study, the authors found that DDR kinase modification of nucleoporins releases the interaction between tethered chromosomes and the pore. Another possible mechanism could involve phosphorylation of KAP1, which is observed throughout the nucleus. KAP1 binds the heterochromatin protein HP1 and as mentioned earlier, KAP1 phosphorylation is important for the repair of breaks in heterochromatin (Goodarzi et al. 2008b). Finally, DSB recruitment of chromatin remodeling factors such as INO80 and histone variants such as H2A.Z may be important to promote the increase in mobility (Kalocsay et al. 2009; Neumann et al. 2012). Discovering the mechanisms by which the DDR kinases regulate chromosome dynamics will provide important information about nuclear architecture and how chromosomal domains are maintained. In addition, these studies have significant implications for the mechanisms driving chromosomal translocations and rearrangements that cause cancer.

Control of Cellular Nucleotide Levels for DNA Repair

Perhaps the best-documented example of how the DDR kinases create a cellular environment conducive for repair is through the regulation of nucleotide metabolism. In yeast, the intracellular concentration of dNTPs increases in response to DNA damage, whereas in mammalian cells increased production may be more localized (Chabes et al. 2003; Hakansson et al. 2006b). Higher concentrations of dNTPs cause an increase in mutation frequency (Chabes et al. 2003). Not surprisingly, maintaining an optimal balance of cellular dNTPs is a process strictly controlled at multiple levels by the DDR kinases.

The rate-limiting step in dNTP production is catalyzed by ribonucleotide reductase (RNR) (Nordlund and Reichard 2006). RNR contains two subunits, R1 and R2, encoded by multiple genes in most organisms. DDR kinases regulate RNR at almost every conceivable level. The transcriptional regulation of RNR subunits was one of the first documented functions of the DDR (Elledge et al. 1993). In human cells, a DDR kinase- and p53-dependent pathway induces expression of the catalytic RNR subunit p53R2 after prolonged exposure to DNA damage (Tanaka et al. 2000).

In addition to RNR gene expression, the DDR kinases directly regulate the stability of RNR subunits. For example, ATM phosphorylation of p53R2 increases its stability (Chang et al. 2008). Furthermore, ATR signaling inhibits Cyclin F-dependent R2 degradation, which may be a rapid way of increasing functional RNR enzyme levels (D'Angiolella et al. 2012).

The ATR pathway also controls the localization of the RNR subunits. In yeast, one of the RNR subunits is exported to the cytoplasm after damage to form an active RNR enzyme (Yao et al. 2003). In mammalian cells, RNR subunits may actually be recruited directly to sites of DNA damage to ensure dNTP production right where it is most needed (Niida et al. 2010).

Finally, in budding and fission yeast, small protein inhibitors of RNR including Dif1, Sml1, and Spd1 are regulated by DDR kinases. Dif1 and Spd1 control the localization of RNR sub-

units by regulating nuclear import (Liu et al. 2003; Lee et al. 2008) whereas Sml1 and Spd1 are direct inhibitors of RNR activity (Zhao et al. 1998; Hakansson et al. 2006a). The proteolysis of all three of these proteins is under control of the DDR pathway (Zhao et al. 2001; Liu et al. 2003; Lee et al. 2008; Wu and Huang 2008).

Thus, the DDR kinases control the timely and appropriate production of dNTPs for DNA repair through transcriptional, posttranscriptional, and localization mechanisms targeting RNR. The importance of this pathway to create an optimal cellular environment for repair and replication is illustrated by the observation that, in budding yeast, the lethality associated with deleting $Mec1^{ATR}$ can be rescued by increasing RNR activity (Desany et al. 1998; Zhao et al. 1998). Whether ATR regulation of RNR function is equally important in human cells is unknown.

CONCLUDING REMARKS

The basic DNA repair machinery is often sufficient to reconstitute simple repair reactions in vitro on naked DNA substrates. However, efficient repair often requires regulation by the DNA damage response. The DDR kinases directly modify repair proteins, change chromatin structure around the DNA lesion, and regulate nuclear and cellular environments. Failures at any of these levels cause genome instability and disease. Not surprisingly, the list of DDR kinase substrates is long and our understanding of their regulation is incomplete. Fortunately, new tools for discovery in multiple systems promise to rapidly move us toward an intimate understanding of mechanism. This knowledge may help in the design of cancer therapeutic opportunities based on manipulation of the DNA damage response, epigenetic therapies, and combinations with existing radiation and chemotherapies that work primarily by damaging DNA.

ACKNOWLEDGMENTS

Research in the Cortez laboratory on the DNA damage response and DNA repair is supported by NIH grants R01CA102729 and R01CA136933. B.M.S. is funded by a Department of Defense Breast Cancer Research Program predoctoral fellowship (W81XWH-10-1-0226), and we thank Swim Across America for their support.

REFERENCES

Al-Hakim A, Escribano-Diaz C, Landry MC, O'Donnell L, Panier S, Szilard RK, Durocher D. 2010. The ubiquitous role of ubiquitin in the DNA damage response. *DNA Repair* **9:** 1229–1240.

Ammazzalorso F, Pirzio LM, Bignami M, Franchitto A, Pichierri P. 2010. ATR and ATM differently regulate WRN to prevent DSBs at stalled replication forks and promote replication fork recovery. *EMBO J* **29:** 3156–3169.

Andreassen PR, D'Andrea AD, Taniguchi T. 2004. ATR couples FANCD2 monoubiquitination to the DNA-damage response. *Genes Dev* **18:** 1958–1963.

Aten JA, Stap J, Krawczyk PM, van Oven CH, Hoebe RA, Essers J, Kanaar R. 2004. Dynamics of DNA double-strand breaks revealed by clustering of damaged chromosome domains. *Science* **303:** 92–95.

Bansbach CE, Cortez D. 2011. Defining genome maintenance pathways using functional genomic approaches. *Crit Rev Biochem Mol Biol* **46:** 327–341.

Bansbach CE, Betous R, Lovejoy CA, Glick GG, Cortez D. 2009. The annealing helicase SMARCAL1 maintains genome integrity at stalled replication forks. *Genes Dev* **23:** 2405–2414.

Bekker-Jensen S, Rendtlew Danielsen J, Fugger K, Gromova I, Nerstedt A, Lukas C, Bartek J, Lukas J, Mailand N. 2010. HERC2 coordinates ubiquitin-dependent assembly of DNA repair factors on damaged chromosomes. *Nat Cell Biol* **12:** pp 81–12.

Bermejo R, Capra T, Jossen R, Colosio A, Frattini C, Carotenuto W, Cocito A, Doksani Y, Klein H, Gomez-Gonzalez B, et al. 2011. The replication checkpoint protects fork stability by releasing transcribed genes from nuclear pores. *Cell* **146:** 233–246.

Betous R, Mason AC, Rambo RP, Bansbach CE, Badu-Nkansah A, Sirbu BM, Eichman BF, Cortez D. 2012. SMARCAL1 catalyzes fork regression and Holliday junction migration to maintain genome stability during DNA replication. *Genes Dev* **26:** 151–162.

Brown EJ, Baltimore D. 2000. ATR disruption leads to chromosomal fragmentation and early embryonic lethality. *Genes Dev* **14:** 397–402.

Casper AM, Nghiem P, Arlt MF, Glover TW. 2002. ATR regulates fragile site stability. *Cell* **111:** 779–789.

Chabes A, Georgieva B, Domkin V, Zhao X, Rothstein R, Thelander L. 2003. Survival of DNA damage in yeast directly depends on increased dNTP levels allowed by relaxed feedback inhibition of ribonucleotide reductase. *Cell* **112:** 391–401.

Chang L, Zhou B, Hu S, Guo R, Liu X, Jones SN, Yen Y. 2008. ATM-mediated serine 72 phosphorylation stabilizes ribonucleotide reductase small subunit p53R2 protein

against MDM2 to DNA damage. *Proc Natl Acad Sci* **105:** 18519–18524.

Charrier JD, Durrant SJ, Golec JM, Kay DP, Knegtel RM, Maccormick S, Mortimore M, O'Donnell ME, Pinder JL, Reaper PM, et al. 2011. Discovery of potent and selective inhibitors of ataxia telangiectasia mutated and Rad3 related (ATR) protein kinase as potential anticancer agents. *J Med Chem* **54:** 2320–2330.

Chen J, Feng W, Jiang J, Deng Y, Huen MS. 2012. Ring finger protein RNF169 antagonises the ubiquitin-dependent signaling cascade at sites of DNA damage. *J Biol Chem* **287:** 27715–27722.

Chiolo I, Minoda A, Colmenares SU, Polyzos A, Costes SV, Karpen GH. 2011. Double-strand breaks in heterochromatin move outside of a dynamic HP1a domain to complete recombinational repair. *Cell* **144:** 732–744.

Chou DM, Elledge SJ. 2006. Tipin and timeless form a mutually protective complex required for genotoxic stress resistance and checkpoint function. *Proc Natl Acad Sci* **103:** 18143–18147.

Ciccia A, Elledge SJ. 2010. The DNA damage response: Making it safe to play with knives. *Mol Cell* **40:** 179–204.

Ciccia A, Nimonkar AV, Hu Y, Hajdu I, Achar YJ, Izhar L, Petit SA, Adamson B, Yoon JC, Kowalczykowski SC, et al. 2012. Polyubiquitinated PCNA recruits the ZRANB3 translocase to maintain genomic integrity after replication stress. *Mol Cell* **47:** 396–409.

Cimprich KA, Cortez D. 2008. ATR: An essential regulator of genome integrity. *Nat Rev Mol Cell Biol* **9:** 616–627.

Cobb JA, Bjergbaek L, Shimada K, Frei C, Gasser SM. 2003. DNA polymerase stabilization at stalled replication forks requires Mec1 and the RecQ helicase Sgs1. *EMBO J* **22:** 4325–4336.

Cobb JA, Schleker T, Rojas V, Bjergbaek L, Tercero JA, Gasser SM. 2005. Replisome instability, fork collapse, and gross chromosomal rearrangements arise synergistically from Mec1 kinase and RecQ helicase mutations. *Genes Dev* **19:** 3055–3069.

Collins NB, Wilson JB, Bush T, Thomashevski A, Roberts KJ, Jones NJ, Kupfer GM. 2009. ATR-dependent phosphorylation of FANCA on serine 1449 after DNA damage is important for FA pathway function. *Blood* **113:** 2181–2190.

Cortez D, Wang Y, Qin J, Elledge SJ. 1999. Requirement of ATM-dependent phosphorylation of brca1 in the DNA damage response to double-strand breaks. *Science* **286:** 1162–1166.

Cortez D, Guntuku S, Qin J, Elledge SJ. 2001. ATR and ATRIP: Partners in checkpoint signaling. *Science* **294:** 1713–1716.

Cortez D, Glick G, Elledge SJ. 2004. Minichromosome maintenance proteins are direct targets of the ATM and ATR checkpoint kinases. *Proc Natl Acad Sci* **101:** 10078–10083.

Cotta-Ramusino C, Fachinetti D, Lucca C, Doksani Y, Lopes M, Sogo J, Foiani M. 2005. Exo1 processes stalled replication forks and counteracts fork reversal in checkpoint-defective cells. *Mol Cell* **17:** 153–159.

D'Angiolella V, Donato V, Forrester FM, Jeong YT, Pellacani C, Kudo Y, Saraf A, Florens L, Washburn MP, Pagano M. 2012. Cyclin F-mediated degradation of ribonucleotide reductase M2 controls genome integrity and DNA repair. *Cell* **149:** 1023–1034.

Davalos AR, Kaminker P, Hansen RK, Campisi J. 2004. ATR and ATM-dependent movement of BLM helicase during replication stress ensures optimal ATM activation and 53BP1 focus formation. *Cell Cycle* **3:** 1579–1586.

de Klein A, Muijtjens M, van Os R, Verhoeven Y, Smit B, Carr AM, Lehmann AR, Hoeijmakers JH. 2000. Targeted disruption of the cell-cycle checkpoint gene ATR leads to early embryonic lethality in mice. *Curr Biol* **10:** 479–482.

De Piccoli G, Katou Y, Itoh T, Nakato R, Shirahige K, Labib K. 2012. Replisome stability at defective DNA replication forks is independent of S phase checkpoint kinases. *Mol Cell* **45:** 696–704.

Desany BA, Alcasabas AA, Bachant JB, Elledge SJ. 1998. Recovery from DNA replicational stress is the essential function of the S-phase checkpoint pathway. *Genes Dev* **12:** 2956–2970.

Dickey JS, Redon CE, Nakamura AJ, Baird BJ, Sedelnikova OA, Bonner WM. 2009. H2AX: Functional roles and potential applications. *Chromosoma* **118:** 683–692.

Dimitrova N, Chen YC, Spector DL, de Lange T. 2008. 53BP1 promotes non-homologous end joining of telomeres by increasing chromatin mobility. *Nature* **456:** 524–528.

Dion V, Kalck V, Horigome C, Towbin BD, Gasser SM. 2012. Increased mobility of double-strand breaks requires Mec1, Rad9 and the homologous recombination machinery. *Nat Cell Biol* **14:** 502–509.

Dobbs TA, Tainer JA, Lees-Miller SP. 2010. A structural model for regulation of NHEJ by DNA-PKcs autophosphorylation. *DNA Repair* **9:** 1307–1314.

Doil C, Mailand N, Bekker-Jensen S, Menard P, Larsen DH, Pepperkok R, Ellenberg J, Panier S, Durocher D, Bartek J, et al. 2009. RNF168 binds and amplifies ubiquitin conjugates on damaged chromosomes to allow accumulation of repair proteins. *Cell* **136:** 435–446.

Elledge SJ, Zhou Z, Allen JB, Navas TA. 1993. DNA damage and cell cycle regulation of ribonucleotide reductase. *Bioessays* **15:** 333–339.

Errico A, Costanzo V, Hunt T. 2007. Tipin is required for stalled replication forks to resume DNA replication after removal of aphidicolin in *Xenopus* egg extracts. *Proc Natl Acad Sci* **104:** 14929–14934.

Fernandez-Capetillo O, Lee A, Nussenzweig M, Nussenzweig A. 2004. H2AX: The histone guardian of the genome. *DNA Repair (Amst)* **3:** 959–967.

Forget AL, Kowalczykowski SC. 2012. Single-molecule imaging of DNA pairing by RecA reveals a three-dimensional homology search. *Nature* **482:** 423–427.

Franchitto A, Pirzio LM, Prosperi E, Sapora O, Bignami M, Pichierri P. 2008. Replication fork stalling in WRN-deficient cells is overcome by prompt activation of a MUS81-dependent pathway. *J Cell Biol* **183:** 241–252.

Garcia-Higuera I, Taniguchi T, Ganesan S, Meyn MS, Timmers C, Hejna J, Grompe M, D'Andrea AD. 2001. Interaction of the Fanconi anemia proteins and BRCA1 in a common pathway. *Mol Cell* **7:** 249–262.

Gari K, Decaillet C, Delannoy M, Wu L, Constantinou A. 2008a. Remodeling of DNA replication structures by the

branch point translocase FANCM. *Proc Natl Acad Sci* **105:** 16107–16112.

Gari K, Decaillet C, Stasiak AZ, Stasiak A, Constantinou A. 2008b. The Fanconi anemia protein FANCM can promote branch migration of Holliday junctions and replication forks. *Mol Cell* **29:** 141–148.

Goodarzi AA, Noon AT, Deckbar D, Ziv Y, Shiloh Y, Lobrich M, Jeggo PA. 2008a. ATM signaling facilitates repair of DNA double-strand breaks associated with heterochromatin. *Mol Cell* **31:** 167–177.

Goodarzi AA, Noon AT, Deckbar D, Ziv Y, Shiloh Y, Löbrich M, Jeggo PA. 2008b. ATM signaling facilitates repair of DNA double-strand breaks associated with heterochromatin. *Mol Cell* **31:** 167–177.

Goodarzi AA, Kurka T, Jeggo PA. 2011. KAP-1 phosphorylation regulates CHD3 nucleosome remodeling during the DNA double-strand break response. *Nat Struct Mol Biol* **18:** 831–839.

Greenberg RA, Sobhian B, Pathania S, Cantor SB, Nakatani Y, Livingston DM. 2006. Multifactorial contributions to an acute DNA damage response by BRCA1/BARD1-containing complexes. *Genes Dev* **20:** 34–46.

Hakansson P, Dahl L, Chilkova O, Domkin V, Thelander L. 2006a. The *Schizosaccharomyces pombe* replication inhibitor Spd1 regulates ribonucleotide reductase activity and dNTPs by binding to the large Cdc22 subunit. *J Biol Chem* **281:** 1778–1783.

Hakansson P, Hofer A, Thelander L. 2006b. Regulation of mammalian ribonucleotide reduction and dNTP pools after DNA damage and in resting cells. *J Biol Chem* **281:** 7834–7841.

Halazonetis TD, Gorgoulis VG, Bartek J. 2008. An oncogene-induced DNA damage model for cancer development. *Science* **319:** 1352–1355.

Huen MS, Grant R, Manke I, Minn K, Yu X, Yaffe MB, Chen J. 2007. RNF8 transduces the DNA-damage signal via histone ubiquitylation and checkpoint protein assembly. *Cell* **131:** 901–914.

Ishiai M, Kitao H, Smogorzewska A, Tomida J, Kinomura A, Uchida E, Saberi A, Kinoshita E, Kinoshita-Kikuta E, Koike T, et al. 2008. FANCI phosphorylation functions as a molecular switch to turn on the Fanconi anemia pathway. *Nat Struct Mol Biol* **15:** 1138–1146.

Jakob B, Splinter J, Taucher-Scholz G. 2009. Positional stability of damaged chromatin domains along radiation tracks in mammalian cells. *Radiat Res* **171:** 405–418.

Joo W, Xu G, Persky NS, Smogorzewska A, Rudge DG, Buzovetsky O, Elledge SJ, Pavletich NP. 2011. Structure of the FANCI-FANCD2 complex: Insights into the Fanconi anemia DNA repair pathway. *Science* **333:** 312–316.

Kalocsay M, Hiller NJ, Jentsch S. 2009. Chromosome-wide Rad51 spreading and SUMO-H2A.Z-dependent chromosome fixation in response to a persistent DNA double-strand break. *Mol Cell* **33:** 335–343.

Karmakar P, Piotrowski J, Brosh RM Jr, Sommers JA, Miller SP, Cheng WH, Snowden CM, Ramsden DA, Bohr VA. 2002. Werner protein is a target of DNA-dependent protein kinase in vivo and in vitro, and its catalytic activities are regulated by phosphorylation. *J Biol Chem* **277:** 18291–18302.

Kim H, D'Andrea AD. 2012. Regulation of DNA cross-link repair by the Fanconi anemia/BRCA pathway. *Genes Dev* **26:** 1393–1408.

Kim H, Chen J, Yu X. 2007. Ubiquitin-binding protein RAP80 mediates BRCA1-dependent DNA damage response. *Science* **316:** 1202–1205.

Kim Y, Lach FP, Desetty R, Hanenberg H, Auerbach AD, Smogorzewska A. 2011. Mutations of the SLX4 gene in Fanconi anemia. *Nat Genet* **43:** 142–146.

Knipscheer P, Raschle M, Smogorzewska A, Enoiu M, Ho TV, Scharer OD, Elledge SJ, Walter JC. 2009. The Fanconi anemia pathway promotes replication-dependent DNA interstrand cross-link repair. *Science* **326:** 1698–1701.

Kolas NK, Chapman JR, Nakada S, Ylanko J, Chahwan R, Sweeney FD, Panier S, Mendez M, Wildenhain J, Thomson TM, et al. 2007. Orchestration of the DNA-damage response by the RNF8 ubiquitin ligase. *Science* **318:** 1637–1640.

Kratz K, Schopf B, Kaden S, Sendoel A, Eberhard R, Lademann C, Cannavo E, Sartori AA, Hengartner MO, Jiricny J. 2010. Deficiency of FANCD2-associated nuclease KIAA1018/FAN1 sensitizes cells to interstrand crosslinking agents. *Cell* **142:** 77–88.

Kruhlak MJ, Celeste A, Dellaire G, Fernandez-Capetillo O, Muller WG, McNally JG, Bazett-Jones DP, Nussenzweig A. 2006. Changes in chromatin structure and mobility in living cells at sites of DNA double-strand breaks. *J Cell Biol* **172:** 823–834.

Lavin MF. 2008. Ataxia-telangiectasia: From a rare disorder to a paradigm for cell signalling and cancer. *Nat Rev Mol Cell Biol* **9:** 759–769.

Lee YD, Wang J, Stubbe J, Elledge SJ. 2008. Dif1 is a DNA-damage-regulated facilitator of nuclear import for ribonucleotide reductase. *Mol Cell* **32:** 70–80.

Lee HS, Park JH, Kim SJ, Kwon SJ, Kwon J. 2010. A cooperative activation loop among SWI/SNF, γ-H2AX and H3 acetylation for DNA double-strand break repair. *EMBO J* **29:** 1434–1445.

Leman AR, Noguchi C, Lee CY, Noguchi E. 2010. Human Timeless and Tipin stabilize replication forks and facilitate sister-chromatid cohesion. *J Cell Sci* **123:** 660–670.

Li W, Kim SM, Lee J, Dunphy WG. 2004. Absence of BLM leads to accumulation of chromosomal DNA breaks during both unperturbed and disrupted S phases. *J Cell Biol* **165:** 801–812.

Liu C, Powell KA, Mundt K, Wu L, Carr AM, Caspari T. 2003. Cop9/signalosome subunits and Pcu4 regulate ribonucleotide reductase by both checkpoint-dependent and -independent mechanisms. *Genes Dev* **17:** 1130–1140.

Liu T, Ghosal G, Yuan J, Chen J, Huang J. 2010. FAN1 acts with FANCI-FANCD2 to promote DNA interstrand cross-link repair. *Science* **329:** 693–696.

Long DT, Raschle M, Joukov V, Walter JC. 2011. Mechanism of RAD51-dependent DNA interstrand cross-link repair. *Science* **333:** 84–87.

Lopes M, Cotta-Ramusino C, Pellicioli A, Liberi G, Plevani P, Muzi-Falconi M, Newlon CS, Foiani M. 2001. The DNA replication checkpoint response stabilizes stalled replication forks. *Nature* **412:** 557–561.

Lovejoy CA, Cortez D. 2009. Common mechanisms of PIKK regulation. *DNA Repair (Amst)* **8:** 1004–1008.

Lovejoy CA, Xu X, Bansbach CE, Glick GG, Zhao R, Ye F, Sirbu BM, Titus LC, Shyr Y, Cortez D. 2009. Functional genomic screens identify CINP as a genome maintenance protein. *Proc Natl Acad Sci* **106:** 19304–19309.

Lucca C, Vanoli F, Cotta-Ramusino C, Pellicioli A, Liberi G, Haber J, Foiani M. 2004. Checkpoint-mediated control of replisome-fork association and signalling in response to replication pausing. *Oncogene* **23:** 1206–1213.

Machwe A, Xiao L, Groden J, Orren DK. 2006. The Werner and Bloom syndrome proteins catalyze regression of a model replication fork. *Biochemistry* **45:** 13939–13946.

Machwe A, Karale R, Xu X, Liu Y, Orren DK. 2011. The Werner and Bloom syndrome proteins help resolve replication blockage by converting (regressed) Holliday junctions to functional replication forks. *Biochemistry* **50:** 6774–6788.

Mailand N, Bekker-Jensen S, Faustrup H, Melander F, Bartek J, Lukas C, Lukas J. 2007. RNF8 ubiquitylates histones at DNA double-strand breaks and promotes assembly of repair proteins. *Cell* **131:** 887–900.

Matsuoka S, Ballif BA, Smogorzewska A, McDonald ER III, Hurov KE, Luo J, Bakalarski CE, Zhao Z, Solimini N, Lerenthal Y, et al. 2007. ATM and ATR substrate analysis reveals extensive protein networks responsive to DNA damage. *Science* **316:** 1160–1166.

Meetei AR, Medhurst AL, Ling C, Xue Y, Singh TR, Bier P, Steltenpool J, Stone S, Dokal I, Mathew CG, et al. 2005. A human ortholog of archaeal DNA repair protein Hef is defective in Fanconi anemia complementation group M. *Nat Genet* **37:** 958–963.

Mine-Hattab J, Rothstein R. 2012. Increased chromosome mobility facilitates homology search during recombination. *Nat Cell Biol* **14:** 510–517.

Misteli T, Soutoglou E. 2009. The emerging role of nuclear architecture in DNA repair and genome maintenance. *Nat Rev Mol Cell Biol* **10:** 243–254.

Moyal L, Lerenthal Y, Gana-Weisz M, Mass G, So S, Wang SY, Eppink B, Chung YM, Shalev G, Shema E, et al. 2011. Requirement of ATM-dependent monoubiquitylation of histone H2B for timely repair of DNA double-strand breaks. *Mol Cell* **41:** 529–542.

Nagai S, Dubrana K, Tsai-Pflugfelder M, Davidson MB, Roberts TM, Brown GW, Varela E, Hediger F, Gasser SM, Krogan NJ. 2008. Functional targeting of DNA damage to a nuclear pore-associated SUMO-dependent ubiquitin ligase. *Science* **322:** 597–602.

Nam EA, Zhao R, Cortez D. 2011. Analysis of mutations that dissociate G_2 and essential S phase functions of human ataxia telangiectasia-mutated and Rad3-related (ATR) protein kinase. *J Biol Chem* **286:** 37320–37327.

Negrini S, Gorgoulis VG, Halazonetis TD. 2010. Genomic instability—An evolving hallmark of cancer. *Nat Rev Mol Cell Biol* **11:** 220–228.

Nelms BE, Maser RS, MacKay JF, Lagally MG, Petrini JH. 1998. In situ visualization of DNA double-strand break repair in human fibroblasts. *Science* **280:** 590–592.

Neumann FR, Dion V, Gehlen LR, Tsai-Pflugfelder M, Schmid R, Taddei A, Gasser SM. 2012. Targeted INO80 enhances subnuclear chromatin movement and ectopic homologous recombination. *Genes Dev* **26:** 369–383.

Niida H, Katsuno Y, Sengoku M, Shimada M, Yukawa M, Ikura M, Ikura T, Kohno K, Shima H, Suzuki H, et al. 2010. Essential role of Tip60-dependent recruitment of ribonucleotide reductase at DNA damage sites in DNA repair during G1 phase. *Genes Dev* **24:** 333–338.

Noon AT, Shibata A, Rief N, Lobrich M, Stewart GS, Jeggo PA, Goodarzi AA. 2010. 53BP1-dependent robust localized KAP-1 phosphorylation is essential for heterochromatic DNA double-strand break repair. *Nat Cell Biol* **12:** 177–184.

Nordlund P, Reichard P. 2006. Ribonucleotide reductases. *Annu Rev Biochem* **75:** 681–706.

Nussenzweig A, Nussenzweig MC. 2010. Origin of chromosomal translocations in lymphoid cancer. *Cell* **141:** 27–38.

Oza P, Jaspersen SL, Miele A, Dekker J, Peterson CL. 2009. Mechanisms that regulate localization of a DNA double-strand break to the nuclear periphery. *Genes Dev* **23:** 912–927.

Paciotti V, Clerici M, Scotti M, Lucchini G, Longhese MP. 2001. Characterization of mec1 kinase-deficient mutants and of new hypomorphic mec1 alleles impairing subsets of the DNA damage response pathway. *Mol Cell Biol* **21:** 3913–3925.

Paulsen RD, Soni DV, Wollman R, Hahn AT, Yee MC, Guan A, Hesley JA, Miller SC, Cromwell EF, Solow-Cordero DE, et al. 2009. A genome-wide siRNA screen reveals diverse cellular processes and pathways that mediate genome stability. *Mol Cell* **35:** 228–239.

Peng G, Yim EK, Dai H, Jackson AP, Burgt I, Pan MR, Hu R, Li K, Lin SY. 2009. BRIT1/MCPH1 links chromatin remodelling to DNA damage response. *Nat Cell Biol* **11:** 865–872.

Pichierri P, Rosselli F, Franchitto A. 2003. Werner's syndrome protein is phosphorylated in an ATR/ATM-dependent manner following replication arrest and DNA damage induced during the S phase of the cell cycle. *Oncogene* **22:** 1491–1500.

Poulsen M, Lukas C, Lukas J, Bekker-Jensen S, Mailand N. 2012. Human RNF169 is a negative regulator of the ubiquitin-dependent response to DNA double-strand breaks. *J Cell Biol* **197:** 189–199.

Qiao F, Mi J, Wilson JB, Zhi G, Bucheimer NR, Jones NJ, Kupfer GM. 2004. Phosphorylation of fanconi anemia (FA) complementation group G protein, FANCG, at serine 7 is important for function of the FA pathway. *J Biol Chem* **279:** 46035–46045.

Rao VA, Fan AM, Meng L, Doe CF, North PS, Hickson ID, Pommier Y. 2005. Phosphorylation of BLM, dissociation from topoisomerase IIIα, and colocalization with γ-H2AX after topoisomerase I-induced replication damage. *Mol Cell Biol* **25:** 8925–8937.

Raschle M, Knipscheer P, Enoiu M, Angelov T, Sun J, Griffith JD, Ellenberger TE, Scharer OD, Walter JC. 2008. Mechanism of replication-coupled DNA interstrand crosslink repair. *Cell* **134:** 969–980.

Reaper PM, Griffiths MR, Long JM, Charrier JD, Maccormick S, Charlton PA, Golec JM, Pollard JR. 2011. Selective killing of ATM- or p53-deficient cancer cells through inhibition of ATR. *Nat Chem Biol* **7:** 428–430.

Sengupta S, Robles AI, Linke SP, Sinogeeva NI, Zhang R, Pedeux R, Ward IM, Celeste A, Nussenzweig A, Chen J, et al. 2004. Functional interaction between BLM helicase and 53BP1 in a Chk1-mediated pathway during S-phase arrest. *J Cell Biol* **166:** 801–813.

Shanbhag NM, Rafalska-Metcalf IU, Balane-Bolivar C, Janicki SM, Greenberg RA. 2010. ATM-dependent chromatin changes silence transcription in *cis* to DNA double-strand breaks. *Cell* **141:** 970–981.

Shell SM, Li Z, Shkriabai N, Kvaratskhelia M, Brosey C, Serrano MA, Chazin WJ, Musich PR, Zou Y. 2009. Checkpoint kinase ATR promotes nucleotide excision repair of UV-induced DNA damage via physical interaction with xeroderma pigmentosum group A. *J Biol Chem* **284:** 24213–24222.

Shi Y, Dodson GE, Mukhopadhyay PS, Shanware NP, Trinh AT, Tibbetts RS. 2007. Identification of carboxyl-terminal MCM3 phosphorylation sites using polyreactive phosphospecific antibodies. *J Biol Chem* **282:** 9236–9243.

Shiloh Y. 2003. ATM and related protein kinases: Safeguarding genome integrity. *Nat Rev Cancer* **3:** 155–168.

Sirbu BM, Couch FB, Feigerle JT, Bhaskara S, Hiebert SW, Cortez D. 2011. Analysis of protein dynamics at active, stalled, and collapsed replication forks. *Genes Dev* **25:** 1320–1327.

Sirbu BM, Couch FB, Cortez D. 2012. Monitoring the spatiotemporal dynamics of proteins at replication forks and in assembled chromatin using isolation of proteins on nascent DNA. *Nat Protoc* **7:** 594–605.

Smogorzewska A, Desetty R, Saito TT, Schlabach M, Lach FP, Sowa ME, Clark AB, Kunkel TA, Harper JW, Colaiacovo MP, et al. 2010. A genetic screen identifies FAN1, a Fanconi anemia-associated nuclease necessary for DNA interstrand crosslink repair. *Mol Cell* **39:** 36–47.

Sobeck A, Stone S, Landais I, de Graaf B, Hoatlin ME. 2009. The Fanconi anemia protein FANCM is controlled by FANCD2 and the ATR/ATM pathways. *J Biol Chem* **284:** 25560–25568.

Sobhian B, Shao G, Lilli DR, Culhane AC, Moreau LA, Xia B, Livingston DM, Greenberg RA. 2007. RAP80 targets BRCA1 to specific ubiquitin structures at DNA damage sites. *Science* **316:** 1198–1202.

Sogo JM, Lopes M, Foiani M. 2002. Fork reversal and ssDNA accumulation at stalled replication forks owing to checkpoint defects. *Science* **297:** 599–602.

Sorensen CS, Hansen LT, Dziegielewski J, Syljuasen RG, Lundin C, Bartek J, Helleday T. 2005. The cell-cycle checkpoint kinase Chk1 is required for mammalian homologous recombination repair. *Nat Cell Biol* **7:** 195–201.

Soutoglou E, Dorn JF, Sengupta K, Jasin M, Nussenzweig A, Ried T, Danuser G, Misteli T. 2007. Positional stability of single double-strand breaks in mammalian cells. *Nat Cell Biol* **9:** 675–682.

Stewart GS, Panier S, Townsend K, Al-Hakim AK, Kolas NK, Miller ES, Nakada S, Ylanko J, Olivarius S, Mendez M, et al. 2009. The RIDDLE syndrome protein mediates a ubiquitin-dependent signaling cascade at sites of DNA damage. *Cell* **136:** 420–434.

Stucki M, Jackson SP. 2006. γH2AX and MDC1: Anchoring the DNA-damage-response machinery to broken chromosomes. *DNA Repair (Amst)* **5:** 534–543.

Tanaka H, Arakawa H, Yamaguchi T, Shiraishi K, Fukuda S, Matsui K, Takei Y, Nakamura Y. 2000. A ribonucleotide reductase gene involved in a p53-dependent cell-cycle checkpoint for DNA damage. *Nature* **404:** 42–49.

Tibbetts RS, Cortez D, Brumbaugh KM, Scully R, Livingston D, Elledge SJ, Abraham RT. 2000. Functional interactions between BRCA1 and the checkpoint kinase ATR during genotoxic stress. *Genes Dev* **14:** 2989–3002.

Toledo LI, Murga M, Zur R, Soria R, Rodriguez A, Martinez S, Oyarzabal J, Pastor J, Bischoff JR, Fernandez-Capetillo O. 2011. A cell-based screen identifies ATR inhibitors with synthetic lethal properties for cancer-associated mutations. *Nat Struct Mol Biol* **18:** 721–727.

Trenz K, Smith E, Smith S, Costanzo V. 2006. ATM and ATR promote Mre11 dependent restart of collapsed replication forks and prevent accumulation of DNA breaks. *EMBO J* **25:** 1764–1774.

Trenz K, Errico A, Costanzo V. 2008. Plx1 is required for chromosomal DNA replication under stressful conditions. *EMBO J* **27:** 876–885.

Tripathi V, Kaur S, Sengupta S. 2008. Phosphorylation-dependent interactions of BLM and 53BP1 are required for their anti-recombinogenic roles during homologous recombination. *Carcinogenesis* **29:** 52–61.

Tsukuda T, Lo YC, Krishna S, Sterk R, Osley MA, Nickoloff JA. 2009. INO80-dependent chromatin remodeling regulates early and late stages of mitotic homologous recombination. *DNA Repair (Amst)* **8:** 360–369.

Unsal-Kacmaz K, Chastain PD, Qu PP, Minoo P, Cordeiro-Stone M, Sancar A, Kaufmann WK. 2007. The human Tim/Tipin complex coordinates an Intra-S checkpoint response to UV that slows replication fork displacement. *Mol Cell Biol* **27:** 3131–3142.

van Attikum H, Gasser SM. 2009. Crosstalk between histone modifications during the DNA damage response. *Trends Cell Biol* **19:** 207–217.

van Attikum H, Fritsch O, Gasser SM. 2007. Distinct roles for SWR1 and INO80 chromatin remodeling complexes at chromosomal double-strand breaks. *EMBO J* **26:** 4113–4125.

Wang B, Matsuoka S, Ballif BA, Zhang D, Smogorzewska A, Gygi SP, Elledge SJ. 2007. Abraxas and RAP80 form a BRCA1 protein complex required for the DNA damage response. *Science* **316:** 1194–1198.

Weterings E, Chen DJ. 2007. DNA-dependent protein kinase in nonhomologous end joining: A lock with multiple keys? *J Cell Biol* **179:** 183–186.

Wilson JB, Yamamoto K, Marriott AS, Hussain S, Sung P, Hoatlin ME, Mathew CG, Takata M, Thompson LH, Kupfer GM, et al. 2008. FANCG promotes formation of a newly identified protein complex containing BRCA2, FANCD2 and XRCC3. *Oncogene* **27:** 3641–3652.

Wood JL, Singh N, Mer G, Chen J. 2007. MCPH1 functions in an H2AX-dependent but MDC1-independent pathway in response to DNA damage. *J Biol Chem* **282:** 35416–35423.

Wu X, Huang M. 2008. Dif1 controls subcellular localization of ribonucleotide reductase by mediating nuclear import of the R2 subunit. *Mol Cell Biol* **28:** 7156–7167.

Wu X, Shell SM, Liu Y, Zou Y. 2007. ATR-dependent checkpoint modulates XPA nuclear import in response to UV irradiation. *Oncogene* **26:** 757–764.

Yan J, Kim YS, Yang XP, Li LP, Liao G, Xia F, Jetten AM. 2007. The ubiquitin-interacting motif containing protein RAP80 interacts with BRCA1 and functions in DNA damage repair response. *Cancer Res* **67:** 6647–6656.

Yang K, Moldovan GL, Vinciguerra P, Murai J, Takeda S, D'Andrea AD. 2011. Regulation of the Fanconi anemia pathway by a SUMO-like delivery network. *Genes Dev* **25:** 1847–1858.

Yannone SM, Roy S, Chan DW, Murphy MB, Huang S, Campisi J, Chen DJ. 2001. Werner syndrome protein is regulated and phosphorylated by DNA-dependent protein kinase. *J Biol Chem* **276:** 38242–38248.

Yao R, Zhang Z, An X, Bucci B, Perlstein DL, Stubbe J, Huang M. 2003. Subcellular localization of yeast ribonucleotide reductase regulated by the DNA replication and damage checkpoint pathways. *Proc Natl Acad Sci* **100:** 6628–6633.

Yoo HY, Shevchenko A, Dunphy WG. 2004. Mcm2 is a direct substrate of ATM and ATR during DNA damage and DNA replication checkpoint responses. *J Biol Chem* **279:** 53353–53364.

Yoshizawa-Sugata N, Masai H. 2007. Human Tim/Timeless-interacting protein, Tipin, is required for efficient progression of S phase and DNA replication checkpoint. *J Biol Chem* **282:** 2729–2740.

Yoshizawa-Sugata N, Masai H. 2009. Roles of human AND-1 in chromosome transactions in S phase. *J Biol Chem* **284:** 20718–20728.

Yusufzai T, Kadonaga JT. 2008. HARP is an ATP-driven annealing helicase. *Science* **322:** 748–750.

Zhao X, Muller EG, Rothstein R. 1998. A suppressor of two essential checkpoint genes identifies a novel protein that negatively affects dNTP pools. *Mol Cell* **2:** 329–340.

Zhao X, Chabes A, Domkin V, Thelander L, Rothstein R. 2001. The ribonucleotide reductase inhibitor Sml1 is a new target of the Mec1/Rad53 kinase cascade during growth and in response to DNA damage. *EMBO J* **20:** 3544–3553.

Zhu B, Zheng Y, Pham AD, Mandal SS, Erdjument-Bromage H, Tempst P, Reinberg D. 2005. Monoubiquitination of human histone H2B: The factors involved and their roles in HOX gene regulation. *Mol Cell* **20:** 601–611.

Ziv Y, Bielopolski D, Galanty Y, Lukas C, Taya Y, Schultz DC, Lukas J, Bekker-Jensen S, Bartek J, Shiloh Y. 2006. Chromatin relaxation in response to DNA double-strand breaks is modulated by a novel ATM- and KAP-1 dependent pathway. *Nat Cell Biol* **8:** 870–876.

OPEN ACCESS Freely available online

PLOS ONE

Inhibition of *Histone Deacetylase 3* Causes Replication Stress in Cutaneous T Cell Lymphoma

Christina E. Wells[1], Srividya Bhaskara[2], Kristy R. Stengel[1], Yue Zhao[1], Bianca Sirbu[1], Benjamin Chagot[1,3], David Cortez[1,4], Dineo Khabele[4,5,6], Walter J. Chazin[1], Andrew Cooper[7], Vincent Jacques[7], James Rusche[7], Christine M. Eischen[4,8], Laura Y. McGirt[4,9]*, Scott W. Hiebert[1,4]*

1 Department of Biochemistry, Vanderbilt University School of Medicine, Nashville, Tennessee, United States of America, **2** Departments of Radiation Oncology and Oncological Sciences, Huntsman Cancer Institute, University of Utah School of Medicine, Salt Lake City, Utah, United States of America, **3** Laboratoire AREMS UMR7214 UL-CNRS, Université de Lorraine, Vandoeuvre-Lés-Nancy, France, **4** Vanderbilt-Ingram Cancer Center, Vanderbilt University School of Medicine, Nashville, Tennessee, United States of America, **5** Department of Cancer Biology, Vanderbilt University Medical Center, Nashville, Tennessee, United States of America, **6** Department of Obstetrics and Gynecology, Division of Gynecologic Oncology, Vanderbilt University Medical Center, Nashville, Tennessee, United States of America, **7** Repligen Corporation, Waltham, Massachusetts, United States of America, **8** Department of Pathology, Microbiology and Immunology, Vanderbilt University Medical Center, Nashville, Tennessee, United States of America, **9** Department of Medicine, Division of Dermatology, Vanderbilt University Medical Center, Nashville, Tennessee, United States of America

Abstract

Given the fundamental roles of histone deacetylases (HDACs) in the regulation of DNA repair, replication, transcription and chromatin structure, it is fitting that therapies targeting HDAC activities are now being explored as anti-cancer agents. In fact, two histone deacetylase inhibitors (HDIs), SAHA and Depsipeptide, are FDA approved for single-agent treatment of refractory cutaneous T cell lymphoma (CTCL). An important target of these HDIs, histone deacetylase 3 (HDAC3), regulates processes such as DNA repair, metabolism, and tumorigenesis through the regulation of chromatin structure and gene expression. Here we show that HDAC3 inhibition using a first in class selective inhibitor, RGFP966, resulted in decreased cell growth in CTCL cell lines due to increased apoptosis that was associated with DNA damage and impaired S phase progression. Through isolation of proteins on nascent DNA (iPOND), we found that HDAC3 was associated with chromatin and is present at and around DNA replication forks. DNA fiber labeling analysis showed that inhibition of HDAC3 resulted in a significant reduction in DNA replication fork velocity within the first hour of drug treatment. These results suggest that selective inhibition of HDAC3 could be useful in treatment of CTCL by disrupting DNA replication of the rapidly cycling tumor cells, ultimately leading to cell death.

Citation: Wells CE, Bhaskara S, Stengel KR, Zhao Y, Sirbu B, et al. (2013) Inhibition of *Histone Deacetylase 3* Causes Replication Stress in Cutaneous T Cell Lymphoma. PLoS ONE 8(7): e68915. doi:10.1371/journal.pone.0068915

Editor: Sue Cotterill, St. Georges University of London, United Kingdom

Received January 25, 2013; **Accepted** June 4, 2013; **Published** July 22, 2013

Funding: This work was supported by the T. J. Martell Foundation, the Robert J. Kleberg, Jr. and Helen C. Kleberg Foundation, National Institutes of Health grants (R01-CA64140, RO1-CA164605, RO1-CA109355) and core services performed through Vanderbilt Digestive Disease Research grant P30DK058404 and the Vanderbilt-Ingram Cancer Center support grant NCI P30CA68485. SB was supported by a fellowship (1F32CA138091) from the National Cancer Institute. LYM is supported by career development awards through the Dermatology Foundation and the NIH (Vanderbilt Clinical Oncology; 5K12CA090625). The funders had no role in study design, data collection and analysis, decision to publish, or preparation of the manuscript.

Competing Interests: Vincent Jacques and James Rusche work for Repligen who has developed the HDAC selective compounds used in this manuscript and have financial interests in this company. All other authors declare that no competing interests exist. This does not alter the authors' adherence to all the PLOS ONE policies on sharing data and materials.

* E-mail: laura.y.mcgirt@Vanderbilt.Edu (LYM); scott.hiebert@vanderbilt.edu (SWH)

Introduction

Cutaneous T cell lymphoma (CTCL) is a heterogeneous group of non-Hodgkin's lymphoma that is characterized by accumulation of malignant T cells in the skin [1–3]. The most common subtypes of CTCL are mycosis fungoides, Sézary Syndrome, and the $CD30^+$ lymphoproliferative disorders, comprising 95% of CTCL [2–5]. Histone deacetylase (HDAC) inhibitors have become an important treatment option for CTCL that progresses to the more aggressive stages of disease. Histone deacetylases are likely to serve as valuable therapeutic targets as they contribute to genomic stability and cell cycle control through their fundamental roles in cell proliferation including the regulation of DNA repair, replication, transcription, and chromatin structure. In fact, due to their success in the treatment of CTCL, HDACs are now being explored as therapeutic targets for multiple cancers [6–9].

Two histone deacetylase inhibitors (HDIs), SAHA (Vorinostat) and Depsipeptide (Romidepsin), are FDA approved for the treatment of refractory CTCL [1,3,10–12]. Both of these compounds inhibit multiple HDACs with SAHA inhibiting class I and II HDACs while Depsipeptide inhibits the class I HDACs and HDAC6 [10,11,13]. However, since these HDIs inhibit multiple HDACs, they may be inhibiting targets that are not integral to CTCL survival and progression, thereby causing unnecessary side effects. Treatment with SAHA or Depsipeptide is less toxic than standard chemotherapy but can be associated with negative impacts on quality of life [3,12,13]. Adverse effects of SAHA and Depsipeptide include nausea, fatigue, gastrointestinal and cardiac toxicity, and hematologic impairment [3,12,13]. Additionally, the roles of HDACs in tumorigenesis and the mechanisms by which HDAC inhibition is effective against cancer remain unclear. Therefore, selective inhibition of HDACs may

decrease side effects by inhibiting only one or two HDACs at a time and allow for further elucidation of the roles of individual HDACs in cancer.

An important target of these HDIs is histone deacetylase 3, or HDAC3. HDAC3 (a class I HDAC) is involved in the regulation of chromatin structure and gene expression, which controls DNA repair, metabolism, and even tumorigenesis [14–18]. While HDACs are often thought of exclusively as transcriptional repressors, mouse embryonic fibroblasts (MEFs) lacking HDAC3 displayed S phase dependent DNA damage accumulation, deregulation of transcription, and apoptosis [17]. Due to this role in DNA damage, selective HDAC3 inhibition could potentially target the rapidly proliferating tumor cells while not harming the surrounding quiescent, non-malignant cells [19–24].

HDACs are classified based on sequence conservation. The class I HDACs (HDACs 1, 2, 3, and 8) are homologous to yeast RPD3 while the class II HDACs are more similar to the yeast Hda1 enzyme [25–28]. HDACs 1 and 2 share 82% identity while these HDACs share 53% and 52% identity, respectively, with HDAC3 [29–31]. The class I HDACs also contain a highly conserved central catalytic domain [30,31] that is 58% identical between HDAC1 and HDAC3. Given the high level of homology between the class I HDACs, it is understandable why a selective inhibitor would be difficult to identify. However, a new class of inhibitors, N-(*o*-aminophenyl) carboxamides, can show 10-fold or higher selectivity for HDAC3, over HDACs 1 and 2 [[32] and Vincent Jacques, Repligen, unpublished data]. This family of inhibitors includes RGFP966 [32–35], which has an IC_{50} of 0.08 μM in *in vitro* substrate assays and inhibition of other HDACs by RGFP966 was not seen at concentrations up to 15 μM [32]. Therefore, we set out to determine the effects of selective HDAC3 inhibition using RGFP966 on cancer cell growth.

Here we treated CTCL cell lines with a selective HDAC3 inhibitor and found that these cells exhibited sensitivity to selective HDAC3 inhibition as demonstrated by decreased cell growth and increased apoptosis. We also found that these cells had increased DNA damage upon HDAC3 inhibition and did not progress normally through the cell cycle due to impaired S phase progression. Consistently, DNA fiber labeling assays demonstrated that inhibition of HDAC3 caused a 50% reduction in DNA replication fork velocity. Through isolation of proteins on nascent DNA (iPOND), we determined that Hdac3 is associated with chromatin and present at and around DNA replication forks. Thus, HDAC3 inhibition caused replication stress in CTCL cells, and selective inhibition of HDAC3 through novel inhibitors may be useful in the treatment of CTCL.

Materials and Methods

Ethics Statement

Mouse studies were performed under an animal protocol approved by the Vanderbilt Institutional Animal Care and Use Committee, Nashville, TN.

Cell Culture

HH ($CD30^+$ lymphoproliferative disorder) cells (ATCC) were cultured in RPMI supplemented with 10% heat inactivated fetal bovine serum (FBS), 50 U/ml penicillin, 50 μg/ml streptomycin, and 2 mM L-glutamine. Hut78 (Sézary Syndrome) cells (ATCC) were cultured in Iscove's Modified Dulbecco's Medium (IMDM) supplemented with 20% heat inactivated FBS, 50 U/ml penicillin, 50 μg/ml streptomycin, and 4 mM L-glutamine. Cells were maintained between 2×10^5–1×10^6 cells/mL.

Antibodies

The following antibodies were purchased from Abcam: Histone H4 [EP10000Y] (acetyl K5) (ab51997), Histone H3 (acetyl K27) (ab4729), HDAC 1 (ab19845), HDAC 2 [Y461] (ab32117), HDAC 3 (ab16047) and Histone H2B (ab1790). Histone H3 [96C10] (3638S) and Histone H4 [L64C1] (2935S) were used as loading controls and purchased from Cell Signaling. Anti-acetyl histone H3 (or H3K9K14ac) (06–599) and Anti-phospho-Histone H2A.X (Ser 139) clone JBW301 (05–636) were purchased from Millipore. Histone H3 (acetyl K56) (2134-1) was purchased from Epitomics, and anti-actin (A2066) was purchased from Sigma Aldrich. PCNA [FL261] was purchased from Santa Cruz (SC7907).

Histone Deacetylase Inhibitors (HDIs) and CTCL Therapeutic Drugs

Depsipeptide (aka Romidepsin, FK228, Depsi) was kindly provided by Celgene. The HDIs RGFP233, RGFP136, and RGFP966 were synthesized and kindly given to us by Repligen Corporation. These compounds are analogs of previously published compounds [34] but have different HDAC inhibition selectivity [32–35]. In purified enzyme assays, RGFP966, 233, and 136 had the following HDAC inhibition IC_{50} values for HDAC1, HDAC2, and HDAC3: RGFP966: >15, >15, 0.08 μM; RGFP233:0.034, 0.059, 3.33 μM; and RGFP136:5.2, 3.0, 0.4 μM. Bexarotene (SML0282), Methotrexate (M8407), and ATRA (R2625) were purchased from Sigma Aldrich.

Protein Preparation and Western Blot Analysis

For preparation of whole cell protein lysates, cell pellets were washed with PBS and then sonicated in radioimmunoprecipitation assay (RIPA) buffer containing protease inhibitors (Roche) and phosphatase inhibitors (Roche). For preparation of liver lysates, livers were minced in RIPA buffer with protease inhibitors with a razor blade and then homogenized using a dounce homogenizer. Samples were sonicated and then cleared by centrifugation. Then samples were diluted 1:2 in Laemmli's sample buffer (Bio-Rad) and subjected to 13% sodium dodecyl sulfate-polyacrylamide gel electrophoresis. Western blot analyses were performed using primary antibodies listed above and for histone modification or γH2ax westerns, fluorophore conjugated secondary antibodies and the Odyssey system (LiCor) were used. For the iPOND experiment, a HRP secondary antibody and Western Lightning Plus enhanced chemiluminescence substrate (PerkinElmer, NEL103001EA) was used.

For protein separation, soluble chromatin obtained from Hela cells was fractionated using a Superose 6 10/300 GL (GE Healthcare) gel filtration column. Fractions (0.5 ml) were collected, concentrated using trichloroacetic acid precipitation, and analyzed by western blotting using the antibodies indicated in the figure legends. Molecular weight standards were added to the sample as controls. Their elution fractions are indicated at top of the figure.

Growth Curves

Alamar blue was purchased from Invitrogen (DAL1100). Cells were counted and split into T25 (Corning) flasks at 2×10^5 cells/mL. Cells were then treated with DMSO, or HDIs once at hour 0. 100 μl aliquots were taken in triplicate from each flask at 0 hr, 24 hrs, 48 hrs, and 72 hrs after treatment, distributed into a flat bottom 96-well plate, and 10 μl of alamar blue added to each well. After a 4 hr incubation, fluorescence was measured using the Biotek Synergy MX Microplate Reader. For the dual treatment

curves, the same protocol was followed except ATRA was re-administered at 48 hrs after the initial treatment.

Annexin V Staining

Annexin V analysis of HH and Hut78 cells was performed using annexin V-fluorescein isothiocyanate (annexin V-FITC) apoptosis detection kit I (BD Pharmingen - 556547) per the manufacturer's instructions. Briefly, cells were treated with DMSO, Depsi, or HDIs for 24 hrs, pelleted, washed with PBS, and counted. Cells were then resuspended in annexin V binding buffer, labeled with annexin V-FITC and propidium iodide (PI), and then analyzed by flow cytometry using the 5-laser BD LSRII instrument in the Vanderbilt Flow Cytometry Core. Here propidium iodide (PI) is used as a vital dye.

BrdU Staining

Cell cycle status was analyzed using the FITC Mouse Anti-BrdU set (BD Pharmingen-556028). Cells were treated with DMSO, Depsi, or HDIs for 24 hrs and then BrdU (20 μM final concentration) was added to each flask one and a half hours before harvesting. The cells were then pelleted, washed with PBS, and counted. 1×10^6 cells per sample were pelleted, resuspended in 200 μl cold PBS and 5 mls of cold 100% ethanol, covered with foil, and stored at 4°C overnight. The next day cells were pelleted, resuspended in 1 mL 2N HCL supplemented with 0.5 mg/mL pepsin, and then incubated for exactly 30 mins at 37°C. Samples were then neutralized with 3 mL 0.1M Sodium Tetraborate (pH 8.5) and pelleted for 7 mins. Then samples were washed 1× with 1 mL of PBS +0.5% BSA, pelleted, washed 1× with PBS +0.5% BSA +0.5% Tween 20, and pelleted again. Samples were then resuspended in FITC-Conjugated anti-BrdU and incubated for 45 mins at room temperature in the dark. Samples were washed one more with PBS +0.5% BSA +0.5% Tween 20 and resuspended in 400 μL of PBS. Propidium iodide and RNase A were added to each sample and then analyzed by flow cytometry using the 5-laser BD LSRII instrument in the Vanderbilt Flow Cytometry Core.

iPOND

Analysis of proteins associated with DNA replication forks was performed using the iPOND (isolated proteins on nascent DNA) method described previously [36]. Briefly, Hut78 cells were pulsed with EdU for 15 mins followed by either no thymidine chase or a 60 minute thymidine chase. The protein-DNA complexes were then crosslinked with 1% (wt/vol) formaldehyde, nascent DNA was conjugated to biotin using click chemistry, and then protein-DNA complexes were purified using Streptavidin beads. The eluted proteins were then analyzed using western blot analysis. A no click reaction sample (No Clk) that did not include biotin azide was used as a negative control. 0.1% input samples were included for positive controls of each protein analyzed. PCNA served as a positive control for a replication fork associated protein and H2B served as a loading control and positive control for a chromatin associated protein.

DNA Fiber Labeling

DNA fiber labeling analysis was used to assess DNA replication fork progression [37] in Hut78 cells treated with DMSO, 10 nM Depsipeptide or 10 μM 966. For experiments where DMSO or HDIs were added prior to labeling, DMSO or HDIs were added 5 mins or 4 hrs prior to the addition of IdU (green). Following a 20 min IdU pulse (20 μM final concentration), cells were washed and drug re-administered along with 100 μM CldU for 20 mins. Cells were then washed with equilibrated HBSS, resuspended in cold PBS at 1×10^6 cells/ml, and mixed with non-labeled cells for better spreading results (20 μL labeled cells +60 μL non-labeled cells). 2 μL of cell suspension and 10 μL of spreading buffer (0.5% SDS, 200 mM Tris-HCl ph 7.4, 50 mM EDTA) was added to each slide, let sit for 6 mins at RT and then tilted to 15 degrees to allow the DNA to run slowly down the slide. 5 slides were made for each sample. Slides were then air dried for at least 40 mins, fixed in 3:1 methanol:acetic acid for 2 mins, air dried again for 20 mins, and then stored at 4°C overnight.

The next day, slides were submerged in 2.5M HCl for 30 mins, rinsed 3× in PBS and then incubated in 10% goat serum/0.1%Triton in PBS for 1 hr. Then slides were incubated in the dark for 1 hr in rat monoclonal anti-CldU (Accurate Chemical OBT0030G) and mouse anti-IdU (Becton Dickinson 347580) diluted 1/100 in 10% goat serum/0.1% Triton in PBS. Slides were then rinsed 3× in PBS and incubated 30 min with secondary antibodies (Invitrogen Alexa Fluor 568 goat anti-rat-IgG A-11077 and Alexa Fluor 488 goat anti-mouse-IgG A-11029) in 10% goat serum/0.1% Triton in PBS in the dark. Slides were then rinsed 3× in PBS, air dried in the dark, mounted with 110 μL of Prolong Gold with no Dapi (Invitrogen P36930) using whole slide coverslips, let dry overnight at RT and then stored at 4°C. Samples were imaged at 1000× and 100 fibers were measured for each sample.

Fork velocity was determined by the total length of fibers (IdU plus CldU) divided by 40 min. The above listed protocol was followed for all experiments except for changes in the labeling scheme as listed below: For experiments where DMSO or HDIs were added after labeling with IdU followed by CldU, cells were labeled with IdU for 20 mins followed by 20 mins of CldU, washed, and then either immediately treated with DMSO or HDIs for 25 mins or incubated in fresh medium for 4 hrs and then treated with DMSO or HDIs for 25 mins. Fork Velocity was determined by the total length of fibers (IdU plus CldU) divided by 40 min pulse or by the length of either the IdU label or CldU label divided by 20 min pulse.

Results

Selectivity of Novel Histone Deacetylase Inhibitors

The development of selective class I HDAC inhibitors has been challenging due to the conservation of the deacetylase domains of HDACs1-3, yet recently some selectivity has been achieved [32–34,38]. To further assess the action of these inhibitors, we sought a histone mark that separates the functions of HDAC1/2 from HDAC3. Deletion of *Hdac3* caused increases in the acetylation of H4K5, H4K8, H4K12, H4K16, H3K9K14, and H3K27 [16], which are also targeted by Hdac1/2 [39]. However, we noted that *Hdac3* deletion did not cause the accumulation of the modification recognized by the rabbit monoclonal antibody to H3K56ac (Figure 1A). While this antibody can also cross react with H3K9ac [40], anti-H3K9ac did increase in $Hdac3^{-/-}$ cells, suggesting that under the conditions used here we did not detect H3K9ac with this antibody (Figure 1A; note that all samples were run on the same gel, but we removed intervening lanes for side by side comparison of WT and $Hdac3^{-/-}$ samples). In contrast, inhibitors of class I HDACs (SAHA, Trichostatin A and sodium butyrate (NaB)), caused a more dramatic accumulation of H3K56ac than nicotinamide, which impairs the Sirtuins (Figure 1B). Therefore, we used siRNAs directed to *Hdac1* and *Hdac2* and found that co-suppression of the expression of both enzymes was necessary to cause H3K56ac to accumulate, suggesting that both of these

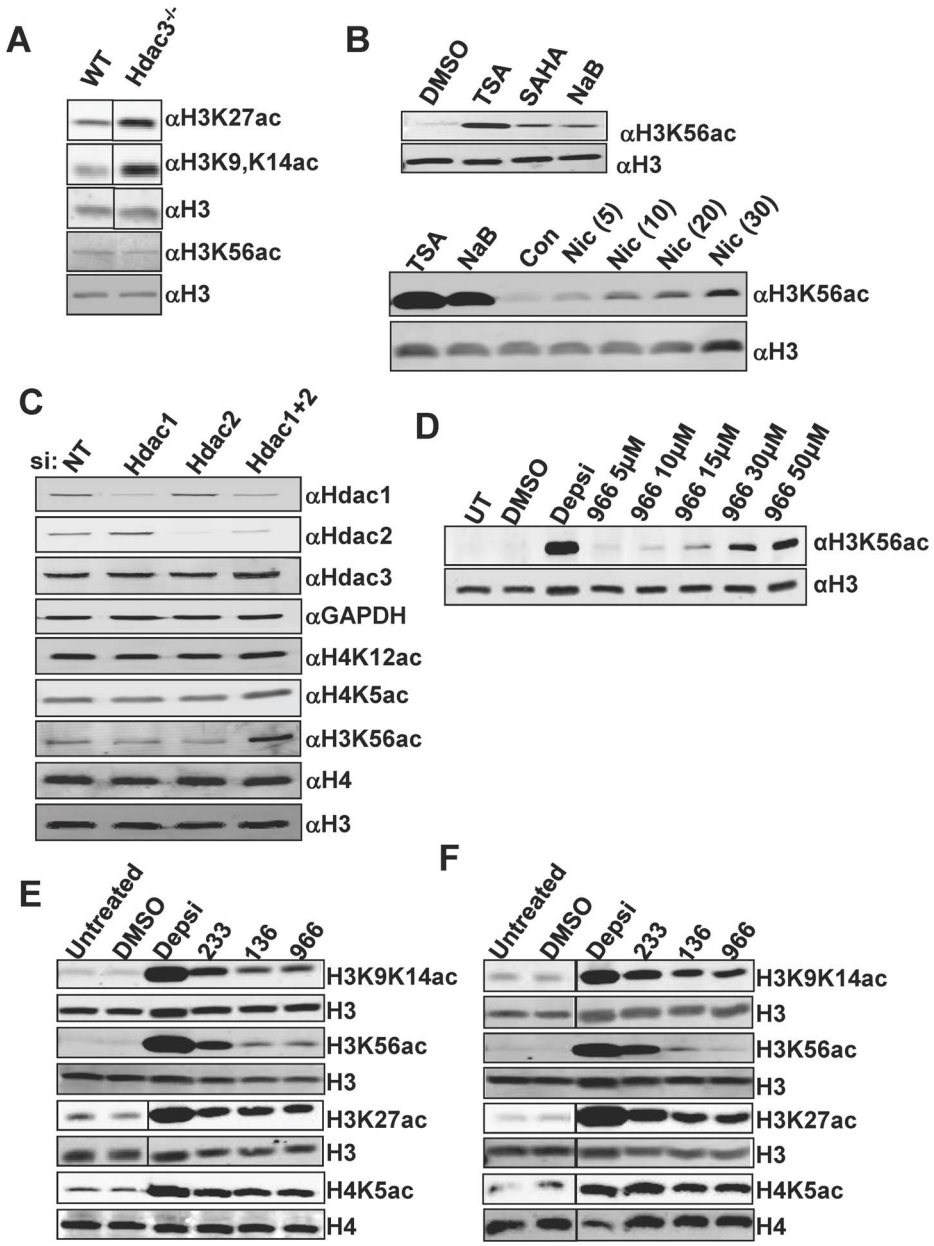

Figure 1. HDIs show selective inhibition of HDACs in CTCL cell lines. (A)Western blot analysis of whole cell lysates from Wild-type (WT) and *Hdac3*-null livers. Histones H3 and H4 served as loading controls. (B) Upper Panel: Western blot analysis of NIH 3T3 cells following treatment with various HDIs (indicated above each lane). Anti-histone H3 was used as a loading control. Lower panel: Western blot analysis of NIH 3T3 cells treated with either Trichostatin A (TSA) (1 μM), sodium butyrate (NaB) (5 mM), or increasing concentrations of nicotinamide (mM). (C) Western blot analysis of whole cell lysates prepared from cells that were transfected with either non-targeting siRNAs (NT) or siRNAs directed to the indicated Hdacs. (D) Western blot analysis of H3K56ac using whole cell lysates prepared from cells treated with the indicated amounts of RGFP966 for 24 hr. (E & F) Western blot analysis of (E) HH or (F) Hut78 cell lines treated with DMSO, 10 nM Depsipeptide (Depsi), 10 μM 233, 10 μM 136, or 10 μM 966. Cells were treated for 24 hr and then harvested for protein isolation. Samples were run on the same gel and probed on the same membrane. Intervening lanes (represented by a black bar) were removed for side-by-side comparison of DMSO and Depsipeptide. Histones H3 and H4 were used as loading controls.
doi:10.1371/journal.pone.0068915.g001

enzymes can target this mark, but that Hdac3 fails to deacetylate this residue (Figure 1C).

Given that H3K56ac separates the action of HDAC1/2 from HDAC3, we tested selective Hdac1/2 (RGFP233) and Hdac3 selective inhibitors (RGFP136 and RGFP966) for specificity. RGFP233 (233) showed 100- and 50-fold selectivity respectively towards HDAC1 and HDAC2 over HDAC3, and RGFP136 (136) and RGFP966 (966) were 10- and >100-fold respectively more selective for HDAC3 in *in vitro* deacetylase assays [32] [Vincent Jacques, Repligen unpublished data]. A titration of RGFP966 showed that at 5–10 μM there was only a modest affect on H3K56ac, which was approximately 15-fold less than found with Depsipeptide (Fig. 1D). Treatment of two CTCL cell lines, HH and Hut78, with the HDAC3-selective inhibitors 966 and 136, for 24 hours prior to western blot analysis resulted in increased acetylation at H3K9/K14, H3K27, and H4K5, but

not H3K56ac (even at 10μM, Figure 1E and F). In contrast, Depsipeptide, an inhibitor of the class I HDACs (HDACs 1, 2, 3, and 8) [10,13], caused the robust accumulation of all of the histone acetylation marks tested, whereas the HDAC1/2-selective inhibitor, 233, caused a less robust accumulation of these same marks. Using the Odyssey imaging system, we measured the fluorescence (integrated intensity units) of each band and found that 966 and 136 were at least 8–10-fold selective for HDAC3 inhibition by these criteria, even when used at relatively high levels (Figure 1E and F), confirming the *in vitro* data that 136 and 966 are selective for HDAC3 inhibition [Vincent Jacques, Repligen unpublished data]. Importantly, 966 was determined to have no inhibition of other HDACs at concentrations up to 15 μM in *in vitro* assays [32], which is consistent with our finding of only modest increases in H3K56ac at 10 μM.

HH and Hut78 CTCL Cell Lines Show Sensitivity to Novel, Selective HDIs and Additive Effects with CTCL Clinical Drugs

To determine how treatment with selective HDIs affects CTCL cell lines, we first performed cell proliferation assays using alamar blue to measure cell growth and viability in the presence of different HDIs. HH and Hut78 cells were treated at hour 0 with either DMSO, Depsipeptide, 233, or 966 and then analyzed at hours 0, 24, 48, and 72 for changes in cell proliferation as measured by changes in alamar blue-dependent fluorescence. Both cell lines were sensitive to treatment with 10 μM 233 or 966, as demonstrated by decreases in cell growth over time (Figure 2A). However, Hut78 cells exhibited a greater sensitivity to these HDIs than HH cells. Neither cell line was affected by the DMSO control, and Depsipeptide, which targets all class 1 HDACs was very efficient at cell killing. Therefore, we tested the combined effects of 233+966 and found additive effects, consistent with the selective targeting of HDAC1/2 and HDAC3 by these compounds (Fig. S1).

Dose curves were performed on each cell line to determine the optimal dose for dual treatment with drugs that are used or have been used to treat CTCL (Figure 2B). Cells were treated with varying concentrations of 233, 136, or 966 at hour 0 and again analyzed using alamar blue cell viability assays. CTCL cells showed dramatic sensitivity to 233 at each concentration, with Hut78 cells again exhibiting heightened sensitivity when compared to HH cells (Figure S2A). Treatment of cells with 136 had only modest effects on cell growth when compared to treatment with 966 (Figure S2B and Figure 2B) in both cell lines. Thus, we discontinued the analysis of 136 in subsequent experiments and focused on the inhibition of Hdac3 using 966.

A number of therapies are currently used for the treatment of CTCL and given that single agent therapy is rarely beneficial, we tested Bexarotene (highly selective retinoid x receptor agonist), Methotrexate (inhibitor of dihydrofolate reductase), or ATRA (All Trans Retinoic Acid, a retinoic acid receptor agonist) [1,41–43] for cooperative cell killing with 966. A dose of 2 μM for 966 was selected for dual treatment experiments so that we could assess additive or synergistic effects when 966 was combined with these drugs. Dose curves for Bexarotene, Methotrexate, and ATRA were performed and concentrations near the IC_{50} were chosen (Figure S3). Both HH and Hut78 cells exhibited increased sensitivity to dual treatment of 966 plus Bexarotene (Figure 3A), while only Hut78 cells showed increased sensitivity to 966 plus Methotrexate or ATRA (Figure 3B and C).

CTCL Cell Lines Undergo Apoptosis, have Increased DNA Damage, and Exhibit Cell Cycle Defects

We next determined whether the decreased cell growth seen when HH and Hut78 cells were treated with selective HDIs (Figures 2 and 3) was due to increased apoptosis. Flow cytometry analysis using Annexin V versus propidium iodide (PI) was performed on HH and Hut78 cells that had been treated for 24 hours with DMSO, 10 nM Depsipeptide, 10 μM 233, or 10 μM 966. HH and Hut78 cells displayed significant increases in Annexin V levels following treatment with HDIs, with Hut78 cells exhibiting the highest Annexin V levels (Figure 4A and Figure S4). Therefore, these cells undergo apoptosis when treated with HDIs. In both cell lines, Depsipeptide treatment resulted in the greatest cell killing, followed by 233 and 966. This trend may reflect the fact that Depsipeptide inhibits all three class I HDACs, 233 inhibits two HDACs, and 966 selectively inhibits a single HDAC.

Deletion of *Hdac3* caused increased DNA damage and cell cycle delays in an S phase dependent manner in fibroblasts [17]. To determine if the apoptosis occurring in Hut78 and HH cells when cells were treated with HDIs was associated with increased DNA damage, we treated cells for 8 hours with DMSO, Depsipeptide, 233 or 966 and performed western blot analysis using anti-γH2aX, which is localized to sites of DNA double-strand breaks [44]. Both cell lines showed approximately a 2.4-fold increase in the amount of γH2aX in samples treated with 966, indicative of an increase in DNA damage when HDAC3 was inhibited in CTCL cells (Figure 4B and Figure S3B). Treatment with Depsipeptide or 233 also caused increased γH2aX levels in both cell lines, with Depsipeptide being the most robust. When HH and Hut78 cells were treated with DMSO, Depsipeptide, 233, or 966 for 24 hours and pulsed with BrdU for 90 min before harvest, Hut78 cells treated with HDIs exhibited decreased BrdU incorporation, and also an increase in cells that were present in S phase but were not incorporating BrdU (Figure 4C–E and Figure S3C–E). These S phase cells that did not incorporate BrdU represent cells that have not completed DNA replication and are arrested in the S phase, suggesting that HDI treatment caused replication stress in CTCL cell lines.

Inhibition of Hdac3 leads to DNA Replication Defects

HDACs 1 and 2 regulate deacetylation of histones deposited on newly synthesized DNA during S phase and are enriched at replication forks [16,39,45] through association with histone chaperones like RbAp48 and CAF1 [25,46–48]. Like HDAC1 and 2, HDAC3 also targets histone deposition marks ([16] and Figure 1), and yeast two-hybrid studies show that HDAC3 can also bind to RbAp48 [49]. Therefore, we tested whether HDAC3 could associate with RbAp48 in mammalian cells. Immunoprecipitation analysis of endogenous HDAC3 and RbAp48 from HeLa cells detected an association, suggesting that HDAC3 could be bound to histone chaperones on chromatin (Figure 5A). To extend this analysis, we used gel filtration to determine the sizes of native HDAC3-containing complexes (Figure 5B). HDAC3 co-eluted with a portion of the RbAp48, but not PCNA, which marks DNA replication complexes (Figure 5B).

The gel filtration analysis suggested that HDAC3 might be associated with histone deposition machinery, yet not directly bound to the DNA replication machinery. Therefore, isolation of proteins on nascent DNA (iPOND) was used to further probe HDAC3 localization to DNA replication forks. A similar analysis in HEK293T cells suggested that, not only were HDAC1 and HDAC2 present at DNA replication forks, but HDAC3 was also detected [45]. To test whether HDAC3 was also present at replication forks in CTCL cells, Hut78 cells were pulsed for 15

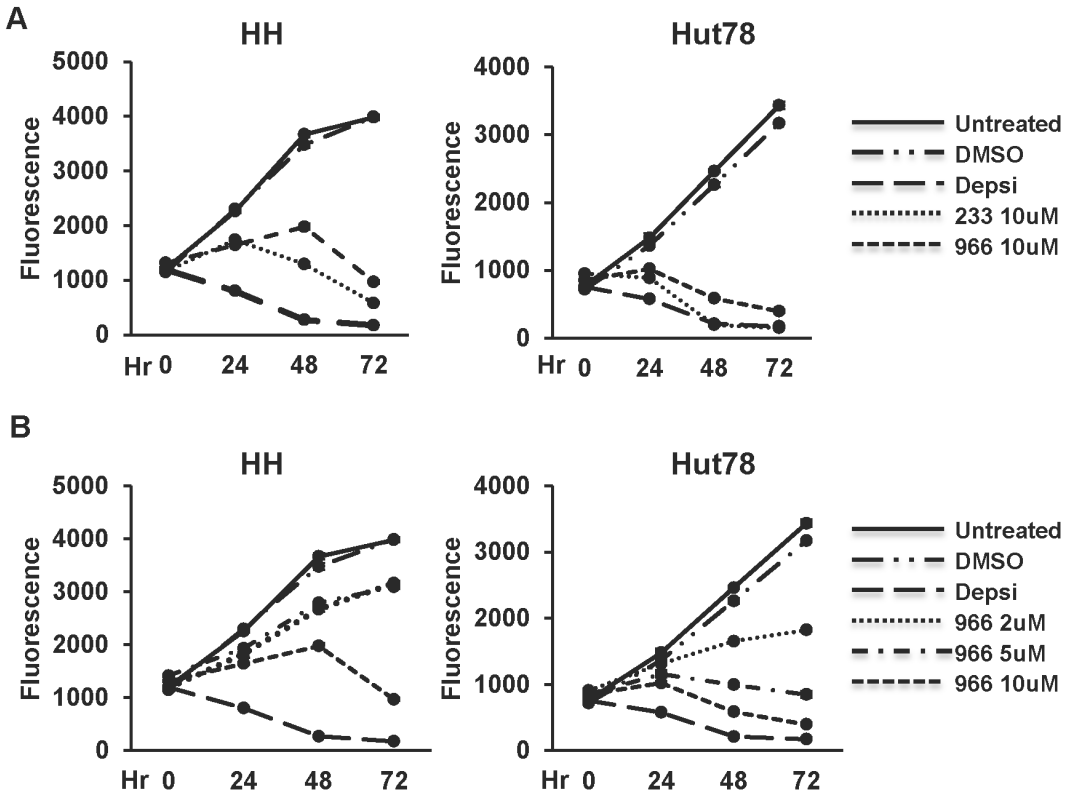

Figure 2. CTCL cell lines are sensitive to pan and selective HDIs. (A) Growth curves of HDI treated HH cells (left) or Hut78 cells (right). Cells were treated once with DMSO, 10 nM Depsipeptide (Depsi), 10 μM 233, or 10 μM 966 at hour 0. Untreated cells and DMSO treated cells were used as controls. Cell growth was assessed at 0, 24, 48, and 72 hours after treatment. (B) Dose curves of 966 treated HH cells (left) and Hut78 cells (right). The experiment was performed in the same manner as (A) except that the cells treated were treated once with 2 μM, 5 μM, or 10 μM of 966 at hour 0. For both (A) and (B), representative curves are shown from experiments performed in triplicate that are consistent with other biological replicates. Statistical analysis was performed using a two-tail paired T-test and comparing the HDI treated cells to DMSO treated cells resulting in the following p values: (A) HH cells (left), Depsi: $p = 0.0008$, 233: $p = 0.004$, and 966: $p = 0.006$. For the Hut78 cells (right), Depsi: $p = 0.002$, 233: $p = 0.006$, and 966: $p = 0.006$. (B) HH cells (left), Depsi: $p = 0.0008$, 966 2 μM: $p = 0.02$, 966 5 μM: $p = 0.01$, and 966 10 μM: $p = 0.006$. For the Hut78 cells (right), Depsi: $p = 0.002$, 966 2 μM: $p = 0.03$, 966 5 μM: $p = 0.01$, and 966 10 μM: $p = 0.006$.
doi:10.1371/journal.pone.0068915.g002

minutes with EdU (5-Ethynyl-2′-deoxyuridine) only or pulsed with EdU for 15 minutes followed by a 60 minute thymidine chase. After the labeling, cells were cross-linked, and the nascent DNA with EdU incorporated was conjugated to biotin using click chemistry. The newly synthesized DNA and the DNA-protein complexes were then purified using streptavidin beads. Proteins that move with the replication fork such as HDAC1 and PCNA [36,45] were enriched immediately after EdU labeling (lanes labeled "0", Figure 6) and then decreased with the thymidine chase. By contrast, western blot analysis showed that HDAC3 was bound to chromatin at and around replication forks, but like H2B, its levels did not significantly drop after the 60 minute chase, suggesting that it did not travel with replication forks (Figure 6).

Although HDAC3 did not appear to move with replication forks using iPOND, loss of HDAC3 activity using siRNA or gene deletion showed a requirement for this deacetylase for optimal DNA replication fork velocity [[50],Summers,unpublished data]. A major advantage of small molecules is that they allow the analysis of HDAC function in short timeframes that cannot be replicated by genetic methods. We started by assessing the minimal time required to achieve HDAC3 inhibition using 966. Hut78 cells were treated with DMSO, Depsipeptide, or 966 for 30 min, 1 hr, 2 hr, and 4 hr and western blot analysis for H4K5ac was used as a measure of HDAC3 inhibition (Figure 7A). In purified enzyme assays, 966 is a slow on/slow off inhibitor when used at nanomolar concentrations, where full potency was observed within approximately 2 hr. Treatment with 10 μM 966 for 30 min did not significantly increase H4K5 acetylation levels, but by 1 hr a noticeable increase in H4K5 acetylation was apparent, and by 4 hr a dramatic accumulation of H4K5 acetylation was observed (Figure 7A) suggesting full inhibition within 4 hr. This suggests that HDAC3-regulated histone acetylation is very dynamic with changes in histone acetylation detectable by western blot occurring within hours of treatment, but within 30 min of Hdac3 inhibition by 966 there were not global effects on histone acetylation.

Next, DNA fiber labeling analysis was used to visualize individual DNA fibers by sequential labeling of cells with IdU and CldU followed by immunofluorescence to detect the incorporation of these analogs [37] in strands of DNA to measure replication fork velocity. Treatment with Depsi or 966 for 4 hrs prior to labeling with IdU followed by CldU resulted in a shortening of the average length of fiber tracks (examples of fibers are shown on the right), which corresponds to slower replication fork progression than the DMSO control (Figure 7B). To ensure that changes in chromatin structure did not affect fiber track length after replication fork progression, which would interfere with accurate measurement of DNA fibers, Hut78 cells were labeled with IdU followed by CldU, washed and then were either immediately treated with DMSO or HDIs for 25 min or

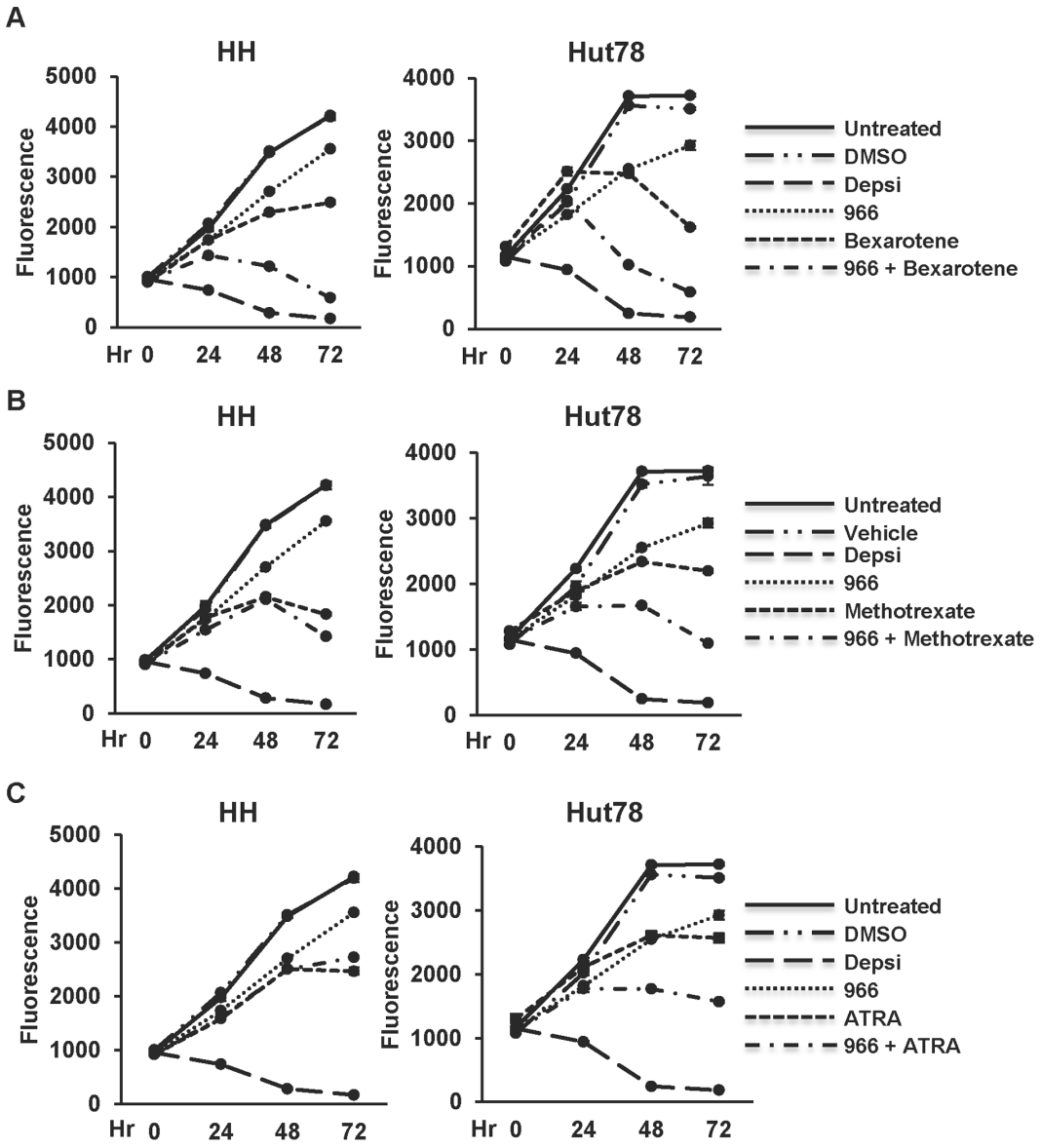

Figure 3. Dual treatment with RGFP966 and CTCL drugs has an additive effect on cell growth. Growth curves of dual treatment on HH cells or Hut78 cells. Cells were treated once at hour 0 with DMSO, 10 nM Depsipeptide (Depsi), 2 μM 966, or a combination of 2 μM 966 and either Bexarotene, Methotrexate, or ATRA. Untreated cells and DMSO treated cells were used as controls. Cell growth was assessed at 0, 24, 48, and 72 hours after treatment. (A) HH cells (left) or Hut78 cells (right) were treated with 20 μM or 75 μM Bexarotene alone or in combination with 966. (B) Cells were treated with 0.1 μM Methotrexate alone or in combination with 966. DMSO and 1 M Na_2CO_3 served as vehicle controls. (C) Cells were treated with 2 μM ATRA alone or in combination with 966. ATRA was administered at hour 0 and re-dosed at 48 hours after treatment. For (A–C), representative curves are shown from experiments performed in triplicate that are consistent with other biological replicates. Statistical analysis was performed using a two-tail paired T-test and comparing the HDI, CTCL drug, or dual treated cells to DMSO treated cells resulting in the following p values: (A) HH cells (left), Depsi: $p = 0.0008$, 966: $p = 0.003$, Bexarotene: $p = 0.003$, and 966 plus Bexarotene: $p = 0.002$. For the Hut78 cells (right), Depsi: $p = 0.001$, 966: $p = 0.08$, Bexarotene: $p = 0.01$, and 966 plus Bexarotene: $p = 0.009$. (B) HH cells (left), Depsi: $p = 0.0008$, 966: $p = 0.003$, Methotrexate: $p = 0.003$, and 966 plus Methotrexate: $p = 0.003$. For the Hut78 cells (right) Depsi: $p = 0.001$, 966: $p = 0.01$, Methotrexate: $p = 0.01$, and 966 plus Methotrexate: $p = 0.004$. (C) HH cells (left), Depsi: $p = 0.0008$, 966: $p = 0.003$, ATRA: $p = 0.002$, and 966 plus ATRA: $p = 0.0007$. For the Hut78 cells (right) Depsi: $p = 0.001$, 966: $p = 0.01$, ATRA: $p = 0.02$, and 966 plus ATRA: $p = 0.004$.
doi:10.1371/journal.pone.0068915.g003

incubated in fresh medium for 4 hr and then treated with DMSO or HDIs for 25 min. Neither of these experiments showed significant changes in fiber track length or fork velocity (Figure 7C & S5), confirming that the effects on replication seen with inhibition of HDAC3 are not due to shortening of fiber track lengths due to global changes in chromatin structure.

Finally, to determine if this replication defect was due to a localized effect, we treated Hut78 cells for 5 min with either Depsi or 966 before labeling with IdU followed by CldU. Remarkably, even treatment within this short timeframe caused a shortening of DNA fiber track lengths and slower fork velocity (Figure 7D). These data suggest that treatment with a HDAC3 selective inhibitor has localized effects on replication at or nearby the replication fork since global changes in H4K5ac were not seen within 30 min of treatment with 966 (Figure 7A).

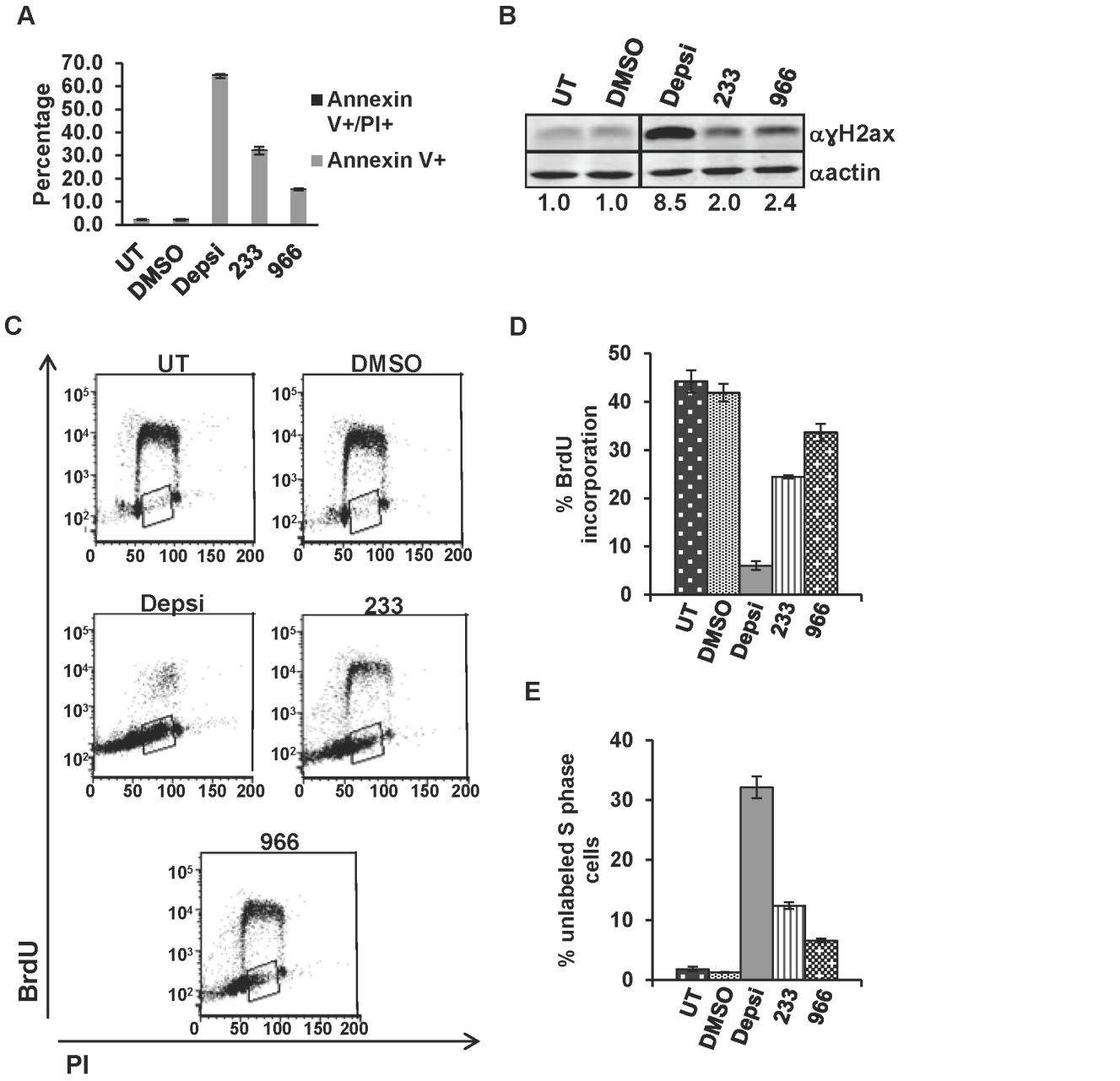

Figure 4. An HDAC3 selective inhibitor triggers apoptosis associated with increased DNA damage and cell cycle defects. (A) Hut78 cells were treated with DMSO, 10 nM Depsipeptide (Depsi), 10 μM 233, or 10 μM 966 for 24 hr and apoptosis assessed by Annexin V staining and flow cytometry. Cells were also labeled with propidium iodide to assess DNA content. Untreated (UT) and DMSO treated cells were used as controls. Shown is a representative graph from an experiment performed in duplicate that is consistent with other biological replicates. (B) Western blot analysis of γH2aX levels in Hut78 cells treated with DMSO, 10 nM Depsi, 10 μM 233, or 10 μM 966 for 8 hrs. Untreated and DMSO treated cells were used as controls. Samples were run on the same gel and probed on the same membrane. Intervening lanes (represented by a black bar) were removed for side by side comparison of DMSO and Depsipeptide. (C) Cell cycle status was analyzed using BrdU incorporation and propidium iodide to assess DNA content by flow cytometry. Hut78 cells were treated with DMSO, 10 nM Depsipeptide (Depsi), 10 μM 233, or 10 μM 966 for 24 hr and pulsed for an hour and a half with BrdU prior to cell harvest and analysis. Shown are representative flow cytometry plots from an experiment performed in duplicate that is consistent with other biological replicates. (D) Graphical representation of BrdU incorporation from the experiment described in (C). (E) Graphical representation of the percent of S phase cells that did not incorporate BrdU (shown by box in panel (C)). Statistical analysis for both the Annexin V and BrdU experiments was performed using a two-tail T-test and comparing the HDI treated cells to the DMSO treated cells resulting in the following p-values: (A) Depsi: $p = 0.0002$, 233: $p = 0.003$, and 966: $p = 0.0003$. (D) Depsi: $p = 0.003$, 233: $p = 0.01$, and 966: $p = 0.08$. (E) Depsi: $p = 0.003$, 233: $p = 0.003$, and 966: $p = 0.004$.
doi:10.1371/journal.pone.0068915.g004

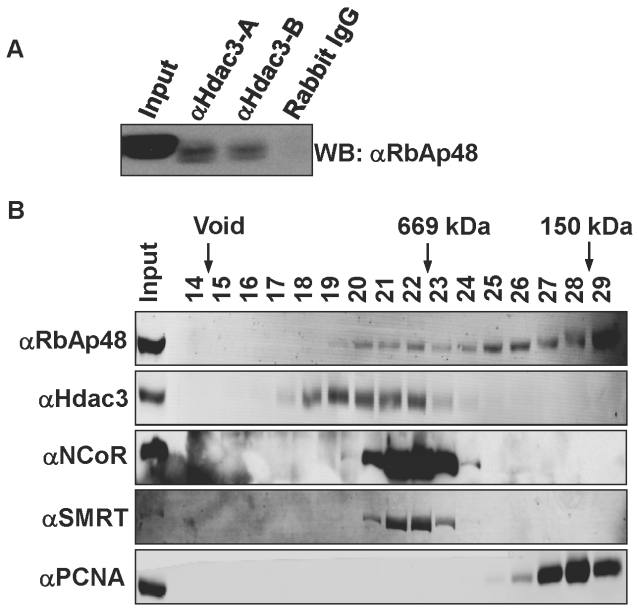

Figure 5. Hdac3 co-purifies with the histone chaperone, RbAp48, in mammalian cells. (A) Immunoprecipitation analysis of endogenous HDAC3 and RbAp48 from HeLa cells. Two different HDAC3 antibodies were used and labeled (A) or (B) and rabbit IgG was included as a negative control. (B) Gel Filtration analysis of HDAC3 containing protein complexes. Nuclear lysates were separated using a Superose 6 gel filtration column and the elution profile of the indicated proteins determined by western blot analysis. The elution of size markers is shown at the top of the blots.
doi:10.1371/journal.pone.0068915.g005

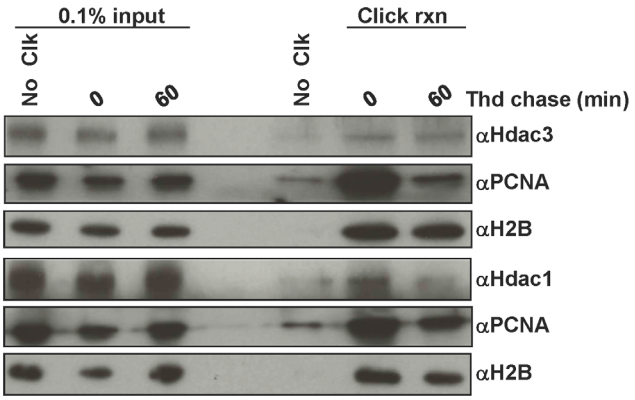

Figure 6. iPOND analysis reveals HDAC3 association with replication forks in Hut78 CTCL cells. Hut78 cells were pulsed for 15 minutes with EdU followed by either no thymidine chase or a 60 minute thymidine chase. The protein-DNA complexes were then cross-linked, nascent DNA was conjugated to biotin using click chemistry, and then protein-DNA complexes were purified using Streptavidin beads. The eluted proteins were then analyzed using western blot analysis. A no click reaction sample (No Clk) that did not include biotin azide was used as a negative control. 0.1% input samples were included for positive controls of each protein analyzed. PCNA served as a positive control for a replication fork bound protein and H2B served as a loading control and positive control for a chromatin bound protein.
doi:10.1371/journal.pone.0068915.g006

Discussion

Cutaneous T cell lymphoma (CTCL) diagnosed during early stage disease generally has an indolent course and good outcome [1–5]. However, late stage, refractory, or aggressive CTCL (such as Sézary Syndrome) has a shortened survival expectancy [1–5]. Two histone deacetylase inhibitors, SAHA and Depsipeptide, have been FDA approved for the treatment of late stage or refractory CTCL [1,3,10–12]. However, since these HDIs target multiple HDACs, it is unknown which of these HDACs must truly be inhibited to achieve the anti-tumor effects observed upon HDI treatment. Furthermore, it is likely that the unnecessary inhibition of other HDACs contributes to the side effects seen with HDI treatment (such as nausea, fatigue, and GI, cardiac and hematologic toxicities). By using selective HDIs, the efficacy of individual HDAC targeting can be assessed and side effects may be lessened, resulting in improved quality of life for patients undergoing treatment. Here, we show that the inhibition of HDAC1/2 or HDAC3 through the use of novel, selective inhibitors, caused decreased cell growth of the CTCL cell lines, HH and Hut78 by triggering apoptosis (Figure 2). While it appears that inhibition of all three of these HDACs was more efficacious (e.g., Depsipeptide worked very well), more potent selective inhibitors may yield better results, or the lower toxicity may allow more intensive or longer-term treatments. Ultimately, having HDAC1/2 versus HDAC3 selective inhibitors will provide flexibility in defining the best schedules and combinations of these compounds to maximize the therapeutic benefit in the treatment of CTCL.

Mechanistically, the apoptosis observed was associated with the accumulation of DNA damage in HDI treated cells (Figure 4 and S3). BrdU-labeling studies showed decreased BrdU incorporation with pan HDAC inhibitors, inhibitors of HDAC1/2 and the HDAC3 selective inhibitors (Figure 4 C–E). These studies also revealed a significant increase in cells that did not incorporate BrdU, but showed increased DNA content, consistent with an S-phase arrest following HDI treatment, suggesting that the DNA damage was due to defects in DNA replication. This prompted an analysis of DNA replication fork velocity using DNA fiber labeling assays, which showed that Depsipeptide treatment and treatment with the Hdac3 selective inhibitor resulted in inefficient or slowed DNA replication (Figure 7). By examining DNA replication shortly after adding the HDIs, we were able to show that this is a very early event, occurring within the first hour of HDI treatment. These data suggest that HDI therapy first affects DNA replication (Figure 7), which would provide a therapeutic window by targeting the cycling cancer cells, and leaving normal, non-cycling cells intact.

The rapid effects of 966 on DNA replication suggest an important role for HDAC3 in DNA replication. In addition, by inhibiting HDAC3 at various times before DNA fiber labeling, we were able to narrow the possible mechanisms by which this might occur to localized effects at or around the DNA replication fork, as it took greater than 30 min before global changes in histone acetylation were observed (Figure 7). However, these studies cannot discriminate whether this is due to a local chromatin effect or whether HDAC3 directly targets the DNA replication machinery. For instance, chromatin in and around the DNA replication fork must be in an open configuration, which is more accessible to HDAC3 than nucleosomes in mature chromatin. Because the histones in newly placed nucleosomes are acetylated prior to deposition, inhibition of HDAC3 could cause the accumulation of acetylation of these histones within minutes of HDI treatment, whereas global accumulation of H4K5ac takes an hour or more (Figure 7A). Alternatively, components of the DNA replication machinery may be regulated by acetylation and deacetylation and HDAC3 could play a regulatory role. One argument against this is that HDAC3 did not co-elute with PCNA in size

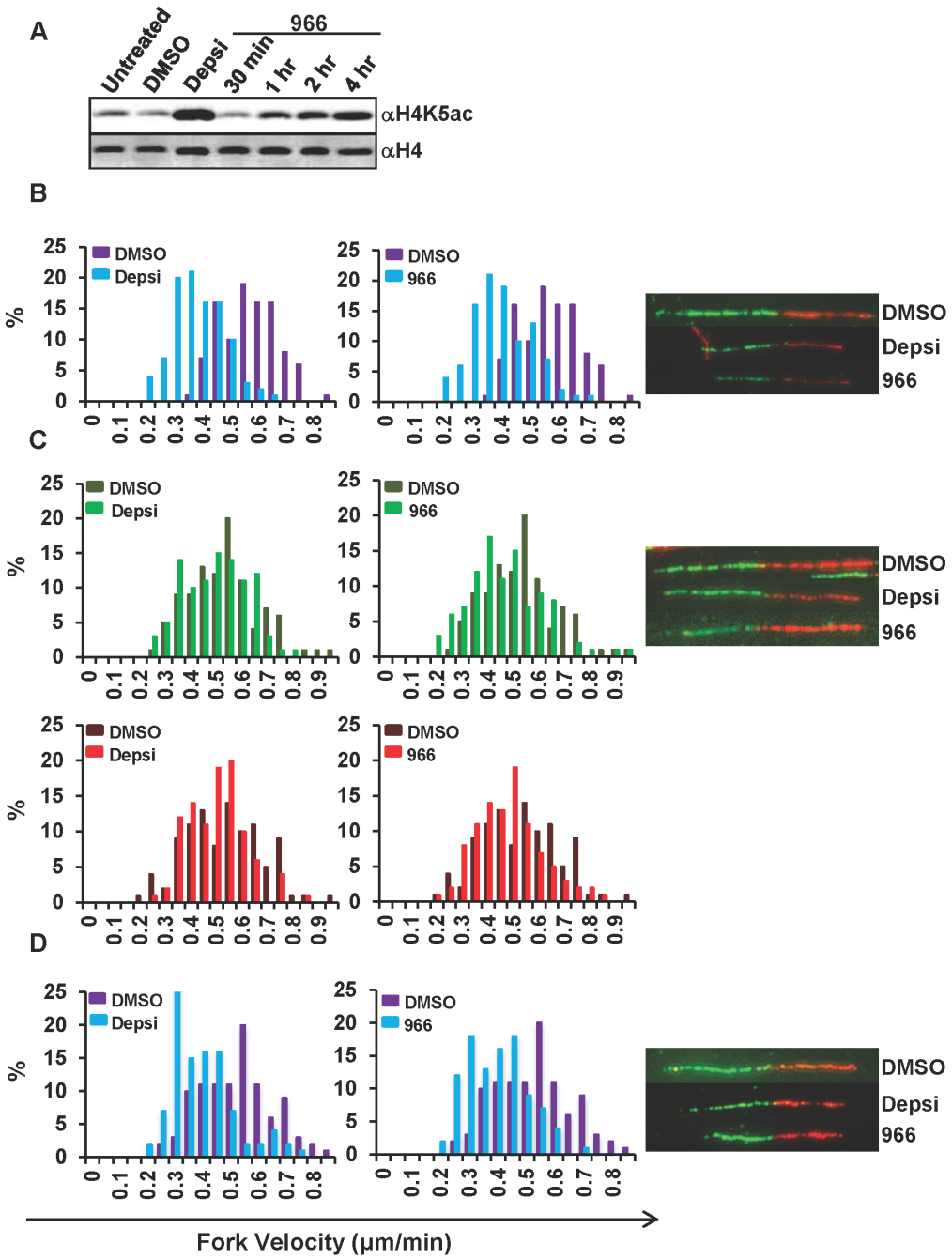

Figure 7. HDAC3 selective inhibitors rapidly cause defects in DNA replication. (A) Western blot analysis of Hut78 cells treated with DMSO or 10 nM Depsipeptide (Depsi) for 4 hrs, or 10 μM 966 for 30 min, 1 hr, 2 hr, and 4 hr. (B, C, and D) DNA fiber labeling analysis was used to assess DNA replication fork progression in Hut78 cells treated with DMSO, 10 nM Depsipeptide (left) or 10 μM 966 (right) for 4 hr (B) or 5 mins (D) prior to labeling with 20 mins of IdU (green) followed by 20 min of CldU (red). Graph of fork velocity (length of fibers divided by 40 min) is shown. (C) Hut78 cells were treated with DMSO, Depsi or 966 immediately after labeling cells with IdU followed by CldU. Graph of fork velocity for either the IdU label or CldU label is shown. Representative fibers are shown. 100 fibers were measured for each sample. Statistical analysis was performed using Mann-Whitney test and standard deviations were calculated. HDI treated cells were compared to DMSO treated cells resulting in the following p-values: (B) Depsi: $p<0.0001$; 966: $p<0.0001$. The average velocities for Depsi and 966 were greater than 3 standard deviations of the DMSO average velocity. (C) Depsi IdU (green): $p=0.1$, Depsi CldU (red): $p=0.1$; 966 IdU (green): $p=0.0011$; 966 CldU (red): $p=0.01$. The average velocities for IdU and CldU in Depsi treated cells were within 1 and 2 standard deviations respectively of the DMSO average velocity. The average velocities for IdU and CldU in 966 treated cells were within 2 standard deviations of the DMSO average velocity. (D) Depsi: $p<0.0001$; 966: $p<0.0001$. The average velocities for Depsi and 966 were greater than 3 standard deviations of the DMSO average velocity.
doi:10.1371/journal.pone.0068915.g007

exclusion chromatography (Figure 5) or move with the DNA replication fork in iPOND purifications (Figure 6). Thus, at this point in time, the evidence best supports a localized effect on chromatin at the replication fork.

Although endogenous HDAC3 can associate with histone chaperones such as RbAp48 (Figure 5), its role in deacetylation of newly formed nucleosomes is largely based on genetic, siRNA and chemical inhibition studies ([16,17] and Figure 7). These studies indicate that HDAC3 targets the same histone deposition marks that HDAC1/2 deacetylate and that HDAC3 is required at replication forks (Figure 6, 7). Historically, HDAC1/2 were biochemically linked to histone deposition [16,39]. These enzymes form nearly stoichiometric complexes with the histone deposition machinery and are thought to be the major enzymes responsible for the deacetylation of new nucleosomes. Moreover, siRNA or genetic impairment of HDAC1 is compensated by higher expression of HDAC2 (e.g., Figure 1C), whereas deletion of *Hdac3* is not compensated for by higher expression of other class 1 Hdacs. Thus, we conclude that HDAC3 plays a distinct role from HDAC1 and HDAC2 during chromatin maturation (Figure 6) and that targeting HDAC3 with small molecule inhibitors will provide additional therapeutic impact in the treatment of CTCL and other cancers.

Currently, SAHA and Depsipeptide are approved as single agents to treat refractory CTCL [1,3,10–12]. However, combinatorial treatment is almost always more beneficial than single agent therapy, so we tested HDAC3 inhibitors with other drugs currently used for CTCL. The combination of 966 and either bexarotene, methotrexate, or ATRA led to further reductions in cell growth than either agent alone in Hut78 cells (Figure 3), but these effects were additive, not synergistic. Nevertheless, these combinations did not negate the responses of these drugs, suggesting that these compounds could be used together in the clinic. Our studies show that individual HDACs can be targeted and that these inhibitors may be useful in the treatment of CTCL by rapidly targeting DNA replication. While the first effects of these compounds may be at replication forks (which provides a therapeutic window), within only 4 hr these drugs also affected global histone acetylation, which indicates that HDAC3 plays a dynamic role in the regulation of histone acetylation and chromatin structure. Thus, these compounds may target multiple fundamental events in the cell cycle to trigger apoptosis in cycling tumor cells that would be beneficial in combination with current therapies for CTCL.

Supporting Information

Figure S1 CTCL cell lines exhibit additive sensitivity to the combination of 233 and 966. Viability curves of Hut78 cells treated with the indicated amounts of RGFP966 and 233. Cells were treated once with DMSO, 10 nM Depsipeptide (Depsi), or different concentrations of either 233 or 966 at hour 0. Untreated cells and DMSO treated cells were used as controls. Cell growth was assessed at 0, 24, 48, and 72 hours after treatment using alamar blue. A representative curve is shown from experiments performed in triplicate that are consistent with other biological replicates.
(TIFF)

Figure S2 CTCL cell lines exhibit sensitivity to multiple doses of 233 and high dose 136. Dose curves of HH cells (left) or Hut78 cells (right) treated with 10 μM 233 (A) or 966 (B). Cells were treated once with DMSO, 10 nM Depsipeptide (Depsi), or different concentrations of either 233 or 136 at hour 0. Untreated cells and DMSO treated cells were used as controls. Cell growth was assessed at 0, 24, 48, and 72 hours after treatment using alamar blue. For both (A) and (B), representative curves are shown from experiments performed in triplicate that are consistent with other biological replicates. Statistical analysis was performed using a two-tail paired T-test and comparing the HDI treated cells to DMSO treated cells resulting in the following p values: (A) HH cells (left), Depsi: $p = 0.0008$, 233 2 μM: $p = 0.005$, 233 5 μM: $p = 0.005$, and 233 10 μM: $p = 0.004$. For the Hut78 cells (right), Depsi: $p = 0.002$, 233 2 μM: $p = 0.01$, 233 5 μM: $p = 0.005$, and 233 10 μM: $p = 0.006$. (B) HH cells (left), Depsi: $p = 0.001$, 136 1 μM: $p = 0.1$, 136 5 μM: $p = 0.1$, and 136 10 μM: $p = 0.006$. For the Hut78 cells (right), Depsi: $p = 0.001$, 136 1 μM: $p = 0.08$, 136 5 μM: $p = 0.02$, and 136 10 μM: $p = 0.005$.
(TIFF)

Figure S3 Dose curves for Bexarotene, Methotrexate, and ATRA reveal optimal concentrations for combination treatments. Dose curves of Bexarotene (A), Methotrexate (B), and ATRA (C) treated HH cells or Hut78 cells. Cells were treated at hour 0 with DMSO, 10 nM Depsipeptide (Depsi), or varying concentrations of Bexarotene, Methotrexate, or ATRA. Cell growth was assessed at 0, 24, 48, and 72 hours after treatment. In all studies except for (A), the HH and Hut78 cells were treated with the same varying concentrations of CTCL drugs. HH cells were treated with 10, 20, or 50 μM of Bexarotene while Hut78 cells were treated with 50,75, or 100 μM of Bexarotene. In (B) DMSO and a solution containing Na_2CO_3 served as vehicle controls. (C) ATRA was administered at hour 0 and re-dosed at 48 hours after treatment. For (A–C), representative curves are shown from experiments performed in triplicate that are consistent with other biological replicates. Statistical analysis was performed using a two-tail paired T-test and comparing the HDI or CTCL drug treated cells to DMSO treated cells resulting in the following p values: (A) HH cells (left), Depsi: $p = 0.0007$; Bexarotene 10 μM: $p = 0.001$; Bexarotene 20 μM: $p = 0.004$; Bexarotene 50 μM: $p = 0.001$. Hut78 cells (right), Depsi: $p = 0.002$; Bexarotene 50 μM: $p = 0.8$; Bexarotene 75 μM: $p = 0.1$; and Bexarotene 100 μM: $p = 0.04$. (B) HH cells (left), Depsi: $p = 0.001$; Methotrexate 0.1 μM: $p = 0.007$; Methotrexate 1 μM: $p = 0.01$; Methotrexate 10 μM: $p = 0.01$; Methotrexate 100 μM: $p = 0.006$. Hut78 cells (right) Depsi: $p = 0.001$; Methotrexate 0.1 μM: $p = 0.005$; Methotrexate 1 μM: $p = 0.006$; Methotrexate 10 μM: $p = 0.004$; Methotrexate 100 μM: $p = 0.004$. (C) HH cells (left), Depsi: $p = 0.001$; ATRA 500 nM: $p = 0.008$; ATRA 1 μM: $p = 0.002$; ATRA 2 μM: $p = 0.003$. Hut78 cells (right) Depsi: $p = 0.001$; ATRA 500 nM: $p = 0.02$; ATRA 1 μM: $p = 0.005$; ATRA 2 μM: $p = 0.006$.
(TIFF)

Figure S4 HDIs increased in apoptosis, DNA damage, and cell cycle defects in HH cells. (A) HH cells were treated with DMSO, 10 nM Depsipeptide (Depsi), 10 μM 233, or 10 μM 966 for 24 hr and apoptosis levels were assessed by Annexin V/PI staining and flow cytometry. Untreated (UT) and DMSO treated cells were used as controls. Shown is a representative graph from an experiment performed in duplicate that is consistent with other biological replicates. (B) Western blot analysis of γH2aX levels in HH cells treated with DMSO, 10 nM Depsi, or 10 μM 966 for 8 hrs. Untreated and DMSO treated cells were used as controls. (C) Cell cycle status was analyzed using BrdU/PI and flow cytometry. HH cells were treated with DMSO, 10 nM Depsipeptide (Depsi), 10 μM 233, or 10 μM 966 for 24 hr and pulsed for an hour and a half with BrdU prior to cell harvest and analysis. Shown are representative flow cytometry plots from an experiment performed in duplicate that is consistent with other biological replicates. (D) Graphical representation of BrdU incorporation from the experiment described in (C). (E) Graphical representation of the percent of S phase cells that did not incorporate BrdU (shown by box in panel (C)). Statistical analysis for both the

Annexin V and BrdU experiments was performed using a two-tail T-test and comparing the HDI treated cells to the DMSO treated cells resulting in the following p-values: (A) Depsi: $p = 0.02$, 233: $p = 0.01$, and 966: $p = 0.06$. (D) Depsi: $p = 0.002$, 233: $p = 0.05$, and 966: $p = 0.3$. (E) Depsi: $p = 0.03$, 233: $p = 0.07$, and 966: $p = 0.8$.
(TIFF)

Figure S5 HDI treatment after labeling with IdU and CldU shows no changes in DNA fiber length. (A) DNA fiber labeling analysis was used to assess DNA fiber length in Hut78 cells treated with either DMSO, 10 nM Depsipeptide (left) or 10 μM 966 (right) 4 hrs after labeling the cells with IdU for 20 mins (green) followed by 20 mins of CldU (red). (A) Graphical representation of fork velocity as determined by the total length of fibers (IdU plus CldU) divided by 40 min pulse is shown. Representative measured fibers are shown at the right for DMSO, Depsi, and 966. 100 fibers were measured for each sample. Statistical analysis was performed using Mann-Whitney test and standard deviations were calculated. HDI treated cells were compared to the DMSO treated cells resulting in the following p-values: Depsi: $p = 0.5$ and 966: $p = 0.4$. The average velocities for both Depsi and 966 were within 1 standard deviation of the average velocity for DMSO.
(TIFF)

Acknowledgments

We thank all the members of the Hiebert lab for helpful discussions, reagents and advice. We thank the Vanderbilt Cell Imaging and Flow Cytometry Shared Resources for services and support.

Author Contributions

Conceived and designed the experiments: CEW SB KRS YZ BS BC DC DK WJC AC CME LYM SWH. Performed the experiments: CEW SB KRS YZ BS BC. Analyzed the data: CEW SB KRS YZ BS BC DC DK WJC AC CME LYM SWH VJ JR. Contributed reagents/materials/analysis tools: AC VJ. Wrote the paper: CEW SB KRS YZ BS BC DC DK WJC AC CME LYM SWH VJ JR.

References

1. Lansigan F, Foss FM (2010) Current and emerging treatment strategies for cutaneous T-cell lymphoma. Drugs 70: 273–286.
2. Wilcox RA (2011) Cutaneous T-cell lymphoma: 2011 update on diagnosis, risk-stratification, and management. Am J Hematol 86: 928–948.
3. Li JY, Horwitz S, Moskowitz A, Myskowski PL, Pulitzer M, et al. (2012) Management of cutaneous T cell lymphoma: new and emerging targets and treatment options. Cancer Manag Res 4: 75–89.
4. Wollina U (2012) Cutaneous T cell lymphoma: update on treatment. Int J Dermatol 51: 1019–1036.
5. Willemze R, Jaffe ES, Burg G, Cerroni L, Berti E, et al. (2005) WHO-EORTC classification for cutaneous lymphomas. Blood 105: 3768–3785.
6. Barneda-Zahonero B, Parra M (2012) Histone deacetylases and cancer. Mol Oncol. 6: 579–89.
7. Cotto M, Cabanillas F, Tirado M, Garcia MV, Pacheco E (2010) Epigenetic therapy of lymphoma using histone deacetylase inhibitors. Clin Transl Oncol 12: 401–409.
8. Melnick A, Licht JD (2002) Histone deacetylases as therapeutic targets in hematologic malignancies. Curr Opin Hematol 9: 322–332.
9. Yoshida M, Furumai R, Nishiyama M, Komatsu Y, Nishino N, et al. (2001) Histone deacetylase as a new target for cancer chemotherapy. Cancer Chemother Pharmacol 48 Suppl 1: S20–26.
10. Prince HM, Bishton MJ, Harrison SJ (2009) Clinical studies of histone deacetylase inhibitors. Clin Cancer Res 15: 3958–3969.
11. Mann BS, Johnson JR, He K, Sridhara R, Abraham S, et al. (2007) Vorinostat for treatment of cutaneous manifestations of advanced primary cutaneous T-cell lymphoma. Clin Cancer Res 13: 2318–2322.
12. Mann BS, Johnson JR, Cohen MH, Justice R, Pazdur R (2007) FDA approval summary: vorinostat for treatment of advanced primary cutaneous T-cell lymphoma. Oncologist 12: 1247–1252.
13. Whittaker SJ, Demierre MF, Kim EJ, Rook AH, Lerner A, et al. (2010) Final results from a multicenter, international, pivotal study of romidepsin in refractory cutaneous T-cell lymphoma. J Clin Oncol 28: 4485–4491.
14. Gallinari P, Di Marco S, Jones P, Pallaoro M, Steinkuhler C (2007) HDACs, histone deacetylation and gene transcription: from molecular biology to cancer therapeutics. Cell Res 17: 195–211.
15. Goodarzi AA, Noon AT, Jeggo PA (2009) The impact of heterochromatin on DSB repair. Biochem Soc Trans 37: 569–576.
16. Bhaskara S, Knutson SK, Jiang G, Chandrasekharan MB, Wilson AJ, et al. (2010) Hdac3 is essential for the maintenance of chromatin structure and genome stability. Cancer Cell 18: 436–447.
17. Bhaskara S, Chyla BJ, Amann JM, Knutson SK, Cortez D, et al. (2008) Deletion of histone deacetylase 3 reveals critical roles in S phase progression and DNA damage control. Mol Cell 30: 61–72.
18. Knutson SK, Chyla BJ, Amann JM, Bhaskara S, Huppert SS, et al. (2008) Liver-specific deletion of histone deacetylase 3 disrupts metabolic transcriptional networks. EMBO J 27: 1017–1028.
19. Insinga A, Monestiroli S, Ronzoni S, Gelmetti V, Marchesi F, et al. (2005) Inhibitors of histone deacetylases induce tumor-selective apoptosis through activation of the death receptor pathway. Nat Med 11: 71–76.
20. Insinga A, Minucci S, Pelicci PG (2005) Mechanisms of selective anticancer action of histone deacetylase inhibitors. Cell Cycle 4: 741–743.
21. Rosato RR, Almenara JA, Dai Y, Grant S (2003) Simultaneous activation of the intrinsic and extrinsic pathways by histone deacetylase (HDAC) inhibitors and tumor necrosis factor-related apoptosis-inducing ligand (TRAIL) synergistically induces mitochondrial damage and apoptosis in human leukemia cells. Mol Cancer Ther 2: 1273–1284.
22. Rosato RR, Grant S (2005) Histone deacetylase inhibitors: insights into mechanisms of lethality. Expert Opin Ther Targets 9: 809–824.
23. Xu WS, Parmigiani RB, Marks PA (2007) Histone deacetylase inhibitors: molecular mechanisms of action. Oncogene 26: 5541–5552.
24. Khan O, La Thangue NB (2012) HDAC inhibitors in cancer biology: emerging mechanisms and clinical applications. Immunol Cell Biol 90: 85–94.
25. Taunton J, Hassig CA, Schreiber SL (1996) A mammalian histone deacetylase related to the yeast transcriptional regulator Rpd3p. Science 272: 408–411.
26. Bernstein BE, Tong JK, Schreiber SL (2000) Genomewide studies of histone deacetylase function in yeast. Proc Natl Acad Sci U S A 97: 13708–13713.
27. Emiliani S, Fischle W, Van Lint C, Al-Abed Y, Verdin E (1998) Characterization of a human RPD3 ortholog, HDAC3. Proc Natl Acad Sci U S A 95: 2795–2800.
28. Grozinger CM, Hassig CA, Schreiber SL (1999) Three proteins define a class of human histone deacetylases related to yeast Hda1p. Proc Natl Acad Sci U S A 96: 4868–4873.
29. Hagelkruys A, Sawicka A, Rennmayr M, Seiser C (2011) The biology of HDAC in cancer: the nuclear and epigenetic components. Handb Exp Pharmacol 206: 13–37.
30. Yang WM, Tsai SC, Wen YD, Fejer G, Seto E (2002) Functional domains of histone deacetylase-3. J Biol Chem 277: 9447–9454.
31. Yang WM, Yao YL, Sun JM, Davie JR, Seto E (1997) Isolation and characterization of cDNAs corresponding to an additional member of the human histone deacetylase gene family. J Biol Chem 272: 28001–28007.
32. Malvaez M, McQuown SC, Rogge GA, Astarabadi M, Jacques V, et al. (2013) HDAC3-selective inhibitor enhances extinction of cocaine-seeking behavior in a persistent manner. Proc Natl Acad Sci U S A. 110: 2647–52.
33. Chou CJ, Herman D, Gottesfeld JM (2008) Pimelic diphenylamide 106 is a slow, tight-binding inhibitor of class I histone deacetylases. J Biol Chem 283: 35402–35409.
34. Rai M, Soragni E, Chou CJ, Barnes G, Jones S, et al. (2010) Two new pimelic diphenylamide HDAC inhibitors induce sustained frataxin upregulation in cells from Friedreich's ataxia patients and in a mouse model. PLoS One 5: e8825.
35. Xu C, Soragni E, Chou CJ, Herman D, Plasterer HL, et al. (2009) Chemical probes identify a role for histone deacetylase 3 in Friedreich's ataxia gene silencing. Chem Biol 16: 980–989.
36. Sirbu BM, Couch FB, Cortez D (2012) Monitoring the spatiotemporal dynamics of proteins at replication forks and in assembled chromatin using isolation of proteins on nascent DNA. Nat Protoc 7: 594–605.
37. Dorn ES, Chastain PD, 2nd, Hall JR, Cook JG (2009) Analysis of re-replication from deregulated origin licensing by DNA fiber spreading. Nucleic Acids Res 37: 60–69.
38. McQuown SC, Barrett RM, Matheos DP, Post RJ, Rogge GA, et al. (2011) HDAC3 is a critical negative regulator of long-term memory formation. J Neurosci 31: 764–774.
39. Yamaguchi T, Cubizolles F, Zhang Y, Reichert N, Kohler H, et al. (2010) Histone deacetylases 1 and 2 act in concert to promote the G1-to-S progression. Genes Dev 24: 455–469.
40. Drogaris P, Villeneuve V, Pomies C, Lee EH, Bourdeau V, et al. (2012) Histone deacetylase inhibitors globally enhance h3/h4 tail acetylation without affecting h3 lysine 56 acetylation. Sci Rep 2: 220.
41. Shen S, O'Brien T, Yap LM, Prince HM, McCormack CJ (2012) The use of methotrexate in dermatology: a review. Australas J Dermatol 53: 1–18.

42. Zhang C, Duvic M (2003) Retinoids: therapeutic applications and mechanisms of action in cutaneous T-cell lymphoma. Dermatol Ther 16: 322–330.
43. Abbott RA, Whittaker SJ, Morris SL, Russell-Jones R, Hung T, et al. (2009) Bexarotene therapy for mycosis fungoides and Sezary syndrome. Br J Dermatol 160: 1299–1307.
44. Fernandez-Capetillo O, Nussenzweig A (2004) Linking histone deacetylation with the repair of DNA breaks. Proc Natl Acad Sci U S A 101: 1427–1428.
45. Sirbu BM, Couch FB, Feigerle JT, Bhaskara S, Hiebert SW, et al. (2011) Analysis of protein dynamics at active, stalled, and collapsed replication forks. Genes Dev 25: 1320–1327.
46. Zhang Y, Iratni R, Erdjument-Bromage H, Tempst P, Reinberg D (1997) Histone deacetylases and SAP18, a novel polypeptide, are components of a human Sin3 complex. Cell 89: 357–364.
47. Ahmad A, Takami Y, Nakayama T (2003) WD dipeptide motifs and LXXLL motif of chicken HIRA are necessary for transcription repression and the latter motif is essential for interaction with histone deacetylase-2 in vivo. Biochem Biophys Res Commun 312: 1266–1272.
48. Tyler JK, Bulger M, Kamakaka RT, Kobayashi R, Kadonaga JT (1996) The p55 subunit of Drosophila chromatin assembly factor 1 is homologous to a histone deacetylase-associated protein. Mol Cell Biol 16: 6149–6159.
49. Rual JF, Venkatesan K, Hao T, Hirozane-Kishikawa T, Dricot A, et al. (2005) Towards a proteome-scale map of the human protein-protein interaction network. Nature 437: 1173–1178.
50. Conti C, Leo E, Eichler GS, Sordet O, Martin MM, et al. (2010) Inhibition of histone deacetylase in cancer cells slows down replication forks, activates dormant origins, and induces DNA damage. Cancer Res 70: 4470–4480.

JBC Papers in Press. Published on September 18, 2013 as Manuscript M113.511337
The latest version is at http://www.jbc.org/cgi/doi/10.1074/jbc.M113.511337

Identification Of Proteins At Active, Stalled, And Collapsed Replication Forks Using Isolation Of Proteins On Nascent DNA (iPOND) Coupled With Mass Spectrometry

Bianca M. Sirbu[1], W. Hayes McDonald[1,3], Huzefa Dungrawala[1], Akosua Badu-Nkansah[1], Gina M. Kavanaugh[1], Yaoyi Chen[2], David L. Tabb[2], David Cortez[#,1]

From the [1]Department of Biochemistry, [2]Department of Biomedical Informatics, and [3]Mass Spectrometry Research Center, Vanderbilt University School of Medicine, Nashville, TN, 37232 USA

*Running title: Identification of proteins on nascent DNA using iPOND-MS

[#]To whom correspondence should be addressed: David Cortez, Department of Biochemistry, Vanderbilt University School of Medicine, Nashville, TN, USA, Tel: (615) 322-8547; Fax: (615) 343-0704; E-mail: david.cortez@vanderbilt.edu

Keywords: DNA damage response, DNA replication, DNA repair, iPOND, ATR, Chromatin

Background: DNA replication and the replication stress response require the coordinated actions of many proteins.
Results: iPOND coupled with mass spectrometry identified 290 proteins associated with active, stalled, or collapsed replication forks.
Conclusion: iPOND-MS provides a useful discovery tool.
Significance: The data increase our understanding of the network of proteins involved in DNA replication and the replication stress response.

ABSTRACT

Both the DNA and chromatin needs to be duplicated each cell division cycle. Replication happens in the context of defects in the DNA template and other forms of replication stress that present challenges to both genetic and epigenetic inheritance. The replication machinery is highly regulated by replication stress responses to accomplish this goal. To identify important replication and stress response proteins we combined Isolation of Proteins on Nascent DNA (iPOND) with quantitative mass spectrometry. We identified 290 proteins enriched on newly replicated DNA at active, stalled, and collapsed replication forks. Approximately 16% of these proteins are known replication or DNA damage response proteins. Genetic analysis indicates that several of the newly identified proteins are needed to facilitate DNA replication especially in stressed conditions. Our data provide a useful resource for investigators studying DNA replication and the replication stress response and validate the use of iPOND combined with mass spectrometry as a discovery tool.

Chromosomal replication requires the coordinated action of a large molecular machine called the replisome consisting of multiple subunits including helicases, polymerases, histone chaperones, and chromatin modifying enzymes. The replisome must work with speed and precision to replicate the DNA and chromatin each cell division cycle. Damage to the DNA template from endogenous and environmental genotoxins, depletion of nucleotide precursors, and even difficult to replicate DNA sequences can impede replication fork progression. Multiple mechanisms respond to this stress to repair the damaged DNA, signal checkpoint activation, ensure the completion of DNA replication, and maintain genome stability. Defects in replication stress response mechanisms cause diseases that are characterized by developmental abnormalities, premature aging, and cancer predisposition.

The Ataxia-telangiectasia and Rad3-related (ATR) protein kinase signaling pathway is a primary regulator of the replication stress response (1). A complex of ATR and its obligate partner ATRIP is activated by interactions with TOPBP1 when DNA polymerase and helicase activities at the replication fork are uncoupled (2-5). Activated ATR stabilizes the stalled fork, promotes fork restart, and regulates cell cycle checkpoints to ensure completion of DNA synthesis prior to mitosis. If ATR is not functional, then forks collapse into double-strand breaks due

to the action of unregulated fork remodeling and nuclease activities (6).

The continued high rate of discovery of new replication stress response proteins suggests that our inventory of replication regulators remains incomplete. Thus, identifying proteins that function at active and damaged replication forks, and characterizing how they work in a coordinated fashion to maintain genome integrity remain critically important research goals. We recently developed a technology called iPOND (isolation of proteins on nascent DNA) that can be used to track protein recruitment to active and damaged replication forks as well as study the processes of chromatin deposition and maturation (7,8). Importantly, the technique provides high resolution and sensitivity and is compatible with unbiased approaches such as mass spectrometry.

iPOND uses the nucleoside analog 5-ethynyl-2'-deoxyuridine (EdU) and click chemistry (8). EdU is rapidly incorporated into newly synthesized DNA when added to cell culture media and does not interfere with replication or cause detectable DNA damage (8,9). An alkyne functional group on EdU can be reacted with an azide linked to biotin using click chemistry. This facilitates a streptavidin-biotin method of purification of the EdU-labeled nascent DNA with associated proteins. Fixation of cells with a reversible crosslinking agent prior to click chemistry and cell lysis permits purification under denaturing conditions making a single-step isolation procedure possible. Crosslink reversal separates the proteins from the DNA fragments, which can then be detected by immunoblotting or mass spectrometry. Here we coupled iPOND to unbiased shotgun proteomics to probe the changes in replisome composition at active, stalled, and collapsed replication forks.

EXPERIMENTAL PROCEDURES

iPOND sample preparation

iPOND was performed largely as previously described (7) with the following modifications. 500 ml of logarithmically growing ($3.3x10^6$ cells/ml) suspension 293T cells (total of $1.6x10^9$ cells) were labeled with 12μM EdU for 15 mins. This length of EdU labeling period may label approximately 15-20 kilobases of DNA depending on the rate of polymerization and how rapidly EdU is imported into the cell and phosphorylated by thymidine kinase (8). Following EdU incorporation the stalled fork sample was incubated in 3mM of HU for 2 hours, and the collapsed fork sample was treated with 3mM HU and 3μM of ATR inhibitor for 2 hours to induce fork collapse (10). After the EdU labeling, the thymidine chase sample was centrifuged at 1,000rpm for 4 mins, media decanted and cells resuspended in media equilibrated for temperature and pH containing 10μM thymidine. The thymidine chase was conducted for 60 mins. All samples were fixed with 1% formaldehyde for 20 mins at room temperature, followed by 5 min incubation with 0.125M glycine to quench the formaldehyde.

Fixed samples were split evenly into six 50ml conical tubes, centrifuged at 2,000rpm at 4°C for 6 mins, washed three times with PBS and frozen at -80°C. Five of the 6 tubes were independently processed on a scale of $2.7x10^8$ cells per sample for iPOND purifications. Briefly, click chemistry reactions were performed to conjugate biotin to the EdU-labeled DNA. Streptavidin beads were used to capture the biotin-conjugated DNA-protein complexes. Captured complexes were washed extensively using SDS and high salt wash buffers. Purified replication fork proteins were eluted under reducing conditions by boiling in 2x SDS-sample buffer for 25 mins. One-sixth of the eluted protein sample was resolved one centimeter into a 10% Novex precast gel (Invitrogen), excised from the gel slice, alkylated, and in-gel trypsin digested using standard procedures.

Mass spectrometric data analysis

Recovered tryptic peptides were subjected to two-dimensional LC-MS/MS (MudPIT) separation as previously described (11). Briefly, digested peptides were separated by a combined strong cation exchange (SCX) and reversed phase (RP) chromatographic strategy. Subsets of peptides were eluted from the SCX onto the RP using a series of ammonium acetate pulses of increasing concentration. This was performed for 8 steps, each followed by a 105 min aqueous to organic separation on the RP column. Eluted peptides were directly nanoelectrospray ionized and introduced into an LTQ-XL mass spectrometer (Thermo Fisher Scientific) where peptide tandem mass spectra (MS/MS) were

collected in a data dependent manner. The peptide spectral data was searched against the canonical human proteome subset of UniProtKB (v155) using the Myrimatch (v1.6.75) (12), Sequest (v27)(13), and Myrimatch and Sequest (14) database search engines. Protein groups were assembled using IDPicker, which uses parsimony to report the minimum number of confident protein identifications (15). Matched peptides were filtered at a 5% peptide and protein false discovery rate and each protein required a minimum of two independent peptides for identification. Protein identifiers were converted to EntrezID unique identifiers using the UniProt ID mapping database (16) and the DAVID bioinformatics database (17).

QuasiTel statistical analysis and protein enrichment filtering criteria

To determine fold enrichments of proteins relative to the negative controls, spectral count data was imported into the statistical software program QuasiTel (18) for pair-wise comparisons. QuasiTel applies a quasi-likelihood model to raw spectral count data and reports protein fold enrichment and statistical significance as a quasi p-value. Spectral count data is normalized for each MudPIT run using the total number of spectra reported for the run. The threshold for spectral counts was set at an average of one spectral count per experimental sample. For example, when comparing the 5 replicates from the replication fork sample to the 5 replicates from the chromatin chase sample, a minimum of 10 total spectral counts was required from the 10 samples for QuasiTel comparisons. Furthermore, to be considered a protein significantly enriched on nascent DNA, the filtering criteria required a minimum of 1.5-fold enrichment above both of the negative controls and a quasi p-value of less than or equal to 0.05.

These filtering criteria were applied to proteins identified using each of the three protein identification search algorithms (Myrimatch plus Sequest, Myrimatch alone and Sequest alone). Therefore, three lists of enriched proteins were generated independently. The final data reported in Tables S1-S3 represent the union of all three lists and report the median fold enrichment relative to the chromatin-bound negative control, median p-value, and median spectral counts. The median p value in some cases is greater than 0.05 since three independent p-values were calculated by QuasiTel for each protein identified by the three different search algorithm methods. If any one of the analyses yielded a p-value less than 0.05, that protein is reported in Table S1-S3 along with the median p-value from the three analyses. It should also be noted that when no spectra were detected in the thymidine-chase negative control, QuasiTel calculates relative fold enrichment using a small, non-zero value in the denominator. This factor may lead to an overestimation of protein enrichment. While these values are included in Tables S1-S3, they are omitted from Figures 2-4.

Bioinformatics data analyses

Proteins identified at elongating, stalled and collapsed replication forks were classified based on gene ontology using ToppGene (19). To display median fold enrichment relative to the thymidine chase negative control, median quasi p-value, and median spectral counts from the experimental sample were graphed using R. Protein network modeling was performed using the GeneMANIA prediction server (20).

Antibodies

Antibodies were obtained as follows: H2A, H2B, MSH2, and SNF2H, Abcam; H1, Millipore; PCNA, Santa Cruz Biotechnology; SNF2L, Cell Signaling; BAZ1B, Novus; MSH6, Bethyl Laboratories.

siRNA screen

Four individual siRNAs for each of the genes arrayed in 384 well dishes were transfected into U2OS cells at 10nM final siRNA concentrations. Three days after transfection, cells were treated with 2mM HU for 24h. HU was removed and cells were incubated with 10 μM EdU for four hours. Cells were then fixed with paraformaldehyde and processed with AlexaFluor 488-coupled biotin azide followed by labeling with antibodies to γH2AX as previously described (21). Images were obtained on a Perkin Elmer Opera automated microscope and the intensities of EdU and γH2AX per nucleus quantitated by Columbus image analysis software. The ratio of γH2AX to EdU intensities was used as the final scoring criteria. Samples with elevated ratios were identified using the Wilcoxon rank sum test

requiring a false-discovery rate adjusted p-value of <0.001 and a ratio of at least 2.0. As a comparison the average ratio for the negative control siRNA was 1.07 with a standard error of 0.026.

RESULTS

iPOND proteomics

To identify proteins associated with nascent DNA at active, stalled, and collapsed replication forks we coupled iPOND purifications to mass spectrometry (iPOND-MS). Five samples were prepared for iPOND-MS (Fig. 1A). For all samples, cells were treated for 15 mins with EdU to label nascent DNA. To examine proteins at active replication forks, EdU labeled cells were collected immediately. To monitor proteins associated with stalled replication forks, EdU labeled cells were treated with 3mM hydroxyurea (HU) for two hours to arrest fork movement and induce a replication stress response. To identify proteins associated with fork collapse, cells were treated with HU and a selective ATR inhibitor (10) for two hours. These conditions elicit fork collapse including accumulation of double-strand breaks and excess single-stranded DNA (ssDNA) at the replication fork (6). EdU remained in the growth media during the HU treatments.

The specificity of replication fork protein purifications was tested relative to two negative controls. The first were cells treated identically to the normal replication fork sample but the biotin azide was omitted during the iPOND procedure. Proteins purified in this "no Click reaction" sample represent those that interact non-specifically with streptavidin-conjugated beads. For the second negative control, cells labeled with EdU were washed and then incubated with media containing a small amount of thymidine for one hour. This procedure allows replication to continue without additional EdU incorporation. The small concentration of thymidine does not interfere with replication but is used to compete for whatever EdU is left in the cell after removing it from the growth media. Thus this negative control monitors proteins bound to mature chromatin, which are no longer close to the replication fork. Proteins detected in this "thymidine chase" sample represent chromatin-bound proteins that are not specifically enriched at replisomes (8).

To test the relative enrichment of replication proteins in the samples submitted for mass spectrometry analyses, iPOND purifications were examined for PCNA levels. As observed previously, PCNA was detected at elongating replication forks and its levels decreased in the thymidine chase sample (Fig. 1B). While still detectable, PCNA levels at stalled and collapsed replication forks are also decreased compared to the active fork sample likely due to unloading of PCNA from the mature Okazaki fragments (8). The equal level of histone H2B detected on isolated chromatin (Fig. 1B) indicates that an equivalent amount of EdU-labeled DNA was purified in each sample.

The five experimental samples were purified independently five times each using the iPOND procedure (Fig. 1C). Eluted proteins were analyzed using two-dimensional liquid chromatography coupled with tandem mass spectrometry (multidimensional protein identification technology MudPIT). The MS/MS spectra were matched to the human protein database using the Myrimatch and Sequest search engines (12-14).

QuasiTel was used to compute fold-enrichment values of each experimental sample relative to both of the negative control samples (22). The final lists include proteins enriched at least 1.5-fold (relative to both negative controls) with p-values from at least one of the search engines yielding a p-value less than or equal to 0.05 as computed by QuasiTel.

These filtering criteria led to the identification of a total of 290 proteins that were enriched in at least one of the three experimental samples compared to both negative controls. Approximately 16 percent of the enriched proteins have previously been documented to function in DNA replication or DNA damage responses. Functional characterization of the dataset revealed that gene ontology categories such as DNA repair, response to DNA damage, DNA metabolic process, DNA replication and cell cycle were highly overrepresented above random chance of expectancy (Fig. 1D). This provides confidence that the iPOND-MS screen successfully identified DNA replication and replication stress response proteins. As expected, abundant chromatin-associated proteins like histones were detected by

mass spectrometry but not enriched above the controls in any of the experimental samples.

Of the total proteins enriched on nascent DNA, 84 were found to accumulate at active forks (Table S1), 139 at stalled forks (Table S2), and 137 at collapsed forks (Table S3). Several established genome maintenance proteins were among the proteins enriched in all three experimental conditions. For example, the interstrand crosslink repair factor FANCI, which is found mutated in Fanconi anemia, the ATR-activating and replication initiation protein TOPBP1, and the chromatin remodeler SMARCAD1 were enriched at replication forks in unperturbed and stressed conditions.

The elongating replisome and associated proteins

Overall, the highest confidence proteins from iPOND-MS have low p-values, are highly enriched relative to both negative controls and are detected with large spectral count numbers. A majority of these high confidence proteins at active replication forks are known replisome components such as PCNA, the RFC complex, and polymerase subunits including POLD1 and POLE (Fig. 2A).

Bioinformatics searches using the GeneMANIA prediction server (20) indicate that approximately one third of the proteins identified at active forks form an interacting network (Fig. 2B). Unsurprisingly, PCNA represents a prominent node in this network since it serves as a binding scaffold for numerous replication and DNA damage proteins (23). Eleven of the iPOND-MS proteins contain predicted PCNA-interacting motifs, which is greater than predicted by chance ($p = 2x10^{-7}$) (Fig. 2C). Proteins containing a PCNA interaction protein motif, or PIP box, include the Williams syndrome transcription factor WSTF (also known as BAZ1B), DNA methyltransferase (DNMT1), ligase 1, mismatch repair proteins MSH3 and MSH6, chromatin remodelers SNF2L and SNF2H, and the E3 ubiquitin ligase UBR5. The centrosomal protein CP110, the DNMT1 recruiting protein UHRF1, and the euchromatic histone methyltransferase EHMT1 have predicted APIM (AlkB homologue 2 PCNA-interacting motif) motifs (24).

To further analyze the proteins, the dataset was compared to two published proteomics screens that identify substrates of the ATM or ATR checkpoint kinase substrates (25,26). At least 19 of the iPOND-MS enriched proteins are putative ATM/ATR substrates that were identified in these proteomic screens (Fig. 2C). This represents a statistically significant over-representation of checkpoint kinase substrates compared to what would be expected by chance ($p = 1x10^{-11}$).

The majority of these kinase substrates are known replication or DNA damage response proteins, such as MSH2, MSH3, MSH6, POLE, RFC1, RFC3, TOPBP1, the TOPB1 ubiquitin ligase UBR5, FANCI, the exonuclease EXO1, the replication initiating factor WDHD1 (also known as AND1), and the alternative PCNA clamp loader ATAD5 (also known as ELG1). Other ATM/ATR substrates that localized to active forks are involved in chromatin assembly and maturation. These include the histone chaperones CAF1A and CAF1B, the chromatin remodeler SMARCAD1, and EHMT1. tRNA methyltransferase (TRMT6) and vacuolar protein sorting homolog B (VPS26) are ATM/ATR substrates that have not been previously linked to DNA replication or replication stress responses, but were identified at elongating forks using iPOND-MS.

The iPOND-MS list was also cross-referenced with large-scale siRNA screens that identified genes that when silenced activate the DNA damage response (27,28). Many of those genes encode DNA replication or replication stress response proteins whose inactivation leads to replication-associated checkpoint signaling. Eleven iPOND-MS proteins cause increased H2AX phosphorylation when silenced including several with no previously described functions in DNA replication such as EP400, HSD17B7, PDCD4, PLOD1, SMARCA1, SNRPD1, or TRMT6 (Fig. 2C).

Finally, the strong enrichment of mismatch repair proteins MSH2, MSH3, and MSH6 at active elongating forks is consistent with recent data from yeast systems indicating that these proteins travel with the replisome (29). We verified that both MSH2 and MSH6 are associated with the replisome in a pattern mirroring PCNA using conventional immunoblotting (data not shown).

Several known replisome proteins were not detected. In some cases not enough peptides were identified or the fold enrichment values and

statistical reproducibility did not meet our stringent criteria. Thus, the dataset should not be considered a full list of replisome proteins.

Proteins recruited to stalled replication forks

Proteins enriched near stalled replication forks are listed in Table S2 and Fig 3A. The dataset is significantly enriched in gene ontologies classified under cellular response to stress ($p = 8x10^{-5}$), DNA metabolic process ($p = 6x10^{-4}$) and cell cycle ($p = 1.7x10^{-3}$).

Several known DNA damage response proteins including MDC1, RPA, RECQL1, XRCC1, FANCD2, FANCI, RAD1, and TOPBP1 were enriched. The identified proteins are also enriched for ATM/ATR substrates (19 proteins, $p = 5x10^{-7}$), five contain PCNA-interacting motifs although this is not larger than expected by chance ($p = 0.07$), and 16 cause elevated DNA damage signaling when depleted (Fig 3B). Over 50% of these proteins have not been previously implicated in DNA replication or stress responses.

One of the ATM/ATR substrates identified at the stalled fork is EHMT2 (also known as G9A). This protein methylates H3K56, which has well studied functions in DNA replication and repair in yeast. Recent experiments also indicate that this histone modification is important in mammalian cells during DNA replication (30) and the presence of EHMT2 at stalled forks supports this observation.

A number of DNA damage response proteins that are known to be recruited to stalled forks including ATR were not identified. In some cases we suspect this is because iPOND only purifies nascent, EdU-labeled DNA. Thus, the unlabeled parental ssDNA signaling platform created by uncoupling of helicase and polymerase activities along with bound checkpoint proteins is only purified if it remains attached to the double-stranded, newly synthesized DNA containing EdU (8). Less aggressive DNA fragmentation may be needed to capture the parental ssDNA adjacent to the labeled nascent double-stranded DNA.

Proteins recruited to collapsed replication forks

Proteins enriched at collapsed forks after combined HU and ATR inhibitor treatment are shown in Table S3 and Figure 4A. The most striking difference between the collapsed fork sample and the other two experimental conditions is a large increase in DNA double-strand break repair and RPA-associated proteins. At least one-fourth of the identified proteins form an interacting network (Fig. 4B). ATM and RPA are major nodes in this interaction network. The recruitment of ATM is consistent with studies demonstrating that ATR inhibition leads to ATM activation (1). The strong enrichment of RPA subunits and RPA-interacting proteins at collapsed forks is consistent with our previous observation that large amounts of nascent-strand ssDNA is generated in these conditions due in part to resection of a double-strand break (6). In addition to all three subunits of RPA, this sample contained the RPA-interacting helicases BLM and WRN, the fork regression enzyme SMARCAL1, and the double-strand break response proteins ATM, MDC1, RAD51, and BRIP1. SMARCAL1 is one of the most highly enriched proteins. ATR phosphorylates SMARCAL1 to limit enzymatic processing of stalled forks and unregulated SMARCAL1 contributes to fork collapse (6). ATR was also enriched in this data set (2.5 fold), however, its p value was just outside the cutoff for significance ($p = 0.054$).

Two of the most enriched proteins at collapsed forks are MMS22L and TONSL. The MMS22L-TONSL complex is recruited to sites of RPA-coated ssDNA to promote recombination repair of damaged replication forks (31-33). The MMS22L-TONSL complex facilitates HR after DNA end resection through promoting RAD51 filament formation. These results are also consistent with the idea that ATR prevents the formation of double-strand breaks and nascent ssDNA at replication forks (6).

The collapsed fork dataset is enriched in ATM/ATR substrates (15 proteins, $p = 3x10^{-5}$), seven have PCNA-interacting motifs ($p = 0.008$), and 23 of the proteins cause increased DNA damage signaling when silenced by siRNA (Fig. 4C).

siRNA screen to identify proteins that have critical functions in the context of replication stress

Of the approximately 240 new putative replication/replication stress response proteins identified in the iPOND-MS screens, we selected 148 for further analysis. Specifically, we were interested in identifying new proteins that might be important for continued replication in stressful

conditions. Therefore, we performed an RNA interference screen using four siRNAs targeting many of the genes encoding proteins without clear functions which had higher enrichment or statistical significance values or for which some published literature or domain structure suggested a function in nucleic acid metabolism. Following siRNA transfection, cells were treated with HU overnight to stall replication, then allowed to recover for four hours in the presence of EdU. Cells were then fixed and stained for EdU and γH2AX intensity. Control U2OS cells recover quickly from this acute replication stress challenge and complete DNA replication with very little loss of viability within the time frame of the experiment (6,34). The expectation is that genes encoding proteins needed to maintain replication fork stability or facilitate replication fork recovery would yield low levels of EdU and high levels of γH2AX after knockdown. Indeed, as a positive control, ATR silencing results in a high ratio of γH2AX to EdU values since forks collapse into DSBs and do not resume DNA synthesis (Fig. 5A). Thus, knockdown of a gene that functions in an ATR or related replication stress response pathway would be predicted to cause high γH2AX/EdU ratios. The results of the screen are shown in Figure 5A and Table S4. Seventeen genes passed our stringent criteria and had at least two individual siRNAs yielding an elevated score (>2) with a false discovery rate adjusted p value less than 0.001.

Two genes, PPP1R10 (PNUTS) and SMARCA1 (SNF2L) had 3 of 4 siRNAs yield an elevated score. PNUTS is a targeting subunit for protein phosphatase 1. It is recruited to sites of ionizing radiation-induced DNA damage, is important for DNA repair, and loss of PNUTS function causes G2 checkpoint activation in unperturbed cells (35). Thus, the PNUTS-PP1c phosphatase likely has critical functions at stalled replication forks or after fork collapse to promote fork restart.

SNF2L is an ATP-dependent chromatin remodeling protein. Interestingly, the highly related protein SNF2H (SMARCA5), did not phenocopy loss of SNF2L in this screen (Fig. 5B) even though we confirmed that both SNF2L and SNF2H are enriched at active elongating replication forks using standard iPOND combined with immunoblotting (Fig. 5C and D). Both of these proteins are motor proteins in ISWI chromatin remodeling complexes, which reposition nucleosomes during transcription and other nucleic acid metabolic processes (36). Each protein forms several protein complexes with accessory factors including BAZ1A and BAZ1B (37). BAZ1B (also known as WSTF) was also identified in our iPOND-MS dataset at active forks and confirmed by immunoblotting (Fig. 5C and D) but like SNF2H it did not yield an elevated γH2AX/EdU ratio compared to controls. A BAZ1B-SNF2H complex interacts with PCNA and regulates chromatin compaction during replication (38). SNF2H is also recruited to double-strand breaks where it functions to help unfold chromatin (39). Less is known about SNF2L function in DNA damage responses but silencing SNF2L by RNA interference increases the amount of DNA damage signaling in cells (40). Since iPOND selectively purifies proteins behind the fork in complexes with newly synthesized DNA, our data suggest SNF2L and SNF2H function on newly deposited chromatin. Silencing of the two chromatin remodelers does not yield identical phenotypes indicating that the proteins perform non-redundant roles, and SNF2L may have an especially important function in the context of replication stress.

DISCUSSION

Coupling iPOND with two-dimensional LC-MS/MS is a powerful discovery tool. We identified 290 proteins at active, stalled, and collapsed forks. Providing validation of the approach, the dataset is highly enriched in proteins known to function in DNA damage responses, cell cycle control, DNA repair and replication. For example, at normally elongating replication forks, 15 of the top 20 proteins, as measured by fold enrichment and p-value, are established replisome components and chromatin replication factors. These include the replicative polymerases, PCNA, the replication-loading complex RFC (RFC1-5), and the chromatin assembly factors CAF1A and CAF1B. The stalled fork dataset enriched for DNA damage response proteins above random chance of occurrence. Collapsed replication forks exhibited strong enrichment of RPA and RPA-interacting proteins, double-strand break repair proteins, and fork remodeling helicases.

While this manuscript was in preparation, the Fernadez-Capetillo group completed a iPOND-MS study only looking at proteins enriched at active forks (41). They identified many of the same replisome components including: ATAD5, BAZ1B, CHAF1A, CHAF1B, DNMT1, EXO1, LIG1, MSH2, MSH3, MSH6, PCNA, POLD1, POLE, RFC1-5, UHRF1, and WIZ. They also identified the MCM helicase complex, which was not enriched in our datasets. In immunoblotting experiments we have observed variable results in detecting the MCM proteins. We suspect the differences are due to how much cleavage of the ssDNA at the fork happens during the iPOND processing. The MCM proteins function to unwind parental DNA and are not directly associated with newly synthesized, EdU-labeled DNA. Thus, detection of the MCM helicase would rely on purifying larger fragments of DNA containing both nascent and parental strands. Other differences in methodologies may further explain differences in the datasets. Most notably, we used approximately 10-fold less cells in our samples and examined HU-stalled and HU/ATRi induced collapsed forks in addition to active forks. The decreased amount of starting material may also explain why many known replication and stress response proteins were not identified. Nonetheless, both datasets provide useful resources for investigators interested in replication and replication stress responses. Finally, we would caution that although we applied stringent criteria for protein identification and enrichment, further validation of the candidate proteins is required especially in cases with higher p-values and lower enrichment scores.

The mismatch repair proteins MSH2, MSH3, and MSH6 were some of the most highly enriched proteins at unperturbed replication forks. The high level of enrichment of MMR proteins is unlikely to be due to the need to remove true mismatches since the polymerase error rate is low. More likely, the MMR proteins are scanning for errors in conjunction with replication as recently shown for the yeast MMR system (29) or possibly involved in removing ribonucleotides from the DNA (42). It is also possible that the MMR proteins may recognize EdU-labeled DNA. However, any DNA damage due to EdU incorporation does not activate a DNA damage signaling pathway, and very little (if any) of the EdU is removed from the DNA since we do not observe a decrease in chromatin capture after growing cells for hours after the EdU labeling (8).

The FANCI and FANCD2 proteins are highly enriched at stalled and collapsed replication forks. FANCI was also detected at active forks. FANCI and FANCD2 function in the ID complex during interstrand crosslink repair (43). These lesions are some of the most difficult to repair substrates, requiring specialized repair mechanisms governed by genes mutated in patients with Fanconi anemia, as well as components of nucleotide excision and DSB repair (44,45). FANCD2 is ubiquitylated in response to HU and even as cells enter a normal S-phase. Thus, the ID complex may recognize DNA structures generated during replication stress such as ssDNA-dsDNA junctions (46), and these proteins may have functions outside of crosslink repair. Indeed, FANCD2 promotes restart of aphidicolin-stalled replication forks (47). Alternatively, it is possible that the FANC proteins were identified due to a small amount of continued EdU incorporation during the beginning of the formaldehyde fixation. If this were the case, it might create protein crosslinks to the DNA, which could recruit the FANC proteins (48).

The high-level enrichment of the heterotrimeric ssDNA-binding protein RPA is a striking feature of stalled replication forks that collapse after ATR inhibition. Concomitant with RPA accumulation, we observed enrichment of the disease-associated helicases BLM, CHD1L, SMARCAL1 and WRN, as well as many other RPA interacting proteins. These data are consistent with the recent observation that ATR inhibition causes the extensive production of nascent-strand ssDNA at replication forks through a process involving fork reversal, enzymatic cleavage, and end resection (6).

Finally, our data confirm important functions for chromatin remodeling enzymes including SNF2L and SNF2H at replication forks. The highly related SNF2H and SNF2L chromatin remodelers are the motor enzymes of ISWI complexes (36). In complex with BAZ1B, SNF2H is recruited to replication forks via an interaction with PCNA to maintain the chromatin landscape through DNA replication (38). The activity of SNF2L at replication forks has not been described, but our data indicate it must have an important

non-redundant function that perhaps is especially needed in the context of replication stress.

Collectively, our data indicate that iPOND can be combined with mass spectrometry to provide a powerful discovery approach. In addition to analyzing normal, stalled, and collapsed forks, there are many other instances in which iPOND-MS analysis would be useful to understand DNA repair, replication, and chromatin biology.

ACKNOWLEDGEMENTS

This work was supported by NIH grants R01 CA136933 and R21 ES22319 to D.C. B.M.S. is supported by a Department of Defense Breast Cancer Research Program predoctoral fellowship (W81XWH-10-1-0226) and a grant from Swim Across America. Funding for Vanderbilt Proteomics Core usage was provided by the Center in Molecular Toxicology, P30 ES000267 and the Vanderbilt-Ingram Cancer Center.

REFERENCES

1. Cimprich, K. A., and Cortez, D. (2008) ATR: an essential regulator of genome integrity. *Nat Rev Mol Cell Biol* **9**, 616-627
2. Cortez, D., Guntuku, S., Qin, J., and Elledge, S. J. (2001) ATR and ATRIP: partners in checkpoint signaling. *Science* **294**, 1713-1716.
3. Kumagai, A., Lee, J., Yoo, H. Y., and Dunphy, W. G. (2006) TopBP1 activates the ATR-ATRIP complex. *Cell* **124**, 943-955
4. Mordes, D. A., Glick, G. G., Zhao, R., and Cortez, D. (2008) TopBP1 activates ATR through ATRIP and a PIKK regulatory domain. *Genes Dev* **22**, 1478-1489
5. Byun, T. S., Pacek, M., Yee, M. C., Walter, J. C., and Cimprich, K. A. (2005) Functional uncoupling of MCM helicase and DNA polymerase activities activates the ATR-dependent checkpoint. *Genes Dev* **19**, 1040-1052
6. Couch, F. B., Bansbach, C. E., Driscoll, R., Luzwick, J. W., Glick, G. G., Betous, R., Carroll, C. M., Jung, S. Y., Qin, J., Cimprich, K. A., and Cortez, D. (2013) ATR phosphorylates SMARCAL1 to prevent replication fork collapse. *Genes Dev* **27**, 1610-1623
7. Sirbu, B. M., Couch, F. B., and Cortez, D. (2012) Monitoring the spatiotemporal dynamics of proteins at replication forks and in assembled chromatin using isolation of proteins on nascent DNA. *Nature protocols* **7**, 594-605
8. Sirbu, B. M., Couch, F. B., Feigerle, J. T., Bhaskara, S., Hiebert, S. W., and Cortez, D. (2011) Analysis of protein dynamics at active, stalled, and collapsed replication forks. *Genes Dev* **25**, 1320-1327
9. Salic, A., and Mitchison, T. J. (2008) A chemical method for fast and sensitive detection of DNA synthesis in vivo. *Proc Natl Acad Sci U S A* **105**, 2415-2420
10. Reaper, P. M., Griffiths, M. R., Long, J. M., Charrier, J. D., Maccormick, S., Charlton, P. A., Golec, J. M., and Pollard, J. R. (2011) Selective killing of ATM- or p53-deficient cancer cells through inhibition of ATR. *Nature chemical biology* **7**, 428-430
11. MacCoss, M. J., McDonald, W. H., Saraf, A., Sadygov, R., Clark, J. M., Tasto, J. J., Gould, K. L., Wolters, D., Washburn, M., Weiss, A., Clark, J. I., and Yates, J. R., 3rd. (2002) Shotgun identification of protein modifications from protein complexes and lens tissue. *Proc Natl Acad Sci U S A* **99**, 7900-7905
12. Tabb, D. L., Fernando, C. G., and Chambers, M. C. (2007) MyriMatch: highly accurate tandem mass spectral peptide identification by multivariate hypergeometric analysis. *Journal of proteome research* **6**, 654-661
13. Yates, J. R., 3rd, Eng, J. K., McCormack, A. L., and Schieltz, D. (1995) Method to correlate tandem mass spectra of modified peptides to amino acid sequences in the protein database. *Analytical chemistry* **67**, 1426-1436

14. Chen, Y. Y., Dasari, S., Ma, Z. Q., Vega-Montoto, L. J., Li, M., and Tabb, D. L. (2012) Refining comparative proteomics by spectral counting to account for shared peptides and multiple search engines. *Analytical and bioanalytical chemistry* **404**, 1115-1125
15. Ma, Z. Q., Dasari, S., Chambers, M. C., Litton, M. D., Sobecki, S. M., Zimmerman, L. J., Halvey, P. J., Schilling, B., Drake, P. M., Gibson, B. W., and Tabb, D. L. (2009) IDPicker 2.0: Improved protein assembly with high discrimination peptide identification filtering. *Journal of proteome research* **8**, 3872-3881
16. UniProt, C. (2012) Reorganizing the protein space at the Universal Protein Resource (UniProt). *Nucleic acids research* **40**, D71-75
17. Huang da, W., Sherman, B. T., and Lempicki, R. A. (2009) Systematic and integrative analysis of large gene lists using DAVID bioinformatics resources. *Nature protocols* **4**, 44-57
18. Li, M., Gray, W., Zhang, H., Chung, C. H., Billheimer, D., Yarbrough, W. G., Liebler, D. C., Shyr, Y., and Slebos, R. J. (2010) Comparative shotgun proteomics using spectral count data and quasi-likelihood modeling. *Journal of proteome research* **9**, 4295-4305
19. Chen, J., Bardes, E. E., Aronow, B. J., and Jegga, A. G. (2009) ToppGene Suite for gene list enrichment analysis and candidate gene prioritization. *Nucleic acids research* **37**, W305-311
20. Warde-Farley, D., Donaldson, S. L., Comes, O., Zuberi, K., Badrawi, R., Chao, P., Franz, M., Grouios, C., Kazi, F., Lopes, C. T., Maitland, A., Mostafavi, S., Montojo, J., Shao, Q., Wright, G., Bader, G. D., and Morris, Q. (2010) The GeneMANIA prediction server: biological network integration for gene prioritization and predicting gene function. *Nucleic acids research* **38**, W214-220
21. Bansbach, C. E., Betous, R., Lovejoy, C. A., Glick, G. G., and Cortez, D. (2009) The annealing helicase SMARCAL1 maintains genome integrity at stalled replication forks. *Genes Dev* **23**, 2405-2414
22. Li, M., Gray, W., Zhang, H., Chung, C. H., Billheimer, D., Yarbrough, W. G., Liebler, D. C., Shyr, Y., and Slebos, R. J. (2010) Comparative shotgun proteomics using spectral count data and quasi-likelihood modeling. *Journal of proteome research* **9**, 4295-4305
23. Moldovan, G. L., Pfander, B., and Jentsch, S. (2007) PCNA, the maestro of the replication fork. *Cell* **129**, 665-679
24. Gilljam, K. M., Feyzi, E., Aas, P. A., Sousa, M. M., Muller, R., Vagbo, C. B., Catterall, T. C., Liabakk, N. B., Slupphaug, G., Drablos, F., Krokan, H. E., and Otterlei, M. (2009) Identification of a novel, widespread, and functionally important PCNA-binding motif. *J Cell Biol* **186**, 645-654
25. Matsuoka, S., Ballif, B. A., Smogorzewska, A., McDonald, E. R., 3rd, Hurov, K. E., Luo, J., Bakalarski, C. E., Zhao, Z., Solimini, N., Lerenthal, Y., Shiloh, Y., Gygi, S. P., and Elledge, S. J. (2007) ATM and ATR substrate analysis reveals extensive protein networks responsive to DNA damage. *Science* **316**, 1160-1166
26. Bensimon, A., Schmidt, A., Ziv, Y., Elkon, R., Wang, S. Y., Chen, D. J., Aebersold, R., and Shiloh, Y. (2010) ATM-dependent and -independent dynamics of the nuclear phosphoproteome after DNA damage. *Science signaling* **3**, rs3
27. Lovejoy, C. A., Xu, X., Bansbach, C. E., Glick, G. G., Zhao, R., Ye, F., Sirbu, B. M., Titus, L. C., Shyr, Y., and Cortez, D. (2009) Functional genomic screens identify CINP as a genome maintenance protein. *Proc Natl Acad Sci U S A* **106**, 19304-19309
28. Paulsen, R. D., Soni, D. V., Wollman, R., Hahn, A. T., Yee, M. C., Guan, A., Hesley, J. A., Miller, S. C., Cromwell, E. F., Solow-Cordero, D. E., Meyer, T., and Cimprich, K. A. (2009) A genome-wide siRNA screen reveals diverse cellular processes and pathways that mediate genome stability. *Molecular cell* **35**, 228-239
29. Hombauer, H., Srivatsan, A., Putnam, C. D., and Kolodner, R. D. (2011) Mismatch repair, but not heteroduplex rejection, is temporally coupled to DNA replication. *Science* **334**, 1713-1716

30. Yu, Y., Song, C., Zhang, Q., DiMaggio, P. A., Garcia, B. A., York, A., Carey, M. F., and Grunstein, M. (2012) Histone H3 lysine 56 methylation regulates DNA replication through its interaction with PCNA. *Molecular cell* **46**, 7-17
31. Duro, E., Lundin, C., Ask, K., Sanchez-Pulido, L., MacArtney, T. J., Toth, R., Ponting, C. P., Groth, A., Helleday, T., and Rouse, J. (2010) Identification of the MMS22L-TONSL complex that promotes homologous recombination. *Molecular cell* **40**, 632-644
32. O'Donnell, L., Panier, S., Wildenhain, J., Tkach, J. M., Al-Hakim, A., Landry, M. C., Escribano-Diaz, C., Szilard, R. K., Young, J. T., Munro, M., Canny, M. D., Kolas, N. K., Zhang, W., Harding, S. M., Ylanko, J., Mendez, M., Mullin, M., Sun, T., Habermann, B., Datti, A., Bristow, R. G., Gingras, A. C., Tyers, M. D., Brown, G. W., and Durocher, D. (2010) The MMS22L-TONSL complex mediates recovery from replication stress and homologous recombination. *Molecular cell* **40**, 619-631
33. O'Connell, B. C., Adamson, B., Lydeard, J. R., Sowa, M. E., Ciccia, A., Bredemeyer, A. L., Schlabach, M., Gygi, S. P., Elledge, S. J., and Harper, J. W. (2010) A genome-wide camptothecin sensitivity screen identifies a mammalian MMS22L-NFKBIL2 complex required for genomic stability. *Molecular cell* **40**, 645-657
34. Yu, D. S., Zhao, R., Hsu, E. L., Cayer, J., Ye, F., Guo, Y., Shyr, Y., and Cortez, D. (2010) Cyclin-dependent kinase 9-cyclin K functions in the replication stress response. *EMBO reports* **11**, 876-882
35. Landsverk, H. B., Mora-Bermudez, F., Landsverk, O. J., Hasvold, G., Naderi, S., Bakke, O., Ellenberg, J., Collas, P., Syljuasen, R. G., and Kuntziger, T. (2010) The protein phosphatase 1 regulator PNUTS is a new component of the DNA damage response. *EMBO reports* **11**, 868-875
36. Struhl, K., and Segal, E. (2013) Determinants of nucleosome positioning. *Nat Struct Mol Biol* **20**, 267-273
37. Yadon, A. N., and Tsukiyama, T. (2011) SnapShot: Chromatin remodeling: ISWI. *Cell* **144**, 453-453 e451
38. Poot, R. A., Bozhenok, L., van den Berg, D. L., Steffensen, S., Ferreira, F., Grimaldi, M., Gilbert, N., Ferreira, J., and Varga-Weisz, P. D. (2004) The Williams syndrome transcription factor interacts with PCNA to target chromatin remodelling by ISWI to replication foci. *Nat Cell Biol* **6**, 1236-1244
39. Toiber, D., Erdel, F., Bouazoune, K., Silberman, D. M., Zhong, L., Mulligan, P., Sebastian, C., Cosentino, C., Martinez-Pastor, B., Giacosa, S., D'Urso, A., Naar, A. M., Kingston, R., Rippe, K., and Mostoslavsky, R. (2013) SIRT6 Recruits SNF2H to DNA Break Sites, Preventing Genomic Instability through Chromatin Remodeling. *Molecular cell*
40. Ye, Y., Xiao, Y., Wang, W., Wang, Q., Yearsley, K., Wani, A. A., Yan, Q., Gao, J. X., Shetuni, B. S., and Barsky, S. H. (2009) Inhibition of expression of the chromatin remodeling gene, SNF2L, selectively leads to DNA damage, growth inhibition, and cancer cell death. *Molecular cancer research : MCR* **7**, 1984-1999
41. Lopez-Contreras, A. J., Ruppen, I., Nieto-Soler, M., Murga, M., Rodriguez-Acebes, S., Remeseiro, S., Rodrigo-Perez, S., Rojas, A. M., Mendez, J., Munoz, J., and Fernandez-Capetillo, O. (2013) A proteomic characterization of factors enriched at nascent DNA molecules. *Cell Rep* **3**, 1105-1116
42. Lujan, S. A., Williams, J. S., Clausen, A. R., Clark, A. B., and Kunkel, T. A. (2013) Ribonucleotides are signals for mismatch repair of leading-strand replication errors. *Molecular cell* **50**, 437-443
43. Ciccia, A., and Elledge, S. J. (2010) The DNA damage response: making it safe to play with knives. *Molecular cell* **40**, 179-204
44. Kim, H., and D'Andrea, A. D. (2012) Regulation of DNA cross-link repair by the Fanconi anemia/BRCA pathway. *Genes Dev* **26**, 1393-1408
45. Sirbu, B. M., and Cortez, D. (2013) DNA damage response: three levels of DNA repair regulation. *Cold Spring Harbor perspectives in biology* **5**

46. Joo, W., Xu, G., Persky, N. S., Smogorzewska, A., Rudge, D. G., Buzovetsky, O., Elledge, S. J., and Pavletich, N. P. (2011) Structure of the FANCI-FANCD2 complex: insights into the Fanconi anemia DNA repair pathway. *Science* **333**, 312-316
47. Chaudhury, I., Sareen, A., Raghunandan, M., and Sobeck, A. (2013) FANCD2 regulates BLM complex functions independently of FANCI to promote replication fork recovery. *Nucleic acids research* **41**, 6444-6459
48. Langevin, F., Crossan, G. P., Rosado, I. V., Arends, M. J., and Patel, K. J. (2011) Fancd2 counteracts the toxic effects of naturally produced aldehydes in mice. *Nature* **475**, 53-58

FIGURE LEGENDS

Figure 1. iPOND proteomics screen workflow. (A) Diagram illustrating the samples analyzed by iPOND-MS. Cells labeled with EdU were processed without the Click reaction reagent (Negative control) or treated with thymidine (Thd) for one hour (Thd chase negative control) prior to iPOND. The active replication fork sample was collected immediately after the EdU pulse (Normal replication fork). EdU labeled cells were treated with 3mM HU for 2 hours (Stalled replication fork), or treated with 3mM HU and ATR inhibitor (Collapsed replication fork) without removing EdU, and samples were then collected for iPOND. (B) Representative iPOND purifications from one of the five replicates submitted for proteomic analyses were blotted for PCNA and H2B. (C) iPOND-MS experimental workflow illustrating how proteins were identified. (D) Toppgene analysis for classification of statistically significant proteins found enriched at normal, stalled, and collapsed replication forks.

Figure 2. iPOND-MS identifies proteins enriched at active replication forks. (A) The fold enrichment relative to the thymidine chase negative control, the p-value and the spectral count data are depicted for the proteins listed in Table S1. The dot size indicates the total number of MS spectra counted in the normal replication fork samples from the five replicate purifications. The dot color represents the median p-value as calculated using QuasiTel. (B) Protein network analyses used GeneMANIA predictions to probe the physical interactions within the normal replication fork dataset. Gene not in query refers to proteins known to physically interact with other proteins in the depicted physical interaction network, but that were not identified in the iPOND-MS screen. (C) Proteins that contain PCNA interacting motifs (24), ATM/ATR phosphorylation sites (25,26), or which cause increased DNA damage signaling when silenced by siRNA (27,28) are listed.

Figure 3. iPOND-MS identifies proteins at stalled replication forks. (A) The fold enrichment relative to the thymidine chase negative control, the p-value and the spectral count data are depicted for the proteins listed in Table S2. (B) Proteins that contain PCNA interacting motifs (24), ATM/ATR phosphorylation sites (25,26), or which cause increased DNA damage signaling when silenced by siRNA (27,28) are listed.

Figure 4. iPOND-MS identifies proteins enriched at collapsed forks caused by replication stress and ATR inhibition. (A) The fold enrichment relative to the chromatin chase negative control, the p-value and the spectral count data are depicted for the proteins listed in Table S3. (B) Protein network analyses probed the physical interactions at collapsed replication forks using the GeneMANIA prediction server. (C) Proteins that contain PCNA interacting motifs (24), interact with RPA (BioGrid3.2), contain ATM/ATR phosphorylation sites (25,26), or which cause increased DNA damage signaling when silenced by siRNA (27,28) are listed.

Figure 5. Functional genomic screen reveals proteins important for replication recovery after an acute stalling of the replication fork. siRNA transfected cells were treated with HU, released from replication stress into normal growth media, and labeled with EdU to monitor restart of DNA replication prior to staining for both EdU and γH2AX to monitor DNA damage. The assay was completed in triplicate for

each siRNA. The mean ratio of γH2AX to EdU values obtained for individual siRNAs targeting the genes of interest are plotted. Colored dots indicate siRNAs yielding a ratio of greater than 2 and elevated compared to non-targeting controls (p-value of <0.001, Wilcoxon rank sum test). The location of the ATR positive control score is indicated. For comparison, the average ratio for the negative control siRNA was 1.07 +/- 0.03. (B) Mean ratios (+/-SE) of γH2AX to EdU for four SNF2L and SNF2H siRNAs compared to the non-targeting control are shown. (C) Cells labeled with EdU for the indicated times, processed by iPOND and immunoblotted for the indicated proteins. (D) Cells were labeled with EdU for 20 minutes, washed, then incubated in thymidine containing media for the indicated times prior to iPOND analysis.

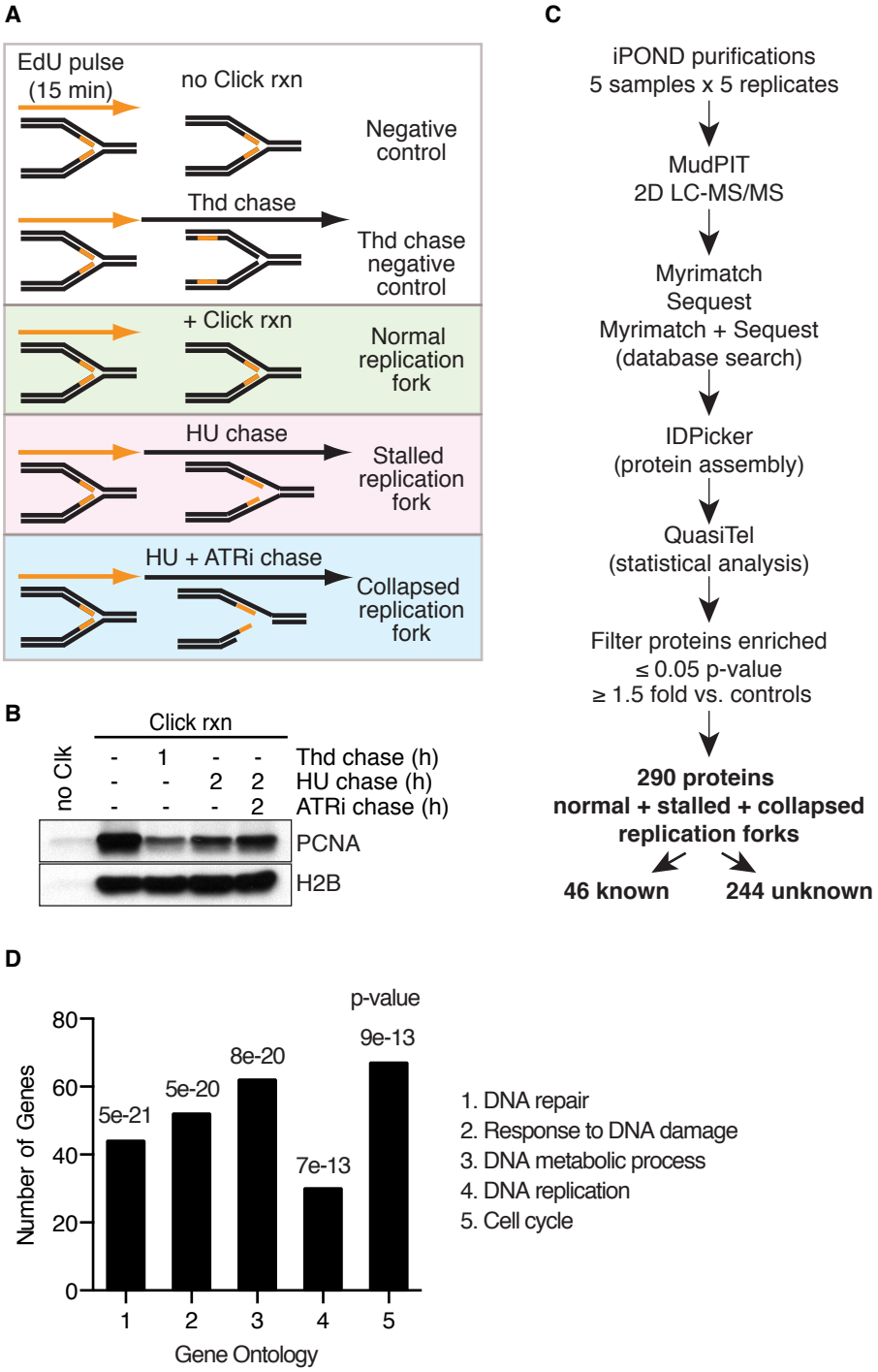

A

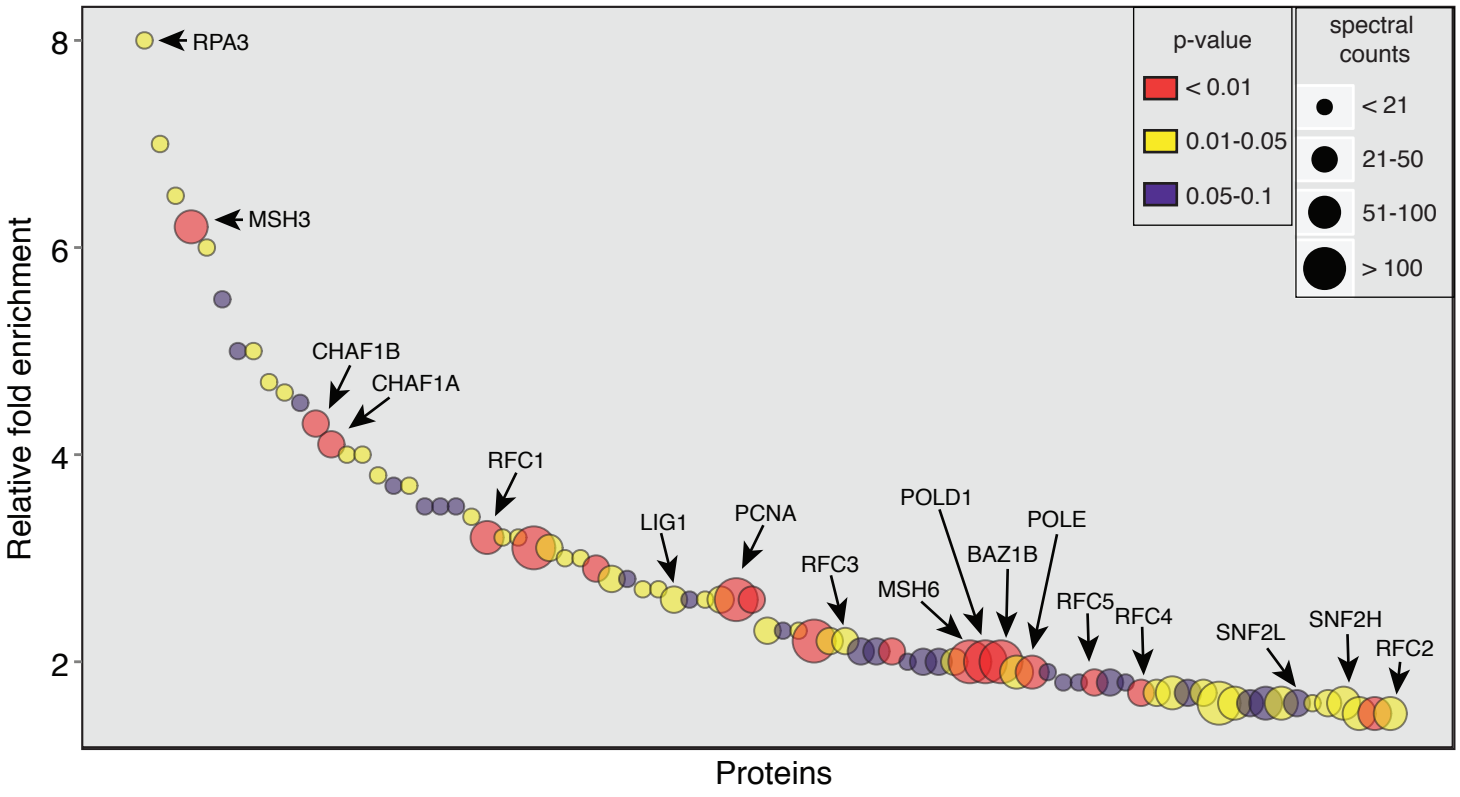

B

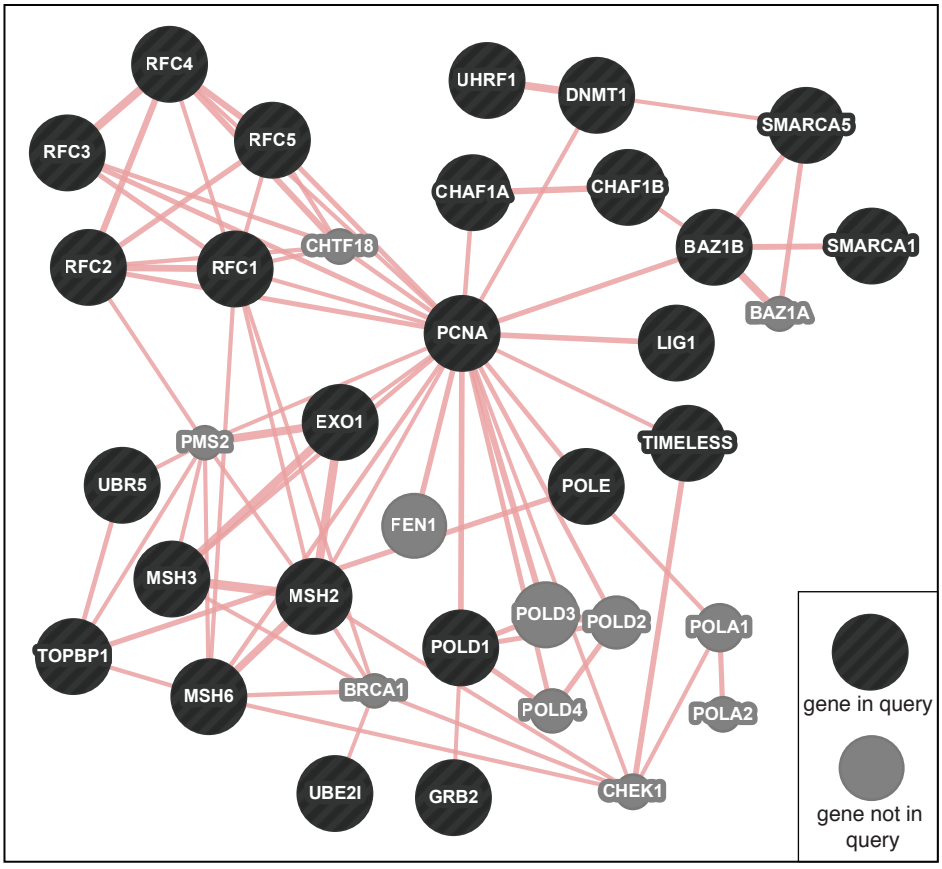

C

Proteins with PCNA-interacting motifs	ATM/ATR substrates	Knockdown causes DNA damage
BAZ1B	ATAD5	EP400
CCP110	BAZ1B	FANCI
DNMT1	CHAF1A	HSD17B7
EHMT1	CHAF1B	PDCD4
LIG1	EHMT1	PLOD1
MSH3	EXO1	RFC2
MSH6	FANCI	RPA3
SMARCA1	MSH2	SMARCA1
SMARCA5	MSH3	SNRPD1
UBR5	MSH6	TIMELESS
UHRF1	POLE	TRMT6
	RFC1	
	RFC3	
	SMARCAD1	
	TOPBP1	
	TRMT6	
	UBR5	
	VPS26B	
	WDHD1	

Sirbu et al., Figure 3

A

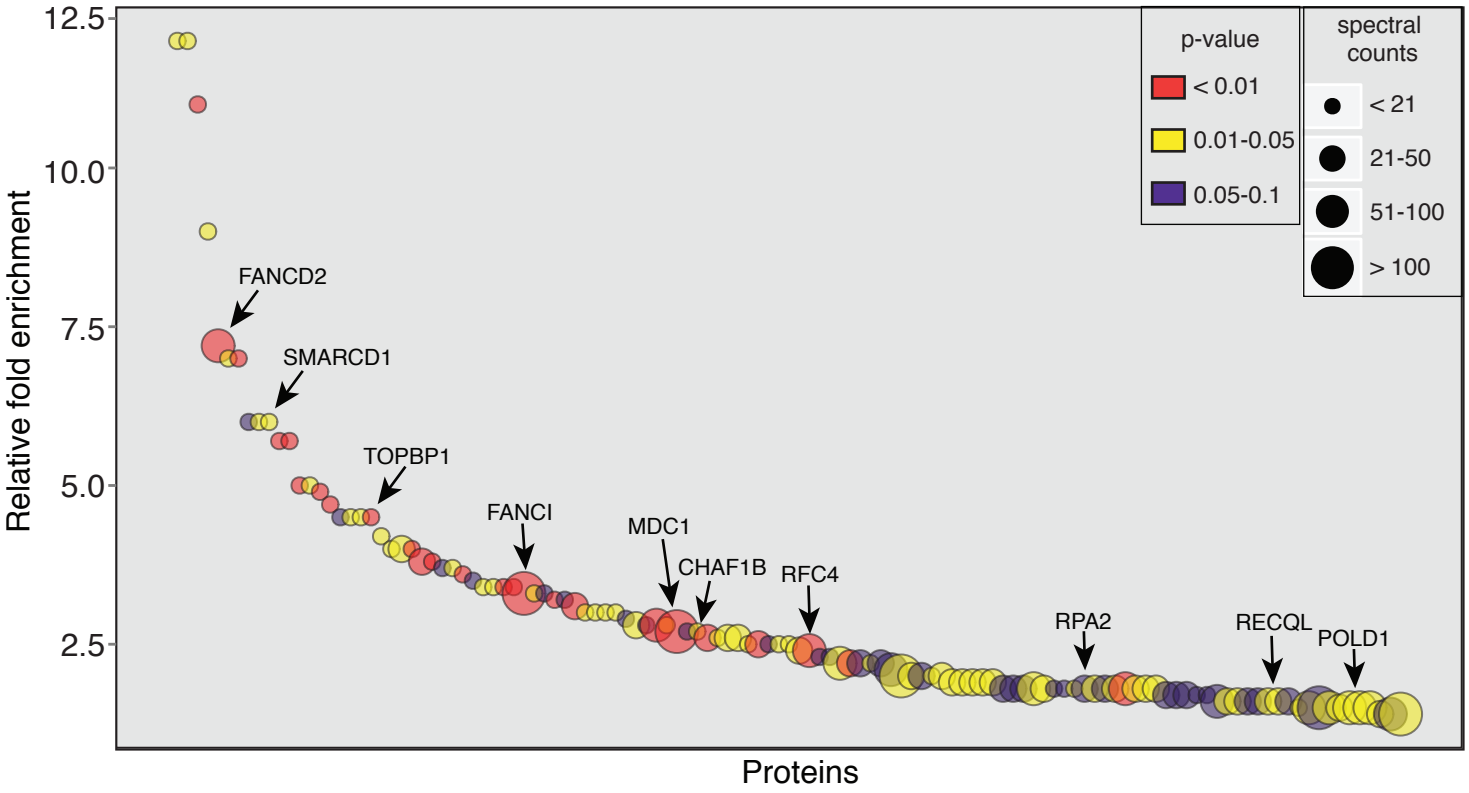

B

Proteins with PCNA-interacting motifs	ATM/ATR substrates	Knockdown causes DNA damage
ASCC3	AKAP12	ADD1
MSH3	CAF1B	ATP6V0D1
OBSCN	CHTF18	CALR
PHF14	EHMT2	COL6A1
RECQL	EIF3D	CUL2
	EPB41L2	FANCI
	FANCD2	KIAA1598
	FANCI	MLL4
	MDC1	ORC7C2
	MSH3	PDC4
	NIN	PSMD8
	PDS5B	RPA2
	PHF14	THUMPD1
	SMARCAD1	TRMT6
	SPG11	TTC27
	TOPBP1	XPO5
	TRMT6	
	ZC3HAV1L	

A

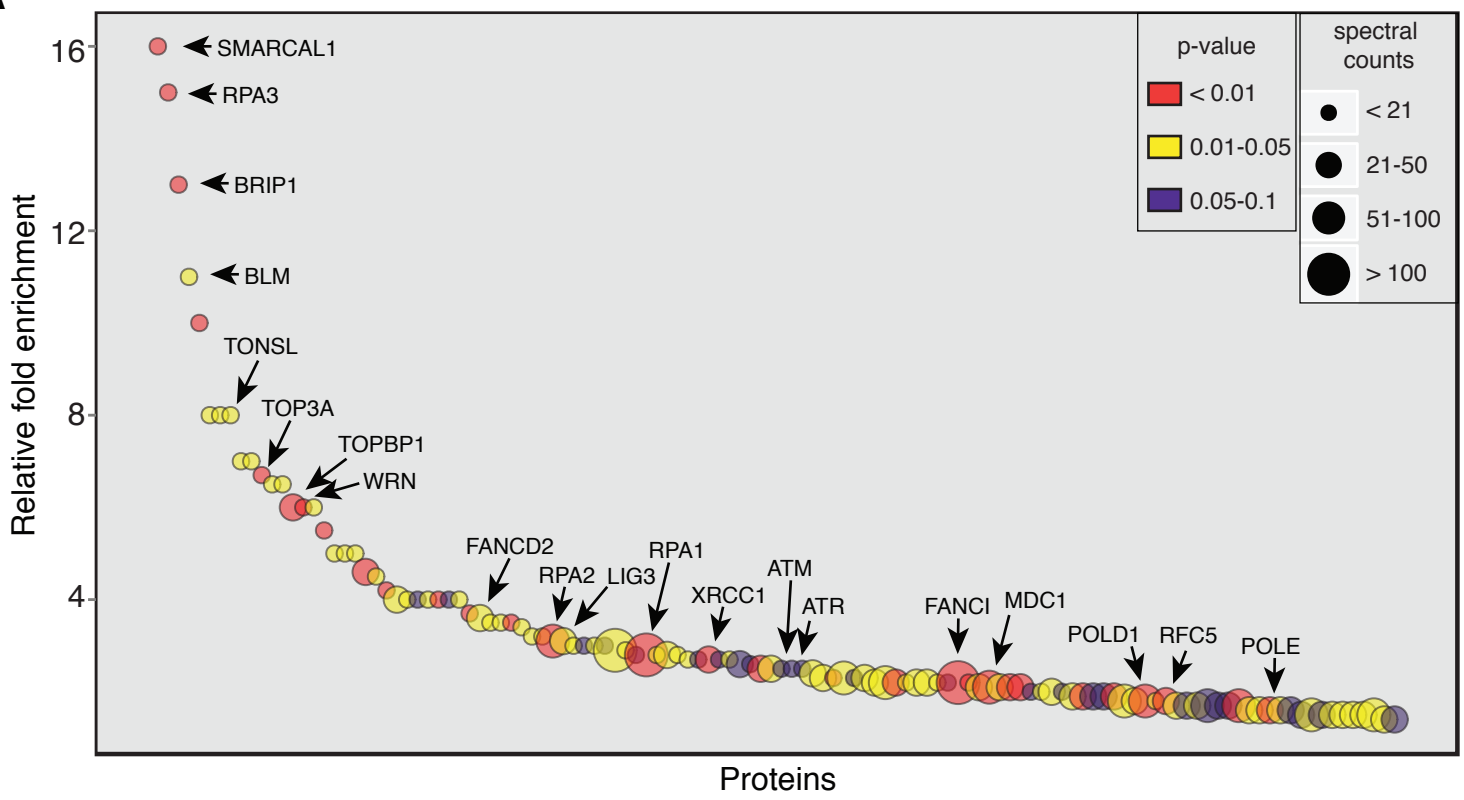

B

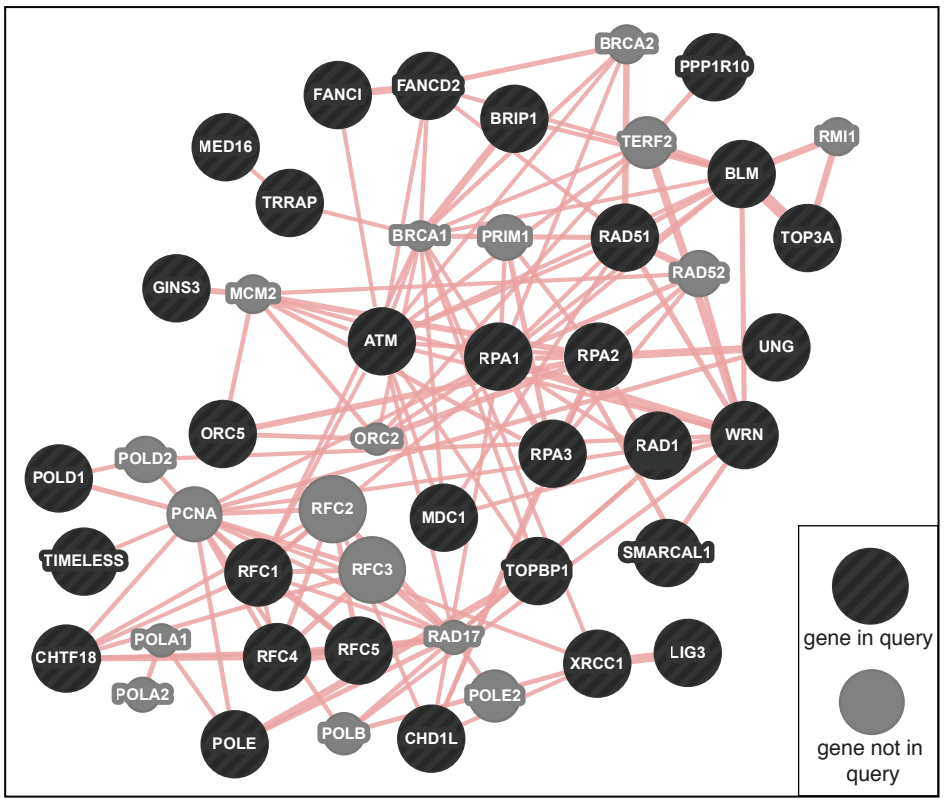

C

Proteins with PCNA-interacting motifs	ATM/ATR substrates	Knockdown causes DNA damage
BTAF1	ATM	ADD1
GTF3C3	CHTF18	BRIP1
MED16	FANCD2	COMT
TONSL	FANCI	CUL2
TRRAP	LIG3	DMD
UNG	MDC1	DNPH1
WRN	PDS5B	FANCI
RPA-interacting proteins	POLE	INCENP
	RFC1	JMJD6
ATM	RPA1	KIAA1598
BLM	SART3	NBAS
BRIP1	SMARCAD1	PDCD4
CHD1L	TOPBP1	PGM3
CUL3	TRMT6	PLIN3
ORC5	WRN	PLRG1
POLD1		RDH14
RAD1		RPA1
RAD51		RPA2
SMARCAL1		RPA3
TOP3A		SLC25A17
TOPBP1		TIMELESS
UNG		TRMT6
WRN		XPO5

Sirbu et al., Figure 5